

SINGLE-REFERENCE COUPLED-CLUSTER METHODS FOR STRONGLY  
CORRELATED SYSTEMS

By

Ilias Magoulas

A DISSERTATION

Submitted to  
Michigan State University  
in partial fulfillment of the requirements  
for the degree of

Chemistry – Doctor of Philosophy

2021

# ABSTRACT

## SINGLE-REFERENCE COUPLED-CLUSTER METHODS FOR STRONGLY CORRELATED SYSTEMS

By

Ilias Magoulas

The development of computationally efficient wavefunction methods that can provide an accurate description of strongly correlated systems and materials is at the heart of electronic structure theory. In general, strong many-electron correlation effects arise from the entanglement of a large number of electrons and are characterized by the unpairing of many electron pairs and their subsequent recoupling to low-spin states, as in the case of Mott metal-insulator transitions where the system traverses from a weakly correlated metallic phase to a strongly correlated insulating one. Although strong correlations have an intrinsically multi-reference nature, multi-reference approaches are not applicable due to the enormous dimensionalities of the underlying model spaces. Therefore, in this dissertation, we focus on single-reference coupled-cluster (CC) approaches, which are widely recognized as the *de facto* standard for high-accuracy electronic structure calculations and whose size extensivity makes them suitable for the study of extended systems and materials. However, it is well established that the traditional CC methodologies that are based on truncating the cluster operator at a given many-body rank, giving rise to the CCSD, CCSDT, CCSDTQ, *etc.* hierarchy, fail to provide physically meaningful solutions in the presence of strong correlations. Thus, in this dissertation, we consider unconventional single-reference CC approaches capable of providing an accurate description of the entire spectrum of many-electron correlation effects, ranging from the weakly to the strongly correlated regimes.

In the first part of this dissertation, we examine the approximate coupled-pair (ACP) theories. The existing ACP methods and their various modifications retain all doubly excited cluster amplitudes, while using subsets of non-linear diagrams of the CCD/CCSD equations. This eliminates failures of conventional CC approaches, including CCSD and even CCSDT or

CCSDTQ, in strongly correlated situations created by the Mott metal–insulator transitions, modeled by linear chains, rings, or cubic lattices of the equally spaced hydrogen atoms, and the  $\pi$ -electron networks described by the Hubbard and Pariser–Parr–Pople Hamiltonians that model one-dimensional metallic systems with periodic boundary conditions. However, typical ACP methods neglect connected triply excited ( $T_3$ ) clusters, which are required to produce quantitative results in most chemical applications. Previous attempts to incorporate these clusters using many-body perturbation theory arguments within the ACP framework have only been partly successful. In this dissertation, we address this concern by employing the active-space ideas to incorporate the dominant  $T_3$  amplitudes in the ACP methods in a robust, yet computationally affordable, manner. Furthermore, taking into consideration that the various diagram modifications defining ACP approaches were derived using minimum-basis-set models, we introduce a novel ACP scheme utilizing basis-set-dependent scaling factors, denoted as  $\text{ACCS}(1, 3 \times \frac{n_o}{n_o+n_u} + 4 \times \frac{n_u}{n_o+n_u})$ , to extend the ACP methodologies to larger basis sets.

In the second part of this dissertation, we discuss a novel approach to extrapolating the exact energetics out of the early stages of full configuration interaction quantum Monte Carlo (FCIQMC) propagations, even in the presence of strong correlations, by merging the ACP approaches with the recently proposed cluster-analysis-driven FCIQMC (CAD-FCIQMC) methodology. In the spirit of externally corrected CC approaches, in the CAD-FCIQMC methodology, one solves CCSD-like equations for the one- and two-body clusters in the presence of their three- and four-body counterparts extracted from the FCIQMC stochastic wavefunction sampling. In this dissertation, we extend CAD-FCIQMC to the strong correlation regime by repartitioning the CC equations so that selected coupled-pair contributions are extracted from FCIQMC as well.

For each new methodology described in this thesis, we discuss the relevant mathematical and computer implementation details and provide numerical examples illustrating its performance in challenging strongly correlated situations.

Copyright by  
ILIAS MAGOULAS  
2021

This dissertation is dedicated to my wife, Ελένη Λύγδα, and daughter, Μαρία Μαγουλά.  
*Πολυαγαπημένες Ελερίτσα και μικρή Μαρία σας ευχαριστώ πάρα πολύ που καθημερινώς ομορφαίρετε τη ζωή μου!*

## ACKNOWLEDGMENTS

To begin with, I would like to thank my doctoral advisor, Professor Piotr Piecuch. As a Master’s student in Greece, I remember that the mere sight of the Feynman diagrams shown on the cover of the “*Many-Body Methods in Chemistry and Physics*” book by R.J. Bartlett and I. Shavitt made me think “*I will never be able to understand coupled-cluster theory*”. Under Professor Piecuch’s training I was able to not only understand the foundations of coupled-cluster and many-body theories, including diagrammatic methods they rely on, but also make a number of non-trivial methodological contributions, including those discussed in this dissertation. I am indebted to Professor Piecuch for entrusting me with the task of developing and implementing new generations of coupled-cluster approaches aimed at an exact or nearly exact treatment of strongly correlated systems, giving me an opportunity to grow substantially as a scientist under his mentorship. I am also very grateful for his continuous support and for doing his best to ensure that my family and I would have a pleasant experience during my Ph.D. studies at Michigan State University.

I would like to thank the remaining members of my guidance committee, namely, Professors Kenneth Merz Jr., James McCusker, and Robert Cukier, for their support, advice, and patience.

I would also like to thank Professors Marcos Dantus, Gary Blanchard, James Jackson, and Babak Borhan and their respective research groups for the fantastic collaboration regarding the photoreactivity of the **FR0**-SB superphotobase that their experimental and our theoretical groups studied together. This project not only gave me the opportunity to learn how to efficiently perform sophisticated electronic structure calculations for large molecules in solution, using explicit and implicit solvation models and embedding techniques, but also piqued my curiosity regarding the various spectroscopic measurements and their underlying physics and chemistry.

I would also like to express my gratitude to former and current members of the Piecuch

group, including Dr. Jun Shen, Dr. Nicholas Bauman, Dr. Adeayo Ajala, Dr. J. Emiliano Deustua, Mr. Stephen Yuwono, Mr. Arnab Chakraborty, and Mr. Karthik Gururangan. In particular, I would like to thank Dr. Nicholas Bauman for introducing me to the codes developed by the Piecuch group and for his invaluable assistance during my initial projects as a graduate student at Michigan State University. I would also like to thank Dr. Jun Shen for providing me with the coupled-cluster codes that formed the basis on which I implemented the novel approaches discussed in this dissertation. I am indebted to Dr. J. Emiliano Deustua for his assistance and guidance during my first steps in coding using the Fortran and Python programming languages as well as for introducing me to the L<sup>A</sup>T<sub>E</sub>X typesetting system. I would also like to thank Mr. Stephen Yuwono for the countless hours of discussions regarding the various projects that we tackled together.

I would also like to thank my undergraduate thesis advisor Professor Aristides Mavridis and my Master's thesis advisor Professor Apostolos Kalamos. They introduced me to the field of electronic structure theory and made me appreciate the importance of precision and ethics in scientific research. Their guidance during my initial steps in this field has been invaluable and I will always be thankful for recommending pursuing a Ph.D. under the supervision of Professor Piecuch.

I would like to acknowledge the support of various friends that helped to make my family's and my stay in East Lansing a very pleasant experience. In particular, I would like to thank Dr. Chrysoula Vasileiou, Professor Elias Strangas, Dr. Jane Turner, Professor Georgios Perdikakis, Professor Artemis Spyrou, Dr. Christos Sidiropoulos, Professor Xanthippi Chatzistavrou, Dr. Christos Grigoriadis, Mr. Ioannis Zachos, Dr. Georgios Psaromiligkos, Mr. Michail Paparizos, Ms. Ana-Maria Raicu, Ms. Andriana Manousidaki, Mr. Dimitris Vardakis, Ms. Christy Natalia, Ms. Laura Castro Diaz, and Mr. Manos Kokarakis. I would also like to thank Dr. Nikolaos Engelis for his steadfast friendship since we first met as freshmen back in Athens in 2007.

At this point, I would like to thank my family for their support and love all these years.

In particular, I would like to thank my parents Themistoklis Magoulas and Maria Nikiforou (deceased), my brother Thanos Magoulas, my wife Eleni Lygda, and my daughter Maria Magoulas. Maria's smile can certainly brighten even the darkest of my days.



# TABLE OF CONTENTS

LIST OF TABLES . . . . .	x
LIST OF FIGURES . . . . .	xiii
CHAPTER 1 INTRODUCTION . . . . .	1
CHAPTER 2 PROJECT OBJECTIVES . . . . .	22
CHAPTER 3 THEORY . . . . .	23
3.1 Introduction to Coupled-Cluster Theory . . . . .	23
3.2 Failure of Conventional Coupled-Cluster Methods in Strongly Correlated Systems . . . . .	30
3.3 Approximate Coupled-Pair Methods with an Active-Space Treatment of Three-Body Clusters . . . . .	40
3.4 Toward the Full Configuration Interaction Limit for Strong Correlation . . . .	54
CHAPTER 4 NUMERICAL RESULTS . . . . .	67
4.1 Application of the Approximate Coupled-Pair Methods with an Active- Space Treatment of Three-Body Clusters to Model Metal–Insulator Transitions	67
4.2 Approaching the Full Configuration Interaction Limit for Strong Correlation Using Semi-Stochastic Ideas . . . . .	86
CHAPTER 5 CONCLUDING REMARKS AND FUTURE OUTLOOK . . . . .	111
APPENDICES . . . . .	120
APPENDIX A COMPUTER IMPLEMENTATION OF THE APPROXI- MATE COUPLED-PAIR METHODS WITH AN ACTIVE- SPACE TREATMENT OF THREE-BODY CLUSTERS . . . .	121
APPENDIX B COMPUTER IMPLEMENTATION OF THE CLUSTER- ANALYSIS-DRIVEN FULL CONFIGURATION INTER- ACTION QUANTUM MONTE CARLO APPROACH FOR STRONGLY CORRELATED SYSTEMS . . . . .	138
BIBLIOGRAPHY . . . . .	149

## LIST OF TABLES

Table 4.1:	A comparison of the energies resulting from the various CC approaches with singles and doubles and the exact FCI data for the symmetric dissociation of the $H_6/cc\text{-pVTZ}$ ring at selected bond distances between neighboring H atoms $R_{H-H}$ (in Å). . . . .	76
Table 4.2:	A comparison of the energies resulting from the various active-space triples CC approaches and the exact FCI data for the symmetric dissociation of the $H_6/cc\text{-pVTZ}$ ring at selected bond distances between neighboring H atoms $R_{H-H}$ (in Å). . . . .	77
Table 4.3:	A comparison of the energies resulting from the various full triples CC approaches and the exact FCI data for the symmetric dissociation of the $H_6/cc\text{-pVTZ}$ ring at selected bond distances between neighboring H atoms $R_{H-H}$ (in Å). . . . .	78
Table 4.4:	A comparison of the energies resulting from the various CC approaches with singles and doubles and the exact FCI data for the symmetric dissociation of the $H_{10}/DZ$ ring at selected bond distances between neighboring H atoms $R_{H-H}$ (in Å). . . . .	79
Table 4.5:	A comparison of the energies resulting from the various active-space triples CC approaches and the exact FCI data for the symmetric dissociation of the $H_{10}/DZ$ ring at selected bond distances between neighboring H atoms $R_{H-H}$ (in Å). . . . .	80
Table 4.6:	A comparison of the energies resulting from the various full triples CC approaches and the exact FCI data for the symmetric dissociation of the $H_{10}/DZ$ ring at selected bond distances between neighboring H atoms $R_{H-H}$ (in Å). . . . .	81
Table 4.7:	A comparison of the energies resulting from the various CC approaches including up to triple excitations and the nearly exact LDMRG(500) data for the symmetric dissociation of the $H_{50}/STO\text{-}6G$ linear chain at selected bond distances between neighboring H atoms $R_{H-H}$ (in bohr). . .	82

Table 4.8: Convergence of the energies resulting from the all-electron $i$ -FCIQMC, CAD-FCIQMC[1–5], and CAD-FCIQMC[1,(3+4)/2] calculations with $\Delta\tau = 0.0001$ a.u. toward FCI for the $\text{H}_2\text{O}$ molecule, as described by the cc-pVDZ basis set, at the equilibrium geometry $R_e$ and the geometry obtained by a simultaneous stretching of both O–H bonds by a factor of 2.0. The $i$ -FCIQMC calculations were initiated by placing 1,000 walkers on the RHF determinant and the $n_a$ parameter of the initiator algorithm was set at 3. . . . .	104
Table 4.9: Convergence of the energies resulting from the $i$ -FCIQMC, CAD-FCIQMC[1–5], and CAD-FCIQMC[1,(3+4)/2] calculations with $\Delta\tau = 0.0001$ a.u. toward FCI for the symmetric dissociation of the $\text{H}_6$ ring, as described by the cc-pVDZ basis set, at two representative values of the distance between neighboring H atoms, including $R_{\text{H-H}} = 1.0$ Å (the region of the minimum on the FCI PEC shown in Figure 4.5(a) characterized by weaker correlations) and $R_{\text{H-H}} = 2.0$ Å (the region characterized by strong correlations involving the entanglement of all six electrons). The $i$ -FCIQMC calculations were initiated by placing 1,500 walkers on the RHF determinant and the $n_a$ parameter of the initiator algorithm was set at 3. . . . .	105
Table 4.10: Same as Table 4.9 for the symmetric dissociation of the $\text{H}_{10}$ ring, as described by the DZ basis set. In analogy to the $\text{H}_6$ ring, $R_{\text{H-H}} = 1.0$ Å corresponds to the region of the minimum on the FCI PEC shown in Figure 4.5(b) characterized by weaker correlations, whereas $R_{\text{H-H}} = 2.0$ Å is the region characterized by strong correlations involving the entanglement of all ten electrons. . . . .	106
Table 4.11: Results of the CAD-FCIQMC calculations based on the AS-FCIQMC wavefunctions obtained after equilibration runs using 1 billion (1B) and 2 billion (2B) walkers. . . . .	107
Table A.1: The spin-orbital Hugenholtz and Brandow diagrams and corresponding algebraic expressions arising from the $\langle \Phi_{ij}^{ab}   (V_{\text{N}}^{\frac{1}{2}} T_2^2)_C   \Phi \rangle$ term. In the last column, we provide the correspondence between the spin-orbital diagrams presented in this table and the spin-adapted ones shown in Figure 3.5. . . . .	122
Table A.2: The spin-integrated Hugenholtz and Brandow diagrams and corresponding algebraic expressions arising from the $\langle \Phi_{IJ}^{AB}   (V_{\text{N}}^{\frac{1}{2}} T_2^2)_C   \Phi \rangle$ term. In the last column, we provide the correspondence between the spin-integrated diagrams presented in this table and the spin-adapted ones shown in Figure 3.5. . . . .	124

Table A.3: The spin-integrated Hugenholtz and Brandow diagrams and corresponding algebraic expressions arising from the $\left\langle \Phi_{IJ}^{A\tilde{B}} \left  \left( V_N \frac{1}{2} T_2^2 \right)_C \right  \Phi \right\rangle$ term. In the last column, we provide the correspondence between the spin-integrated diagrams presented in this table and the spin-adapted ones shown in Figure 3.5. . . . . .	127
--	-----

Table A.4: The spin-integrated Hugenholtz and Brandow diagrams and corresponding algebraic expressions arising from the $\left\langle \Phi_{IJ}^{\tilde{A}\tilde{B}} \left  \left( V_N \frac{1}{2} T_2^2 \right)_C \right  \Phi \right\rangle$ term. In the last column, we provide the correspondence between the spin-integrated diagrams presented in this table and the spin-adapted ones shown in Figure 3.5. . . . . .	132
--	-----

## LIST OF FIGURES

Figure 3.1:	The ground-state PECs of $H_2$ in the presence of 0, 2, 4, and 6 Ne atoms as obtained with (a) CCSD/cc-pVDZ and (b) CISD/cc-pVDZ. The Ne atoms were located such that they do not interact among themselves and with the $H_2$ molecule. In panel (b), we also include the RHF PEC for comparison. All PECs have been aligned such that the corresponding electronic energies at the internuclear separation $R_{H-H} = 4.0 \text{ \AA}$ are identical and set at 0 kcal/mol. . . . .	26
Figure 3.2:	A comparison of the energies resulting from the all-electron CCSD, CCSDT, and CCSDTQ computations for the $H_2O$ molecule, as described by the cc-pVDZ basis set [276], at the equilibrium and two displaced geometries obtained by simultaneous stretching of both O–H bonds by factors of 1.5 and 2.0 [277]. . . . .	30
Figure 3.3:	Schematic representation of the models of cyclic polyenes $C_NH_N$ with (a) $N = 6$ , (b) $N = 10$ , and (c) $N = 14$ . The pertinent molecular orbital diagrams are presented as well. . . . .	32
Figure 3.4:	Branching diagram illustrating the total spin as a function of the number of $s = \frac{1}{2}$ coupled spins. The integers inside the circles indicate the number of independent spin states associated with a given total spin and number of $s = \frac{1}{2}$ spins coupled. . . . .	41
Figure 3.5:	Goldstone–Brandow diagrams for the $\frac{1}{2}T_2^2$ contributions $\Lambda_k^{(2)}(AB, IJ; S_r)$ , $k = 1-5$ , to the CC equations projected on the singlet pp-hh coupled orthogonally spin-adapted doubly excited $ \Phi_{IJ}^{AB}\rangle_{S_r}$ states. The intermediate spin quantum number $S_r$ in defining $ \Phi_{IJ}^{AB}\rangle_{S_r}$ and the corresponding doubly excited cluster amplitudes $^{[S_r]}t_{AB}^{IJ}$ is 0 or 1. The occupied orbital indices $M$ and $N$ , the unoccupied orbital indices $E$ and $F$ , and the intermediate spin quantum numbers $\tilde{S}_r^1$ , $\tilde{S}_r^2$ , and $\tilde{S}_r$ are summed over. . . . .	42

Figure 3.6:	Ground-state PECs characterizing the $D_{6h}$ -symmetric dissociation of the $H_6$ /STO-6G ring, as obtained with the various ACCSD approaches that rely on subsets of the non-linear diagrams shown in Figure 3.5: (a) diagrams D1–D5 are neglected resulting in linearized CCSD, (b) all but one of the diagrams D1–D5 are neglected, (c) all but two of the diagrams D1–D5 are neglected, (d) all but three of the diagrams D1–D5 are neglected, (e) all but four of the diagrams D1–D5 are neglected, and (f) all diagrams are considered, <i>i.e.</i> , full CCSD. The dashed horizontal line designates the exact dissociation limit for the employed basis set corresponding to 6 non-interacting H atoms. . . . .	48
Figure 3.7:	Schematic representation of the partitioning of orbitals into four disjoint groups, namely, core (magenta), active occupied (olive), active unoccupied (blue), and virtual (red), employed in active-space SRCC approaches. . . . .	53
Figure 3.8:	Flowchart outlining the key steps of the CAD-FCIQMC algorithm. . . .	65
Figure 4.1:	Ground-state PECs [panels (a)–(c)] and errors relative to FCI [panels (d)–(f)] for the symmetric dissociation of the $H_6$ ring resulting from the CCSD and various ACCSD calculations [panels (a) and (d)], the active-space CCSDt and ACCSDt computations [panels (b) and (e)], and the full CCSDT and ACCSDT methods [panels (c) and (f)], using the cc-pVTZ basis set. The active-space triples approaches employed a minimum active space built from the 1s orbitals of individual hydrogen atoms. The FCI PEC is included in panels (a)–(c) to facilitate the comparisons. . . . .	83
Figure 4.2:	Ground-state PECs [panels (a)–(c)] and errors relative to FCI [panels (d)–(f)] for the symmetric dissociation of the $H_{10}$ ring resulting from the CCSD and various ACCSD calculations [panels (a) and (d)], the active-space CCSDt and ACCSDt computations [panels (b) and (e)], and the full CCSDT and ACCSDT methods [panels (c) and (f)], using the DZ basis set. The active-space triples approaches employed a minimum active space built from the 1s orbitals of individual hydrogen atoms. The FCI PEC is included in panels (a)–(c) to facilitate the comparisons. . . . .	84
Figure 4.3:	Ground-state PECs for the symmetric dissociation of the $H_{50}$ linear chain resulting from the CCSD and ACCSD( $1, 3 \times \frac{n_o}{n_o+n_u} + 4 \times \frac{n_u}{n_o+n_u}$ ) calculations [panel (a)] and their full triples extensions [panel (b)] using the STO-6G basis set. The nearly exact LDMRG(500) PEC of Reference [175] is included in both panels to facilitate the comparisons. The insets show the errors relative to LDMRG(500) in millihartree ( <i>cf.</i> Table 4.7). . . . .	85

- Figure 4.4: Convergence of the energies resulting from the all-electron *i*-FCIQMC, CAD-FCIQMC[1–5], and CAD-FCIQMC[1,(3+4)/2] calculations with  $\Delta\tau = 0.0001$  a.u. toward FCI for the H<sub>2</sub>O molecule, as described by the cc-pVDZ basis set, at (a) the equilibrium geometry and (b) the geometry obtained by a simultaneous stretching of both O–H bonds by a factor of 2 without changing the  $\angle(\text{H-O-H})$  angle (both geometries were taken from [277]). The *i*-FCIQMC calculations were initiated by placing 1,000 walkers on the RHF determinant and the  $n_a$  parameter of the initiator algorithm was set at 3. All energies are errors relative to FCI in millihartree, and the insets show the percentages of triply (%T) and quadruply (%Q) excited determinants captured during the *i*-FCIQMC propagations. . . . . 108
- Figure 4.5: Ground-state PECs for the symmetric dissociation of the (a) H<sub>6</sub>/cc-pVDZ and (b) H<sub>10</sub>/DZ systems resulting from the CCSD, CCSDT, and FCI calculations. . . . . 108
- Figure 4.6: Convergence of the energies resulting from the *i*-FCIQMC, CAD-FCIQMC[1–5], and CAD-FCIQMC[1,(3+4)/2] calculations with  $\Delta\tau = 0.0001$  a.u. toward FCI for the symmetric dissociation of the H<sub>6</sub>/cc-pVDZ [panels (a) and (b)] and H<sub>10</sub>/DZ [panels (c) and (d)] systems at two representative values of the distance between neighboring H atoms, including  $R_{\text{H-H}} = 1.0$  Å [panels (a) and (c)] and  $R_{\text{H-H}} = 2.0$  Å [panels (b) and (d)]. The *i*-FCIQMC calculations were initiated by placing 1,500 walkers on the RHF determinant and the  $n_a$  parameter of the initiator algorithm was set at 3. All energies are errors relative to FCI in millihartree, and the insets show the percentages of triply (%T) and quadruply (%Q) excited determinants captured during the *i*-FCIQMC propagations. The CAD-FCIQMC[1–5] curve is absent in panel (d), since the solution of the CC equations defining the deterministic part of the CAD-FCIQMC[1–5] procedure for the H<sub>10</sub>/DZ system could not be continued beyond  $R_{\text{H-H}} = 1.75$  Å. . . . . 109

Figure 4.7: A comparison of the energies resulting from the *i*-FCIQMC, CAD-FCIQMC[1–5], and CAD-FCIQMC[1,(3+4)/2] calculations at 50,000 [panels (a) and (d)], 100,000 [panels (b) and (e)], and 150,000 [panels (c) and (f)] *i*-FCIQMC iterations using time step  $\Delta\tau = 0.0001$  a.u., along with the corresponding fully deterministic CCSD, CCSDT, and ACCSD(1, $\frac{3+4}{2}$ ) data, for the symmetric dissociation of the H<sub>6</sub>/cc-pVDZ [panels (a)–(c)] and H<sub>10</sub>/DZ [panels (d)–(f)] systems at selected distances between neighboring H atoms,  $R_{\text{H-H}}$ , ranging from the weakly correlated (smaller  $R_{\text{H-H}}$ ) to the strongly correlated (larger  $R_{\text{H-H}}$ ) regions. The *i*-FCIQMC calculations were initiated by placing 1,500 walkers on the RHF determinant and the  $n_a$  parameter of the initiator algorithm was set at 3. All energies are errors relative to FCI in millihartree. The insets show the entire range of errors relative to FCI. . . . . 110

Figure A.1: Excerpt of the code that computes the scaled  $\frac{1}{2}v_{MN}^{EF}t_{AF}^{NM}$  intermediate, which eventually multiplies  $t_{E\tilde{B}}^{I\tilde{J}}$  and results in the D3 contribution of the  $\left\langle \Phi_{I\tilde{J}}^{A\tilde{B}} \middle| (V_{\text{NA}}T_{2\text{A}}T_{2\text{B}})_C \middle| \Phi \right\rangle$  term (*cf.* Table A.3). . . . . 136

Figure A.2: Excerpt of the code that computes the scaled D1 and D2 diagrams arising from the  $\left\langle \Phi_{IJ}^{AB} \middle| (V_{\text{NC}}\frac{1}{2}T_{2\text{B}}^2)_C \middle| \Phi \right\rangle$  term (*cf.* Table A.2). . . . . 137

Figure B.1: Portion of a list containing Slater determinants and numbers of signed walkers inhabiting them corresponding to the last time step, namely, 160,000 MC iterations, of a *i*-FCIQMC simulation for H<sub>10</sub>/DZ with  $R_{\text{H-H}} = 1.0$  Å. The first column contains serial numbers for each determinant. The second column contains the information about the signed walker populations while the remaining columns list the spin-orbital indices occupied in a given determinant. Odd (even) spin-orbital indices correspond to  $\alpha$  ( $\beta$ ) spin functions. . . . . 138

Figure B.2: Excerpt of the code that computes the deterministic  $\text{diag3} \times \Lambda_3^{(2)}$  contribution of the  $\left\langle \Phi_{IJ}^{AB} \middle| (V_{\text{NA}}\frac{1}{2}T_{2\text{A}}^2)_C \middle| \Phi \right\rangle$  term (*cf.* Table A.2). . . . . 147

Figure B.3: Excerpt of the code that computes the stochastic  $(1 - \text{diag3})\Lambda_3^{(2),(\text{MC})}$  contribution of the  $\left\langle \Phi_{IJ}^{AB} \middle| (V_{\text{NA}}\frac{1}{2}T_{2\text{A}}^2)_C \middle| \Phi \right\rangle$  term (*cf.* Table A.2). . . . . 148



# CHAPTER 1

## INTRODUCTION

*Every attempt to refer chemical questions to mathematical doctrines must be considered, now and always, profoundly irrational, as being contrary to the nature of the phenomena.*

---

A. Comte, *Positive Philosophy*, translated by H. Martineau (Calvin Blanchard, New York, 1858).

The first applications of the Schrödinger equation to molecular systems appeared just one year after the publication of Schrödinger’s seminal papers [1–6], when Burrau examined the ground state of the  $\text{H}_2^+$  species [7] and Heitler and London studied the ground state of  $\text{H}_2$  [8], the simplest one- and two-electron molecules, respectively, giving birth to the field of quantum chemistry. The prospect of elucidating the nature of the chemical bond using the then newly formulated quantum mechanics lead Heitler to exclaim “We can, then, eat Chemistry with a spoon” in a letter to London in 1927 [9]. However, it was soon realized that the application of the Schrödinger equation to many-electron systems leads to formidable equations that cannot be solved analytically [10]. This can be understood by examining the electronic Schrödinger equation, the central tenet of quantum chemistry, which, from the mathematical point of view, is an eigenvalue problem:  $H\Psi_\mu(\mathbf{X}; \mathbf{R}) = E_\mu(\mathbf{R})\Psi_\mu(\mathbf{X}; \mathbf{R})$ , where  $H$  is the electronic Hamiltonian for the system of interest,  $\Psi_\mu$  is the many-electron wavefunction characterizing the  $\mu$ th electronic state, with  $\mu = 0$  denoting the ground state and  $\mu > 0$  designating excited states, and  $E_\mu$  is the corresponding total electronic energy. Thanks to the use of the Born–Oppenheimer approximation [11], which decouples the electronic and nuclear motions, the electronic Schrödinger equation is somewhat simpler than the underlying molecular Schrödinger equation from which it is obtained, but it is still a highly complex multi-dimensional mathematical and numerical problem when realistic systems are

examined. Indeed, the many-electron wavefunction depends explicitly on the spatial and spin coordinates of all electrons, collectively denoted as  $\mathbf{X}$ , and parametrically or implicitly on the nuclear coordinates,  $\mathbf{R}$ , while the total electronic energy, when calculated by solving the electronic Schrödinger equation at multiple values of  $\mathbf{R}$ , becomes a function of the nuclear coordinates. For molecules other than small few-electron systems, solving the electronic Schrödinger equation becomes a major challenge, even when one is interested in single-point calculations (calculations at a single nuclear geometry).

In general, the electronic Hamiltonian contains one- and two-body terms. In this dissertation, we focus on a non-relativistic description, where the electronic Hamiltonian for a system comprised of  $N$  electrons and  $M$  nuclei takes the form, in atomic units,  $H = \sum_{i=1}^N z_i + \sum_{i<j}^N v_{ij} = \sum_{i=1}^N \left( -\frac{1}{2} \nabla_i^2 - \sum_{A=1}^M \frac{Z_A}{r_{iA}} \right) + \sum_{i<j}^N \frac{1}{r_{ij}}$ , with  $Z_A$  denoting the nuclear charge associated with the  $A$ th nucleus. The one-body terms,  $z_i$ , describe the kinetic energy of the electrons and their coulombic attraction to the fixed nuclei, while the two-body terms,  $v_{ij}$ , represent the interelectronic coulombic repulsions. The two-body terms,  $r_{ij}^{-1} \equiv \left[ (x_i - x_j)^2 + (y_i - y_j)^2 + (z_i - z_j)^2 \right]^{-\frac{1}{2}}$ , inextricably couple the motions of the electrons and, thus, prohibit closed-form solutions to the many-electron Schrödinger equation. One can go beyond the non-relativistic theory by extending the Dirac equation [12, 13] to many-electron systems, adopting, for example, the Dirac–Coulomb or other relativistic Hamiltonians (see Reference [14] for a review), but in this dissertation we focus on a non-relativistic case.

The simplest (conceptually and numerically) approach to describing many-electron systems is offered by the independent-particle models (IPMs), where one replaces electronic wavefunctions by products of one-electron functions called spin-orbitals. The oldest method in this category was introduced by Hartree in 1928 [15, 16] and the resulting IPM bears his name. In the Hartree model, the spin-orbitals are determined iteratively through a self-consistent field (SCF) procedure, invoking the variational principle. To be more precise, they are optimized by solving a system of coupled one-electron equations, in which an electron

is moving in the external field of the nuclei and the mean field resulting from the electrons occupying the remaining spin-orbitals, until self-consistency is reached. The Hartree model played an important role in the early days of quantum mechanics, but it had to be replaced by better IPMs, since it has a fundamental deficiency that renders it unsuitable for a more quantitative description consistent with the fact that electrons in atoms and molecules are indistinguishable; its many-electron wavefunction, called a Hartree product, violates the Pauli exclusion principle [17] and the underlying spin-statistics theorem [18], which require many-electron wavefunctions to be antisymmetric with respect to the exchange of the spatial and spin coordinates of any pair of electrons.

In 1929, Slater introduced the simplest form of an antisymmetric many-electron wavefunction in the form of an antisymmetrized product of spin-orbitals, called a Slater determinant [19]. The following year, Fock improved Hartree’s SCF approach by replacing the Hartree product with a Slater determinant [20, 21] (see Reference [22] for a similar suggestion by Slater). This gave rise to the Hartree–Fock (HF) approach, the most widely used IPM to date (other than the Kohn–Sham density functional theory [23, 24]). Although the numerical solution of the HF integro-differential equations for orbitals treated as functions of electronic coordinates, without any reference to basis sets, is possible for atoms and diatomics, it is generally not tractable in the case of polyatomic species. The routine application of the HF approach to polyatomic molecules became possible after Hall [25] and Roothaan [26] recasted the HF equations in matrix form by introducing finite one-electron basis sets of atomic spin-orbitals and expressing their molecular counterparts as linear combinations of these atomic spin-orbitals. The resulting set of molecular spin-orbitals, obtained by solving the HF equations in a basis set using an SCF procedure, is partitioned into the disjoint subsets of occupied (hole) and unoccupied (particle) ones, where the antisymmetrized product of the former defines the underlying HF Slater determinant. In the limit of an infinite-dimensional one-electron basis, one arrives at the true HF limit corresponding to the aforementioned integro-differential representation of the HF equations.

The HF methodology is capable of recovering the lion’s share of the total electronic energy, but is far from being a good solution to the many-electron problem, since the error in the calculated total electronic energy is comparable to the magnitude of various observables of chemical interest, such as energies of chemical bonds, excitation energies, ionization energies, and activation barriers. The HF description also neglects important physical effects, such as dispersion in van der Waals molecules. Furthermore, HF provides a poor description of fragmentation phenomena when a closed-shell species dissociates into open-shell fragments. In such cases, the restricted HF (RHF) approach, where each spatial molecular orbital can be occupied by up to two electrons with opposite spin, significantly overbinds the system. This is a consequence of the fact that a single RHF Slater determinant overemphasizes ionic structures. One might resort to unrestricted HF (UHF), using, for example, different spatial orbitals for different spins, to improve the description of bond breaking phenomena, but UHF introduces various new problems related to symmetry breaking (see, for example, References [27] and [28] for the classification of the various symmetry-broken UHF solutions). The single bond breaking of the  $F_2$  diatomic showcases the deficiencies associated with both flavors of the HF approach. In this case, RHF significantly overbinds the system, since it forces  $F_2$  to dissociate into  $F^+$  and  $F^-$ , while the UHF method of the different orbitals for different spins type produces a repulsive potential energy curve (PEC), with no minimum on it [29]. The problems associated with the HF approach stem from the fact that, like its Hartree model predecessor, it is a mean field approximation and, thus, neglects many-electron correlation effects, leading to the uncorrelated motion of the electrons, which is unphysical.

It is interesting to note that when Hartree introduced his SCF approach in 1928 he “*hoped that when the time is ripe for the practical evaluation of the exact solution of the many-electron problem, the self-consistent fields... may be helpful as providing first approximations*” [16]. Indeed, the HF approach, while having many deficiencies, such as those mentioned above, often serves as a starting point for constructing correlated many-electron wavefunctions, which allow us to systematically approach the numerically exact solutions of

the many-electron Schrödinger equation. To that end, one begins by defining a one-electron basis set of molecular spin-orbitals, which are usually determined from an SCF mean-field approach, such as HF, as discussed above. In the exact case, the dimensionality of the one-electron basis is infinite, but in practice finite-dimensional basis sets are employed. Subsequently, one constructs all possible Slater determinants that can be formed from the finite basis of molecular spin-orbitals. Using one of these determinants (*e.g.*, the HF determinant) as a reference state, one can construct the remaining determinants in the electronic wavefunction by particle-hole (ph) excitations starting from singly excited Slater determinants, where one electron is excited from an occupied molecular spin-orbital to an unoccupied one in all possible ways, and going all the way to  $N$ -tuply excited Slater determinants, in which all electrons of the  $N$ -electron system are excited from the occupied to unoccupied molecular spin-orbitals. The resulting set of Slater determinants afforded by the chosen one-electron basis spans the many-electron Hilbert space and, thus, forms a natural many-electron basis set for constructing many-electron wavefunctions. This implies that, in a given one-electron basis, the exact wavefunctions can always be expressed as linear combinations of all possible Slater determinants that this one-electron basis permits. This recasts the many-electron Schrödinger equation into a purely algebraic matrix eigenvalue problem  $\mathbf{H} \cdot \mathbf{C}_\mu = E_\mu \mathbf{C}_\mu$ , where  $\mathbf{H}$  is the Hamiltonian matrix involving Slater determinants defining the electronic wavefunction and  $\mathbf{C}_\mu$  is the vector of coefficients in the expansion of the electronic wavefunction  $|\Psi_\mu\rangle$  in terms of Slater determinants. By diagonalizing the resulting Hamiltonian matrix  $\mathbf{H}$  in a complete many-electron Hilbert space, one obtains the exact wavefunctions and total electronic energies corresponding to the one-electron basis used in the calculations. This procedure is referred to as the full configuration interaction (FCI) approach. To arrive at the numerically exact eigenvalues  $E_\mu$  and eigenfunctions  $|\Psi_\mu\rangle$  of the Hamiltonian, one needs to employ sufficiently large basis sets that are practically equivalent to the complete basis set (CBS) limit or repeat the calculations using several basis sets of growing size and extrapolate the CBS limit. If properly executed, the above procedure provides us with

an exact description of the many-electron correlation effects neglected by HF and similar approximations and the associated correlation energy.

The first use of the term “correlation energy” can be traced to a paper by Wigner published in 1934 [30], while its modern definition as the difference between the exact eigenvalue of the Hamiltonian and the energy obtained from HF was introduced by Löwdin in 1959 [31]. It is customary to divide correlation effects into dynamic and non-dynamic or static [32], although the distinction between them is not always possible. Dynamic correlation effects are associated with the dynamical motion of the electrons, which avoid one another due to interelectronic repulsion, and typically manifest themselves as numerous excited Slater determinants having small coefficients in the electronic wavefunction. On the other hand, static correlation effects characterize situations in which several Slater determinants become quasi-degenerate, having large CI coefficients, or sometimes even degenerate, as in open-shell singlet and many other classes of low-spin states.

At this point, it is important to reiterate the fact that although correlation energy is usually just a fraction of the total electronic energy, its neglect leads to a very poor, sometimes even unphysical, description of chemical properties and phenomena. This showcases and emphasizes the significance of many-electron correlation effects, which lie at the heart of modern quantum chemistry effort (see Reference [33] for a historical overview of the electron correlation problem). At the same time, the computational costs characterizing exact Hamiltonian diagonalizations, which would enable us to describe many-electron correlation effects exactly, render the FCI approach inapplicable to systems with more than a few electrons, even when smaller basis sets are employed and even when one takes advantage of the state-of-the-art matrix-diagonalization algorithms and largest supercomputers. To make matters worse, taking into account the steep scaling of the dimensionality of the FCI problem, which scales factorially with the system size [34, 35], it is highly unlikely that FCI will be routinely applied to the majority of problems of chemical interest for a very long time, despite rapid software and hardware advances. Therefore, efficient alternative quantum chemistry

methods that can provide an accurate, near FCI, description of many-electron correlation effects at the small fraction of the computational cost associated with FCI Hamiltonian diagonalizations are required.

The colossal theoretical and technical advances in the treatment of electron correlation effects that have taken place since the dawn of quantum chemistry have enabled numerous high-accuracy quantum mechanical calculations that have successfully addressed problems of experimental interest. In fact, I benefited from these advances in my own work in the Piecuch group, where I was involved in computational studies aimed at the virtually exact determination of the electronic structure of challenging diatomics, such as NaI, Be<sub>2</sub>, and Mg<sub>2</sub>, providing important insights into ultrafast [36] and high-resolution spectroscopy [37–39], and high-precision calculations for larger polyatomic species, including, for instance, novel super photobases, such as **FR0**-SB [40–42], whose light-induced excited-state solvent-to-solute proton transfer is amenable to spatial and temporal control rendering them perfect candidates for precision chemistry. Nonetheless, there still are situations that remain challenging for many contemporary quantum chemistry methods, such as quasi-degenerate electronic states in instances involving biradical and polyradical species, multiple bond breaking, and excited states characterized by two- and other many-electron transitions, and strongly correlated systems in general. These situations, which are of interest in this dissertation, require the use of electronic structure methods that are capable of providing FCI-quality results for the entire spectrum of many-electron correlation effects, including the weakly and strongly correlated regimes and dynamical and static correlations, while retaining tractable polynomial computational costs. We focus on the development of such methods, which adopt concepts based on the coupled-cluster (CC) theory [43–48], in this thesis research. The reason we will rely on the CC theory is its well-known efficiency in balancing accuracy and computational costs.

Historically, the CC theory emerged as an infinite-order generalization of the finite-order many-body perturbation theory (MBPT) by summing linked wavefunction and connected

energy diagrams to infinite order, as dictated by the linked [49–52] and connected [51, 52] cluster theorems. These fundamental theorems guarantee that CC methods, unlike other wavefunction-based approaches, such as truncated configuration interaction (CI), satisfy several important conditions of the exact theory. For example, CC methods that rely on linked wavefunction and connected energy expressions are size extensive, *i.e.*, no loss in accuracy occurs when the size of the system is increased. Furthermore, as long as the underlying reference state is separable, the exponential ansatz defining CC wavefunctions, which was introduced by Hubbard and Hugenholtz in 1957 [51, 52], ensures the separability or size-consistency of the many-electron wavefunctions in the non-interacting limit, enabling CC methods to provide a proper description of fragmentation phenomena. Fast convergence toward FCI as a consequence of representing higher-order correlation effects via products of low-rank excitation operators is another very important feature of the exponential CC ansatz. These paramount properties of the CC theory and its other characteristics that will be stated later in this dissertation have established CC-based methods as the *de facto* standard for high-accuracy electronic structure calculations. Nowadays this includes larger molecular systems with hundreds of correlated electrons and thousands of basis functions, where the use of size-extensive methods is imperative.

Within the CC framework one can distinguish between two broad classes of formalisms that depend on the dimensionality of the reference or model space which provides the zeroth-order description of the many-electron problem of interest. The first and historically oldest formalism, which is called the single-reference (SR) CC approach, is based on a one-dimensional model space spanned by a single Slater determinant that serves as the Fermi vacuum. The second category of CC methods adopts multi-dimensional model spaces and is called multi-reference (MR) CC. Since, as already mentioned above, we are interested in an accurate description of quasi-degenerate and strongly correlated electronic states, which are intrinsically MR problems, it seems natural to turn to MRCC approaches. In MRCC schemes, a multi-dimensional model space, consisting of multiple reference Slater determi-



nants, is constructed in such a way that a proper zeroth-order description of the problem of interest can be attained. The remaining, mostly dynamical, correlation effects are then captured through ph excitations from each reference determinant. Unfortunately, unlike in the SRCC formalism, there is no unambiguous way of writing an exponential wavefunction ansatz within the MR framework, leaving room for a wide variety of MRCC-type ideas, reviewed, for example, in References [53–56]. The situation is further complicated by the fact that MRCC methods cannot match the ease of use and application of their SR counterparts, which can often be converted into computational “black boxes” that can be used by non-experts. In particular, many interesting problems in chemistry, especially when transition metal atoms are involved, require enormous reference spaces, running into similar challenges to those characterizing FCI. This is particularly true in strongly correlated situations examined in this dissertation. For these and other reasons, in this dissertation we focus on SRCC-type ideas, where one recovers strong non-dynamical correlation effects dynamically, *i.e.*, through conventional ph excitations from a single Slater determinant defining the Fermi vacuum, *e.g.*, the HF determinant.

In the SRCC formalism [43–48], the exact ground-state  $N$ -electron wavefunction is expressed as  $|\Psi_0\rangle = e^T |\Phi\rangle$ , where  $|\Phi\rangle$  is a suitably chosen IPM reference state that serves as the Fermi vacuum, usually a HF Slater determinant, and the cluster operator  $T$  is expressed in terms of its many-body components as  $T = \sum_{n=1}^N T_n$ . When  $T_n$  acts on the reference Slater determinant  $|\Phi\rangle$ , it creates all possible fully connected  $n$ -tuply excited components of the exact ground-state wavefunction  $|\Psi_0\rangle$ . Powers of  $T$  in  $e^T$  generate the remaining linked disconnected components of  $|\Psi_0\rangle$ . The study of excited states in the SRCC framework can be enabled by, for example, the equation-of-motion (EOM) formalism [57–61], where a linear, CI-like, excitation operator  $R_\mu$  is applied to the ground-state CC wavefunction  $|\Psi_0\rangle$ , so that excited-state wavefunctions are represented as  $|\Psi_\mu\rangle = R_\mu e^T |\Phi\rangle$ . In analogy to the cluster operator  $T$ ,  $R_\mu$  is expressed in terms of its many-body components as  $R_\mu = r_{\mu,0} \mathbf{1} + \sum_{n=1}^N R_{\mu,n}$  (recall that  $\mu = 0$  corresponds to the ground state and  $\mu > 0$

means excited states; we use symbol  $\mathbf{1}$  to designate the unit operator). In the conventional treatment of SRCC theory, a sequence of approximate methods is obtained by truncating  $T$  and  $R_\mu$  at a particular excitation rank  $m_A < N$  (usually  $m_A \ll N$ ), giving rise to the CC approach with singles and doubles (CCSD) [62, 63], the CC approach with singles, doubles, and triples (CCSDT) [64, 65], the CC approach with singles, doubles, triples, and quadruples (CCSDTQ) [66–68], *etc.*, and their EOM excited-state extensions, EOMCCSD [59–61], EOMCCSDT [69–73], EOMCCSDTQ [71, 72, 74, 75], *etc.* At this point, it is also worth mentioning that the flexibility of the EOM formalism allows one to formulate particle–non-conserving theories by replacing the aforementioned particle-conserving  $R_\mu$  operator by its particle–non-conserving electron-attachment (EA) [76–82] and ionization (IP) [78, 80–90] counterparts. These approaches allow the study of ground and excited electronic states of open-shell species, such as radicals, by attaching an electron to (EA-EOMCC) or removing an electron from (IP-EOMCC) the underlying closed-shell core. One of the major advantages of the EA- and IP-EOMCC methodologies is that they automatically lead to orthogonally spin-adapted wavefunctions of the  $(N \pm 1)$ -electron system, due to the use of a closed-shell CC reference wavefunction. The study of species having more than one electron outside the  $N$ -electron closed-shell core is possible by turning to multiple electron-attached and multiple ionized theories, such as the doubly electron-attached (DEA) EOMCC approach and its doubly ionized (DIP) counterpart [91–101] that are well-suited for the study of diradicals. Because we are interested in an accurate description of strongly correlated systems in their ground electronic states, for the remainder of this dissertation we will focus on the ground-state SRCC methods.

The basic SRCC method, CCSD, performs well in the weakly correlated regime, significantly outperforming its CI counterpart, abbreviated as CISD, which is also size inextensive. One of the main reasons for the superiority of CCSD over CISD is the fact that CCSD captures higher–than–doubly excited determinants, absent in CISD, such as the  $\frac{1}{2}T_2^2$  disconnected quadruple excitations, which in the weakly correlated regime are more important

than their connected  $T_4$  counterparts and other ways of exciting four electrons ( $T_1T_3$ ,  $\frac{1}{2}T_1^2T_2$ ,  $\frac{1}{24}T_1^4$ ) [45, 48, 102–104]. In addition, the relatively low computational cost of CCSD, having iterative CPU steps that scale as  $n_o^2n_u^4$  or  $\mathcal{N}^6$ , where  $n_o$  ( $n_u$ ) is the number of correlated occupied (unoccupied) orbitals and  $\mathcal{N}$  is a measure of the size of the system, allows its application to systems containing hundreds of correlated electrons and basis functions. The study of even larger systems is possible by turning to local correlation CC approaches (see, *e.g.*, References [105–118]), which can reduce the computational costs to linear scaling. Unfortunately, CCSD provides qualitatively wrong results in situations dominated by larger non-dynamical correlations, such as bond breaking, because the effects of higher-than-pair connected clusters, such as  $T_3$  and  $T_4$ , which are completely neglected in CCSD, become significant. This can be addressed by taking advantage of the fact that the SRCC methods with a full treatment of higher-than-pair clusters, including CCSDT, CCSDTQ, and their higher-order counterparts, rapidly converge to the exact, FCI, limit in typical MR situations in chemistry, allowing one to incorporate the dynamical and non-dynamical correlation effects dynamically, but the computational costs associated with higher-level SRCC methods, such as  $n_o^3n_u^5$  ( $\mathcal{N}^8$ ) in the CCSDT case or  $n_o^4n_u^6$  ( $\mathcal{N}^{10}$ ) in the case of CCSDTQ, limit their application to systems with a dozen or so correlated electrons and relatively small basis sets. The key challenge has been how to incorporate higher-rank clusters, especially  $T_3$  and  $T_4$ , within the SRCC framework in a computationally affordable yet robust manner in order to handle typical MR situations.

Historically, the contributions of higher-than-pair clusters, such as  $T_3$  and  $T_4$ , were estimated using MBPT arguments, either iteratively, as in the CCSDT- $n$  [119–122] or CCSDTQ- $n$  [123] schemes, or non-iteratively, in methods such as CCD + ST(CCD) [124], CCSD + T(CCSD)  $\equiv$  CCSD[T] [125], CCSD(T) [126], and CCSD(TQ<sub>f</sub>) [127], to mention a few representative examples. Unfortunately, despite the significant reduction of the computational costs compared to CCSDT and CCSDTQ, these methods, like all finite-order MBPT-based approaches, break down in MR situations. Among the new generations of SRCC

methodologies that incorporate the physics of higher-than-pair clusters in a robust manner, suitable for the description of typical cases of electronic quasi-degeneracies in chemistry, including single bond breaking, biradicals, and excited states dominated by two-electron transitions, without turning to genuine MR considerations, are the completely renormalized (CR) CC/EOMCC schemes resulting from the formalism of the method of moments of CC equations [128–144] and a broad category of the active-space CC theories [69, 70, 80–82, 98–100, 145–160]. In the former approaches, one adds non-iterative corrections to the energies resulting from methods employing a conventional truncation in the cluster operator  $T$ , such as CCSD, for the correlation effects due to the higher-order connected excitations that are neglected in the initial CC calculation without utilizing MBPT. The active-space CC methods incorporate higher-than-two-body clusters, such as  $T_3$  or  $T_3$  and  $T_4$ , in an iterative and yet relatively inexpensive manner using small subsets of active orbitals, while allowing the lower-order cluster amplitudes to relax in the presence of the dominant higher-order ones. The culmination of these efforts, all aimed at eliminating failures of perturbative CC methods, such as CCSD(T), in typical MR situations in chemistry, while avoiding high computational costs of CCSDT or CCSDTQ, was the introduction of the deterministic CC( $P;Q$ ) framework [37, 38, 144, 161–163], which is a merger of the CR-CC and active-space CC ideas, and its semi-stochastic variant [164–166], where one automates the selection of active spaces utilizing stochastic wavefunction sampling. In the ground-state CC( $P;Q$ ) formalism, for example, one corrects the energies obtained with methods relying on a conventional or unconventional truncation in the cluster operator  $T$  for the correlation effects due to the higher-rank determinants neglected in the initial CC calculation. It has been demonstrated that the deterministic and semi-stochastic CC( $P;Q$ ) hierarchies not only greatly improve the results of both the active-space CC and CR-CC methods, but also faithfully and accurately reproduce the respective parent full CC schemes, such as CCSDT, CCSDTQ, and EOMCCSDT, at a small fraction of the computational cost [37, 38, 144, 161–166].

Despite all of the aforementioned impressive methodological advances, the CC( $P;Q$ ) hi-

erarchy is not a panacea for all the problems facing CC methods, since even the parent high-level SRCC approaches, such as CCSDT or CCSDTQ, can completely break down in challenging strongly correlated situations, which are the focus of the present dissertation. Indeed, it is well established that the conventional CCSD, CCSDT, CCSDTQ, *etc.* hierarchy may exhibit slow or even erratic convergence toward the exact, FCI, limit if the system under consideration is characterized by strong correlations beyond single, double, or triple bond breaking or systems with small numbers of electrons outside closed shells. In general, strongly correlated systems involve the entanglement of a large number of electrons and are characterized by the unpairing of many electron pairs and their subsequent recoupling to low-spin states, as in the Mott metal–insulator transitions [167–169], which can be modeled by the Hubbard Hamiltonian [170–172] (see, *e.g.*, References [173] and [174] and references therein) or linear chains, rings, or cubic lattices of the equally spaced hydrogen atoms that change from a state with weaker metallic correlations at compressed geometries to an insulating state with strong correlations in the dissociation region (see, *e.g.*, References [175–181]). The analogous challenges apply to the strongly correlated  $\pi$ -electron networks in cyclic polyenes [182, 183], described by the Hubbard and Pariser–Parr–Pople [184–186] (PPP) Hamiltonians, which can be used to model one-dimensional metallic-like systems with Born–von Kármán periodic boundary conditions and a half-filled band [187–194]. Molecular examples of strongly correlated systems can be found in situations involving multiple bond breaking, typically more than three, as in the dissociation of transition metal diatomics such as the formidable chromium dimer (see, for example, Reference [195] and references therein). At the same time, when the numbers of strongly correlated electrons and open-shell sites from which these electrons originate become larger, traditional MR approaches, relying on model spaces generated by complete active-space SCF (CASSCF) [196, 197], are no longer applicable due to astronomical dimensionalities of the corresponding model spaces. Capturing dynamical correlation effects, needed to obtain a quantitative description, on top of CASSCF is prohibitively expensive too. Even the increasingly popular substitute for CASSCF, namely,

the density-matrix renormalization group (DMRG) approach [198–203], begins to wear out when the number of strongly correlated electrons exceeds  $\sim 50$  and prospects for incorporating dynamical correlation effects on top of the large-active-space DMRG references in an accurate and computationally manageable manner, when one needs to use basis sets much larger than the minimum one and the generally expensive post-DMRG steps [204–208], remain, at least at this time, uncertain. It is, therefore, worth understanding the origin of the erratic behavior of SRCC approaches, which, as already mentioned, are characterized by an ease of implementation and application that cannot be matched by MR schemes, in the presence of strong electron correlation effects and proposing unconventional SRCC schemes capable of accurately describing both the weak and strong correlation regimes.

The catastrophic failures of the traditional CCSD, CCSDT, CCSDTQ, *etc.* hierarchy in all of the aforementioned and similar situations, relevant to condensed matter physics, materials science, and the most severe cases of multiple bond breaking (*e.g.*, the celebrated chromium dimer), are related to the observation that in order to describe wavefunctions for  $N$  strongly correlated electrons one is essentially forced to deal with a FCI-level description of these  $N$  electrons, which in a conventional CC formulation requires the incorporation of virtually all cluster components  $T_n$ , including  $T_N$ . As shown in Figure 2 of Reference [209], using the 12-site, half-filled attractive pairing Hamiltonian with equally spaced levels, the higher-order  $T_n$  components of the cluster operator, which normally decrease with  $n$ , in a strongly correlated regime remain large for larger  $n$  values approaching  $N$ . This is not a problem when the number of strongly correlated electrons  $N$  is small (*e.g.*, 2 in single bond breaking or 4 in double bond breaking), but becomes a major issue when  $N$  is larger.

The consequences of the above observations manifest themselves in various, sometimes dramatic, ways. For example, one experiences a disastrous behavior of the traditional CCSD, CCSDT, CCSDTQ, *etc.* hierarchy, which produces large errors, branch point singularities, and unphysical complex solutions in calculations for strongly correlated one-dimensional systems modeled by the Hubbard and PPP Hamiltonians or  $H_n$  rings, linear chains, and cubic

lattices undergoing metal–insulator transitions [187–194, 209–212]. One can also show, using spin-symmetry breaking and restoration arguments, combined with the Thouless theorem [213, 214] and a subsequent cluster analysis of the wavefunction within a projected UHF (PUHF) [215–218] framework, similar to Reference [219] and its predecessor [220], that if we insist on the wavefunction ansatz using a function of low-order cluster components, such as  $T_2$ , the resulting strongly correlated PUHF state has a non-intuitive polynomial rather than the usual exponential form [221–223] (*cf.*, also, References [209, 211, 212]). This means that in seeking a computationally manageable CC-type solution to a problem of strong correlation involving many electrons, which would avoid the exponential scaling of FCI, while eliminating dramatic failures of the traditional CCSD, CCSDT, CCSDTQ, *etc.* hierarchy, one has to rely on non-traditional approaches, such as those discussed in References [209–212, 221–223], replacing the conventional CC exponential wavefunction ansatz with the cluster operator  $T$  truncated at a given many-body rank by entirely different formulations. In our view, one of the most promising ideas in this area is that of the approximate coupled-pair (ACP) approaches [187–194, 219, 220, 224–231] and their various recent reincarnations or modifications, including the 2CC approach and its  $n$ CC extensions [232, 233], parameterized CCSD (pCCSD) [234] and its CCSDT counterpart [235], and distinguishable cluster approximation with doubles (DCD) or singles and doubles (DCSD) [180, 236–239] (see, also, References [240] and [241]) and its DCSDT extension to connected triples [235, 242], to name a few examples (*cf.* Reference [243] for a review).

The ACP methods and their various modifications retain all doubly excited cluster amplitudes of CCD or CCSD in the calculations, *i.e.*, they have the relatively inexpensive  $n_o^2 n_u^4$  ( $\mathcal{N}^6$ ) costs of standard CCD/CCSD, but they use subsets of non-linear diagrams/terms of the CCD/CCSD amplitude equations. Interestingly, this not only greatly improves the performance of CCD/CCSD in situations involving single and multiple bond dissociations [180, 234, 236–240, 244], but also, what is most intriguing, eliminates the complete failures of conventional SRCC approaches, such as CCSD, CCSDT, and CCSDTQ, in the strongly

correlated regime of low-dimensional metallic-like systems and symmetrically stretched hydrogen rings, linear chains, and cubic lattices [180, 187–194]. As further elaborated on below, these great improvements in the performance of conventional CC approaches are not a coincidence; one can prove that there exist subsets of CCSD diagrams that result in an exact description of certain strongly correlated minimum-basis-set model systems [191, 219, 220]. Thus, the ACP methodologies provide a rigorous basis for developing relatively inexpensive SRCC-like approaches for addressing the challenge of strong correlations in many-electron systems, which lie at the heart of contemporary quantum chemistry effort.

Having stated all of the above, there remain several open problems that need to be addressed before the ACP methods can be routinely applied to realistic strongly correlated systems, *i.e.*, systems involving larger numbers of strongly correlated electrons described by *ab initio* Hamiltonians and larger basis sets. The main problem is concerned with the neglect of connected triply excited ( $T_3$ ) clusters in typical ACP methods. Low-dimensional model systems with small band gaps do not suffer from this a lot, since their accurate description relies on  $T_n$  clusters with even values of  $n > 2$ , but one cannot produce quantitative results in the majority of chemistry applications without  $T_3$ . All previous attempts to incorporate connected triply excited clusters using conventional MBPT-like arguments, similar to those exploited in CCSD[T] [125], CCSD(T) [126], or CCSDT-1 [119, 120], within the ACP framework have only been partly successful [190, 192, 193, 219, 231]. Another major problem pertains to the fact that the combinations of diagrams that result in the improved performance of ACP methods in the strongly correlated regime of minimum-basis-set model systems are not necessarily optimum when larger basis sets are employed.

In this dissertation, we successfully address both of these problems. We deal with the issue regarding the missing  $T_3$  physics by adopting and further developing the active-space CC ideas [69, 70, 80–82, 98–100, 145–160] to incorporate the dominant  $T_3$  amplitudes in the ACP methods in a robust, yet computationally affordable, manner. As shown in this dissertation, the active-space triples ACP approaches are immune to the various issues plaguing conven-



tional MBPT-based connected triples energy corrections, which suffer from vanishingly small perturbative denominators in the strong correlation regime. Furthermore, the active-space CC methodologies and their ACP counterparts developed in this thesis research incorporate the leading higher-than-two-body clusters in an iterative manner, allowing the lower-order cluster amplitudes to relax in the presence of the dominant higher-order ones. In addition, the active-space CC and ACP schemes systematically converge to their corresponding parent methods by simply increasing the size of the active space, the limit being reached when all orbitals become active. Finally, we address the concern of extending the ACP methods to larger basis sets by proposing a new ACP variant that utilizes basis-set-dependent scaling factors multiplying the pertinent CCSD diagrams. As shown in this dissertation, this novel ACP scheme reduces to DCSD when a minimum basis set is employed, *i.e.*, it remains exact for strongly correlated model systems, while becoming asymptotically equivalent to ACCSD(1,4), *i.e.*, to the original ACP-D14 scheme of Piecuch and Paldus [191] augmented with singles, in a CBS limit. This is a desired behavior because, based on our numerical observations, the ACCSD(1,4) approach corrected for connected triples provides, among the various tested triples-corrected ACP schemes, the most accurate description for the entire spectrum of correlation effects (from weak to strong correlations) for larger basis sets.

The ACP schemes examined in this dissertation, especially those incorporating connected three-body clusters, provide an accurate description of electron correlation effects, including both the weakly and strongly correlated regimes, and become exact in the strong correlation limit of model minimum-basis-set Hamiltonians or in the atomization limit of lattices of hydrogen atoms, but they may have limitations in some situations. One of the successes of this dissertation is the development and implementation of a novel semi-stochastic approach with CCSD-like computational cost that can provide FCI-quality energetics for the entire range of correlation effects, including both the weakly and strongly correlated regimes. Before we proceed with the information about this new semi-stochastic methodology, we give a brief introduction to quantum Monte Carlo (QMC) approaches, on which the novel semi-stochastic

approach developed in this thesis research is based.

In general, Monte Carlo (MC) methods provide solutions to problems of either probabilistic or deterministic nature by virtue of stochastic sampling. The original realizations of MC approaches required scientists to perform a series of experiments, *i.e.*, samplings, and the overall outcome was inferred by means of statistical analysis. One such example was the experimental determination of the mathematical constant  $\pi$  in 1873 [245] using Buffon's needle [246, 247], but instances of such experimental mathematics can be traced back to ancient Babylon and Old Testament times [248]. Pivotal in the development of modern MC approaches was the replacement of costly and sometimes impractical or even impossible experiments by the numerical processing of random or pseudorandom numbers. The invention of MC in the form that is used today is attributed to Fermi, who used it in his unpublished work on neutron moderation in the early 1930s [249]. However, the accurate MC study of complex physical processes, which require the collection of an enormous number of sampling points, was not possible until the advent of electronic digital computers in the late 1940s. Around that time, the foundations of modern MC methods were laid down at Los Alamos in the pioneering works of Ulam, von Neumann, Fermi, Metropolis, and others [249–252]. The application of MC methods to address problems of quantum mechanical nature are termed QMC (see, for example, Reference [253] for a review regarding the use of QMC methods to solve the electronic Schrödinger equation).

We begin our discussion of QMC approaches starting with variational MC (VMC) [254, 255]. In analogy with other variational approaches, one starts with a trial wavefunction for the problem of interest that contains one or more parameters. Subsequently, one invokes the variational principle, solving the various integrals using MC integration sampling the wavefunction probability distribution, and evaluating the energy expectation value as the average of the local energy values, to obtain the optimum parameters that result in the lowest-energy wavefunction of a given functional form. The accuracy of the resulting VMC wavefunction and energy depends on the quality of the trial wavefunction. An alternative QMC approach

that is less sensitive to the quality of trial wavefunction is diffusion MC (DMC). The basic idea behind the DMC methodology was already stated in 1949, when Fermi recognized that the time-dependent Schrödinger equation in imaginary time resembles a diffusion equation that can be solved stochastically [250]. As long as the initial trial wavefunction has a non-zero overlap with the exact wavefunction, it is guaranteed that by propagating the time-dependent Schrödinger equation in imaginary time the exact wavefunction will be projected out in the infinite imaginary time limit. One of the advantages of DMC is that the underlying computer codes are easy to parallelize across multiple nodes and they require relatively modest computational resources. In addition, DMC schemes directly sample the real space of  $3N$  electronic coordinates allowing them to recover, in principle, the exact solution to the Schrödinger equation, unlike conventional quantum chemistry approaches operating in the  $N$ -electron Hilbert space spanned by Slater determinants, which are limited by the size and quality of the one- and  $N$ -electron basis sets.

Unfortunately, the DMC methods outlined above are plagued by a major problem that makes their applicability to molecular systems difficult. If no constraints are enforced on the trial wavefunction, propagating the time-dependent Schrödinger equation in imaginary time will eventually project out a bosonic state, *i.e.*, the true ground state of the spin-free Schrödinger equation, albeit violating the Pauli exclusion principle. This problem can be remedied by using what is known as the fixed-node approximation [256–259]. In this case, one imposes the node structure of an approximate wavefunction, obtained using conventional quantum chemistry approaches, on the trial wavefunction, essentially forcing the DMC solution to be antisymmetric. Of course, by introducing the nodes of an approximate wavefunction, the DMC approach can no longer yield the exact solution to the many-electron Schrödinger equation and the quality of the DMC results may heavily depend on the quality of the approximate wavefunction and its ability to properly locate the nodes.

Recently, a novel QMC approach was formulated that alleviates the issues introduced by the fixed-node approximation. This is accomplished by propagating the time-dependent

Schrödinger equation in the  $N$ -electron Hilbert space spanned by Slater determinants, rather than in the real space of  $3N$  electronic coordinates [260]. The fact that Slater determinants obey the Pauli exclusion principle by construction ensures that the resulting wavefunction will be antisymmetric. Similar to the DMC case, the stochastic sampling of the  $N$ -electron Hilbert space is made possible through a walker population dynamics algorithm that places more walkers on important determinants and less walkers on the less important ones. The resulting approach is called FCIQMC, since, in analogy to FCI, the walkers are allowed to explore the entire  $N$ -electron Hilbert space, and this provides the numerically exact solution to the  $N$ -electron Schrödinger equation in a basis set equivalent to FCI in the limit of infinite propagation time [260]. The convergence of the FCIQMC approach can be slow, but this can be addressed by employing an initiator approach, giving rise to the *i*-FCIQMC scheme, that dramatically decreases the total walker population required for obtaining accurate results [261, 262], and other powerful algorithms, such as the adaptive-shift approach developed in References [263, 264].

Although the FCIQMC approach is guaranteed to provide the numerically exact solution in a given basis set, one needs tens or hundreds of thousands of MC time steps, called MC iterations, for this to be accomplished. Furthermore, in the presence of strong many-electron correlation effects, the convergence of FCIQMC is decelerated considerably. One of the major successes of this dissertation is the introduction of a novel semi-stochastic electronic structure approach that is capable of extrapolating FCI-quality energetics, even in the strong correlation regime, out of the early stages of FCIQMC propagations. This methodology, called cluster-analysis-driven FCIQMC (CAD-FCIQMC) [265, 266], is based on the fact that, for Hamiltonians containing up to two-body terms, as is the case in quantum chemistry, the correlation energy depends only on the one- and two-body clusters,  $T_1$  and  $T_2$ , respectively, which, in turn, couple with their three- and four-body counterparts, but no more than that, through the CC equations projected on singles and doubles. This implies that extracting the exact  $T_3$  and  $T_4$  components of the cluster operator  $T$  and solving

CCSD-like equations for  $T_1$  and  $T_2$  in their presence should yield the exact  $T_1$  and  $T_2$  and consequently, the exact, FCI, energy. This observation is the driving force behind externally corrected CC approaches [219, 220, 230, 243, 267–274] in which one extracts the three- and four-body clusters from a non-CC source that provides a good description of the many-electron system of interest. In our case, we take advantage of the *i*-FCIQMC stochastic wavefunction sampling as a good source of FCI-quality  $T_3$  and  $T_4$ . Although the original CAD-FCIQMC approach provides nearly exact energetics out of the early stages of the *i*-FCIQMC propagations, even in the presence of electronic quasi-degeneracies such as those characterizing the double bond dissociation of  $\text{H}_2\text{O}$  [265], it may fail or display problems in the strong correlation regime. In this dissertation, we extend the CAD-FCIQMC approach to strong many-electron correlation effects by exploiting the ACP ideas within the CAD-FCIQMC formalism, so that one can obtain FCI-quality energetics for the entire spectrum of electron correlation effects.

## CHAPTER 2

### PROJECT OBJECTIVES

1. Extension of the ACP methodologies, especially those based on the ACP-D13, ACP-D14, and ACP-D1(3 + 4)/2 ideas, to allow for the explicit incorporation of  $T_3$  clusters via active-space CC considerations.
2. Development and testing of a novel ACP approach using basis-set-dependent scaling factors, suitable for the study of systems with realistic basis sets.
3. Development and implementation of the semi-stochastic CAD-FCIQMC methodology and its extension to the strongly correlated regime.
4. Application of the above novel methodologies to low-dimensional model systems relevant to metal-insulator transitions, such as hydrogen clusters, as well as to problems of chemical interest, such as the double bond dissociation of  $\text{H}_2\text{O}$  and the ground-state energy of  $\text{C}_6\text{H}_6$ .

## CHAPTER 3

### THEORY

#### 3.1 Introduction to Coupled-Cluster Theory

*...believe it or not, it is taken from one of the  
Chemistry Journals!*

---

Remark made by R. McWeeny during his 1967 Inaugural Lecture at the University of Sheffield referring to the L-CCD diagrams and CCD equations shown in Reference [45] [quote taken from J. Paldus, in *Theory and Applications of Computational Chemistry: The First Forty Years*, edited by C. E. Dykstra, G. Frenking, K. S. Kim, and G. E. Scuseria (Elsevier, Amsterdam, 2005) pp. 115–147].

As mentioned in the Introduction, in the SRCC formalism the exact ground-state wavefunction of an  $N$ -electron system is expressed as

$$|\Psi_0\rangle = e^T |\Phi\rangle, \quad T = \sum_{n=1}^N T_n, \quad (3.1)$$

where  $|\Phi\rangle$  is an IPM reference state that serves as the Fermi vacuum (usually a HF Slater determinant) and  $T$  is the cluster operator. The  $n$ -body component of  $T$  is defined as

$$T_n = \sum_{\substack{i_1 < \dots < i_n \\ a_1 < \dots < a_n}} t_{a_1 \dots a_n}^{i_1 \dots i_n} E_{i_1 \dots i_n}^{a_1 \dots a_n}, \quad (3.2)$$

where  $t_{a_1 \dots a_n}^{i_1 \dots i_n}$  are the corresponding cluster amplitudes and  $E_{i_1 \dots i_n}^{a_1 \dots a_n}$  are the elementary  $n$ -particle– $n$ -hole excitation operators defined as  $E_{i_1 \dots i_n}^{a_1 \dots a_n} = a^{a_1} \dots a^{a_n} a_{i_n} \dots a_{i_1}$ , with  $a^p$  and  $a_p$  representing the usual creation and annihilation operators associated with the spin-orbital  $|p\rangle$ , that generate excited determinants  $|\Phi_{i_1 \dots i_n}^{a_1 \dots a_n}\rangle$  when acting on  $|\Phi\rangle$ . We use the usual convention regarding spin-orbital indices, so that indices  $i_1, i_2, \dots$  or  $i, j, \dots$  ( $a_1, a_2, \dots$

or  $a, b, \dots$ ) denote spin-orbitals that are occupied (unoccupied) in the reference determinant  $|\Phi\rangle$  and  $p_1, p_2, \dots$  or  $p, q, \dots$  designate generic spin-orbitals. By inserting the exponential ansatz for the wavefunction, Equation (3.1), into the Schrödinger equation and multiplying from the left by  $e^{-T}$ , we obtain the connected cluster form of the Schrödinger equation,

$$\overline{H_N} |\Phi\rangle = \Delta E_0 |\Phi\rangle, \quad (3.3)$$

where  $\overline{H_N} = e^{-T} H_N e^T = (H_N e^T)_C$  is the similarity-transformed Hamiltonian, with  $H_N = H - \langle \Phi | H | \Phi \rangle$  representing the Hamiltonian in the normal-ordered form and  $C$  designating the connected operator product, and  $\Delta E_0 = E_0 - \langle \Phi | H | \Phi \rangle$  is the ground-state correlation energy. By projecting Equation (3.3) on the manifold of excited determinants that correspond to the content of  $T$ , we arrive at an energy-independent system of non-linear equations for the cluster amplitudes  $t_{a_1 \dots a_n}^{i_1 \dots i_n}$ ,

$$\langle \Phi_{i_1 \dots i_n}^{a_1 \dots a_n} | \overline{H_N} | \Phi \rangle = 0, \quad (3.4)$$

where  $i_1 < \dots < i_n$ ,  $a_1 < \dots < a_n$ , and  $n = 1, \dots, N$ . Taking into account that the electronic Hamiltonian contains only up to two-body terms, the above system of equations contains at most quartic terms in the cluster amplitudes. After solving the above system of non-linear equations, which is usually done by employing an iterative procedure, we calculate the ground-state correlation energy in a single step by projecting Equation (3.3) on the reference determinant  $|\Phi\rangle$ ,

$$\Delta E_0 = \langle \Phi | \overline{H_N} | \Phi \rangle. \quad (3.5)$$

Using the facts that one needs to consider only fully contracted terms when computing expectation values in  $|\Phi\rangle$  and that the electronic Hamiltonian contains only up to two-body terms, the CC correlation energy, Equation (3.5), depends on the one- and two-body clusters only, independent of the level of truncation of the cluster operator.

The theory presented so far provides a numerically exact solution of the electronic Schrödinger equation within a given basis set, *i.e.*, the full CC (FCC) approach, which



is equivalent to FCI and, therefore, usually prohibitively expensive. Thus, in the vast majority of applications of chemical interest, we truncate the cluster operator  $T$  at some excitation rank  $m_A < N$  (usually  $m_A \ll N$ ), replacing the exact  $T$ , Equation (3.1), by its approximate form  $T^{(A)} = \sum_{n=1}^{m_A} T_n$  and limit the projections in Equation (3.4) to excited determinants  $|\Phi_{i_1 \dots i_n}^{a_1 \dots a_n}\rangle$  with  $n \leq m_A$ . The correlation energy resulting from such truncated CC calculations will be denoted as  $\Delta E_0^{(A)}$ . This procedure results in a hierarchy of conventional SRCC approaches, such as CCSD, where  $m_A = 2$ , CCSDT, where  $m_A = 3$ , CCSDTQ, where  $m_A = 4$ , *etc.* In CCSD, for example, the cluster operator is expressed as  $T^{(\text{CCSD})} = T_1 + T_2$ , and Equation (3.3) is projected on all singly and doubly excited determinants,  $|\Phi_i^a\rangle$  and  $|\Phi_{ij}^{ab}\rangle$ , respectively, to obtain the corresponding amplitude equations.

As already mentioned in the Introduction, the CC theory emerged as an infinite-order generalization of finite-order MBPT and as such it satisfies important theorems of many-body physics, including the linked and connected cluster theorems. These theorems guarantee that the CC approaches satisfy important conditions of the exact theory, independent of truncation in  $T$ . We now proceed to discuss these properties in more detail. We begin with the fact that the cluster operator  $T$  represents connected diagrams only. As a result, the CC correlation energy is expressed using strictly connected quantities that lead to its size extensivity. Consequently, unlike truncated CI, methods based on the CC theory lead to approximations that do not lose accuracy as the system size is increased. The importance of size-extensive electronic structure methodologies is illustrated in Figure 3.1, where we examine the ground-state PEC of  $\text{H}_2$  in the presence of a few non-interacting Ne atoms using the CCSD and CISD methodologies. Of course, in the absence of Ne atoms, both CCSD and CISD approaches provide an exact description for the two-electron  $\text{H}_2$  diatomic. In the case of CCSD, which is rigorously size extensive, we notice that the PEC obtained by subtracting the energies of the added Ne atoms remains invariant under the presence of any number of non-interacting Ne atoms. In particular, CCSD provides the exact PEC for the single bond dissociation of  $\text{H}_2$  even when the number of correlated electrons is increased by

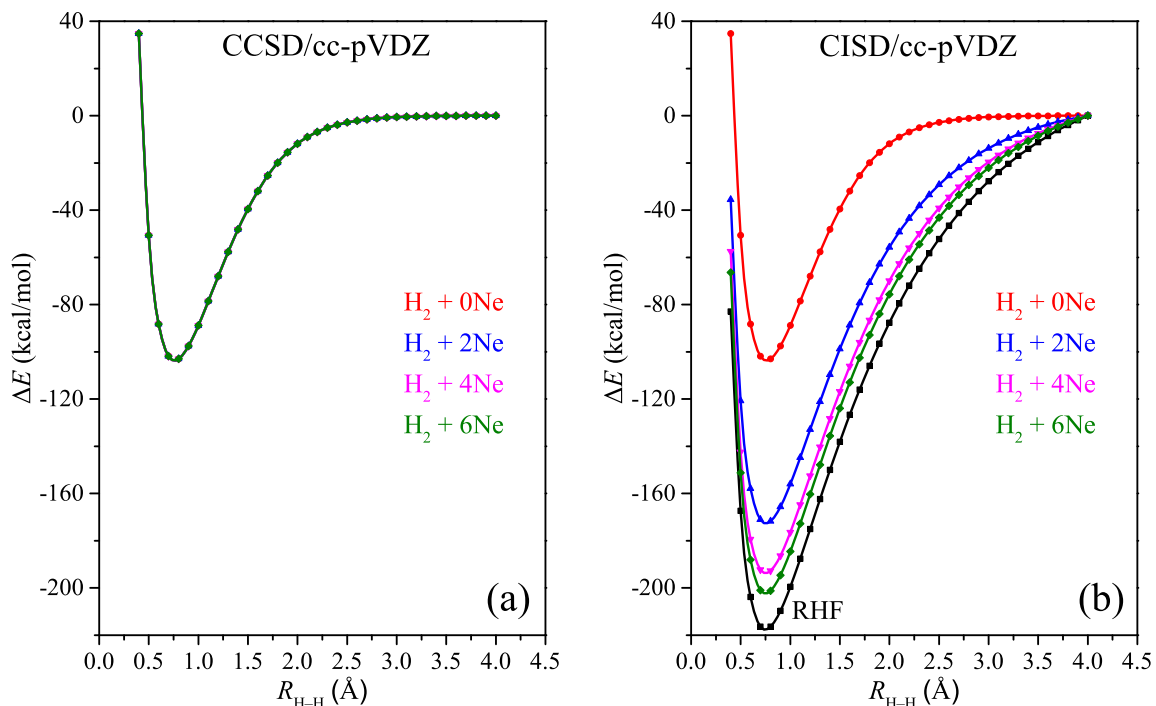


Figure 3.1: The ground-state PECs of  $H_2$  in the presence of 0, 2, 4, and 6 Ne atoms as obtained with (a) CCSD/cc-pVDZ and (b) CISD/cc-pVDZ. The Ne atoms were located such that they do not interact among themselves and with the  $H_2$  molecule. In panel (b), we also include the RHF PEC for comparison. All PECs have been aligned such that the corresponding electronic energies at the internuclear separation  $R_{H-H} = 4.0$  Å are identical and set at 0 kcal/mol.

a factor of more than 30. On the other end of the spectrum, we see that the performance of the CISD approach, which is not size extensive, gradually deteriorates as the size of the system is increased. In fact, in the thermodynamic limit, the CISD approach will not recover any many-electron correlation effects, rendering it equivalent in this example to RHF, which is a known behavior (see, for example, Reference [275]).

Another important advantage of the CC theory is that it can be made size consistent, enabling the proper description of fragmentation phenomena, as long as the underlying reference state is separable. This property is bestowed upon the CC theory due to the properties of the exponential mapping defining the CC wavefunction. For example, let us examine the fragmentation of a system into two non-interacting subsystems, denoted as  $A$  and  $B$ . The fact that there is no coupling between subsystems  $A$  and  $B$  suggests that the

Hamiltonian of the entire system has the form  $H_{AB} = H_A + H_B$ . In this case, using the fact that  $T_A$  and  $T_B$  are defined on different, *i.e.*, orthogonal, many-electron Hilbert spaces, we have that  $T = T_A + T_B$  and  $[T_A, T_B] = 0$ . Assuming that the underlying reference is separable, namely, that  $|\Phi_{AB}\rangle = |\Phi_A\rangle |\Phi_B\rangle$ , the wavefunction of the entire system becomes

$$\begin{aligned} |\Psi_{AB}\rangle &= e^{T_{AB}} |\Phi_{AB}\rangle \\ &= e^{T_A} |\Phi_A\rangle e^{T_B} |\Phi_B\rangle \\ &= |\Psi_A\rangle |\Psi_B\rangle. \end{aligned} \tag{3.6}$$

The corresponding energy can then be computed using the asymmetric expression equivalent to Equation (3.5)

$$\begin{aligned} E_{AB} &= \langle \Phi_{AB} | H_{AB} | \Psi_{AB} \rangle \\ &= \langle \Phi_A | H_A | \Psi_A \rangle \langle \Phi_B | \Psi_B \rangle + \langle \Phi_B | H_B | \Psi_B \rangle \langle \Phi_A | \Psi_A \rangle \\ &= E_A + E_B. \end{aligned} \tag{3.7}$$

We, thus, see that the CC theory provides a correct description of fragmentation processes, namely, it correctly predicts the multiplicative nature of the total wavefunction and the additivity of the total electronic energy of a system consisting of non-interacting subsystems. Other mainstream correlated electronic structure approaches, such as truncated CI and finite-order MBPT, are not size consistent, emphasizing once more the significance of CC approaches.

One of the most important characteristics of the CC exponential ansatz, which is very useful in practice, is the rapid convergence of the conventional CC hierarchy toward the exact, FCI, solutions in typical molecular applications relevant to chemistry. This property becomes apparent when one examines the structure of the FCI and FCC wavefunctions. Using the intermediate normalization, the FCI wavefunction can be expressed as

$$|\Psi_0\rangle = (\mathbf{1} + C) |\Phi\rangle, \quad C = \sum_{n=1}^N C_n, \tag{3.8}$$

where  $C$  is a linear excitation operator. The many-body components of  $C$  are defined in a similar manner to Equation (3.4). As mentioned above, the FCI and FCC wavefunctions are

equivalent, giving rise to the operator equality

$$\begin{aligned}
\mathbf{1} + C &= e^T \Rightarrow \\
\mathbf{1} + C &= \mathbf{1} + \sum_{n=1}^N \frac{T^n}{n!} \Rightarrow \\
\sum_{m=1}^N C_m &= \sum_{n=1}^N \frac{(\sum_{l=1}^N T_l)^n}{n!} \Rightarrow \\
\sum_{m=1}^N C_m &= \sum_{n=1}^N \left[ \frac{1}{n!} \sum_{\substack{k_1+\dots+k_N=n \\ k_1+\dots+k_N=m}} \binom{n}{k_1, \dots, k_N} \prod_{j=1}^N T_j^{k_j} \right].
\end{aligned} \tag{3.9}$$

As a result, the  $m$ -body component of  $C$  can be expressed in terms of the many-body components of the cluster operator  $T$  as

$$C_m = \sum_{n=1}^m \left[ \frac{1}{n!} \sum_{\substack{k_1+\dots+k_m=n \\ k_1+\dots+k_m=m}} \binom{n}{k_1, \dots, k_m} \prod_{j=1}^m T_j^{k_j} \right]. \tag{3.10}$$

Using Equation (3.10) for  $m = 1, 2, 3$ , and 4 yields

$$C_1 = T_1, \tag{3.11a}$$

$$C_2 = T_2 + \frac{1}{2}T_1^2, \tag{3.11b}$$

$$C_3 = T_3 + T_2T_1 + \frac{1}{3!}T_1^3, \tag{3.11c}$$

and

$$C_4 = T_4 + T_3T_1 + \frac{1}{2}T_2^2 + T_2\frac{1}{2}T_1^2 + \frac{1}{4!}T_1^4. \tag{3.11d}$$

A simple inspection of Equation (3.11) reveals that CC wavefunctions are substantially richer than the corresponding CI wavefunctions truncated at the same excitation level. Focusing on singles and doubles approaches, for example, we see that the CISD wavefunction contains up to doubly excited Slater determinants. On the other hand, due to the exponential wavefunction ansatz, the CCSD wavefunction already has the dimension of the FCI vector, the difference between the two being in the coefficients multiplying the Slater determinants, which in CCSD are parameterized by  $t_a^i$  and  $t_{ab}^{ij}$  amplitudes. A further aspect that points

to the superiority of CCSD relative to CISD is that the former incorporates higher-than-doubly excited determinants, absent in CISD, including disconnected quadruples in the form of  $\frac{1}{2}T_2^2$ , which are the dominant form of quadruple excitations in a weakly correlated regime. A final remark is that going from singles and doubles to singles, doubles, and triples is not bringing a lot of information in the case of CISDT, while CCSDT contains all terms of CISDTQ other than connected quadruples, which in weakly correlated systems are negligible compared to  $\frac{1}{2}T_2^2$ , and many classes of higher-order correlations absent in CISDTQ summed to infinite order. Of course, one must always keep in mind that CCSDT is size extensive and, thus (putting aside computational costs), allows the study of larger systems without loss of accuracy, while the performance of the size-inextensive CISDTQ approach will gradually deteriorate with increasing numbers of correlated electrons. All of these observations corroborate the fact that the traditional hierarchy of CC methods provides fast convergence toward the FCI limit in weakly correlated situations.

The hierarchy of traditional CC methods exhibits fast convergence toward the FCI solutions in the presence of electronic quasi-degeneracies, such as those characterizing single and double bond dissociations, as well. This is demonstrated in Figure 3.2 using the symmetric double bond dissociation of  $\text{H}_2\text{O}$  as an example. In this case, we see that the performance of the CCSD methodology gradually deteriorates as both bonds are stretched from their equilibrium positions by factors of 1.5 and 2. The CCSDT approach constitutes a dramatic improvement over CCSD, being characterized with small errors across all geometries shown in Figure 3.2, and the energetics obtained with CCSDTQ can hardly be distinguished from their FCI counterparts.

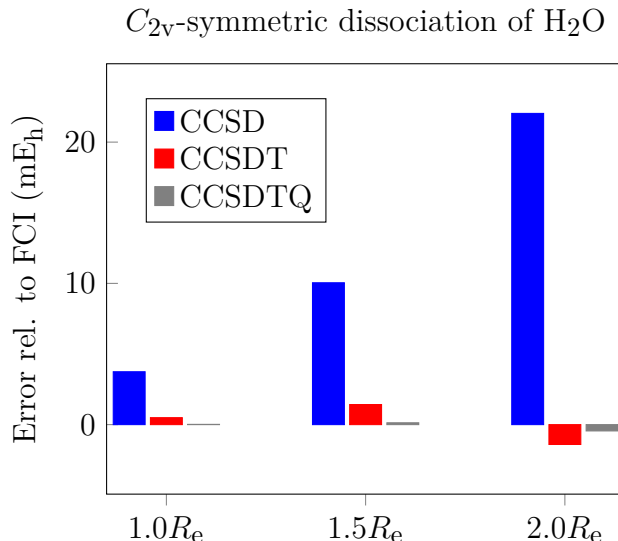


Figure 3.2: A comparison of the energies resulting from the all-electron CCSD, CCSDT, and CCSDTQ computations for the  $H_2O$  molecule, as described by the cc-pVDZ basis set [276], at the equilibrium and two displaced geometries obtained by simultaneous stretching of both O–H bonds by factors of 1.5 and 2.0 [277].

### 3.2 Failure of Conventional Coupled-Cluster Methods in Strongly Correlated Systems

*Thus, we can expect an increasing role to be played not only by the  $T_4$  clusters, but also by the  $T_{2n}$  ( $n \geq 3$ ) clusters in general.*

---

J. Paldus, M. Takahashi, and R. W. H. Cho, Int. J. Quantum Chem. Symp. **18**, 237 (1984).

In the previous section we saw that the conventional hierarchy of CC methods is characterized by a fast convergence to the FCI solution not only in the weakly correlated regime, but also in the presence of electronic quasi-degeneracies arising, for example, from single and double bond dissociations. However, as already mentioned in the Introduction, there exist strongly correlated systems and materials for which high-level CC schemes, including CCSDT and CCSDTQ, completely break down. In fact, in severe cases of strong correlation, where a large number of Slater determinants become degenerate with the reference (*e.g.*, HF) one, the only meaningful CC approach would be FCC. To gain insights regarding the failures

plaguing traditional CC methods in the strong correlation regime, we examine a few problems involving model Hamiltonians.

We begin our discussion with the models of cyclic polyenes,  $C_NH_N$  with  $N = 4\nu + 2$  and  $\nu = 1, 2, \dots$ , as described by the Hubbard and the PPP Hamiltonians [187–193, 220]. As shown in Figure 3.3, in the case of the Hubbard and PPP models of cyclic polyenes, each carbon atom is placed on a vertex of a regular  $N$ -gon and is described by a single  $2p_z$  electron. Thus, they can model aromatic compounds, the first member of the series being benzene ( $N = 6$ ), or, alternatively, and in the case of our work more importantly, they can be viewed as models of one-dimensional solids with a half-filled band, on which periodic boundary conditions have been imposed. These model Hamiltonians have several advantages, such as the availability of analytical or numerically exact solutions as well as the possibility of achieving a smooth transition from the weakly to the strongly correlated regime by continuously varying appropriate parameters that dictate the HOMO–LUMO or band gap.

The PPP Hamiltonian modeling the  $C_NH_N$  cyclic polyenes has the form [35, 187–193, 278]

$$H = \beta \sum_{\mu=0}^{N-1} \left( E_{\mu\mu+1} + E_{\mu\mu+1}^\dagger \right) + \frac{1}{2} \sum_{\mu,\nu=0}^{N-1} \gamma_{\mu\nu} (E_{\mu\mu} - 1) (E_{\nu\nu} - 1), \quad (3.12)$$

where  $E_{\mu\nu} = \sum_{\sigma} a^{\mu\sigma} a_{\nu\sigma}$  are the generators of the orbital unitary group  $U(N)$  [279],  $\sigma = \uparrow$  or  $\sigma = \downarrow$  corresponds to the spin up and spin down function associated with a given  $2p_z$  atomic spin-orbital, *i.e.*,  $|\mu\sigma\rangle = |\mu\rangle |\sigma\rangle$ , with  $\mu = 0, 1, \dots, N-1$ . The one-electron part of the PPP Hamiltonian, Equation (3.12), describes the hopping of an electron between nearest neighbors and depends on a single parameter  $\beta \leq 0$ , called the resonance integral. The two-electron term is an approximation to the interelectronic repulsions, considering only up to two-center two-electron integrals,  $\gamma_{\mu\nu} = \langle \mu\nu | \hat{v} | \mu\nu \rangle$ . The Hubbard Hamiltonian has the same form as the PPP one, but employs a more drastic approximation to electron–electron repulsions, neglecting all but the on-site ones, *i.e.*,  $\gamma_{\mu\nu} = \gamma \delta_{\mu\nu}$ . The Hubbard and PPP Hamiltonians provide a framework for examining the entire range of many-electron correlation effects

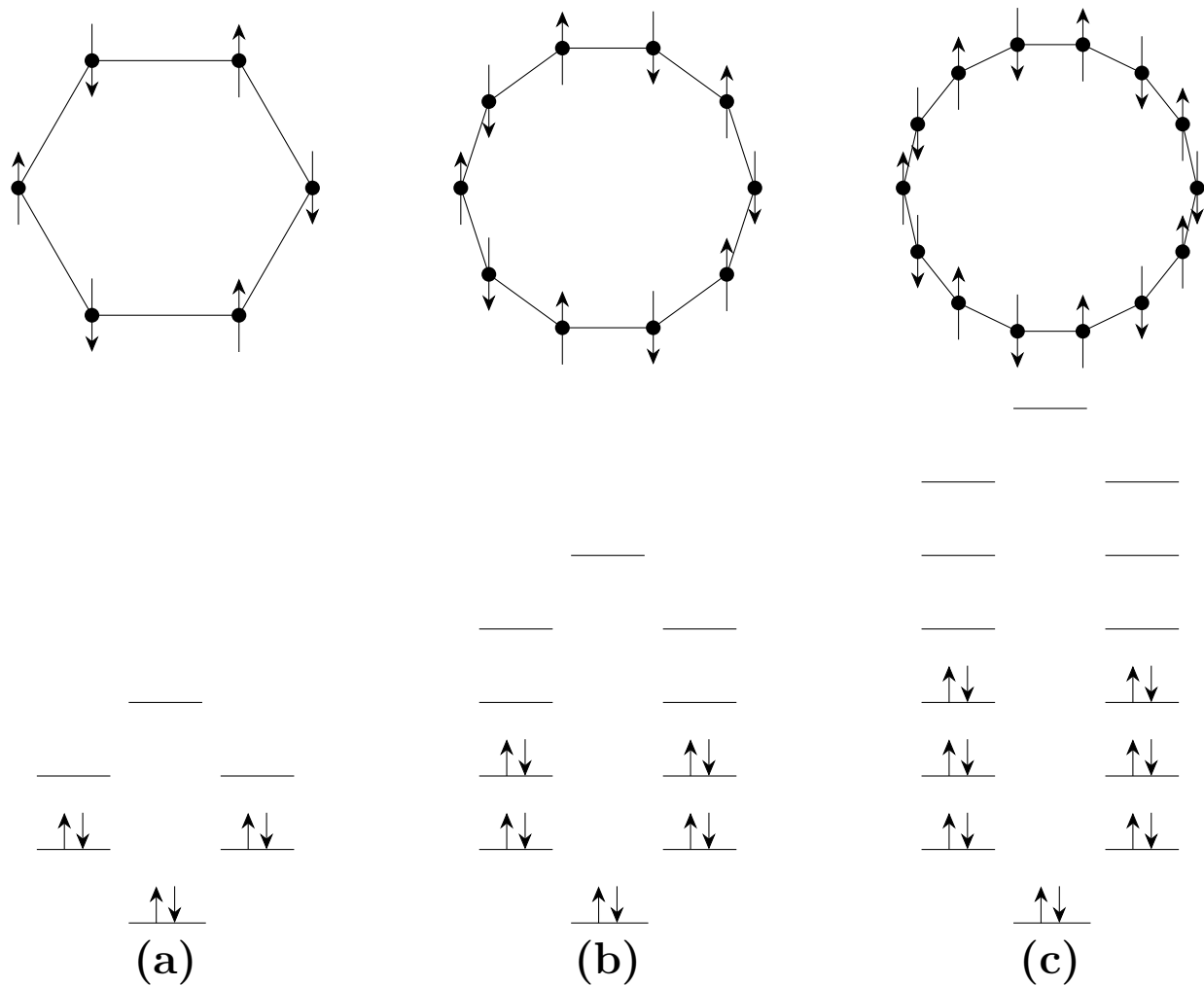


Figure 3.3: Schematic representation of the models of cyclic polyenes  $C_NH_N$  with (a)  $N = 6$ , (b)  $N = 10$ , and (c)  $N = 14$ . The pertinent molecular orbital diagrams are presented as well.

by varying the value of the parameter  $\beta$ . The weakly correlated regime is approached as  $\beta \rightarrow -\infty$ . In this case, the hopping one-body term dominates in Equation (3.12) and the electrons are essentially free to move from one site to the next without experiencing any interelectronic repulsions, *i.e.*, the system behaves like a metal. At the other end of the electron correlation strength, when  $\beta \rightarrow 0^-$  the hoping term is negligible and the whole system is driven by electron correlation effects, giving rise to a strongly correlated insulating phase. Note that  $\beta \approx -2.4$  eV corresponds to a physical value of the resonance integral that reproduces experimental spectroscopic data for benzene [185].



Further insights regarding the implications of  $\beta \rightarrow 0^-$ , especially the various complications regarding post-RHF approaches, such as CCSD, CCSDT, and CCSDTQ, can be gained by examining the RHF orbital energies,  $\epsilon_P$ , of the PPP and Hubbard models of cyclic polyenes [278],

$$\epsilon_P = 2\beta \cos\left(\frac{2\pi P}{N}\right) + \sum_{\mu=0}^{N-1} \gamma_{0\mu} + \frac{1}{N} \sum_{J=-\kappa}^{\kappa} \sum_{\mu=0}^{N-1} \gamma_{0\mu} e^{\frac{2\pi i(P-J)\mu}{N}}, \quad (3.13)$$

where the summation over  $J$  extends over the set of  $2\kappa + 1$  occupied molecular orbitals (we use a convention, where capital letters  $P, Q, \dots$  represent spatial molecular orbitals, with  $I, J, \dots$  being occupied and  $A, B, \dots$  unoccupied). Thus, in analogy to benzene in a  $\pi$ -electron approximation, the RHF molecular orbitals, which are fully determined by symmetry and equivalent to Bloch and Brueckner ( $T_1 = 0$ ) orbitals, are pairwise degenerate,  $\epsilon_P = \epsilon_{-P}$ , with the exceptions of the lowest- and highest-energy ones (*cf.* Figure 3.3). An interesting observation that played an important role in the development of ACP approaches, including the ones introduced in this dissertation, is that the PPP and Hubbard models of cyclic polyenes satisfy the Coulson–Rushbrooke pairing theorem for polynuclear hydrocarbons [280], which, in the case of cyclic polyenes, states that for every occupied molecular orbital there exists an unoccupied one with opposite RHF orbital energy, *i.e.*, the system is characterized by ph symmetry (see Figure 3.3). The  $\Delta\epsilon_P \equiv \epsilon_{P+1} - \epsilon_P$  energy gap is

$$\begin{aligned} \Delta\epsilon_P = 2\beta \left\{ \cos\left[\frac{2\pi(P+1)}{N}\right] - \cos\left(\frac{2\pi P}{N}\right) \right\} \\ + \frac{1}{N} \sum_{J=-\kappa}^{\kappa} \sum_{\mu=0}^{N-1} \gamma_{0\mu} \left[ e^{\frac{2\pi i(P+1-J)\mu}{N}} - e^{\frac{2\pi i(P-J)\mu}{N}} \right]. \end{aligned} \quad (3.14)$$

Equation (3.14) reveals that, in the case of the PPP Hamiltonian, when  $\beta \rightarrow 0^-$  the molecular orbitals become quasi-degenerate. When the Hubbard Hamiltonian is considered, the RHF orbitals become exactly degenerate for  $\beta = 0$ . In addition, according to Equation (3.14), quasi-degeneracies can also occur for non-zero values of  $\beta$ , as long as one examines cyclic polyenes  $C_NH_N$  with large enough values of  $N$ . A complete orbital degeneracy is attained in the thermodynamic limit, which, based on numerical observations, is reached

rather quickly [187, 220]. In fact, it has been shown that the  $\text{C}_{10}\text{H}_{10}$  electron density resembles more that of an infinite one-dimensional solid than that of the benzene, *i.e.*,  $N = 6$ , analog [281].

The above analysis heralds the catastrophic failure of conventional SRCC approaches, such as CCSD, CCSDT, CCSDTQ, *etc.*, in the strong correlation regime of cyclic polyenes as described by the Hubbard and PPP Hamiltonians. For example, Podeszwa *et al.* [194] examined the performance of CCSD, CCSDT, and CCSDTQ in reproducing the FCI energetics for the PPP model of cyclic polyenes  $\text{C}_N\text{H}_N$  with  $N = 6, 10, 14$ , and  $18$ , varying the parameter  $\beta$  from physical values to the fully correlated, *i.e.*,  $\beta = 0$ , limit. A simple inspection of Figures 1–4 of Reference [194] reveals that the CCSD and CCSDT approaches quickly begin to overcorrelate upon departing from the range of  $\beta$  values that correspond to the weakly correlated regime. Furthermore, for rings larger than benzene, CCSD and CCSDT completely break down and no convergence is obtained after reaching a critical value of  $\beta$ ,  $\beta_c$ . Consistent with the analysis presented above, the larger the cyclic polyene the closer the value of  $\beta_c$  is to its physical range. Even the high-level CCSDTQ methodology is not immune to the onset of strong many-electron correlation effects. Although CCSDTQ closely reproduces the FCI correlation energies for weaker correlations, it exhibits a similar catastrophic behavior to CCSD and CCSDT, albeit it is more robust, failing only for the larger cyclic polyenes studied in Reference [194].

The nature of the singularities that prevent the convergence of traditional SRCC approaches for values of the resonance integral larger than the critical ones were investigated as early as 1984 [187]. In their early work, Paldus *et al.* showed, under certain very plausible assumptions, that no real solutions to the CCSD amplitude equations can be found for  $\beta < \beta_c$  [187]. In fact, they provided numerical evidence that in the vicinity of  $\beta_c$  correlation energy has the form  $\Delta E(\beta) \approx \Delta E(\beta_c) + \Delta E^{(1)}(\beta - \beta_c)^{\frac{1}{2}}$ , implying that for  $\beta < \beta_c$  one obtains complex correlation energies. A few years later, a more detailed study of this singular behavior, including CCSD (equivalent in this case to CCD) and higher-order

CC methods with connected triples, revealed that the critical values of the resonance integral  $\beta_c$  correspond to branch point singularities in the complex plane, resulting in real branches representing multiple solutions of the CC system in the  $\beta > \beta_c$  region becoming complex when  $\beta < \beta_c$ , so that the correlation energies around  $\beta_c$  satisfy the Laurent series  $\Delta E(\beta) = \Delta E(\beta_c) + \Delta E^{(1)}(\beta - \beta_c)^{\frac{1}{2}} + \mathcal{O}(\beta - \beta_c)$  [190]. It was also demonstrated, by deriving the analytical formula for the exact doubly excited cluster amplitudes of the PPP and Hubbard Hamiltonian models and back substitution, that these exact amplitudes do not satisfy the CCD system at  $\beta = 0$  [191].

As a final nail in the coffin of conventional SRCC approaches, we will prove analytically that in the strong correlation regime the only meaningful CC scheme is FCC. This was already anticipated since the early 1980s, when Paldus *et al.* [188, 278] showed that, in the  $\beta \rightarrow 0^-$  limit of the Hubbard and PPP models of the  $N = 6$  and 10 cyclic polyenes, the dominant quadruples were the connected ones, by cluster analysis of FCI wavefunctions. Furthermore, they speculated that  $T_{2n}$  clusters with  $n \geq 3$  would play an important role for larger cyclic polyenes, since the CISDTQ approach was already struggling with  $C_{10}H_{10}$ .

To simplify the mathematical manipulations, we shall examine the 12-site half-filled attractive pairing Hamiltonian [282–284], which constitutes a simple model for superconductivity by phenomenologically describing the Cooper problem of bound electron pairs [285–287]. The attractive pairing Hamiltonian has the form [209]

$$H = \sum_{P,\sigma} \epsilon_P a^{P\sigma} a_{P\sigma} - G \sum_{PQ} a^{P\uparrow} a^{P\downarrow} a_{Q\uparrow} a_{Q\downarrow}, \quad G \geq 0, \quad (3.15)$$

and, as was the case with the Hubbard and PPP Hamiltonians, depends on two parameters, namely, the orbital energies  $\epsilon_P$  and the interaction strength  $G$ . By varying the value of  $G$  from 0 to  $\infty$  one can continuously go from the weakly to the strongly correlated regime. A simple inspection of Equation (3.15) reveals that the attractive pairing Hamiltonian preserves the seniority number, which is the number of unpaired electrons. As a result, all odd-number-excited cluster components, which necessarily break the pairing of electrons, are zero, *i.e.*,  $T_{2n+1} = 0, \forall n \in \mathbb{Z}^+ \cup \{0\}$ , which constitutes a major simplification.

We begin our proof by examining the fully correlated limit of the attractive pairing Hamiltonian. We assume that in this regime all Slater determinants become exactly degenerate with the RHF one. By examining the structure of the corresponding FCI wavefunction,  $|\Psi_0\rangle = (\mathbf{1} + \sum_{n \in \mathbb{Z}^+} C_{2n}) |\Phi\rangle$ , we notice that the degeneracy condition forces all determinants to have a weight of 1, namely,  $c_{A\uparrow A\downarrow}^{I\uparrow I\downarrow} = 1, \forall I \in \text{occ.}, A \in \text{unocc.}, c_{A\uparrow A\downarrow B\uparrow B\downarrow}^{I\uparrow I\downarrow J\uparrow J\downarrow} = 1, \forall I < J \in \text{occ.}, A < B \in \text{unocc.}$ , and so on (occ. and unocc. stand for occupied and unoccupied orbital sets). In the next step, we will compute the values of the cluster amplitudes of the FCC wavefunction by cluster analyzing the aforementioned FCI wavefunction. To that end, we need to develop an expression similar to Equation (3.10), this time relating an  $m$ -body connected cluster with the CI excitation operators of rank up to  $m$ . This is accomplished in a similar fashion to Equation (3.9) and the final expression is

$$T_m = \sum_{j=1}^m \frac{(-1)^{j-1}}{j} \left[ \sum_{\substack{l_1+l_2+\dots+l_m=j \\ l_1+2l_2+\dots+ml_m=m}} \binom{j}{l_1, l_2, \dots, l_m} \prod_{k=1}^m C_k^{l_k} \right]. \quad (3.16)$$

Using Equation (3.16) for  $m = 2, 4, 6, 8, 10$ , and  $12$  we obtain

$$T_2 = C_2, \quad (3.17a)$$

$$T_4 = C_4 - \frac{1}{2}C_2^2, \quad (3.17b)$$

$$T_6 = C_6 - C_4C_2 + \frac{1}{3}C_2^3, \quad (3.17c)$$

$$T_8 = C_8 - C_6C_2 - \frac{1}{2}C_4^2 + C_4C_2^2 - \frac{1}{4}C_2^4, \quad (3.17d)$$

$$T_{10} = C_{10} - C_8C_2 - C_6C_4 + C_6C_2^2 + C_4^2C_2 - C_4C_2^3 + \frac{1}{5}C_2^5, \quad (3.17e)$$

and

$$\begin{aligned} T_{12} = & C_{12} - C_{10}C_2 - C_8C_4 + C_8C_2^2 - \frac{1}{2}C_6^2 + 2C_6C_4C_2 - C_6C_2^3 \\ & + \frac{1}{3}C_4^3 - \frac{3}{2}C_4^2C_2^2 + C_4C_2^4 - \frac{1}{6}C_2^6, \end{aligned} \quad (3.17f)$$

where we already took advantage of the fact that for the attractive pairing Hamiltonian the odd-number-excited clusters vanish. The explicit expressions connecting the cluster and CI excitation amplitudes can be derived diagrammatically by using Equation (3.17) and

computing matrix elements of the form  $\left\langle \Phi_{I_1 \uparrow I_1 \downarrow \dots I_n \uparrow I_n \downarrow}^{A_1 \uparrow A_1 \downarrow \dots A_n \uparrow A_n \downarrow} \middle| T_n \middle| \Phi \right\rangle$ . This yields

$$t_{A \uparrow A \downarrow}^{I \uparrow I \downarrow} = c_{A \uparrow A \downarrow}^{I \uparrow I \downarrow}, \quad (3.18a)$$

$$\begin{aligned} t_{A \uparrow A \downarrow B \uparrow B \downarrow}^{I \uparrow I \downarrow J \uparrow J \downarrow} &= c_{A \uparrow A \downarrow B \uparrow B \downarrow}^{I \uparrow I \downarrow J \uparrow J \downarrow} \\ &\quad - \mathcal{S}_{ABC} c_{A \uparrow A \downarrow}^{I \uparrow I \downarrow} c_{B \uparrow B \downarrow}^{J \uparrow J \downarrow}, \end{aligned} \quad (3.18b)$$

$$\begin{aligned} t_{A \uparrow A \downarrow B \uparrow B \downarrow C \uparrow C \downarrow}^{I \uparrow I \downarrow J \uparrow J \downarrow K \uparrow K \downarrow} &= c_{A \uparrow A \downarrow B \uparrow B \downarrow C \uparrow C \downarrow}^{I \uparrow I \downarrow J \uparrow J \downarrow K \uparrow K \downarrow} \\ &\quad - \mathcal{S}_{AB/C} \mathcal{S}^{IJ/K} c_{A \uparrow A \downarrow B \uparrow B \downarrow}^{I \uparrow I \downarrow J \uparrow J \downarrow} c_{C \uparrow C \downarrow}^{K \uparrow K \downarrow} \\ &\quad + 2 \mathcal{S}_{ABC} c_{A \uparrow A \downarrow}^{I \uparrow I \downarrow} c_{B \uparrow B \downarrow}^{J \uparrow J \downarrow} c_{C \uparrow C \downarrow}^{K \uparrow K \downarrow}, \end{aligned} \quad (3.18c)$$

$$\begin{aligned} t_{A \uparrow A \downarrow B \uparrow B \downarrow C \uparrow C \downarrow D \uparrow D \downarrow}^{I \uparrow I \downarrow J \uparrow J \downarrow K \uparrow K \downarrow L \uparrow L \downarrow} &= c_{A \uparrow A \downarrow B \uparrow B \downarrow C \uparrow C \downarrow D \uparrow D \downarrow}^{I \uparrow I \downarrow J \uparrow J \downarrow K \uparrow K \downarrow L \uparrow L \downarrow} \\ &\quad - \mathcal{S}_{ABC/D} \mathcal{S}^{IJK/L} c_{A \uparrow A \downarrow B \uparrow B \downarrow C \uparrow C \downarrow}^{I \uparrow I \downarrow J \uparrow J \downarrow K \uparrow K \downarrow} c_{D \uparrow D \downarrow}^{L \uparrow L \downarrow} \\ &\quad - \mathcal{S}_{AB/CD} \mathcal{S}^{IJ/K} c_{A \uparrow A \downarrow B \uparrow B \downarrow}^{I \uparrow I \downarrow J \uparrow J \downarrow} c_{C \uparrow C \downarrow D \uparrow D \downarrow}^{K \uparrow K \downarrow L \uparrow L \downarrow} \\ &\quad + 2 \mathcal{S}_{AB/C/D} \mathcal{S}^{IJ/KL} c_{A \uparrow A \downarrow B \uparrow B \downarrow}^{I \uparrow I \downarrow J \uparrow J \downarrow} c_{C \uparrow C \downarrow}^{K \uparrow K \downarrow} c_{D \uparrow D \downarrow}^{L \uparrow L \downarrow} \\ &\quad - 6 \mathcal{S}_{ABCD} c_{A \uparrow A \downarrow}^{I \uparrow I \downarrow} c_{B \uparrow B \downarrow}^{J \uparrow J \downarrow} c_{C \uparrow C \downarrow}^{K \uparrow K \downarrow} c_{D \uparrow D \downarrow}^{L \uparrow L \downarrow}, \end{aligned} \quad (3.18d)$$

$$\begin{aligned} t_{A \uparrow A \downarrow B \uparrow B \downarrow C \uparrow C \downarrow D \uparrow D \downarrow E \uparrow E \downarrow}^{I \uparrow I \downarrow J \uparrow J \downarrow K \uparrow K \downarrow L \uparrow L \downarrow M \uparrow M \downarrow} &= c_{A \uparrow A \downarrow B \uparrow B \downarrow C \uparrow C \downarrow D \uparrow D \downarrow E \uparrow E \downarrow}^{I \uparrow I \downarrow J \uparrow J \downarrow K \uparrow K \downarrow L \uparrow L \downarrow M \uparrow M \downarrow} \\ &\quad - \mathcal{S}_{ABCD/E} \mathcal{S}^{IJKL/M} c_{A \uparrow A \downarrow B \uparrow B \downarrow C \uparrow C \downarrow D \uparrow D \downarrow}^{I \uparrow I \downarrow J \uparrow J \downarrow K \uparrow K \downarrow L \uparrow L \downarrow} c_{E \uparrow E \downarrow}^{M \uparrow M \downarrow} \\ &\quad - \mathcal{S}_{ABC/DE} \mathcal{S}^{IJK/LM} c_{A \uparrow A \downarrow B \uparrow B \downarrow C \uparrow C \downarrow}^{I \uparrow I \downarrow J \uparrow J \downarrow K \uparrow K \downarrow} c_{D \uparrow D \downarrow E \uparrow E \downarrow}^{L \uparrow L \downarrow M \uparrow M \downarrow} \\ &\quad + 2 \mathcal{S}_{ABC/D/E} \mathcal{S}^{IJK/LM} c_{A \uparrow A \downarrow B \uparrow B \downarrow C \uparrow C \downarrow}^{I \uparrow I \downarrow J \uparrow J \downarrow K \uparrow K \downarrow} c_{D \uparrow D \downarrow}^{L \uparrow L \downarrow} c_{E \uparrow E \downarrow}^{M \uparrow M \downarrow} \\ &\quad + \mathcal{S}_{AB/CD/E} \mathcal{S}^{IJ/KL/M} c_{A \uparrow A \downarrow B \uparrow B \downarrow}^{I \uparrow I \downarrow J \uparrow J \downarrow} c_{C \uparrow C \downarrow D \uparrow D \downarrow}^{K \uparrow K \downarrow L \uparrow L \downarrow} c_{E \uparrow E \downarrow}^{M \uparrow M \downarrow} \\ &\quad - 6 \mathcal{S}_{AB/C/D/E} \mathcal{S}^{IJ/KLM} c_{A \uparrow A \downarrow B \uparrow B \downarrow}^{I \uparrow I \downarrow J \uparrow J \downarrow} c_{C \uparrow C \downarrow}^{K \uparrow K \downarrow} c_{D \uparrow D \downarrow}^{L \uparrow L \downarrow} c_{E \uparrow E \downarrow}^{M \uparrow M \downarrow} \\ &\quad + 24 \mathcal{S}_{ABCDE} c_{A \uparrow A \downarrow}^{I \uparrow I \downarrow} c_{B \uparrow B \downarrow}^{J \uparrow J \downarrow} c_{C \uparrow C \downarrow}^{K \uparrow K \downarrow} c_{D \uparrow D \downarrow}^{L \uparrow L \downarrow} c_{E \uparrow E \downarrow}^{M \uparrow M \downarrow}, \end{aligned} \quad (3.18e)$$

and

$$\begin{aligned}
t_{A\uparrow A\downarrow B\uparrow B\downarrow C\uparrow C\downarrow D\uparrow D\downarrow E\uparrow E\downarrow F\uparrow F\downarrow}^{I\uparrow I\downarrow J\uparrow J\downarrow K\uparrow K\downarrow L\uparrow L\downarrow M\uparrow M\downarrow N\uparrow N\downarrow} &= c_{A\uparrow A\downarrow B\uparrow B\downarrow C\uparrow C\downarrow D\uparrow D\downarrow E\uparrow E\downarrow F\uparrow F\downarrow}^{I\uparrow I\downarrow J\uparrow J\downarrow K\uparrow K\downarrow L\uparrow L\downarrow M\uparrow M\downarrow N\uparrow N\downarrow} \\
&- \mathcal{S}_{ABCDE/F} \mathcal{S}^{IJKLM/N} c_{A\uparrow A\downarrow B\uparrow B\downarrow C\uparrow C\downarrow D\uparrow D\downarrow E\uparrow E\downarrow}^{I\uparrow I\downarrow J\uparrow J\downarrow K\uparrow K\downarrow L\uparrow L\downarrow M\uparrow M\downarrow} c_{F\uparrow F\downarrow}^{N\uparrow N\downarrow} \\
&- \mathcal{S}_{ABCD/EF} \mathcal{S}^{IJKL/MN} c_{A\uparrow A\downarrow B\uparrow B\downarrow C\uparrow C\downarrow D\uparrow D\downarrow}^{I\uparrow I\downarrow J\uparrow J\downarrow K\uparrow K\downarrow L\uparrow L\downarrow} c_{E\uparrow E\downarrow F\uparrow F\downarrow}^{M\uparrow M\downarrow N\uparrow N\downarrow} \\
&+ 2\mathcal{S}_{ABCD/E/F} \mathcal{S}^{IJKL/MN} c_{A\uparrow A\downarrow B\uparrow B\downarrow C\uparrow C\downarrow D\uparrow D\downarrow}^{I\uparrow I\downarrow J\uparrow J\downarrow K\uparrow K\downarrow L\uparrow L\downarrow} c_{E\uparrow E\downarrow}^{M\uparrow M\downarrow} c_{F\uparrow F\downarrow}^{N\uparrow N\downarrow} \\
&- \mathcal{S}_{ABC/DEF} \mathcal{S}^{IJK/LM} c_{A\uparrow A\downarrow B\uparrow B\downarrow C\uparrow C\downarrow}^{I\uparrow I\downarrow J\uparrow J\downarrow K\uparrow K\downarrow} c_{D\uparrow D\downarrow E\uparrow E\downarrow F\uparrow F\downarrow}^{L\uparrow L\downarrow M\uparrow M\downarrow N\uparrow N\downarrow} \\
&+ 2\mathcal{S}_{ABC/DE/F} \mathcal{S}^{IJK/LM/N} c_{A\uparrow A\downarrow B\uparrow B\downarrow C\uparrow C\downarrow}^{I\uparrow I\downarrow J\uparrow J\downarrow K\uparrow K\downarrow} c_{D\uparrow D\downarrow E\uparrow E\downarrow}^{L\uparrow L\downarrow M\uparrow M\downarrow} c_{F\uparrow F\downarrow}^{N\uparrow N\downarrow} \\
&- 6\mathcal{S}_{ABC/D/E/F} \mathcal{S}^{IJK/LMN} c_{A\uparrow A\downarrow B\uparrow B\downarrow C\uparrow C\downarrow}^{I\uparrow I\downarrow J\uparrow J\downarrow K\uparrow K\downarrow} c_{D\uparrow D\downarrow}^{L\uparrow L\downarrow} c_{E\uparrow E\downarrow}^{M\uparrow M\downarrow} c_{F\uparrow F\downarrow}^{N\uparrow N\downarrow} \\
&+ 2\frac{1}{6}\mathcal{S}_{AB/CD/EF} \mathcal{S}^{IJ/KL/MN} c_{A\uparrow A\downarrow B\uparrow B\downarrow}^{I\uparrow I\downarrow J\uparrow J\downarrow} c_{C\uparrow C\downarrow D\uparrow D\downarrow}^{K\uparrow K\downarrow L\uparrow L\downarrow} c_{E\uparrow E\downarrow F\uparrow F\downarrow}^{M\uparrow M\downarrow N\uparrow N\downarrow} \\
&- 6\frac{1}{4}\mathcal{S}_{AB/CD/E/F} \mathcal{S}^{IJ/KL/M/N} c_{A\uparrow A\downarrow B\uparrow B\downarrow}^{I\uparrow I\downarrow J\uparrow J\downarrow} c_{C\uparrow C\downarrow D\uparrow D\downarrow}^{K\uparrow K\downarrow L\uparrow L\downarrow} c_{E\uparrow E\downarrow}^{M\uparrow M\downarrow} c_{F\uparrow F\downarrow}^{N\uparrow N\downarrow} \\
&+ 24\mathcal{S}_{AB/C/D/E/F} \mathcal{S}^{IJ/KLMN} c_{A\uparrow A\downarrow B\uparrow B\downarrow}^{I\uparrow I\downarrow J\uparrow J\downarrow} c_{C\uparrow C\downarrow}^{K\uparrow K\downarrow} c_{D\uparrow D\downarrow}^{L\uparrow L\downarrow} c_{E\uparrow E\downarrow}^{M\uparrow M\downarrow} c_{F\uparrow F\downarrow}^{N\uparrow N\downarrow} \\
&- 120\mathcal{S}_{ABCDEF} c_{A\uparrow A\downarrow}^{I\uparrow I\downarrow} c_{B\uparrow B\downarrow}^{J\uparrow J\downarrow} c_{C\uparrow C\downarrow}^{K\uparrow K\downarrow} c_{D\uparrow D\downarrow}^{L\uparrow L\downarrow} c_{E\uparrow E\downarrow}^{M\uparrow M\downarrow} c_{F\uparrow F\downarrow}^{N\uparrow N\downarrow},
\end{aligned} \tag{3.18f}$$

where the  $\mathcal{S}$  symbols denote symmetrizing operators with respect to the relevant permutations of given sets of orbital indices. To be precise, symmetrizers of the form  $\mathcal{S}_{P_1 \dots P_n} \equiv \mathcal{S}^{P_1 \dots P_n}$  incorporate all  $n!$  permutations of the  $n$  indices, while symmetrizers with slashes exclude permutations of indices belonging to the same group. For instance, the number of permutations included in  $\mathcal{S}_{P_1 \dots P_\alpha / Q_1 \dots Q_\beta / R_1 \dots R_\gamma / S_1 \dots S_\delta} \equiv \mathcal{S}^{P_1 \dots P_\alpha / Q_1 \dots Q_\beta / R_1 \dots R_\gamma / S_1 \dots S_\delta}$  is  $\frac{(\alpha + \beta + \gamma + \delta)!}{\alpha! \beta! \gamma! \delta!}$ . At a first glance, the appearance of symmetrizers instead of antisymmetrizers might seem surprising, but this is related to the fact that the Hamiltonian preserves the seniority number. As a result, any permutation of orbital indices gives rise to a product of two permutations over the corresponding spin-orbital indices, resulting in symmetrizing, rather than antisymmetrizing, operators. For example,  $\mathcal{S}_{PQR} \equiv \mathcal{S}^{PQR} = \mathbf{1} + (PQ) + (PR) + (QR) + (PQR) + (PRQ) \equiv \mathbf{1} + (P\uparrow Q\uparrow)(P\downarrow Q\downarrow) + (P\uparrow R\uparrow)(P\downarrow R\downarrow) + (Q\uparrow R\uparrow)(Q\downarrow R\downarrow) + (P\uparrow Q\uparrow R\uparrow)(P\downarrow Q\downarrow R\downarrow) + (P\uparrow R\uparrow Q\uparrow)(P\downarrow R\downarrow Q\downarrow)$  and  $\mathcal{S}_{PQ/R} \equiv \mathcal{S}^{PQ/R} = \mathbf{1} + (PR) + (QR) \equiv \mathbf{1} + (P\uparrow R\uparrow)(P\downarrow R\downarrow) + (Q\uparrow R\uparrow)(Q\downarrow R\downarrow)$ .

We are now in a position to calculate the values of the cluster amplitudes in the strong correlation limit of the 12-site half-filled attractive pairing Hamiltonian. To that end, we use Equation (3.18) together with the fact that in this regime all CI excitation amplitudes are equal to one and obtain

$$t_{A\uparrow A\downarrow}^{I\uparrow I\downarrow} = 1, \quad \forall I \in \text{occ.}, A \in \text{unocc.}, \quad (3.19a)$$

$$t_{A\uparrow A\downarrow B\uparrow B\downarrow}^{I\uparrow I\downarrow J\uparrow J\downarrow} = -1, \quad \forall I < J \in \text{occ.}, A < B \in \text{unocc.}, \quad (3.19b)$$

$$t_{A\uparrow A\downarrow B\uparrow B\downarrow C\uparrow C\downarrow}^{I\uparrow I\downarrow J\uparrow J\downarrow K\uparrow K\downarrow} = 4, \quad \forall I < J < K \in \text{occ.}, A < B < C \in \text{unocc.}, \quad (3.19c)$$

$$t_{A\uparrow A\downarrow B\uparrow B\downarrow C\uparrow C\downarrow D\uparrow D\downarrow}^{I\uparrow I\downarrow J\uparrow J\downarrow K\uparrow K\downarrow L\uparrow L\downarrow} = -33, \quad \forall I < J < K < L \in \text{occ.}, \quad (3.19d)$$

$$A < B < C < D \in \text{unocc.},$$

$$t_{A\uparrow A\downarrow B\uparrow B\downarrow C\uparrow C\downarrow D\uparrow D\downarrow E\uparrow E\downarrow}^{I\uparrow I\downarrow J\uparrow J\downarrow K\uparrow K\downarrow L\uparrow L\downarrow M\uparrow M\downarrow} = 456, \quad \forall I < J < K < L < M \in \text{occ.}, \quad (3.19e)$$

$$A < B < C < D < E \in \text{unocc.},$$

and

$$t_{A\uparrow A\downarrow B\uparrow B\downarrow C\uparrow C\downarrow D\uparrow D\downarrow E\uparrow E\downarrow F\uparrow F\downarrow}^{I\uparrow I\downarrow J\uparrow J\downarrow K\uparrow K\downarrow L\uparrow L\downarrow M\uparrow M\downarrow N\uparrow N\downarrow} = -9460, \quad \forall I < J < K < L < M < N \in \text{occ.}, \quad (3.19f)$$

$$A < B < C < D < E < F \in \text{unocc.}$$

This clearly shows that in the fully correlated limit of the half-filled attractive pairing Hamiltonian the higher the many-body rank of a connected cluster component the higher its magnitude is. The same behavior was observed numerically by Degroote *et al.* in their investigation of the 12-site half-filled attractive pairing Hamiltonian [209], but, to the best of our knowledge, this is the first time that this is shown analytically rather than numerically. Furthermore, the above derivation, although rationalized in the context of the attractive pairing Hamiltonian, is, in fact, more general, as it applies to any strongly correlated situation in which all determinants in the FCI expansion have an equal weight and in which the seniority number is conserved.

The above observations clearly demonstrate that the fabric of traditional SRCC approaches is utterly destroyed in the strong correlation limit. The enormous success of the hierarchy of conventional SRCC approaches, including CCSD, CCSDT, and CCSDTQ, in de-

describing weakly and moderately correlated systems is based on the fact that in these regimes  $T_2 > T_3 > T_4 > \dots > T_N$ . This conventional paradigm is destroyed, being often reversed, in a strongly correlated regime, so that the only meaningful conventional SRCC approach capable of properly describing strong correlations is FCC, where all many-body components of  $T$  must be included in the calculations.

### 3.3 Approximate Coupled-Pair Methods with an Active-Space Treatment of Three-Body Clusters

*... the neglect of nonlinear nonfactorizable diagrams  
... must simulate the higher excited-cluster contri-  
butions, such as  $T_4$  and  $T_6$ .*

---

J. Paldus, M. Takahashi, and R. W. H. Cho, Int. J. Quantum Chem. Symp. **18**, 237 (1984).

A crucial step in the discovery and subsequent understanding of ACP schemes was the development of the orthogonally spin-adapted CC formalism [219, 220, 230, 288–290]. Therefore, before we proceed to the discussion of ACP approaches, we present the salient features of singlet spin-adapted CC theory, using the CC with doubles (CCD) [45, 291, 292] as an example.

The first step in developing an orthogonally spin-adapted CC formalism is to define the  $\left| \Phi_{I_1 \dots I_n}^{A_1 \dots A_n}; \{\tilde{\mathbf{S}}_{\mathbf{r}}\} S M_S \right\rangle$  configuration state functions that span the many-electron Hilbert space, where indices  $I_1, I_2, \dots$  or  $I, J, \dots$  ( $A_1, A_2, \dots$  or  $A, B, \dots$ ) designate orbitals that are occupied (unoccupied) in the closed-shell (*e.g.*, RHF) reference determinant,  $S$  and  $M_S$  denote the total spin and its projection on the  $z$ -axis, respectively, and  $\tilde{\mathbf{S}}_{\mathbf{r}}$  represents the relevant intermediate spin quantum numbers resulting in the final  $|S, M_S\rangle$  spin state (note that the closed-shell reference determinant is singlet spin-adapted by construction). Since we are interested in singlet spin-adapted CCD, we need to consider doubly excited configuration state functions of the form  $\left| \Phi_{IJ}^{AB}; \{\tilde{\mathbf{S}}_{\mathbf{r}}\} 00 \right\rangle$ , which require the coupling of four  $s = \frac{1}{2}$  spins involved in 2-particle–2-hole excitation via the intermediate spins  $\tilde{\mathbf{S}}_{\mathbf{r}}$ . Although there exist a



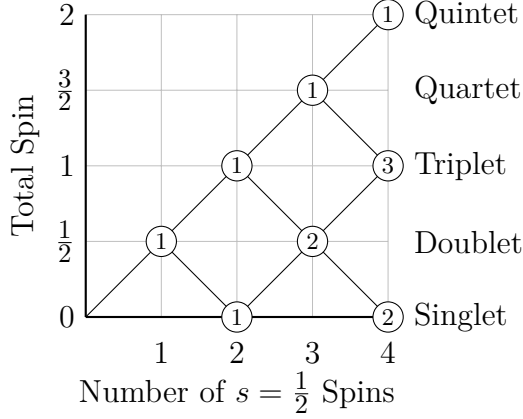


Figure 3.4: Branching diagram illustrating the total spin as a function of the number of  $s = \frac{1}{2}$  coupled spins. The integers inside the circles indicate the number of independent spin states associated with a given total spin and number of  $s = \frac{1}{2}$  spins coupled.

few ways of coupling the spins of the four spin-orbitals, it has been shown that the particle-particle-hole-hole (pp-hh) scheme leads to the most symmetric and simple expressions [293]. In the pp-hh approach, one obtains two intermediate spins denoted as  $S_{r_{pp}}$  and  $S_{r_{hh}}$  by separately coupling the spins of the two particle and the two hole states, respectively, that are subsequently coupled to the final  $S, M_S$  spin state. The fact that the final state is a singlet imposes the restriction  $S_{r_{pp}} = S_{r_{hh}} = S_r$ . Therefore, as one might anticipate from the branching diagram [294] shown in Figure 3.4, there are two independent classes of doubly excited configuration state functions, namely, those that arise from an intermediate singlet,  $S_r = 0$ , and those originating from an intermediate triplet,  $S_r = 1$ . To distinguish between the two, the kets representing the singlet pp-hh coupled orthogonally spin-adapted doubly excited configuration state functions  $|\Phi_{IJ}^{AB}; \{S_r S_r\} 00\rangle$  can be designated as  $|\Phi_{IJ}^{AB}\rangle_{S_r}$ , where  $S_r = 0$  or  $1$ .

Having defined the configuration state functions, we now proceed to the discussion of the cluster operator. In CCD, the cluster operator is approximated by its two-body component, *i.e.*,  $T^{(\text{CCD})} = T_2$ . Based on the analysis presented in the previous paragraph, it comes as no surprise that  $T_2$ , as a two-body operator, has two independent singlet-coupled components, *i.e.*,  $T_2 = T_2^{[0]} + T_2^{[1]}$ , defined as  $T_2^{[S_r]} |\Phi\rangle = \sum_{I \geq J, A \geq B} [S_r] t_{AB}^{IJ} |\Phi_{IJ}^{AB}\rangle_{S_r}$ . Thus, the CC

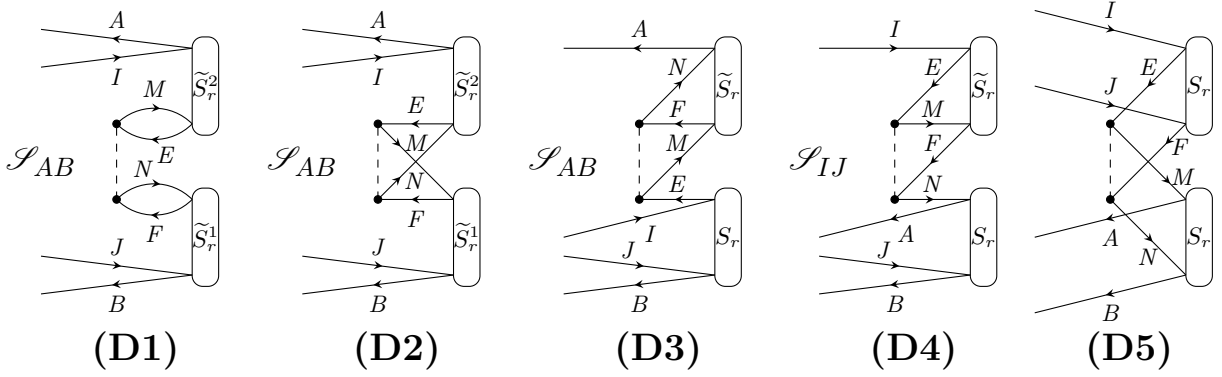


Figure 3.5: Goldstone–Brandow diagrams for the  $\frac{1}{2}T_2^2$  contributions  $\Lambda_k^{(2)}(AB, IJ; S_r)$ ,  $k = 1-5$ , to the CC equations projected on the singlet pp-hh coupled orthogonally spin-adapted doubly excited  $|\Phi_{IJ}^{AB}\rangle_{S_r}$  states. The intermediate spin quantum number  $S_r$  in defining  $|\Phi_{IJ}^{AB}\rangle_{S_r}$  and the corresponding doubly excited cluster amplitudes  $^{[S_r]}t_{AB}^{IJ}$  is 0 or 1. The occupied orbital indices  $M$  and  $N$ , the unoccupied orbital indices  $E$  and  $F$ , and the intermediate spin quantum numbers  $\tilde{S}_r^1$ ,  $\tilde{S}_r^2$ , and  $\tilde{S}_r$  are summed over.

amplitude equations for singlet spin-adapted CCD are

$$0 = {}_{S_r}\langle \Phi_{IJ}^{AB} | \left[ H_N \left( \mathbf{1} + T_2 + \frac{1}{2} T_2^2 \right) \right]_C | \Phi \rangle \Rightarrow \quad (3.20)$$

$$0 = {}_{S_r}\langle \Phi_{IJ}^{AB} | [H_N (\mathbf{1} + T_2)]_C | \Phi \rangle + \sum_{k=1}^5 \Lambda_k^{(2)}(AB, IJ; S_r), \quad (3.21)$$

where in the last step resulting in Equation (3.21) we isolated the bilinear  $\Lambda_k^{(2)}(AB, IJ; S_r)$ ,  $k = 1-5$ , terms that correspond to  $\frac{1}{2}T_2^2$  contributions and that form the basis of the various ACP approaches. In Figure 3.5, we provide the Goldstone–Brandow diagrams associated with these five non-linear terms.

We now proceed to the discussion of the ACP approaches, especially how they came into existence, the reasons behind their success in the presence of strong many-electron correlation effects, and their novel extensions to connected triples and realistic basis sets introduced in this dissertation. We, thus, begin with a brief historical overview of the development of the ACP family of methods.

In the late 1970s and early 1980s, Paldus, Jankowski, and Adams performed a series of investigations aimed at developing reliable approximations to orthogonally spin-adapted

CCD [224–227]. The motivation behind these efforts can be traced to the following two facts. First, at that time, the construction of intermediates by diagram factorization (see, for example, Reference [295]) was still in its infancy and researchers were faced with the computationally demanding task of solving a system of non-linear CC equations. This lead Jankowski and Paldus to state that “*it seems quite unlikely that*” CCD “*can be routinely used in the near future for larger than 10–20 electron systems or even smaller problems requiring very extensive orbital basis sets*” [225]. Second, the performance of the approximations to CCD that were available at that time was often worse than that of full CCD when electronic quasi-degeneracies were present (see, for example, References [224] and [225] and references therein). Among the schemes facing problems were linearized CCD (L-CCD) [45], which completely neglects the non-linear contributions shown in Figure 3.5, and coupled electron pair approximation (CEPA) methodologies [296–305] that simplify the quadratic  $\frac{1}{2}T_2^2$  contributions by considering only the exclusion principle violating terms that can be expressed as the product of a pair-energy contribution times a  $T_2$  matrix element.

To address the above problems, while attempting to avoid the use of full CCD, Paldus and co-workers devised an approximate CCD approach, abbreviated as ACP-D45, that replaces the  $\sum_{k=1}^5 \Lambda_k^{(2)}(AB, IJ; S_r)$  terms in Equation (3.20) by  $\Lambda_4^{(2)}(AB, IJ; S_r) + \Lambda_5^{(2)}(AB, IJ; S_r)$  [224, 225], *i.e.*, only diagrams D4 and D5 shown in Figure 3.5 are retained. In doing so, they were partly inspired by the CEPA family of methods, since only diagrams D4 and D5 can produce exclusion principle violating terms containing pair energies. In this regard, the various CEPA schemes can be viewed as approximations to ACP-D45. The same ACP-D45 scheme was rediscovered (under a different name) by Chiles and Dykstra in 1981 [228] (see also Reference [229]) using different argumentation. By examining the CCD equations in the limit of separated electron pairs, Chiles and Dykstra proved that diagrams D1–D3 cancel out and proposed the ACCD approach neglecting diagrams D1–D3, which is identical to ACP-D45 of Paldus *et al.*

The performance of the ACP-D45 scheme in the presence of electronic quasi-degeneracies

was originally tested by Paldus and co-workers on four-electron species, including the Be atom [226, 227], the minimum-basis-set  $H_4$  models [225], and *cis*-butadiene as described by the PPP Hamiltonian [225]. The last two systems allow one to examine the entire range of electron correlation effects, either by changing the nuclear geometry ( $H_4$ ) or by varying the parameters defining the PPP Hamiltonian (*cis*-butadiene). In all cases, the CCD methodology produced energetics of generally good quality, slightly overcorrelating after the onset of degeneracies. The performance of the ACP-D45 approach ignoring diagrams D1–D3 was remarkable, closely reproducing the CCD results in the weakly correlated regime and outperforming it in the presence of electronic quasi-degeneracies. In fact, ACP-D45 became practically exact in the strong correlation limit of the PPP model of *cis*-butadiene. At the same time, the ACP-D123 scheme, which is the complement of ACP-D45 keeping diagrams D1–D3 and neglecting the D4 and D5 contributions, became singular in the strong correlation regime, as was the case with L-CCD. Furthermore, Paldus and co-workers searched for other combinations of the D1–D5 non-linear diagrams that could possibly handle the quasi-degeneracy present in the case of the Be atom [226]. Among the 32 possible ACP variants, ACP-D45 performed the best, faithfully reproducing the CCD correlation energy. An additional interesting observation was that the results of the ACP-D123 calculations were very close to those obtained with L-CCD. This suggested that a mutual cancellation of diagrams D1–D3 takes place, explaining why ACP-D45 was an excellent approximation to CCD.

Motivated by the success of the ACP-D45 method, Paldus and co-workers turned their attention to the Hubbard and PPP models of cyclic polyenes [187, 188, 220], which, as emphasized in the previous section, exhibit severe electronic quasi-degeneracies as the resonance integral  $\beta$  approaches 0. They demonstrated that, unlike CCSD (equivalent in this case to CCD), which eventually overcorrelates or becomes singular, the ACP-D45 approach was well-behaved in the entire range of electron correlation effects characterizing the  $C_6H_6$  and  $C_{10}H_{10}$  cyclic polyenes. In fact, ACP-D45 provided the exact correlation energies in the strong correlation limit of the Hubbard Hamiltonian, while being very accurate in the case of

the PPP model. The fact that the  $T_{2n}$  components of the cluster operator  $T$  with  $n \geq 2$  become important in the strong correlation regime of these model Hamiltonians suggests that the ACP-D45 approach provides a mechanism for simulating the effect of these higher-than-two-body clusters. Indeed, in the spirit of externally corrected CC methodologies, Paldus and co-workers proved analytically that, as long as the PUHF approach [215–218] is exact and singles do not contribute, *i.e.*,  $C_1 = T_1 = 0$ , which is the case for the strongly correlated limit of the Hubbard and PPP models of cyclic polyenes, the  $S_r \langle \Phi_{IJ}^{AB} | (V_N T_4)_C | \Phi \rangle$  term with  $T_4$  extracted from PUHF cancels diagrams D1–D3 and multiplies diagram D5 by a factor of 9 when projected on the doubly excited configuration state functions with an intermediate triplet,  $|\Phi_{IJ}^{AB}\rangle_1$ , [220]. In principle, the three-body clusters should have been extracted as well, but the PUHF wavefunction does not contain singlet spin-adapted connected triples. The resulting approach, which uses  $\Lambda_4^{(2)}(AB, IJ; S_r) + (2S_r + 1)^2 \Lambda_5^{(2)}(AB, IJ; S_r)$  instead of  $\sum_{k=1}^5 \Lambda_k^{(2)}(AB, IJ; S_r)$  in Equation (3.20) and is, therefore, almost identical to ACP-D45, was termed ACP-D45g or ACPQ, to emphasize the *de facto* presence of  $T_4$  contribution in the latter acronym. The ACPQ approach, being formally an approximation to CCD, is much better than CCD, becoming exact in the strong correlation limit of cyclic polyenes as described by the Hubbard and PPP Hamiltonians. Furthermore, in the case of the Hubbard Hamiltonian, where D5 is zero when projections onto  $|\Phi_{IJ}^{AB}\rangle_1$  are considered, ACPQ becomes equivalent to the original ACP-D45 approach, explaining the exactness of the latter in the  $\beta = 0$  limit of the Hubbard Hamiltonian model. As already alluded to above, in their original derivation [220], Paldus and co-workers assumed that the PUHF wavefunction, expressed in terms of the RHF Slater determinant using the Thouless theorem, has no singlet monoexcitation component, which, although correct in the case of the Hubbard and PPP models of cyclic polyenes since the RHF orbitals are completely determined by symmetry rendering them simultaneously Brueckner orbitals, is not true in general. Piecuch *et al.* generalized the aforementioned derivation for cases where singlet monoexcitations do not vanish [219]. They demonstrated that not only the singlet-coupled three-body clusters continued to be

absent in the PUHF wavefunction, but also that the diagram cancellation defining the ACPQ approach augmented for  $T_1$  clusters remains valid. The resulting ACCSD' approach, which reduces to ACCD' = ACPQ when  $T_1 = 0$ , provides exact electronic energetics whenever the PUHF state offers an exact description.

As it turns out, the combination of D4 and D5 diagrams is not unique in providing exact results in the  $\beta = 0$  limit of cyclic polyene models. Paldus and co-workers realized that, due to the ph symmetry characterizing the Hubbard and PPP models of cyclic polyenes, diagrams D3 and D4 are equivalent, *i.e.*,  $\Lambda_3^{(2)}(AB, IJ; S_r) = \Lambda_4^{(2)}(AB, IJ; S_r)$ , suggesting that ACP-D35g is also exact in the fully correlated limit of these models. In fact, using any combination of the form

$$\lambda \Lambda_3^{(2)}(AB, IJ; S_r) + (1 - \lambda) \Lambda_4^{(2)}(AB, IJ; S_r) + (2S_r + 1)^2 \Lambda_5^{(2)}(AB, IJ; S_r) \quad (3.22)$$

instead of  $\sum_{k=1}^5 \Lambda_k^{(2)}(AB, IJ; S_r)$  in Equation (3.20) would be exact in the strong correlation limit of cyclic polyenes described by the PPP and Hubbard Hamiltonians, for any value of the real parameter  $\lambda$  (the Hubbard Hamiltonian only if the  $(2S_r + 1)^2$  factor at  $\Lambda_5^{(2)}(AB, IJ; S_r)$  is ignored). Interestingly, Piecuch and Paldus demonstrated, analytically and numerically, that the exact doubly excited clusters corresponding to the strong correlation limit of the cyclic polyene models, as extracted by cluster analysis of the PUHF wavefunction, satisfy the ACPQ equations, but are not a solution of the CCD ones [191]. As a by-product of their effort, they also demonstrated that in the  $\beta = 0$  limit  $\Lambda_1^{(2)}(AB, IJ; S_r) = (2S_r + 1)^2 \Lambda_5^{(2)}(AB, IJ; S_r)$ . This observation implies that the ACP-D14 approach proposed in Reference [191], in which one retains only the  $\frac{1}{2}T_2^2$  terms associated with diagrams D1 and D4 shown in Figure 3.5, *i.e.*, replacing  $\sum_{k=1}^5 \Lambda_k^{(2)}(AB, IJ; S_r)$  in Equation (3.20) by  $\Lambda_1^{(2)}(AB, IJ; S_r) + \Lambda_4^{(2)}(AB, IJ; S_r)$ , is exact in the fully correlated limit of cyclic polyene models, too. Piecuch and Paldus implemented the ACP-D14 methodology and showed that it performs as well as the ACPQ approach for the  $C_NH_N$  systems with  $N = 6, 10, 14, 18$ , and 22 for the entire range of  $\beta$  values. Both are accurate and capable of removing branch point singularities seen in CCD calculations for  $N \geq 14$  and both become

exact when  $\beta = 0$ . In addition, and in light of the ph symmetry, the identical behavior is anticipated for any ACP scheme using

$$\Lambda_1^{(2)}(AB, IJ; S_r) + \lambda \Lambda_3^{(2)}(AB, IJ; S_r) + (1 - \lambda) \Lambda_4^{(2)}(AB, IJ; S_r), \quad (3.23)$$

with  $\lambda \in \mathbb{R}$ , instead of  $\sum_{k=1}^5 \Lambda_k^{(2)}(AB, IJ; S_r)$  in Equation (3.20).

A graphical illustration of the above observations is provided in Figure 3.6, where we examine the performance of all 32 combinations of diagrams D1–D5 in describing the  $D_{6h}$ -symmetric dissociation of the minimum-basis-set (STO-6G [306])  $H_6$  ring using codes interfaced with the integral, RHF and restricted open-shell HF, and CC routines available in the GAMESS package [307–309], which were developed in this thesis research. In this and similar hydrogen clusters, which can be viewed as the simplest *ab initio* analogs of the PPP and Hubbard Hamiltonian models of cyclic polyenes, one can examine the entire spectrum of electron correlation effects by varying the radius  $R$  of the ring, transitioning from a weakly correlated metallic phase at small  $R$  values to a strongly correlated insulating phase as  $R \rightarrow \infty$ , mimicking the Mott transitions. To distinguish between the original orthogonally spin-adapted ACP approaches and their various spin-integrated counterparts implemented in this thesis research that incorporate  $T_1$  clusters as well, we commonly denote the latter approaches as ACCSD. In each ACCSD approach, the subset of the five  $\frac{1}{2}T_2^2$  diagrams that are retained in the CC equations corresponding to projections on doubly excited determinants,  $|\Phi_{ij}^{ab}\rangle$ , is provided inside parentheses. For example, the ACCSD(4,5) scheme incorporates only diagrams D4 and D5, *i.e.*, it is the spin-integrated analog of the original singlet spin-adapted ACP-D45 approach extended to singles. Out of the 32 possible ACCSD variants, only ACCSD(3), ACCSD(4), ACCSD(1,3), ACCSD(1,4), ACCSD(3,4), ACCSD(3,5), ACCSD(4,5), ACCSD(1,3,4), ACCSD(3,4,5), and ACCSD(1,3,4,5) provide qualitatively correct PECs. As anticipated in light of the above discussion regarding the Hubbard and PPP models of cyclic polyenes, only ACCSD(1,3), ACCSD(1,4), ACCSD(3,5), and ACCSD(4,5) become exact at the symmetric  $H_6 \rightarrow 6H$  dissociation, *i.e.*, in the strongly correlated, limit.

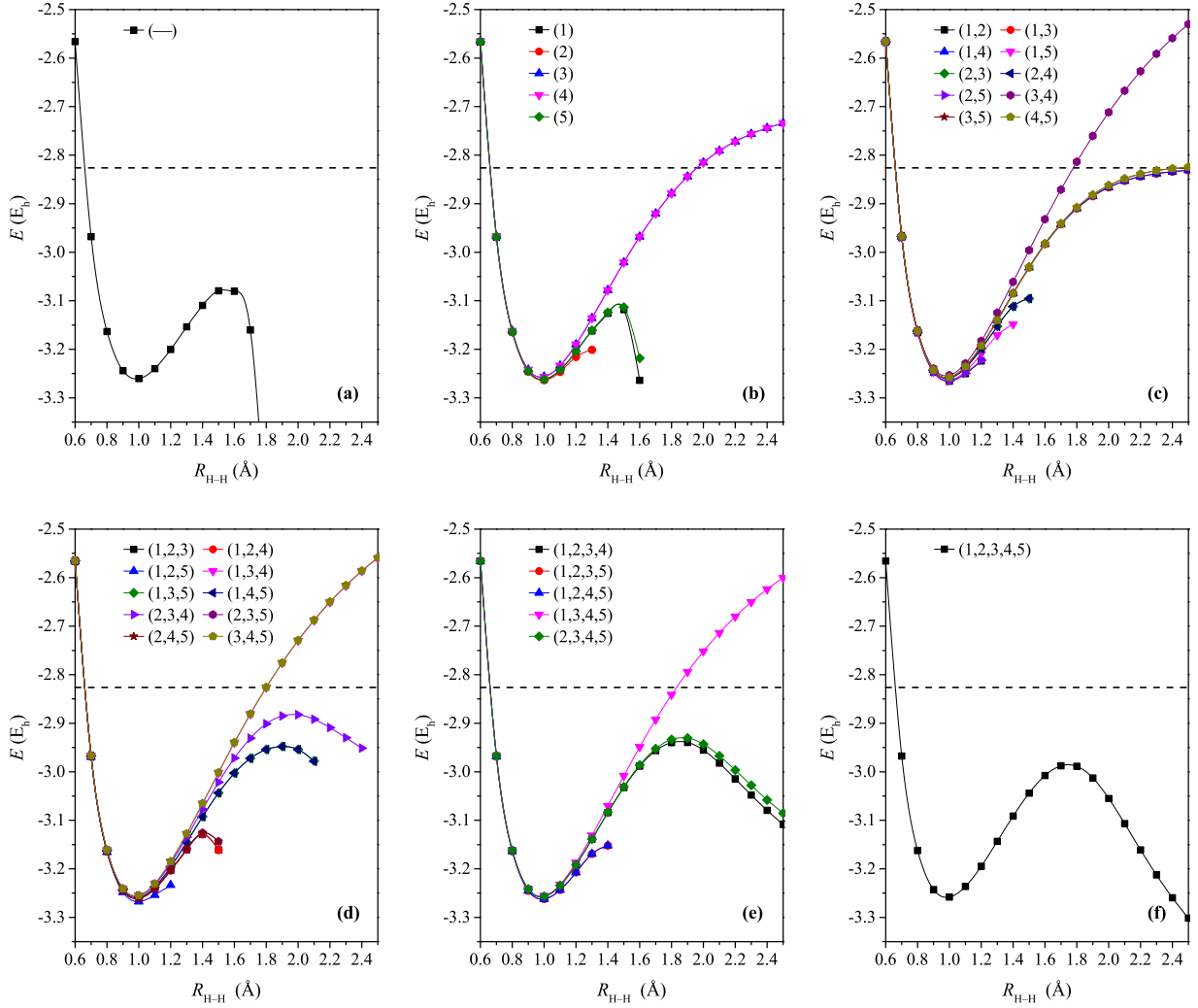


Figure 3.6: Ground-state PECs characterizing the  $D_{6h}$ -symmetric dissociation of the  $H_6$ /STO-6G ring, as obtained with the various ACCSD approaches that rely on subsets of the non-linear diagrams shown in Figure 3.5: (a) diagrams D1–D5 are neglected resulting in linearized CCSD, (b) all but one of the diagrams D1–D5 are neglected, (c) all but two of the diagrams D1–D5 are neglected, (d) all but three of the diagrams D1–D5 are neglected, (e) all but four of the diagrams D1–D5 are neglected, and (f) all diagrams are considered, *i.e.*, full CCSD. The dashed horizontal line designates the exact dissociation limit for the employed basis set corresponding to 6 non-interacting H atoms.

It is also interesting to note that any scheme that incorporates D2 is either overcorrelating or plagued by singularities.

At this point, we would like to recall that three additional classes of ACP approaches have recently emerged, namely, 2CC [232, 233], pCCSD( $\alpha, \beta$ ) [234], and DCSD [180]. The



philosophy behind these newer families of ACP schemes is more in line with the original motivation of Chiles and Dykstra, *i.e.*, it does not focus on the behavior in the strongly correlated regime as is the case in the work of Paldus, Čížek, Piecuch, and co-workers summarized above. They were derived by seeking modifications in the diagrams arising from the  $\frac{1}{2}T_2^2$  contributions to the CCSD equations that would result in approaches that are exact for two-electron systems and separated electron pairs. It is, thus, not surprising that all three classes include ACCSD(4,5) as a special case. In fact, 2CC is the same as ACCSD(4,5), *i.e.*, there is nothing new about it. The pCCSD( $\alpha, \beta$ ) scheme of Reference [234], where one replaces the non-linear terms of Equation (3.20) by

$$\beta \sum_{k=1}^3 \Lambda_k^{(2)}(AB, IJ; S_r) + \frac{1+\alpha}{2} \Lambda_4^{(2)}(AB, IJ; S_r) + \alpha \Lambda_5^{(2)}(AB, IJ; S_r), \quad (3.24)$$

remains exact for two-electron systems and separated electron pairs for any values of the real parameters  $\alpha$  and  $\beta$ . Another parameterization of the terms quadratic in  $T_2$  that gives rise to approaches that are exact for two-electron systems and separated electron pairs is [180]

$$\begin{aligned} \Lambda_1^{(2)}(AB, IJ; S_r) + (1 + 2\alpha) \Lambda_2^{(2)}(AB, IJ; S_r) + (1 + \alpha) \Lambda_3^{(2)}(AB, IJ; S_r) \\ + (1 + \beta) \Lambda_4^{(2)}(AB, IJ; S_r) + (1 + 2\beta) \Lambda_5^{(2)}(AB, IJ; S_r). \end{aligned} \quad (3.25)$$

Note that in this case diagrams D1 and D2 are not necessarily treated on an equal footing. Setting  $\alpha = \beta = -\frac{1}{2}$  enforces ph symmetry, even if it is not a real symmetry of the system of interest, and yields the DCSD  $\equiv$  ACCSD( $1, \frac{3+4}{2}$ ) methodology, which corresponds to setting  $\lambda$  in Equation (3.23) at  $\frac{1}{2}$ . However, one needs to keep in mind that exactness for two-electron systems and separated electron pairs does not guarantee that a given method can provide qualitatively, let alone quantitatively, correct results in the presence of strong non-dynamical correlation effects. In light of the above discussion, it is, thus, not surprising that among these new generations of ACP methods only DCSD  $\equiv$  ACCSD( $1, \frac{3+4}{2}$ ) is well-behaved in situations characterized by electronic quasi-degeneracies, since it satisfies Equation (3.23) with  $\lambda = \frac{1}{2}$ . Furthermore, the extensions of these schemes to connected triples ( $T_3$  clusters), via the 3CC [232, 233], pCCSDT [235], and DCSDT [235, 242] approaches, cannot handle

strong correlations, because they are based on diagram cancellations/modifications on the triples projection, *i.e.*, they retain all diagrams of CCSDT corresponding to projections on doubles, which is not a correct design for strong correlations.

The above discussion implies that the ACP-D13, ACP-D14, ACP-D1(3+4)/2  $\equiv$  DCD, ACP-D45, and ACPQ approaches, obtained by considering subsets of  $\frac{1}{2}T_2^2$  diagrams within the CCD system, Equation (3.20), and their extensions incorporating  $T_1$  clusters are more robust than the traditional CCSD, CCSDT, CCSDTQ, *etc.* hierarchy in strongly correlated situations, but the main rationale behind their usefulness is based on considering strongly correlated limits of highly symmetric, minimum-basis-set, model Hamiltonians. It is far from obvious that the same combinations of  $\frac{1}{2}T_2^2$  diagrams are optimum when one uses *ab initio* Hamiltonians and larger basis sets, required by quantitative quantum chemistry. In this dissertation, we address the issue of extending the ACP framework to larger basis sets and an *ab initio* description by taking advantage of the fact that Equations (3.22) and (3.23) define continuous classes of ACP approaches that retain the exactness in the strongly correlated limit of cyclic polyene models as described by the Hubbard and PPP Hamiltonians (the Hubbard Hamiltonian only when the  $(2S_r + 1)^2$  factor in Equation (3.22) is ignored). Between the two families, we focus on the one based on diagrams D1, D3, and D4, *i.e.*, we use Equation (3.23), because such methods are also exact in the  $\beta = 0$  limit of the more realistic PPP Hamiltonian.

Among the various ACP and ACCSD approaches originating from the use of Equation (3.23) instead of  $\sum_{k=1}^5 \Lambda_k^{(2)}(AB, IJ; S_r)$  in the CCD or CCSD amplitude equations projected on doubles, only ACP-D1(3+4)/2 and its ACCSD( $1, \frac{3+4}{2}$ ) or DCSD extension incorporating  $T_1$  clusters, where one uses  $\lambda = \frac{1}{2}$ , enforce ph symmetry. Naturally, this is desired for the Hubbard and PPP models of cyclic polyenes, which have an intrinsic ph symmetry, and is also justified in the case of strongly correlated systems described by *ab initio* Hamiltonians, such as the hydrogen clusters examined in this dissertation, as long as one uses a minimum basis set, for which ph symmetry is approximately satisfied. However, this does not necessarily

mean that  $\lambda = \frac{1}{2}$  in Equation (3.23) is an appropriate choice for realistic basis sets, especially when  $n_o \ll n_u$ . By numerically examining several strongly correlated systems treated with various basis sets, including dissociating rings and linear chains composed of varying numbers of hydrogen atoms, we have noticed that the ACP-D14 approximation augmented for  $T_1$  clusters, *i.e.*, ACCSD(1,4), which uses  $\lambda = 0$ , works better as the basis set becomes larger than ACCSD(1,  $\frac{3+4}{2}$ ), especially when one incorporates the three-body  $T_3$  clusters within the ACP or ACCSD framework. This numerical observation suggests that one might want to scale up diagram D4 by decreasing the coefficient  $\lambda$  when  $n_u$  gets larger. To that end, in this dissertation project, we introduce the method abbreviated as ACCSD(1,  $3 \times \frac{n_o}{n_o+n_u} + 4 \times \frac{n_u}{n_o+n_u}$ ), where we set  $\lambda = \frac{n_o}{n_o+n_u}$  in Equation (3.23) to take into account the effect of the dimensionality of the basis set in the calculations. This value of  $\lambda$  has two advantages. First, in the case of  $n_o = n_u$ , which is true, for example, in the Hubbard and PPP models of cyclic polyenes and the various hydrogen clusters as described by a minimum basis set, the novel method is equivalent to ACCSD(1,  $\frac{3+4}{2}$ ) or DCSD, which is well-behaved in the presence of strong many-electron correlation effects when the minimum basis set is employed. Second, as one approaches the CBS limit, the ACCSD(1,  $3 \times \frac{n_o}{n_o+n_u} + 4 \times \frac{n_u}{n_o+n_u}$ ) scheme becomes ACCSD(1,4), which is a desired behavior as well, since, based on our numerical observations, ACCSD(1,4), especially when corrected for the connected triples, performs the best out of all tested ACP approaches.

Another issue that is successfully addressed in this dissertation is the incorporation of connected triples in the ACP (meaning, ACCSD) approaches. As already mentioned earlier in this thesis, the PUHF wavefunction, which was used in deriving the ACPQ and ACCSD' equations and explaining the origin of the exceptional behavior of these ACP schemes in the presence of strong correlations, does not contain any information regarding the three-body clusters. Of course, one could incorporate connected triples fully, yielding CCSDT-like ACP schemes, but the associated computational costs would prohibit the application of such triples-corrected methods to realistic strongly correlated systems and materials. Histori-

cally, the  $T_3$  physics was incorporated within the ACP framework using MBPT arguments, similar to those exploited in the CCSDT-1 [119–122] and CCD+ST(CCD) [124] methodologies. Naturally, the use of MBPT already implies that such schemes will have difficulties in the presence of electronic quasi-degeneracies due to the vanishingly small perturbative denominators. Indeed, the resulting ACPTQ [190, 230] and ACPQ+T(ACPQ) [192, 231] methodologies, which are the ACPQ analogs of CCSDT-1 and CCD+T(CCD), respectively, were only partly successful [190, 192, 193, 219, 231]. Therefore, in this study, we explore the various diagram selections/modifications characterizing the ACP family of methods within the active-space CC framework [69, 70, 80–82, 98–100, 145–160], which avoids dangerous denominators while being computationally affordable.

In the active-space CC methods, the spin-orbitals used in the calculations are partitioned into four distinct groups, namely, core, active occupied, active unoccupied, and virtual spin-orbitals, and the higher-order cluster components, such as  $T_3$ , are approximated with the help of active orbitals, while the lower-order ones, *i.e.*,  $T_1$  and  $T_2$ , are treated fully. This has several advantages. By selecting, for example, the  $T_3$  cluster amplitudes using active orbitals, we save a lot in the computer effort without significant loss of accuracy when compared to the parent full CCSDT approach. At the same time, by keeping the dominant  $T_3$  amplitudes in the calculations, we provide a mechanism for relaxing  $T_1$  and  $T_2$  amplitudes in the presence of  $T_3$ , which is not available in non-iterative triples energy corrections of the CCSD[T] and CCSD(T) types.

In the CC approach with singles, doubles, and an active-space treatment of triples, abbreviated as CCSDt, which is most relevant to this thesis work, we approximate the cluster operator  $T$  as

$$T \approx T^{(\text{CCSDt})} = T_1 + T_2 + t_3, \quad (3.26)$$

where  $T_1$  and  $T_2$  are the standard one- and two-body components of  $T$ , treated fully, and

$$t_3 = \sum_{\substack{i < j < \mathbf{K} \\ \mathbf{A} < b < c}} t_{\mathbf{ABC}}^{ij\mathbf{K}} E_{ij\mathbf{K}}^{\mathbf{A}bc} \quad (3.27)$$

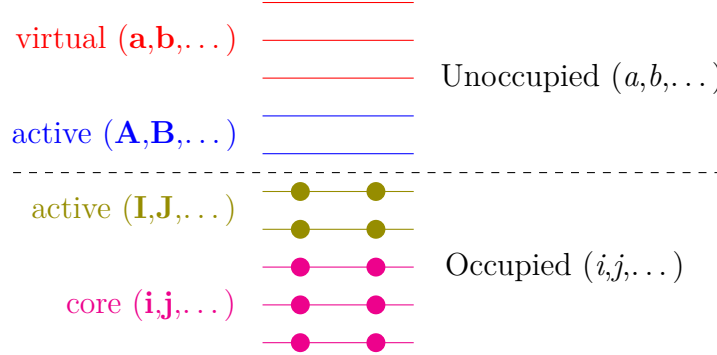


Figure 3.7: Schematic representation of the partitioning of orbitals into four disjoint groups, namely, core (magenta), active occupied (olive), active unoccupied (blue), and virtual (red), employed in active-space SRCC approaches.

is an approximate form of  $T_3$  defined using active orbitals. We use a convention where uppercase bold letters  $\mathbf{I}, \mathbf{J}, \mathbf{K}, \dots$  are the active occupied spin-orbitals, whereas  $\mathbf{A}, \mathbf{B}, \mathbf{C}, \dots$  designate the active unoccupied spin-orbitals. We continue using the lower-case italic indices,  $i, j, \dots$  for the occupied and  $a, b, \dots$  for the unoccupied spin-orbitals, if the active/inactive character is not specified. The  $t_a^i$ ,  $t_{ab}^{ij}$ , and  $t_{ij\mathbf{K}}^{\mathbf{A}bc}$  cluster amplitudes are obtained by solving the CC amplitude equations, Equation (3.4), projected on the excited Slater determinants corresponding to the definition of  $T^{(\text{CCSDt})}$ , *i.e.*, on all singly ( $|\Phi_i^a\rangle$ ) and doubly ( $|\Phi_{ij}^{ab}\rangle$ ) excited determinants and a subset of the triply excited determinants,  $|\Phi_{ij\mathbf{K}}^{\mathbf{A}bc}\rangle$ , defined using active orbitals. This simplification on the CC amplitude equations results in significant CPU time savings. The computational cost associated with the CCSDt method equals that of CCSD times a small prefactor that depends on the numbers of active occupied ( $N_o$ ) and active unoccupied ( $N_u$ ) orbitals. To be precise, the most expensive computational steps of the CCSDt calculations scale as  $N_o N_u n_o^2 n_u^4$ . Once the corresponding cluster amplitudes are computed, the active-space CC energy is obtained, in direct analogy with the conventional SRCC methods, by projecting the connected cluster form of the Schrödinger equation, Equation (3.3), on the reference determinant, *i.e.*, we continue using Equation (3.5).

The active-space triples extensions of the CCSD-like ACP schemes examined in this work, namely ACCSD(1,3), ACCSD(1,4), ACCSD( $1, \frac{3+4}{2}$ ), and ACCSD( $1, 3 \times \frac{n_o}{n_o+n_u} + 4 \times \frac{n_u}{n_o+n_u}$ ), are denoted as ACCSDt(1,3), ACCSDt(1,4), ACCSDt( $1, \frac{3+4}{2}$ ), and ACCSDt( $1, 3 \times$

$\frac{n_o}{n_o+n_u} + 4 \times \frac{n_u}{n_o+n_u}$ ), respectively. By allowing all orbitals to become active, one obtains the parent full triples ACP approaches ACCSDT(1,3), ACCSDT(1,4), ACCSDT(1, $\frac{3+4}{2}$ ), and ACCSDT(1, $3 \times \frac{n_o}{n_o+n_u} + 4 \times \frac{n_u}{n_o+n_u}$ ). In extending the various ACP approaches to connected triples, we focus on modifications of the  $\frac{1}{2}T_2^2$  diagrams in the CC equations projected on the doubly excited determinants,  $|\Phi_{ij}^{ab}\rangle$ , to retain the applicability of the resulting CCSDt- and CCSDT-like ACP schemes in strongly correlated systems. To be precise, the various specifications given inside parentheses following the ACCSDt and ACCSDT acronyms continue to designate the modifications of the  $\frac{1}{2}T_2^2$  diagrams in the CC equations projected on doubles only, while all terms appearing in the CC equations projected on triples are included.

### 3.4 Toward the Full Configuration Interaction Limit for Strong Correlation

*The only good Monte Carlos are dead Monte Carlos.*

---

H. F. Trotter and J. W. Turkey, in *Symposium on Monte Carlo Methods*, edited by H. A. Meyer (Wiley, New York, 1956) pp. 64–79.

Although the ACP approaches, especially those incorporating  $T_1$  and  $T_3$  clusters, are well-suited for the study of strongly correlated systems and can be very accurate in general, they are not exact, with the exceptions of the fully correlated limit of model Hamiltonians and the atomization threshold of hydrogen clusters. Here, we discuss the salient features of a novel semi-stochastic quantum chemistry approach, developed as part of this thesis research, that is capable of providing FCI-quality energetics, even in the presence of electronic quasi-degeneracies, at the computational cost of CCSD calculations combined with relatively inexpensive stochastic and deterministic preparatory steps. This is accomplished by merging the ACP schemes with the recently proposed semi-stochastic CAD-FCIQMC methodology [265], which accelerates convergence toward FCI energetics by solving CCSD-like equations in the presence of the three- and four-body clusters extracted from the early stages of FCIQMC [260–262] propagations.

The philosophy behind the CAD-FCIQMC methodology draws heavily from externally corrected CC approaches [219, 220, 230, 243, 267–274]. It is, thus, based on the observation that, for Hamiltonians containing up to two-body interactions, the CC correlation energy, Equation (3.5), depends only on the one- and two-body clusters,

$$\Delta E_0 = \langle \Phi | \left[ H_N \left( 1 + T_1 + T_2 + \frac{1}{2} T_1^2 \right) \right]_C | \Phi \rangle, \quad (3.28)$$

independent of the level of truncation of the cluster operator, while  $T_1$  and  $T_2$  directly couple with their three- and four-body counterparts through the CC equations corresponding to projections onto singly and doubly excited Slater determinants,

$$\langle \Phi_i^a | \left[ H_N \left( 1 + T_1 + T_2 + \frac{1}{2} T_1^2 + T_3 + T_1 T_2 + \frac{1}{3!} T_1^3 \right) \right]_C | \Phi \rangle = 0, \quad (3.29)$$

and

$$\begin{aligned} \langle \Phi_{ij}^{ab} | \left[ H_N \left( 1 + T_1 + T_2 + \frac{1}{2} T_1^2 + T_3 + T_1 T_2 + \frac{1}{3!} T_1^3 \right. \right. \\ \left. \left. + T_4 + T_1 T_3 + \frac{1}{2} T_2^2 + \frac{1}{2} T_1^2 T_2 + \frac{1}{4!} T_1^4 \right) \right]_C | \Phi \rangle = 0, \end{aligned} \quad (3.30)$$

respectively. Of course, setting  $T_3 = T_4 = 0$  in Equations (3.29) and (3.30) and neglecting projections onto higher-than-doubly excited Slater determinants gives rise to the standard CCSD approach. What is more interesting, however, is that if one extracts high-quality  $T_3$  and  $T_4$  clusters from a well-behaved non-CC source and solves Equations (3.29) and (3.30) for  $T_1$  and  $T_2$  in the presence of  $T_3$  and  $T_4$  obtained in this way, one can obtain high-quality values of the one- and two-body clusters and, consequently, the much improved correlation energy. In fact, extracting  $T_3$  and  $T_4$  from FCI and solving the CCSD-like system of equations shown in Equations (3.29) and (3.30) would generate the exact  $T_1$  and  $T_2$  and, thus, the exact (FCI) correlation energy. Historically, various non-CC sources have been used for extracting  $T_3$  and  $T_4$  clusters. For example, in the previous section we discussed the ACP family of methods that were discovered by extracting the exact four-body clusters from PUHF (recall that  $T_3 = 0$  for PUHF). The PUHF wavefunction was also used in the design of the ACCSD' and CCSDQ' approaches [219]. In the case of the latter approach, no

assumption was made regarding the exactness of four-body clusters extracted from PUHF. Other sources of  $T_3$  and  $T_4$  that have been explored over the years are valence bond theory [267], CASSCF [268, 269], MRCI [271, 272], and selected CI [270, 273, 274]. In the case of the CAD-FCIQMC approach, we employ the stochastic FCIQMC methodology of Alavi and co-workers [260–262] as a source of high-quality  $T_3$  and  $T_4$  clusters, which are guaranteed to become exact in the infinite-imaginary-time limit. In what follows, we give a brief overview of FCIQMC starting with its DMC predecessor.

As mentioned in the Introduction, the DMC approach is capable of producing numerically exact solutions to the electronic Schrödinger equation by directly sampling the  $N$ -electron wavefunction in the real space of  $3N$  electronic coordinates. This can be accomplished by realizing that the time-dependent Schrödinger equation resembles a diffusion equation if expressed in imaginary time,  $\tau = it$ , so that by propagating the resulting wavefunction  $|\Psi(\tau)\rangle$  along the imaginary time axis one can project out the exact ground state  $|\Psi_0\rangle$ ,

$$\lim_{\tau \rightarrow \infty} |\Psi(\tau)\rangle = \lim_{\tau \rightarrow \infty} e^{-(H-S)\tau} |\Phi_0\rangle = \begin{cases} c_0 |\Psi_0\rangle, & \text{for } S = E_0 \\ \infty, & \text{for } S > E_0, \\ 0, & \text{for } S < E_0 \end{cases} \quad (3.31)$$

where  $|\Phi_0\rangle$  is the reference state satisfying  $\langle \Phi_0 | \Psi_0 \rangle \neq 0$  (in our case, the RHF determinant  $|\Phi\rangle$ ) and  $S$  is the energy shift controlling wavefunction evolution.

Unfortunately, traditional DMC approaches run into the notorious Fermion sign problem, *i.e.*, an unconstrained imaginary-time propagation of  $|\Psi(\tau)\rangle$  in the coordinate space will cause the trial wavefunction to collapse to a totally symmetric bosonic state, which is the mathematical ground state of the spin-free non-relativistic electronic Hamiltonian. To alleviate this problem, the fixed-node approximation is employed in conventional DMC simulations. In this case, one enforces the nodal structure of an antisymmetric approximate wavefunction, obtained using one of the relatively inexpensive quantum chemistry approaches, on  $|\Psi(\tau)\rangle$ . By doing so the final wavefunction  $|\Psi_0\rangle$  and the corresponding en-



ergy  $E_0$  are not exact anymore and their quality is bound to the quality of the approximate nodes. This issue is addressed in the FCIQMC approach of Alavi and co-workers, who replaced the propagation in the coordinate space by the propagation in the many-electron Hilbert space spanned by Slater determinants. The fact that Slater determinants satisfy the proper fermionic antisymmetry by construction ensures that the final projected wavefunction will be antisymmetric as well, without having to resort to a fixed-node approximation.

The first step in the FCIQMC methodology is to express the  $N$ -electron time-dependent wavefunction  $|\Psi(\tau)\rangle$  as a linear combination of all Slater determinants afforded by the one-electron basis set, *i.e.*, a FCI-type expansion with the imaginary-time-dependent CI expansion coefficients,

$$|\Psi(\tau)\rangle = \sum_K c_K(\tau) |\Phi_K\rangle, \quad (3.32)$$

where  $|\Phi_K\rangle$  are the Slater determinants used to represent  $|\Psi(\tau)\rangle$ . Inserting this expression for  $|\Psi(\tau)\rangle$  into the imaginary-time Schrödinger equation, in which we have applied an energy shift  $S$  to the electronic Hamiltonian, yields a system of coupled differential equations for the  $c_K(\tau)$  coefficients,

$$\frac{\partial}{\partial \tau} c_K(\tau) = -(H_{KK} - S) c_K(\tau) - \sum_{L(\neq K)} H_{KL} c_L(\tau), \quad (3.33)$$

where  $H_{KL} = \langle \Phi_K | H | \Phi_L \rangle$  are matrix elements of the Hamiltonian involving Slater determinants engaged in the calculation. In light of Equation (3.31),  $\lim_{\tau \rightarrow \infty} |\Psi(\tau)\rangle = c_0 |\Psi_0\rangle$ , as long as  $\lim_{\tau \rightarrow \infty} S = E_0$ . This implies that in the infinite imaginary-time limit the state becomes stationary, meaning  $\frac{\partial}{\partial \tau} c_K(\tau) = 0, \forall K$ . As a result, if all Slater determinants are allowed in the calculations, in the  $\tau = \infty$  limit Equation (3.33) becomes equivalent to the FCI diagonalization of the Hamiltonian matrix in a given basis set,  $\sum_L H_{KL} c_L(\infty) = E_0 c_K(\infty)$ .

A direct numerical integration of the set of coupled differential equations shown in Equation (3.33) would require the entire set of  $c_K(\tau)$  coefficients to be available at every time step, resulting in a formidable computational cost of FCI times the number of time steps. To address this issue, Alavi and co-workers replaced the deterministic approach to Equation

3.33 by employing a walker population dynamics algorithm, in accord with DMC approaches. Of course, one needs to keep in mind that in DMC the walkers sample a continuum space of  $3N$  electronic coordinates, while in FCIQMC the walkers sample the discrete set of Slater determinants. Walkers can be thought of as fictitious signed particles that populate, in the case of FCIQMC, the various Slater determinants. In the FCIQMC approach, the CI coefficient at a given Slater determinant is proportional to the signed sum of walkers residing on this determinant, *i.e.*,

$$c_K(\tau) \propto N_K = \sum_{\alpha} s_{\alpha} \delta_{K, K_{\alpha}}, \quad (3.34)$$

where  $s_{\alpha} = \pm 1$  is the sign associated with the  $\alpha$ th walker and the summation extends over all walkers. As in the case of CI expansion coefficients, the walker population at a given determinant can be either positive or negative. On the other hand, the total population of walkers,  $N_w$ , is strictly positive and computed as  $N_w = \sum_K |N_K|$ . At this point it is worth mentioning that, although the FCIQMC approach guarantees the proper fermionic antisymmetry of the final projected state, it does not alleviate completely the fermion sign problem, since the stochastically determined sign structure of the FCIQMC wavefunction is not necessarily the same, up to a phase, with the one of the FCI vector. This is why, in addition to the birth/death and spawning processes controlling walker dynamics, further elaborated on below, one needs to annihilate walkers with opposite signs at each time  $\tau$ .

In light of Equation (3.34), the coupled differential equations shown in Equation (3.33) become

$$\frac{d}{d\tau} N_K(\tau) = - (H_{KK} - S) N_K(\tau) - \sum_{L(\neq K)} H_{KL} N_L(\tau). \quad (3.35)$$

The structure of the coupled differential equations shown in Equation (3.35) reveals that the walker population dynamics is essentially driven by the matrix elements of the Hamiltonian. Consequently, two kinds of processes can be identified. On the one hand, the off-diagonal matrix elements of the Hamiltonian define the spawning of walkers on different determinants. To be precise, for each (parent) walker  $\alpha$  residing on a given Slater determinant

$|\Phi_K\rangle$ , a Slater determinant  $|\Phi_L\rangle$ , coupled to  $|\Phi_K\rangle$  through the Hamiltonian, is selected with probability  $p_{\text{gen}}(L|K)$  and the spawning of one or more (child) walkers is attempted with probability  $p_s(L|K) = \Delta\tau|H_{KL}|/p_{\text{gen}}(L|K)$ , where  $\Delta\tau$  designates the imaginary-time step, compared to a number between 0 and 1 produced by random number generator. The sign of the matrix element of the Hamiltonian dictates also the sign of the spawned walker; the spawned walker will have the same sign as the parent walker in the case of  $H_{KL} < 0$  and opposite otherwise. We also see that this step of the algorithm is responsible for sampling the many-electron Hilbert space spanned by Slater determinants by placing walkers on new determinants. Taking into account that the electronic Hamiltonian contains up to two-body terms, the spawning step at a given time  $\tau$  can explore Slater determinants  $|\Phi_L\rangle$  that differ from  $|\Phi_K\rangle$  by at most two spin-orbitals. On the other hand, the diagonal matrix elements of the Hamiltonian define the birth or death of walkers, meaning the increase or decrease of the walker population on a given Slater determinant  $|\Phi_K\rangle$ . In this step, for each parent walker residing on  $|\Phi_K\rangle$ , a probability  $p_d(K) = \Delta\tau(H_{KK} - S)$  is computed. If  $p_d > 0$  ( $p_d < 0$ ), the walker dies (is cloned) with probability  $p_d$  ( $|p_d|$ ). It is also apparent that the growth of the walker population depends on the value of the shift energy  $S$ . For example, in light of Equation (3.31), if a rapid walker population growth is desired, the shift energy  $S$  is set at a value that is larger than  $E_0$ ; this is done in the early stages of the FCIQMC propagations. On the other hand, once a total walker population becomes sufficiently large, one starts using the energy shift  $S$  to stabilize walker population and reach convergence. As already alluded to above, the final step of the walker population dynamics algorithm involves the annihilation of oppositely signed walkers inhabiting a given determinant. As with birth/death and spawning, this is done at each time  $\tau$  during the propagation.

Having discussed the key elements of the walker population dynamics algorithm, we provide a brief outline of a FCIQMC simulation. We start with the original algorithm [260]. We begin by placing a certain number of walkers on one or more reference determinants (in our case, one, RHF) and setting the energy shift  $S$  above the exact ground-state energy  $E_0$ ,

$S > E_0$ , to promote the growth of the walker population [*cf.* Equation (3.31)]. At every imaginary-time step  $\tau$ , the three major processes driving the walker population dynamics are attempted, namely, spawning, birth/death, and annihilation. Initially, the simulation is characterized by an exponential growth of the walker population until a plateau is reached, corresponding to a system-dependent critical population of walkers,  $N_c$ . The plateau is a manifestation of a steady state, where the rate of walker creation equals the combined rate of death and annihilation. During this stage of the simulation, the annihilation process “purifies” the FCIQMC wavefunction, leading to a converged sign structure. Once the proper sign structure is attained, the walker population begins to rise again. At this point, the energy shift  $S$  is allowed to vary in an attempt to stabilize the walker population. Based on Equation (3.31), a constant walker population implies that  $S \rightarrow E_0$  and, thus, convergence is reached.

The performance of the FCIQMC methodology was originally tested on the Ne atom and oligoatomic species, including  $N_2$ ,  $C_2$ , and  $H_2O$ , as described by the aug-cc-pVDZ and cc-pVDZ basis sets, respectively. It was demonstrated that, even when starting with a single walker inhabiting the RHF Slater determinant, the FCIQMC simulation was able to converge to the deterministic FCI energy with submillihartree accuracy. What is, perhaps, more interesting is the fact that this kind of accuracy was obtained with critical walker populations, which define the computational bottleneck of FCIQMC, less than the total number of Slater determinants afforded by the one-electron basis,  $N_{\text{FCI}}$ . This observation suggests that FCIQMC is capable of providing FCI-quality results without having to sample the entire many-electron Hilbert space. Although in many cases  $f_c \equiv \frac{N_c}{N_{\text{FCI}}} \ll 1$ , in the original FCIQMC work [260] there were a few challenging situations in which  $f_c$  was as large as 0.9, implying that for some systems a population of walkers comparable to the dimensionality of the FCI problem was required for the convergence of the correct sign structure of the wavefunction. In addition, despite the fact that the critical number of walkers was always less than the dimension of the many-electron Hilbert space,  $N_c < N_{\text{FCI}}$ ,

it still grew exponentially with the size of the system. These observations forced Alavi and co-workers to remark that the FCIQMC approach should be “perhaps best thought of as an alternative method to FCI, with a smaller prefactor (proportional to  $f_c$ ), which in some cases is substantially so”. They also forced them to work on improving the FCIQMC algorithm.

Alavi and co-workers addressed the above issues by augmenting the original FCIQMC approach with an initiator criterion, giving rise to the initiator FCIQMC (*i*-FCIQMC) scheme [261, 262]. To be precise, at a given time step, out of all Slater determinants inhabited by walkers only a subset of them, called initiators, are allowed to spawn progeny to unpopulated Slater determinants. For a Slater determinant to become an initiator, it has to be populated by more than a preset value of walkers, denoted  $n_a$ . During the imaginary-time propagation, the population of walkers inhabiting each Slater determinant changes, meaning that the set of initiator determinants is dynamically updated. In fact, as the total number of walkers grows during a simulation, the *i*-FCIQMC approach eventually becomes equivalent to FCIQMC, since each sampled determinant, which contributes to the wavefunction, will eventually have a walker population greater than  $n_a$ . Of course, the same applies if one sets  $n_a = 0$ , meaning that as long as a determinant is inhabited by at least one signed walker it can act as an initiator. As a consequence of the initiator approach, the total number of walkers required for *i*-FCIQMC to achieve the same level of accuracy as the original FCIQMC methodology was significantly reduced, sometimes by a few orders of magnitude, compared to the original algorithm discussed in Reference [260]. The success of *i*-FCIQMC can be traced to the fact that determinants that are populated by more than  $n_a$  walkers have a much higher probability of having a converged sign structure. Taking into account that the sign of a child walker depends, in addition to the matrix elements of the Hamiltonian, on the sign of the parent walker, the initiator approach allows for the sign-coherent sampling of the many-electron Hilbert space, minimizing the role of annihilation.

Having said all of the above, the initiator approach may introduce a systematic error related to the undersampling of non-initiator determinants. This is not a major concern for

small to medium size molecules, but becomes a potential issue in larger systems whose many-electron Hilbert spaces are characterized by immense dimensionalities. In fact, in some cases *i*-FCIQMC fails to converge to the exact, FCI, energetics as a consequence of the initiator bias (see, for example, References [310] and [263]). To ameliorate the systematic error introduced by the initiator approximation, Alavi and co-workers modified the algorithm driving the walker population dynamics, such that for each non-initiator Slater determinant  $|\Phi_K\rangle$  a local, reduced, energy shift  $S_K$  is applied by scaling the full energy shift  $S$  [263, 264]. The scaling factor depends on the ratio of accepted spawning events from  $|\Phi_K\rangle$  over the total attempted spawns from the same Slater determinant (see Reference [263] for the details). Once a Slater determinant accumulates more than  $n_a$  walkers, the full shift  $S$  is applied. This means that as the total walker population grows, one always recovers the original FCIQMC algorithm. This novel FCIQMC approach is called adaptive-shift FCIQMC (AS-FCIQMC) and has been shown to significantly reduce the errors introduced by the initiator approximation [263, 264]. Furthermore, it has been demonstrated that one can obtain near-exact energetics with relatively modest total walker populations, even when the many-electron Hilbert space is spanned by about  $10^{35}$  determinants [263, 266].

Having briefly discussed the intricacies of the FCIQMC, *i*-FCIQMC, and AS-FCIQMC approaches, we now proceed to the recently proposed CAD-FCIQMC methodology [265, 266]. As already mentioned above, CAD-FCIQMC accelerates convergence toward FCI energetics by solving a CCSD-like system of equations, Equations (3.29) and (3.30), in which singly and doubly excited clusters, needed to determine the energy, Equation (3.28), are iterated in the presence of their three- and four-body counterparts extracted from FCIQMC propagations. Before performing cluster analysis of a given FCIQMC wavefunction, we need to express it using intermediate normalization,

$$\left| \Psi_0^{(\text{MC})}(\tau) \right\rangle = [\mathbf{1} + \sum_{n=1}^N C_n^{(\text{MC})}(\tau)] |\Phi\rangle. \quad (3.36)$$

To that end, the walker population of each Slater determinant is divided by the walker population of the reference determinant  $|\Phi\rangle$  (in our case, the RHF determinant). The cor-

responding CI excitation operators are expressed as

$$C_n^{(\text{MC})}(\tau) = \sum_K c_K(\tau) E_K, \quad c_K(\tau) = \frac{N_K}{N_0}, \quad (3.37)$$

where  $E_K$  is the elementary ph excitation operator that generates  $|\Phi_K\rangle$  upon acting on the reference determinant  $|\Phi\rangle$ ,  $E_K |\Phi\rangle = |\Phi_K\rangle$ . Subsequently, we cluster analyze the FCIQMC wavefunction by rewriting it in a CC-like form,

$$|\Psi_0^{(\text{MC})}(\tau)\rangle = \exp \left[ \sum_{n=1}^N T_n^{(\text{MC})} \right] |\Phi\rangle, \quad (3.38)$$

and use Equation (3.16) for  $m = 1-4$ , resulting in

$$\begin{aligned} T_1^{(\text{MC})} &= C_1^{(\text{MC})}, \\ T_2^{(\text{MC})} &= C_2^{(\text{MC})} - \frac{1}{2} \left( C_1^{(\text{MC})} \right)^2, \\ T_3^{(\text{MC})} &= C_3^{(\text{MC})} - C_1^{(\text{MC})} C_2^{(\text{MC})} + \frac{1}{3} \left( C_1^{(\text{MC})} \right)^3, \\ T_4^{(\text{MC})} &= C_4^{(\text{MC})} - C_1^{(\text{MC})} C_3^{(\text{MC})} - \frac{1}{2} \left( C_2^{(\text{MC})} \right)^2 + \left( C_1^{(\text{MC})} \right)^2 C_2^{(\text{MC})} - \frac{1}{4} \left( C_1^{(\text{MC})} \right)^4, \end{aligned} \quad (3.39)$$

where the “(MC)” superscripts emphasize the origin of the amplitudes defining the various excitation operators. In writing Equation (3.39), we dropped the explicit imaginary-time dependence of the operators for the sake of clarity. As might have been anticipated, all one needs to extract  $T_3^{(\text{MC})}(\tau)$  and  $T_4^{(\text{MC})}(\tau)$  is the knowledge of the FCIQMC wavefunction up to quadruples ( $C_4^{(\text{MC})}$  contributions). This significantly simplifies the cluster analysis algorithm and reduces the memory and storage requirements.

The various steps involved in a CAD-FCIQMC calculation are summarized as follows. First, we initialize a FCIQMC simulation by placing a certain number of walkers on the reference determinant  $|\Phi\rangle$ . At a given time  $\tau$ , we extract  $C_1^{(\text{MC})}(\tau)$ ,  $C_2^{(\text{MC})}(\tau)$ ,  $C_3^{(\text{MC})}(\tau)$ , and  $C_4^{(\text{MC})}(\tau)$  using Equation (3.37) from the instantaneous FCIQMC wavefunction,  $|\Psi^{(\text{MC})}(\tau)\rangle$ . Subsequently, we use Equation (3.39) to perform cluster analysis of the FCIQMC wavefunction at time  $\tau$  and extract the corresponding triply and quadruply excited clusters, *i.e.*,

$T_3^{(\text{MC})}(\tau)$  and  $T_4^{(\text{MC})}(\tau)$  components, respectively. In the next step, we solve the CCSD-like system of equations, Equations (3.29) and (3.30), in the presence of  $T_3^{(\text{MC})}(\tau)$  and  $T_4^{(\text{MC})}(\tau)$  to determine the one- and two-body clusters and the ground-state correlation energy  $\Delta E_0(\tau)$ . Finally, we check the convergence by recomputing  $T_1$ ,  $T_2$ , and  $\Delta E_0$  in the presence of  $T_3^{(\text{MC})}(\tau')$  and  $T_4^{(\text{MC})}(\tau')$  extracted from a FCIQMC wavefunction at time  $\tau' > \tau$ . It is guaranteed that in the infinite imaginary-time limit  $\Delta E_0(\tau)$  approaches the exact, FCI, ground-state correlation energy. The above procedure is given in graphical form in Figure 3.8.

It has been demonstrated in our work [265, 266] that the CAD-FCIQMC methodology is capable of producing FCI-quality energetics out of the early stages of FCIQMC propagations, even in challenging situations involving electronic quasi-degeneracies, such as those characterizing the  $C_{2v}$ -symmetric double bond dissociation of  $\text{H}_2\text{O}$  [265]. However, CAD-FCIQMC, as described above, breaks down in the presence of strong many-electron correlation effects. A simple inspection of Equations (3.29) and (3.30) reveals the origin behind this failure. At  $\tau = 0$ , the FCIQMC wavefunction is equivalent to the reference Slater determinant, usually the RHF determinant  $|\Phi\rangle$ . Thus,  $T_3^{(\text{MC})}(\tau = 0) = T_4^{(\text{MC})}(\tau = 0) = 0$  and the CAD-FCIQMC approach reduces to CCSD. Considering the poor, sometimes even singular, behavior of CCSD in the strong correlation regime, it is natural that CAD-FCIQMC may struggle with strongly correlated systems involving large numbers of strongly correlated electrons.

In this dissertation, we extend the CAD-FCIQMC approach to the strong correlation regime by merging it with the ACP approaches. As discussed in the previous section, the key to tackling strong many-electron correlation effects lies in the  $\frac{1}{2}T_2^2$  contributions to the CC equations projected on doubles. To that end, in order to incorporate the ACP ideas within the CAD-FCIQMC framework, we repartition Equation (3.30) such that selected



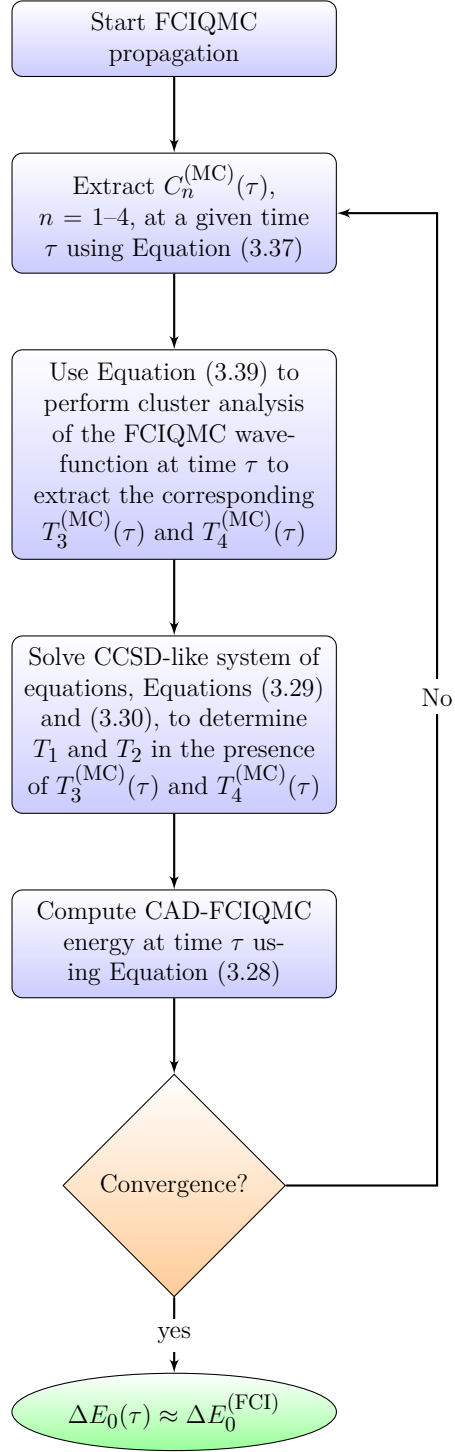


Figure 3.8: Flowchart outlining the key steps of the CAD-FCIQMC algorithm.

coupled-pair contributions are extracted from FCIQMC as well,

$$\begin{aligned} \langle \Phi_{ij}^{ab} | \left[ H_N \left( 1 + T_1 + T_2 + \frac{1}{2} T_1^2 + T_3^{(\text{MC})} + T_1 T_2 + \frac{1}{3!} T_1^3 \right. \right. \\ \left. \left. + T_4^{(\text{MC})} + T_1 T_3^{(\text{MC})} + \frac{1}{2} T_1^2 T_2 + \frac{1}{4!} T_1^4 \right) \right]_C | \Phi \rangle + \sum_i^5 \left[ \xi_i \Lambda_i^{(2)} + (1 - \xi_i) \Lambda_i^{(2),(\text{MC})} \right] = 0. \end{aligned} \quad (3.40)$$

In other words, we assume that in addition to  $T_3$  and  $T_4$ , which are extracted from the FCIQMC wavefunction as summarized above, we extract selected  $\frac{1}{2}T_2^2$  diagrams responsible for weak correlations from FCIQMC as well (they are marked in Equation (3.40) as  $\Lambda_i^{(2),(\text{MC})}$  terms). Like its CAD-FCIQMC predecessor of Reference [265], this new scheme is guaranteed to provide numerically exact, FCI, energetics in the infinite imaginary-time limit. Furthermore, it offers an additional flexibility that extends its application to the strong correlation regime. To be precise, the success behind this modification to the original CAD-FCIQMC algorithm lies in the fact that the  $\frac{1}{2}T_2^2$  part that is responsible for good behavior in strongly correlated systems is treated deterministically, while its complement, which is, more or less, the weakly correlated part of  $\frac{1}{2}T_2^2$ , is extracted from FCIQMC. For example, setting  $\xi_1 = 1$ ,  $\xi_2 = 0$ ,  $\xi_3 = \xi_4 = \frac{1}{2}$ , and  $\xi_5 = 0$  gives rise to the CAD-FCIQMC[1,(3+4)/2] variant, where the numbers in square brackets designate the  $\frac{1}{2}T_2^2$  diagrams, shown in Figure 3.5 in the case of the spin-adapted CC formalism, that are treated deterministically. Consequently, the starting point of CAD-FCIQMC[1,(3 + 4)/2] is ACCSD( $1, \frac{3+4}{2}$ )  $\equiv$  DCSD, which is already well-behaved in the presence of strong correlations. The remaining many-electron correlation effects are extracted from FCIQMC. Within this framework, the original CAD-FCIQMC approach is designated as CAD-FCIQMC[1–5].

## CHAPTER 4

### NUMERICAL RESULTS

#### 4.1 Application of the Approximate Coupled-Pair Methods with an Active-Space Treatment of Three-Body Clusters to Model Metal–Insulator Transitions

We begin the discussion of the numerical results by assessing the performance of the deterministic ACP methods, including the ACCSD(1,3), ACCSD(1,4), ACCSD( $1, \frac{3+4}{2}$ ), and ACCSD( $1, 3 \times \frac{n_o}{n_o+n_u} + 4 \times \frac{n_u}{n_o+n_u}$ ) approaches and their active-space and full triples extensions, developed and implemented in this dissertation project, in challenging situations involving strong many-electron correlation effects. In particular, we examine their ability to reproduce the exact or nearly exact PECs characterizing the symmetric dissociations of the  $H_6$  and  $H_{10}$  rings and the  $H_{50}$  linear chain of equidistant hydrogen atoms, in which the degree of entanglement of the electrons is continuously varied as the systems depart their weakly correlated metallic phases around the respective potential minima and approach the insulating atomization regions governed by strong correlations of all electrons present in the system. To facilitate the discussion and emphasize the power of the ACP methods, without and with the connected triples, in properly handling strong correlations, we also provide the pertinent CCSD, CCSDt, and CCSDT PECs.

All of the CC calculations reported in this subsection were based on RHF reference functions. The CCSD, CCSDt, and full CCSDT computations were performed using the active-space CC codes developed by our group [144, 161, 162] that have been recently incorporated in the official GAMESS package [307–309]. The various ACCSD, ACCSDt, and full ACCSDT calculations were carried out using a local version of GAMESS, where we made suitable modifications in our CCSD, CCSDt, and CCSDT routines. For the  $H_6$  and  $H_{10}$  rings, we employed the largest basis sets that would allow us to perform the exact, FCI

computations, namely, cc-pVTZ [276] in the case of  $H_6$  and DZ [311, 312] in the  $H_{10}$  case. The pertinent FCI calculations were carried out using the determinantal FCI code [313–315] available in GAMESS. When considering the symmetric dissociation of the  $H_{50}$  linear chain, we used the minimum STO-6G [306] basis set, since the nearly exact LDMRG(500)/STO-6G results are available for it [175] (in this case, FCI calculations, even with minimum basis sets, are not possible). The active-space CC approaches, including CCSDt and ACCSDt, employed active spaces that consisted of the orbitals associated with the  $1s$  shells of the hydrogen atoms, *i.e.*, three active occupied and three active unoccupied orbitals for the  $H_6$  ring and 5 active occupied and 5 active unoccupied orbitals in the case of the  $H_{10}$  ring. In the case of the  $H_{50}$  linear chain, where we used the minimum STO-6G basis set, the only meaningful active space is that incorporating all occupied and unoccupied orbitals, resulting in computations with a full treatment of connected triples. Thus, in this case, we performed the CCSDT and ACCSDT computations, in addition to CCSD and ACCSD. Due to the fact that the  $H_{50}$ /STO-6G system is characterized by  $n_o = n_u$ , meaning an approximate ph symmetry, we only considered the ACCSD( $1, \frac{3+4}{2}$ ) and ACCSDT( $1, \frac{3+4}{2}$ ) methods using  $\lambda = \frac{n_o}{n_o+n_u}$  in Equation (3.23). All of our calculations for the symmetric dissociations of the  $H_6$  and  $H_{10}$  rings employed the following grid of internuclear separations between neighboring hydrogen atoms: 0.6, 0.7, 0.8, 0.9, 1.0, 1.1, 1.2, 1.3, 1.4, 1.5, 1.6, 1.7, 1.8, 1.9, 2.0, 2.1, 2.2, 2.3, 2.4, and 2.5 Å. The PECs characterizing the symmetric dissociation of the  $H_{50}$  linear chain were calculated at the geometries reported in Reference [175], namely, 1.0, 1.2, 1.4, 1.6, 1.8, 2.0, 2.4, 2.8, 3.2, 3.6, and 4.2 bohr.

We begin by examining the  $D_{6h}$ -symmetric dissociation of the six-membered hydrogen ring, as described by the cc-pVTZ basis set. The ground-state PECs of the  $H_6$ /cc-pVTZ system resulting from the conventional CCSD approach, the various ACP methods, including ACCSD(1,3), ACCSD(1,4), ACCSD( $1, \frac{3+4}{2}$ ), and ACCSD( $1, 3 \times \frac{n_o}{n_o+n_u} + 4 \times \frac{n_u}{n_o+n_u}$ ), their active-space and full triples counterparts, and the exact FCI diagonalization are presented in Tables 4.1–4.3 and Figure 4.1.

As shown in Tables 4.1–4.3 and Figure 4.1, the CCSD approach and even the active-space-based CCSDt scheme and its parent CCSDT counterpart break down rather quickly as the distance between neighboring hydrogen atoms,  $R_{\text{H-H}}$ , increases. In fact, CCSD already overcorrelates around  $R_{\text{H-H}} = 2.0 \text{ \AA}$ , *i.e.*, at about twice the equilibrium  $R_{\text{H-H}}$  distance, by almost  $25 \text{ mE}_h$ , when compared to the exact FCI results. As one stretches the  $R_{\text{H-H}}$  distance even further, the deviation from FCI dramatically increases, resulting in an unphysical hump and the PEC going downhill, so that when the largest H–H distance considered in this work, namely,  $R_{\text{H-H}} = 2.5 \text{ \AA}$ , is considered, the unsigned difference between the CCSD and FCI energies reaches a gargantuan value of more than  $237 \text{ mE}_h$ . Adding triples on top of CCSD using the full CCSDT approach results in a significant improvement of the PEC around the equilibrium geometry, with errors relative to the FCI energetics of about  $0.1 \text{ mE}_h$ . However, as one approaches the strong correlation regime, CCSDT eventually follows the same catastrophic path as CCSD. On a side note, it is worth mentioning that the active-space CCSDt approach, using an active space comprised of the six  $1s$  orbitals of the individual H atoms, faithfully reproduces the parent CCSDT energetics, with deviations from CCSDT not exceeding  $\sim 2 \text{ mE}_h$  (see Tables 4.2 and 4.3), but at a small fraction of the computational effort. To be precise, the CPU time of a CCSDt iteration for the  $\text{H}_6/\text{cc-pVTZ}$  system was 6 s, using a single core and without taking advantage of point group symmetry. This should be contrasted with the 98 s per CCSDT iteration ran the same way as the CCSDt computation.

A quick inspection of Figure 4.1 reveals that all ACP methods examined in this study, without and with the connected triples, provide qualitatively correct PECs for the  $D_{6h}$ -symmetric dissociation of the  $\text{H}_6/\text{cc-pVTZ}$  ring, *i.e.*, they do not overcorrelate as one approaches the strong correlation limit and remain close to FCI. Focusing on the ACP methodologies with up to two-body clusters, meaning the ACCSD approaches, the ACCSD(1,3) scheme, where  $\lambda = 1$  in Equation (3.23), performs the best, generating a PEC that closely reproduces its FCI counterpart, as illustrated by the small mean unsigned error (MUE) and mean signed error (MSE) values relative to FCI of  $0.675 \text{ mE}_h$  and  $-0.311 \text{ mE}_h$ , respec-

tively (see Table 4.1). At the other end of the spectrum, the ACCSD(1,4) approach, where one sets  $\lambda = 0$  in Equation (3.23), does not reproduce the FCI energetics as good as the ACCSD(1,3) variant, having MUE and MSE values relative to FCI of 9.349 mE<sub>h</sub> and 9.349 mE<sub>h</sub>, respectively. As one might have anticipated, the ACCSD(1,  $\frac{3+4}{2}$ )  $\equiv$  DCSD method, which treats diagrams D3 and D4 shown in Figure 3.5 on an equal footing by setting  $\lambda = 0.5$  in Equation (3.23), produces a PEC that is more or less the average of the ACCSD(1,3) and ACCSD(1,4) ones [see panels (a) and (d) of Figure 4.1 and Table 4.1]. Furthermore, the ACCSD(1,  $3 \times \frac{n_o}{n_o+n_u} + 4 \times \frac{n_u}{n_o+n_u}$ ) PEC characterizing the symmetric dissociation of the H<sub>6</sub>/cc-pVTZ system is almost identical, yet slightly better in reproducing the exact FCI data, to that resulting from the ACCSD(1,4) calculations. Taking into account the size of the cc-pVTZ basis set, where  $n_o = 3$  and  $n_u = 81 = 27n_o$ , this is not a surprise, since, by construction, the ACCSD(1,  $3 \times \frac{n_o}{n_o+n_u} + 4 \times \frac{n_u}{n_o+n_u}$ ) approach converges to ACCSD(1,4) with increasing basis set size ( $\frac{n_u}{n_o}$  approaching  $\infty$ ).

From the above discussion, one might crown the ACCSD(1,3) scheme the best ACP approach examined in this dissertation. However, we believe that the excellent performance of the ACCSD(1,3) method in producing the FCI-quality energetics for the metal–insulator transition in the H<sub>6</sub>/cc-pVTZ system is rather fortuitous. As already mentioned, the ACP methods are very effective in recovering non-dynamical correlation effects by taking advantage of various diagram cancellations in the CCD/CCSD equations projected on doubly excited configuration state functions. However, these diagram cancellations do not describe the  $T_3$  physics, needed to capture dynamical correlations and obtain a quantitative description of realistic systems described by *ab initio* Hamiltonians. Before proceeding to the detailed discussion of the performance of the various ACP methods with the connected triply excited clusters considered in this work, we note that the ACP approaches with an active-space treatment of  $T_3$  components, *i.e.*, the ACCSDt schemes, closely reproduce their parent full triples ACCSDT counterparts. At the same time, the active-space triples framework replaces the expensive  $n_o^3 n_u^5$  computational time steps associated with a full treatment of connected

triply excited clusters by the relatively inexpensive  $N_o N_u n_o^2 n_u^4$  ones, *i.e.*, the computational costs are reduced to those of CCSD times a small prefactor on the order of the number of singles in the active space. For example, the 98 s per single ACCSDT( $1, 3 \times \frac{n_o}{n_o+n_u} + 4 \times \frac{n_u}{n_o+n_u}$ ) iteration, ran on a single core using  $C_1$  point group symmetry, are reduced to just 6 s when the active-space triples ACCSDt( $1, 3 \times \frac{n_o}{n_o+n_u} + 4 \times \frac{n_u}{n_o+n_u}$ ) approach is employed, consistent with the computational time savings observed in the CCSDT/CCSDt case. This is an important observation, especially when one realizes that the ultimate goal of our effort in the long term is to extend the ACP approaches to large systems, allowing us to study strongly correlated materials.

The inclusion of connected triples on top of the various ACP schemes examined in this dissertation results in a dramatic improvement of the ACCSD(1,4) and ACCSD( $1, 3 \times \frac{n_o}{n_o+n_u} + 4 \times \frac{n_u}{n_o+n_u}$ ) energetics when compared to the exact, FCI, data. To be precise, the MSE values characterizing the  $H_6$ /cc-pVTZ PECs obtained with the active-space-based ACCSDt(1,4) and ACCSDt( $1, 3 \times \frac{n_o}{n_o+n_u} + 4 \times \frac{n_u}{n_o+n_u}$ ) approaches are 2.129 mE<sub>h</sub> and 1.818 mE<sub>h</sub>, respectively (*cf.* Table 4.2). As a result, the ACCSDt(1,4) and, especially, ACCSDt( $1, 3 \times \frac{n_o}{n_o+n_u} + 4 \times \frac{n_u}{n_o+n_u}$ ) PECs can be hardly distinguished from the FCI one. To better appreciate the significance of this finding, we compare the ACCSDt( $1, 3 \times \frac{n_o}{n_o+n_u} + 4 \times \frac{n_u}{n_o+n_u}$ ) and FCI CPU timings, which are 6 s per iteration on a single core, without taking advantage of point group symmetry, in the former case, and more than 7 h per iteration, on the same core, in the latter case, in which we used the  $D_{2h}$  symmetry in the calculations. The full treatment of three-body clusters further reduces the already small deviations from FCI even further, as illustrated by the MSE values of 1.189 mE<sub>h</sub>, for ACCSDT(1,4), and 0.875 mE<sub>h</sub>, in the case of ACCSDT( $1, 3 \times \frac{n_o}{n_o+n_u} + 4 \times \frac{n_u}{n_o+n_u}$ ) (see Table 4.3). On the other hand, the PECs characterizing the symmetric dissociation of the  $H_6$ /cc-pVTZ ring generated by the connected-triples extensions of the ACCSD(1,3) and ACCSD( $1, \frac{3+4}{2}$ ) approaches are of a poorer quality when compared to their  $\lambda = 0$  [ACCSDt(1,4)/ACCSDT(1,4)] and  $\lambda = \frac{n_o}{n_o+n_u}$  [ACCSDt( $1, 3 \times \frac{n_o}{n_o+n_u} + 4 \times \frac{n_u}{n_o+n_u}$ )/ACCSDT( $1, 3 \times \frac{n_o}{n_o+n_u} + 4 \times \frac{n_u}{n_o+n_u}$ )] counterparts.

Tables 4.1–4.3 reveal the following relationship regarding the ability of the various ACP schemes considered here to reproduce the FCI energetics:  $\text{ACCSd}(1,3) > \text{ACCSdt}(1,3) \approx \text{ACCSdt}(1,3)$  and  $\text{ACCSd}(1, \frac{3+4}{2}) > \text{ACCSdt}(1, \frac{3+4}{2}) \approx \text{ACCSdt}(1, \frac{3+4}{2})$ . This implies that the  $\text{ACCSd}(1,3)$  and  $\text{ACCSd}(1, \frac{3+4}{2})$  variants of ACP approaches are not systematically improvable, contrary to their  $\text{ACCSd}(1,4)$  and  $\text{ACCSd}(1, 3 \times \frac{n_o}{n_o+n_u} + 4 \times \frac{n_u}{n_o+n_u})$  counterparts, where the following accuracy patterns are observed:  $\text{ACCSd}(1,4) < \text{ACCSdt}(1,4) \approx \text{ACCSdt}(1,4)$  and  $\text{ACCSd}(1, 3 \times \frac{n_o}{n_o+n_u} + 4 \times \frac{n_u}{n_o+n_u}) < \text{ACCSdt}(1, 3 \times \frac{n_o}{n_o+n_u} + 4 \times \frac{n_u}{n_o+n_u}) \approx \text{ACCSdt}(1, 3 \times \frac{n_o}{n_o+n_u} + 4 \times \frac{n_u}{n_o+n_u})$ . An additional important observation, in favor of the  $\lambda = 0$  and  $\lambda = \frac{n_o}{n_o+n_u}$  variants, is that the  $\text{ACCSd}(1,4)$  and  $\text{ACCSd}(1, 3 \times \frac{n_o}{n_o+n_u} + 4 \times \frac{n_u}{n_o+n_u})$  approaches recover 94–98% of the exact, FCI, correlation energy characterizing the  $D_{6h}$ -symmetric dissociation of the  $\text{H}_6/\text{cc-pVTZ}$  ring and their connected triples extensions are practically exact, consistently retrieving about 99% of the FCI correlation energy.

To further explore the usefulness of ACP methods, especially those that incorporate  $T_3$  physics, in faithfully reproducing FCI-level energetics in the presence of strong non-dynamical electron correlation effects, we studied the  $D_{10h}$ -symmetric dissociation of the ten-membered hydrogen ring as described by the DZ basis set. This challenging system involves the entanglement of 10 electrons, which translates into an about 67% increase in the number of strongly correlated electrons compared to the smaller  $\text{H}_6$  hydrogen cluster. This has a severe effect on the performance of the CCSD, CCSDt, and CCSDT approaches, which, as illustrated in Tables 4.4–4.6 and Figure 4.2, fail catastrophically; they overcorrelate rather quickly and no convergence is obtained for distances between neighboring H atoms beyond 1.7 Å. Nevertheless, as was the case with the smaller  $\text{H}_6$  ring, all ACP methods examined in this work, without and with the connected triples, produce qualitatively correct PECs for the metal–insulator transition in the challenging  $\text{H}_{10}$  cluster (see Figure 4.2). Even though the DZ basis set, where  $n_o = 5$  and  $n_u = 15$ , is rather small compared to that used in the  $\text{H}_6$  case, which translates into the various ACP schemes behaving more or less similarly (*cf.* Tables 4.4–4.6 and Figure 4.2), we still observe the same patterns regarding the



ability of the ACP methods, without and with the connected triples, to reproduce the FCI energetics. For example, focusing on the ACP approaches with up to two-body clusters, the ACCSD(1,3) energetics are the closest to the FCI ones ( $\text{MUE} = \text{MSE} = 12.572 \text{ mE}_h$ ), followed by ACCSD( $1, \frac{3+4}{2}$ ) ( $\text{MUE} = \text{MSE} = 14.315 \text{ mE}_h$ ), ACCSD( $1, 3 \times \frac{n_o}{n_o+n_u} + 4 \times \frac{n_u}{n_o+n_u}$ ) ( $\text{MUE} = \text{MSE} = 14.980 \text{ mE}_h$ ), and ACCSD(1,4) ( $\text{MUE} = \text{MSE} = 15.505 \text{ mE}_h$ ), as was the case with the smaller  $\text{H}_6$  ring. The inclusion of a subset of connected triple excitations, selected via an active space of 1s orbitals, results in a dramatic improvement of the results, as illustrated by the about 2–4 times reduction in the MUE and MSE values and favors the ACCSDt( $1, 3 \times \frac{n_o}{n_o+n_u} + 4 \times \frac{n_u}{n_o+n_u}$ ) scheme (see Tables 4.4 and 4.5). Consistent with the  $\text{H}_6$  case, ordering the various active-space triples ACP approaches based on their ability to reproduce the FCI data yields  $\text{ACCSDt}(1, 3 \times \frac{n_o}{n_o+n_u} + 4 \times \frac{n_u}{n_o+n_u}) > \text{ACCSDt}(1, 4) > \text{ACCSDt}(1, \frac{3+4}{2}) > \text{ACCSDt}(1, 3)$ , with their MUE and MSE values being  $3.770 \text{ mE}_h$  and  $-3.770 \text{ mE}_h$  for ACCSDt( $1, 3 \times \frac{n_o}{n_o+n_u} + 4 \times \frac{n_u}{n_o+n_u}$ ),  $3.790 \text{ mE}_h$  and  $-3.790 \text{ mE}_h$  for ACCSDt(1,4),  $4.110 \text{ mE}_h$  and  $-4.110 \text{ mE}_h$  for ACCSDt( $1, \frac{3+4}{2}$ ), and  $5.793 \text{ mE}_h$  and  $-5.793 \text{ mE}_h$  in the case of ACCSDt(1,3). The full inclusion of three-body clusters does not change the scenery, since, due to the small size of the DZ basis set, the active-space approaches already recover the lion’s share of  $T_3$  physics. Finally, the ACCSD(1,4) and ACCSD( $1, 3 \times \frac{n_o}{n_o+n_u} + 4 \times \frac{n_u}{n_o+n_u}$ ) schemes consistently recover about 96% of the exact, FCI, correlation energies characterizing the  $D_{10h}$ -symmetric dissociation of  $\text{H}_{10}/\text{DZ}$ , with their connected-triples counterparts being virtually exact, recovering  $\sim 99\%$  of the FCI correlation energies, similar to the smaller  $\text{H}_6$  ring. Therefore, the  $\text{H}_{10}/\text{DZ}$  results reinforce our conclusion that the ACCSD(1,4) and ACCSD( $1, 3 \times \frac{n_o}{n_o+n_u} + 4 \times \frac{n_u}{n_o+n_u}$ ) methods are systematically improvable by the inclusion of connected triples and exhibit the best performance in reproducing the corresponding FCI PECs, once connected triples are included.

Having established the ability of the various ACP approaches, especially those incorporating three-body clusters, to closely reproduce the FCI PECs characterizing the symmetric dissociation of the six- and ten-membered hydrogen rings, we now proceed to examine the

symmetric dissociation of the  $H_{50}$  linear chain into individual hydrogen atoms, which is a problem that involves the entanglement of 50 strongly correlated electrons. As already mentioned above, even when a minimum basis set, such as STO-6G, is employed, the sheer dimensionality of the many-electron Hilbert space, which is spanned by  $1.21 \times 10^{27}$  singlet-spin-adapted configuration state functions, renders FCI calculations prohibitively expensive. As mentioned earlier, in the case of the  $H_{50}$  linear chain, we relied on the nearly exact LDMRG(500)/STO-6G data of Hachmann *et al.* [175] in assessing the performance of the ACP schemes, without and with the connected triples. However, we recall that the various ACP methodologies provide essentially identical results when applied to hydrogen clusters described by minimum basis sets, as a consequence of the approximate ph symmetry. Furthermore, the smallest meaningful active space in the case of hydrogen clusters dissociating into individual atoms is comprised of the  $1s$  orbitals of the hydrogen atoms, suggesting that only full triples approaches can be applied when minimum basis sets are employed. We, thus, examined only the  $ACCS(1, 3 \times \frac{n_o}{n_o+n_u} + 4 \times \frac{n_u}{n_o+n_u})$  and  $ACCS(1, 3 \times \frac{n_o}{n_o+n_u} + 4 \times \frac{n_u}{n_o+n_u})$  approaches in properly describing the symmetric dissociation of the  $H_{50}$ /STO-6G linear chain, which in this case, where  $n_o = n_u$ , are equivalent to  $ACCS(1, \frac{3+4}{2}) \equiv DCSD$  and  $ACCS(1, \frac{3+4}{2})$ .

Figure 4.3 shows the PECs characterizing the symmetric dissociation of the  $H_{50}$  linear chain into 50 hydrogen atoms using CCSD, CCSDT,  $ACCS(1, 3 \times \frac{n_o}{n_o+n_u} + 4 \times \frac{n_u}{n_o+n_u})$ , and  $ACCS(1, 3 \times \frac{n_o}{n_o+n_u} + 4 \times \frac{n_u}{n_o+n_u})$ , along with the nearly exact LDMRG(500) data of Reference [175]. A quick inspection of Figure 4.3 immediately reveals the complete breakdown of the conventional CCSD and CCSDT approaches, which fail to converge even for geometries in close proximity to the equilibrium one. On the other hand, the  $ACCS(1, 3 \times \frac{n_o}{n_o+n_u} + 4 \times \frac{n_u}{n_o+n_u})$  scheme and its connected triples extension provide qualitatively correct PECs, closely reproducing the LDMRG(500) one. This is a remarkable observation, especially when one realizes that the number of strongly correlated electrons is five times greater than in the already challenging  $H_{10}$  ring. Focusing on the  $ACCS(1, 3 \times \frac{n_o}{n_o+n_u} + 4 \times \frac{n_u}{n_o+n_u})$

energetics reported in Table 4.7, we see that the MSE and MUE values with respect to the nearly exact LDMRG(500) data of Reference [175] are 51.33 mE<sub>h</sub>. Even though this is larger than the MSE values relative to FCI characterizing the ACCSD( $1, 3 \times \frac{n_o}{n_o+n_u} + 4 \times \frac{n_u}{n_o+n_u}$ ) PECs in the H<sub>6</sub> and H<sub>10</sub> cases, this is a very promising result. Even in the H<sub>50</sub> torture test the ACCSD( $1, 3 \times \frac{n_o}{n_o+n_u} + 4 \times \frac{n_u}{n_o+n_u}$ ) approach captures about 97% of the nearly exact, DMRG, correlation energies. This is an important observation, since the ACCSD( $1, 3 \times \frac{n_o}{n_o+n_u} + 4 \times \frac{n_u}{n_o+n_u}$ ) scheme consistently recovered approximately 96% of the exact or nearly exact correlation energies for all examined systems, *i.e.*, independent of the number of strongly correlated electrons or the size of the basis set. Furthermore, and more importantly, once three-body clusters are included, there is a significant improvement of the ACCSD( $1, 3 \times \frac{n_o}{n_o+n_u} + 4 \times \frac{n_u}{n_o+n_u}$ ) total electronic energies, even when the symmetric dissociation of the H<sub>50</sub> linear chain is considered. To be precise, the ACCSDT( $1, 3 \times \frac{n_o}{n_o+n_u} + 4 \times \frac{n_u}{n_o+n_u}$ ) PEC can hardly be distinguished from the nearly exact LDMRG(500) one, reducing the MUE and MSE values of 51.33 mE<sub>h</sub> and 51.33 mE<sub>h</sub> in the case of ACCSD( $1, 3 \times \frac{n_o}{n_o+n_u} + 4 \times \frac{n_u}{n_o+n_u}$ ) to 19.14 mE<sub>h</sub> and -6.08 mE<sub>h</sub>, respectively, when the ACCSDT( $1, 3 \times \frac{n_o}{n_o+n_u} + 4 \times \frac{n_u}{n_o+n_u}$ ) approach is used. This is yet another example that showcases the importance of  $T_3$  physics within the ACP framework in attaining a quantitative description of strongly correlated systems.

Table 4.1: A comparison of the energies resulting from the various CC approaches with singles and doubles and the exact FCI data for the symmetric dissociation of the H<sub>6</sub>/cc-pVTZ ring at selected bond distances between neighboring H atoms  $R_{\text{H-H}}$  (in Å).<sup>a</sup>

$R_{\text{H-H}}$	CCSD	ACCS				FCI
		(1,3)	$(1, \frac{3+4}{2})$	$(1, 3 \times \frac{n_o}{n_o+n_u} + 4 \times \frac{n_u}{n_o+n_u})$	(1,4)	
0.6	3.422	−0.242	1.557	3.144	3.262	−2.858958
0.7	3.593	−0.320	1.618	3.321	3.448	−3.176147
0.8	3.823	−0.417	1.695	3.541	3.679	−3.331124
0.9	4.103	−0.534	1.788	3.809	3.959	−3.396176
1.0	4.424	−0.665	1.906	4.132	4.297	−3.410069
1.1	4.774	−0.805	2.059	4.522	4.705	−3.394673
1.2	5.139	−0.944	2.263	5.003	5.206	−3.362943
1.3	5.489	−1.068	2.543	5.608	5.833	−3.322850
1.4	5.758	−1.156	2.934	6.381	6.634	−3.279466
1.5	5.802	−1.175	3.479	7.377	7.662	−3.236119
1.6	5.309	−1.088	4.219	8.638	8.960	−3.195040
1.7	3.647	−0.865	5.165	10.165	10.529	−3.157716
1.8	−0.380	−0.508	6.266	11.872	12.280	−3.125051
1.9	−8.826	−0.071	7.388	13.563	14.012	−3.097433
2.0	−24.720	0.350	8.337	14.963	15.445	−3.074787
2.1	−51.331	0.660	8.931	15.813	16.314	−3.056686
2.2	−89.837	0.803	9.073	15.975	16.478	−3.042507
2.3	−137.197	0.782	8.776	15.463	15.951	−3.031571
2.4	−187.824	0.635	8.135	14.417	14.876	−3.023237
2.5	−237.074	0.416	7.277	13.027	13.447	−3.016948
MUE <sup>b</sup>	39.624	0.675	4.770	9.037	9.349	—
MSE <sup>c</sup>	−34.095	−0.311	4.770	9.037	9.349	—

<sup>a</sup> The FCI energies are total energies in hartree, whereas all of the remaining energies are errors relative to FCI in millihartree.

<sup>b</sup> Mean unsigned error.

<sup>c</sup> Mean signed error.

Table 4.2: A comparison of the energies resulting from the various active-space triples CC approaches and the exact FCI data for the symmetric dissociation of the  $H_6$ /cc-pVTZ ring at selected bond distances between neighboring H atoms  $R_{H-H}$  (in Å).<sup>a</sup>

$R_{H-H}$	CCSDt	ACCSDt				FCI
		(1,3)	$(1, \frac{3+4}{2})$	$(1, 3 \times \frac{n_o}{n_o+n_u} + 4 \times \frac{n_u}{n_o+n_u})$	(1,4)	
0.6	2.548	-1.234	0.615	2.243	2.365	-2.858958
0.7	2.419	-1.660	0.345	2.103	2.235	-3.176147
0.8	2.235	-2.247	-0.043	1.880	2.023	-3.331124
0.9	2.018	-2.962	-0.515	1.608	1.766	-3.396176
1.0	1.804	-3.757	-1.021	1.339	1.514	-3.410069
1.1	1.609	-4.592	-1.519	1.114	1.309	-3.394673
1.2	1.414	-5.454	-1.992	0.953	1.170	-3.362943
1.3	1.111	-6.428	-2.504	0.809	1.053	-3.322850
1.4	0.669	-7.437	-2.974	0.766	1.040	-3.279466
1.5	-0.074	-8.459	-3.375	0.855	1.163	-3.236119
1.6	-1.438	-9.451	-3.673	1.104	1.451	-3.195040
1.7	-4.014	-10.345	-3.837	1.516	1.904	-3.157716
1.8	-8.888	-11.062	-3.852	2.051	2.478	-3.125051
1.9	-17.983	-11.538	-3.744	2.611	3.069	-3.097433
2.0	-34.481	-11.755	-3.576	3.059	3.535	-3.074787
2.1	-62.336	-11.747	-3.432	3.266	3.744	-3.056686
2.2	-102.675	-11.583	-3.387	3.160	3.624	-3.042507
2.3	-150.692	-11.337	-3.483	2.735	3.172	-3.031571
2.4	-199.899	-11.068	-3.726	2.041	2.442	-3.023237
2.5	-246.321	-10.805	-4.094	1.154	1.516	-3.016948
MUE <sup>b</sup>	42.231	7.746	2.585	1.818	2.129	—
MSE <sup>c</sup>	-40.649	-7.746	-2.489	1.818	2.129	—

<sup>a</sup> The FCI energies are total energies in hartree, whereas all of the remaining energies are errors relative to FCI in millihartree. All active-space CC approaches employed three active occupied and three active unoccupied orbitals, corresponding to the 1s shells of the individual H atoms.

<sup>b</sup> Mean unsigned error.

<sup>c</sup> Mean signed error.

Table 4.3: A comparison of the energies resulting from the various full triples CC approaches and the exact FCI data for the symmetric dissociation of the H<sub>6</sub>/cc-pVTZ ring at selected bond distances between neighboring H atoms  $R_{\text{H-H}}$  (in Å).<sup>a</sup>

$R_{\text{H-H}}$	CCSDT	ACCSDT				FCI
		(1,3)	$(1, \frac{3+4}{2})$	$(1, 3 \times \frac{n_{\text{o}}}{n_{\text{o}}+n_{\text{u}}} + 4 \times \frac{n_{\text{u}}}{n_{\text{o}}+n_{\text{u}}})$	(1,4)	
0.6	0.079	-3.952	-1.996	-0.279	-0.151	-2.858958
0.7	0.095	-4.233	-2.123	-0.277	-0.139	-3.176147
0.8	0.116	-4.609	-2.304	-0.295	-0.146	-3.331124
0.9	0.140	-5.074	-2.530	-0.325	-0.162	-3.396176
1.0	0.160	-5.621	-2.792	-0.356	-0.175	-3.410069
1.1	0.166	-6.241	-3.079	-0.374	-0.174	-3.394673
1.2	0.137	-6.932	-3.381	-0.365	-0.143	-3.362943
1.3	0.031	-7.692	-3.686	-0.307	-0.059	-3.322850
1.4	-0.235	-8.512	-3.973	-0.172	0.106	-3.279466
1.5	-0.823	-9.369	-4.213	0.072	0.385	-3.236119
1.6	-2.046	-10.216	-4.371	0.457	0.808	-3.195040
1.7	-4.493	-10.982	-4.411	0.989	1.380	-3.157716
1.8	-9.245	-11.585	-4.316	1.631	2.061	-3.125051
1.9	-18.225	-11.959	-4.109	2.286	2.747	-3.097433
2.0	-34.617	-12.084	-3.855	2.817	3.296	-3.074787
2.1	-62.392	-11.995	-3.635	3.095	3.576	-3.056686
2.2	-102.685	-11.760	-3.526	3.048	3.514	-3.042507
2.3	-150.676	-11.452	-3.567	2.673	3.111	-3.031571
2.4	-199.857	-11.129	-3.764	2.019	2.421	-3.023237
2.5	-246.248	-10.820	-4.092	1.165	1.528	-3.016948
MUE <sup>b</sup>	41.623	8.811	3.486	1.150	1.304	—
MSE <sup>c</sup>	-41.531	-8.811	-3.486	0.875	1.189	—

<sup>a</sup> The FCI energies are total energies in hartree, whereas all of the remaining energies are errors relative to FCI in millihartree.

<sup>b</sup> Mean unsigned error.

<sup>c</sup> Mean signed error.

Table 4.4: A comparison of the energies resulting from the various CC approaches with singles and doubles and the exact FCI data for the symmetric dissociation of the H<sub>10</sub>/DZ ring at selected bond distances between neighboring H atoms  $R_{\text{H-H}}$  (in Å).<sup>a</sup>

$R_{\text{H-H}}$	CCSD	ACCS				FCI
		(1,3)	$(1, \frac{3+4}{2})$	$(1, 3 \times \frac{n_{\text{O}}}{n_{\text{O}}+n_{\text{U}}} + 4 \times \frac{n_{\text{U}}}{n_{\text{O}}+n_{\text{U}}})$	(1,4)	
0.6	2.461	0.412	0.945	1.204	1.458	−4.581177
0.7	2.942	0.498	1.071	1.348	1.619	−5.133564
0.8	3.519	0.708	1.314	1.606	1.890	−5.400721
0.9	4.157	1.053	1.689	1.992	2.285	−5.513021
1.0	4.878	1.591	2.265	2.582	2.886	−5.538852
1.1	5.691	2.435	3.164	3.501	3.821	−5.516586
1.2	6.510	3.744	4.552	4.917	5.257	−5.468944
1.3	7.013	5.701	6.620	7.022	7.388	−5.409818
1.4	6.288	8.451	9.520	9.972	10.370	−5.347723
1.5	1.896	11.987	13.258	13.773	14.209	−5.287756
1.6	−13.106	16.041	17.575	18.168	18.647	−5.232798
1.7	−66.276	20.069	21.930	22.618	23.144	−5.184271
1.8	NC <sup>b</sup>	23.410	25.650	26.446	27.026	−5.142644
1.9	NC <sup>b</sup>	25.531	28.163	29.075	29.715	−5.107796
2.0	NC <sup>b</sup>	26.191	29.172	30.197	30.903	−5.079254
2.1	NC <sup>b</sup>	25.462	28.691	29.809	30.585	−5.056349
2.2	NC <sup>b</sup>	23.636	26.967	28.146	28.985	−5.038308
2.3	NC <sup>b</sup>	21.090	24.372	25.568	26.453	−5.024332
2.4	NC <sup>b</sup>	18.193	21.298	22.468	23.370	−5.013655
2.5	NC <sup>b</sup>	15.248	18.087	19.193	20.080	−5.005591
MUE <sup>c</sup>	NA <sup>d</sup>	12.572	14.315	14.980	15.505	—
MSE <sup>e</sup>	NA <sup>d</sup>	12.572	14.315	14.980	15.505	—

<sup>a</sup> The FCI energies are total energies in hartree, whereas all of the remaining energies are errors relative to FCI in millihartree.

<sup>b</sup> No convergence.

<sup>c</sup> Mean unsigned error.

<sup>d</sup> Could not be determined because CCSD does not converge at larger distances.

<sup>e</sup> Mean signed error.

Table 4.5: A comparison of the energies resulting from the various active-space CC approaches and the exact FCI data for the symmetric dissociation of the H<sub>10</sub>/DZ ring at selected bond distances between neighboring H atoms  $R_{\text{H-H}}$  (in Å).<sup>a</sup>

$R_{\text{H-H}}$	CCSDt	ACCSDt				FCI
		(1,3)	$(1, \frac{3+4}{2})$	$(1, 3 \times \frac{n_{\text{O}}}{n_{\text{O}}+n_{\text{U}}} + 4 \times \frac{n_{\text{U}}}{n_{\text{O}}+n_{\text{U}}})$	(1,4)	
0.6	0.455	-1.751	-1.181	-0.904	-0.633	-4.581177
0.7	0.554	-2.110	-1.502	-1.209	-0.922	-5.133564
0.8	0.416	-2.726	-2.081	-1.773	-1.473	-5.400721
0.9	0.349	-3.218	-2.541	-2.221	-1.912	-5.513021
1.0	0.181	-3.735	-3.019	-2.686	-2.369	-5.538852
1.1	-0.084	-4.169	-3.399	-3.050	-2.724	-5.516586
1.2	-0.650	-4.477	-3.634	-3.266	-2.933	-5.468944
1.3	-1.956	-4.591	-3.654	-3.266	-2.931	-5.409818
1.4	-4.961	-4.457	-3.399	-2.994	-2.672	-5.347723
1.5	-11.879	-4.091	-2.881	-2.468	-2.182	-5.287756
1.6	-28.679	-3.630	-2.233	-1.824	-1.609	-5.232798
1.7	-81.643	-3.315	-1.692	-1.300	-1.193	-5.184271
1.8	NC <sup>b</sup>	-3.398	-1.510	-1.144	-1.178	-5.142644
1.9	NC <sup>b</sup>	-4.043	-1.862	-1.523	-1.712	-5.107796
2.0	NC <sup>b</sup>	-5.295	-2.810	-2.494	-2.832	-5.079254
2.1	NC <sup>b</sup>	-7.106	-4.333	-4.029	-4.497	-5.056349
2.2	NC <sup>b</sup>	-9.380	-6.355	-6.055	-6.626	-5.038308
2.3	NC <sup>b</sup>	-12.001	-8.762	-8.462	-9.114	-5.024332
2.4	NC <sup>b</sup>	-14.806	-11.381	-11.083	-11.806	-5.013655
2.5	NC <sup>b</sup>	-17.551	-13.966	-13.660	-14.471	-5.005591
MUE <sup>c</sup>	NA <sup>d</sup>	5.793	4.110	3.770	3.790	—
MSE <sup>e</sup>	NA <sup>d</sup>	-5.793	-4.110	-3.770	-3.790	—

<sup>a</sup> The FCI energies are total energies in hartree, whereas all of the remaining energies are errors relative to FCI in millihartree. All active-space CC approaches employed five active occupied and five active unoccupied orbitals, corresponding to the 1s shells of the individual H atoms.

<sup>b</sup> No convergence.

<sup>c</sup> Mean unsigned error.

<sup>d</sup> Could not be determined because CCSDt does not converge at larger distances.

<sup>e</sup> Mean signed error.



Table 4.6: A comparison of the energies resulting from the various full triples CC approaches and the exact FCI data for the symmetric dissociation of the H<sub>10</sub>/DZ ring at selected bond distances between neighboring H atoms  $R_{\text{H-H}}$  (in Å).<sup>a</sup>

$R_{\text{H-H}}$	CCSDT	ACCSDT				FCI
		(1,3)	$(1, \frac{3+4}{2})$	$(1, 3 \times \frac{n_{\text{O}}}{n_{\text{O}}+n_{\text{U}}} + 4 \times \frac{n_{\text{U}}}{n_{\text{O}}+n_{\text{U}}})$	(1,4)	
0.6	0.065	-2.167	-1.591	-1.311	-1.037	-4.581177
0.7	0.094	-2.602	-1.986	-1.688	-1.398	-5.133564
0.8	0.110	-3.054	-2.404	-2.093	-1.790	-5.400721
0.9	0.101	-3.485	-2.805	-2.482	-2.172	-5.513021
1.0	0.035	-3.894	-3.175	-2.841	-2.523	-5.538852
1.1	-0.170	-4.262	-3.491	-3.141	-2.815	-5.516586
1.2	-0.703	-4.535	-3.691	-3.323	-2.989	-5.468944
1.3	-1.991	-4.631	-3.693	-3.305	-2.969	-5.409818
1.4	-4.986	-4.487	-3.428	-3.023	-2.700	-5.347723
1.5	-11.897	-4.115	-2.904	-2.490	-2.205	-5.287756
1.6	-28.687	-3.649	-2.251	-1.842	-1.626	-5.232798
1.7	-81.631	-3.330	-1.706	-1.313	-1.206	-5.184271
1.8	NC <sup>b</sup>	-3.408	-1.520	-1.153	-1.187	-5.142644
1.9	NC <sup>b</sup>	-4.049	-1.867	-1.528	-1.717	-5.107796
2.0	NC <sup>b</sup>	-5.296	-2.811	-2.494	-2.833	-5.079254
2.1	NC <sup>b</sup>	-7.101	-4.329	-4.025	-4.493	-5.056349
2.2	NC <sup>b</sup>	-9.371	-6.346	-6.045	-6.618	-5.038308
2.3	NC <sup>b</sup>	-11.988	-8.750	-8.449	-9.100	-5.024332
2.4	NC <sup>b</sup>	-14.790	-11.365	-11.068	-11.791	-5.013655
2.5	NC <sup>b</sup>	-17.533	-13.927	-13.644	-14.459	-5.005591
MUE <sup>c</sup>	NA <sup>d</sup>	5.887	4.202	3.863	3.881	—
MSE <sup>e</sup>	NA <sup>d</sup>	-5.887	-4.202	-3.863	-3.881	—

<sup>a</sup> The FCI energies are total energies in hartree, whereas all of the remaining energies are errors relative to FCI in millihartree.

<sup>b</sup> No convergence.

<sup>c</sup> Mean unsigned error.

<sup>d</sup> Could not be determined because CCSDT does not converge at larger distances.

<sup>e</sup> Mean signed error.

Table 4.7: A comparison of the energies resulting from the various CC approaches including up to triple excitations and the nearly exact LDMRG(500) data for the symmetric dissociation of the  $H_{50}/STO-6G$  linear chain at selected bond distances between neighboring H atoms  $R_{H-H}$  (in a.u.).<sup>a</sup>

$R_{H-H}$	CCSD	$ACCS(1,3 \times \frac{n_o}{n_o+n_u} + 4 \times \frac{n_u}{n_o+n_u})$	CCSDT	$ACCS(1,3 \times \frac{n_o}{n_o+n_u} + 4 \times \frac{n_u}{n_o+n_u})$	LDMRG(500)
1.0	11.90	6.30	0.27	-6.68	-17.28407
1.2	16.28	9.12	0.29	-9.08	-22.94765
1.4	20.99	12.78	-0.10	-11.37	-25.59378
1.6	26.01	17.82	-1.71	-13.26	-26.71944
1.8	31.00	24.87	-6.96	-14.62	-27.03865
2.0	34.60	34.30	NC <sup>b</sup>	-15.73	-26.92609
2.4	NC <sup>b</sup>	59.23	NC <sup>b</sup>	-22.04 <sup>c</sup>	-26.16057
2.8	NC <sup>b</sup>	86.24	NC <sup>b</sup>	-22.47 <sup>c</sup>	-25.27480
3.2	NC <sup>b</sup>	106.45	NC <sup>b</sup>	-18.78 <sup>c</sup>	-24.56828
3.6	NC <sup>b</sup>	113.43	NC <sup>b</sup>	-4.66 <sup>c</sup>	-24.10277
4.2	NC <sup>b</sup>	94.08	NC <sup>b</sup>	71.86 <sup>c</sup>	-23.74971
MUE <sup>d</sup>	NA <sup>e</sup>	51.33	NA <sup>f</sup>	19.14	—
MSE <sup>g</sup>	NA <sup>e</sup>	51.33	NA <sup>f</sup>	-6.08	—

<sup>a</sup> The LDMRG(500) energies were taken from Reference [175] and are total energies in hartree. The remaining energies are errors relative to LDMRG(500) in millihartree.

<sup>b</sup> No convergence.

<sup>c</sup> We were unable to converge these energies beyond  $1 \times 10^{-3}$  hartree. The reported values correspond to the respective last CC iteration.

<sup>d</sup> Mean unsigned error.

<sup>e</sup> Could not be determined because CCSD does not converge at larger distances.

<sup>f</sup> Could not be determined because CCSDT does not converge at larger distances.

<sup>g</sup> Mean signed error.

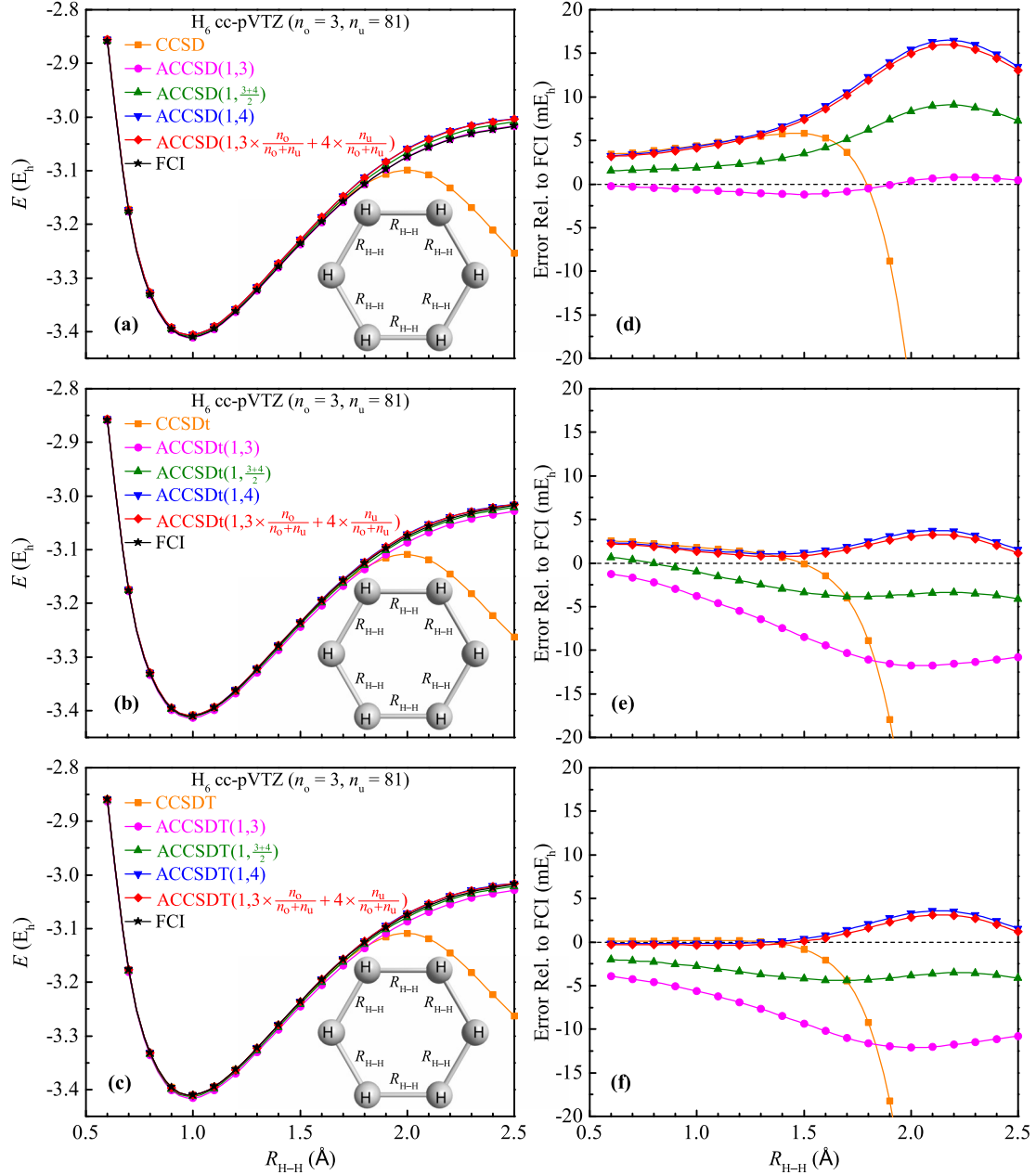


Figure 4.1: Ground-state PECs [panels (a)–(c)] and errors relative to FCI [panels (d)–(f)] for the symmetric dissociation of the  $H_6$  ring resulting from the CCSD and various ACCSD calculations [panels (a) and (d)], the active-space CCSDt and ACCSDt computations [panels (b) and (e)], and the full CCSDT and ACCSDT methods [panels (c) and (f)], using the cc-pVTZ basis set. The active-space triples approaches employed a minimum active space built from the  $1s$  orbitals of individual hydrogen atoms. The FCI PEC is included in panels (a)–(c) to facilitate the comparisons.

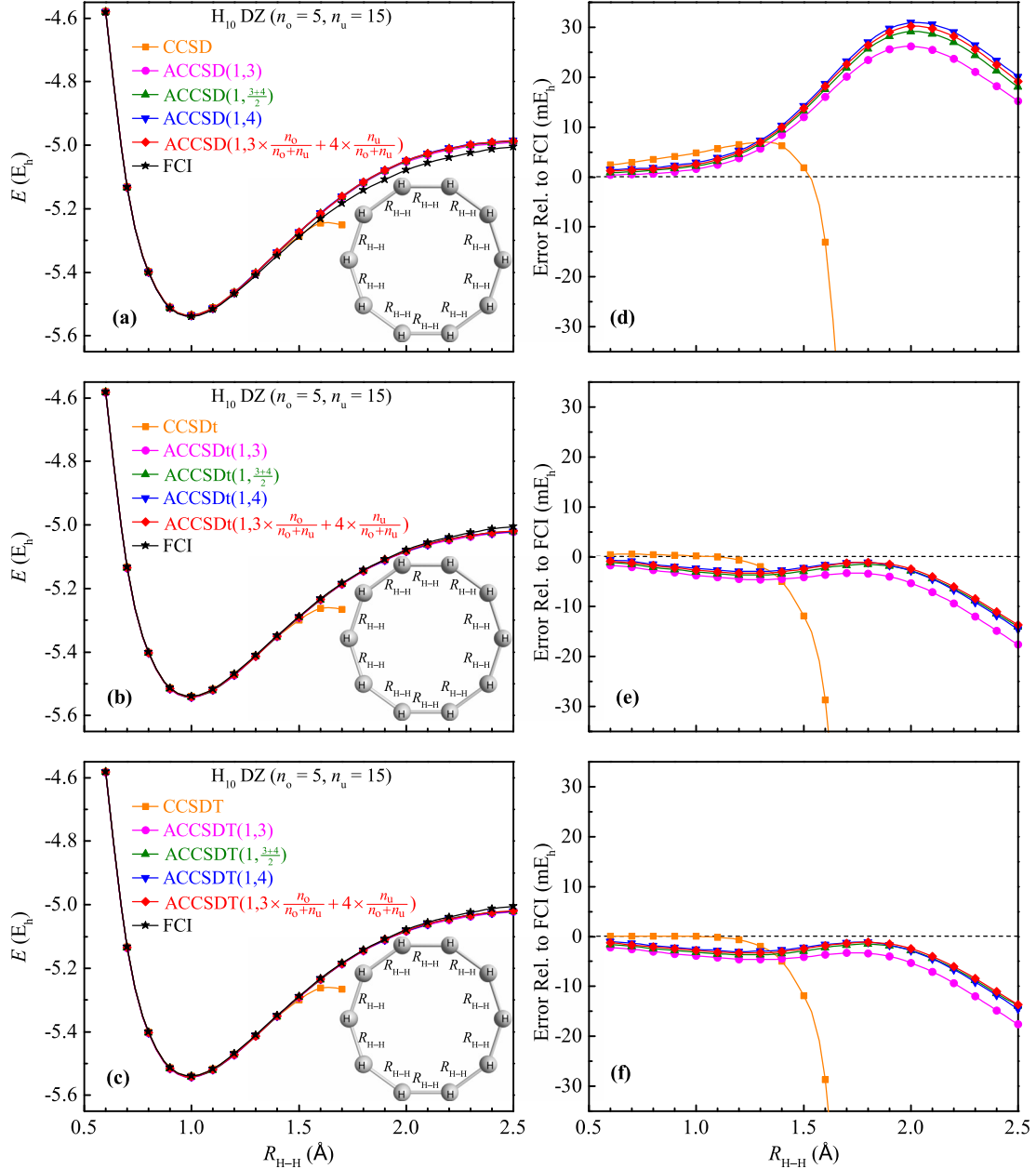


Figure 4.2: Ground-state PECs [panels (a)–(c)] and errors relative to FCI [panels (d)–(f)] for the symmetric dissociation of the  $H_{10}$  ring resulting from the CCSD and various ACCSD calculations [panels (a) and (d)], the active-space CCSDt and ACCSDt computations [panels (b) and (e)], and the full CCSDT and ACCSDT methods [panels (c) and (f)], using the DZ basis set. The active-space triples approaches employed a minimum active space built from the  $1s$  orbitals of individual hydrogen atoms. The FCI PEC is included in panels (a)–(c) to facilitate the comparisons.

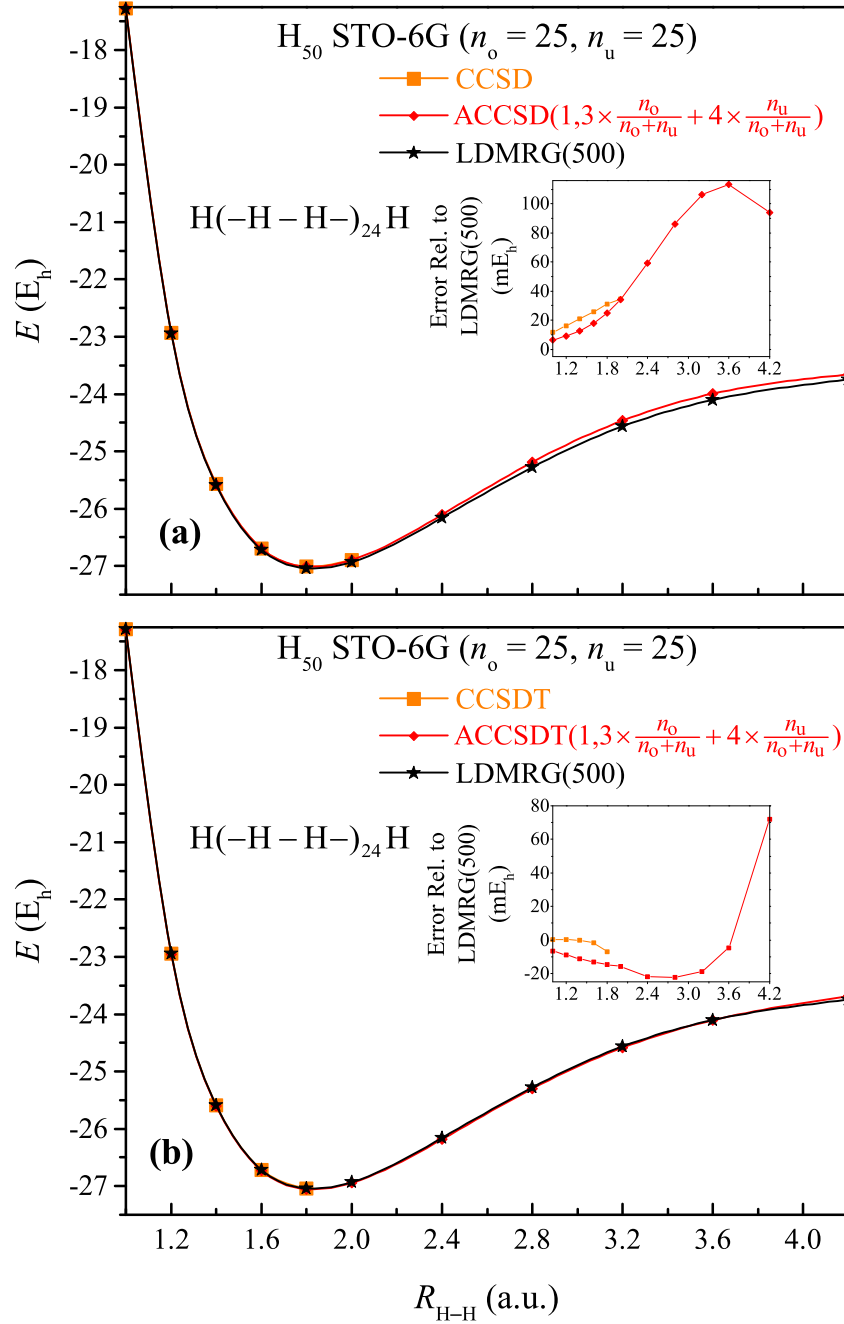


Figure 4.3: Ground-state PECs for the symmetric dissociation of the  $H_{50}$  linear chain resulting from the CCSD and ACCSD( $1, 3 \times \frac{n_o}{n_o+n_u} + 4 \times \frac{n_u}{n_o+n_u}$ ) calculations [panel (a)] and their full triples extensions [panel (b)] using the STO-6G basis set. The nearly exact LDMRG(500) PEC of Reference [175] is included in both panels to facilitate the comparisons. The insets show the errors relative to LDMRG(500) in millihartree (*cf.* Table 4.7).

## 4.2 Approaching the Full Configuration Interaction Limit for Strong Correlation Using Semi-Stochastic Ideas

In this section, we examine the performance of the novel CAD-FCIQMC[1,(3+4)/2] methodology introduced in this dissertation. In particular, we compare its rate of convergence toward the exact, FCI, energetics against the one characterizing the underlying FCIQMC simulations in challenging strongly correlated situations. Before we proceed, however, we first demonstrate that in the absence of strong many-electron correlation effects the CAD-FCIQMC[1,(3+4)/2] approach yields similar results to the original CAD-FCIQMC[1–5] scheme. This is a desired behavior since CAD-FCIQMC[1–5] is characterized by a rapid convergence, much faster than FCIQMC itself, toward the exact energy values for problems involving weak or moderately strong correlations [265].

To that end, we studied the  $C_{2v}$ -symmetric double bond dissociation of  $H_2O$  as described by the cc-pVDZ basis set, which served as the testing ground of the original CAD-FCIQMC[1–5] algorithm [265]. In particular, we considered two geometries of  $H_2O$ , namely, equilibrium,  $R_{O-H} = R_e$ , and one additional geometry obtained by the simultaneous stretch of both O–H bonds by a factor of 2.0,  $R_{O-H} = 2.0R_e$ , while keeping the  $\angle H-O-H$  angle fixed to its equilibrium value. The geometries and corresponding all-electron FCI energy values were obtained from Reference [277]. The *i*-FCIQMC propagations, which provided the source of  $T_3^{(MC)}(\tau)$  and  $T_4^{(MC)}(\tau)$  clusters, were performed with the HANDE package [316]. For each examined geometry of the  $H_2O$  triatomic, the *i*-FCIQMC stochastic wavefunction sampling was initiated by placing 1,000 walkers on the RHF Slater determinant, while the time step used in propagations was  $\Delta\tau = 0.0001$  a.u. To accelerate convergence, the  $n_a$  parameter of the initiator algorithm was set at 3, meaning that, at any given time step  $\tau$ , only determinants inhabited by more than 3 walkers were allowed to spawn progeny on unpopulated determinants. At every 1,000 time steps, we cluster analyzed the *i*-FCIQMC wavefunction and solved the CCSD-like system of equations, Equations (3.29) and (3.40), in which  $T_3^{(MC)}(\tau)$ ,  $T_4^{(MC)}(\tau)$ , and selected coupled-pair contributions were extracted from

*i*-FCIQMC, for  $T_1$  and  $T_2$  using codes developed by the Piecuch group. Finally, both the *i*-FCIQMC calculations and the CC computations were performed using the same set of one- and two-body molecular integrals extracted from GAMESS [307–309].

The results of the original CAD-FCIQMC[1–5] scheme, the CAD-FCIQMC[1,(3+4)/2] methodology introduced in this dissertation, and the underlying *i*-FCIQMC simulations for the double bond dissociation of H<sub>2</sub>O are shown in Figure 4.4 and, for selected time steps, in Table 4.8. As might have been anticipated, the deviation between the two CAD-FCIQMC variants is largest at the initial steps of the simulation and is gradually bridged as one approaches the infinite imaginary time limit, owing to the fact that both schemes converge to the exact, FCI, energetics. At  $\tau = 0$ , the original CAD-FCIQMC[1–5] methodology becomes equivalent to CCSD, while its CAD-FCIQMC[1,(3+4)/2] extension to the strong correlation regime reduces to ACCSD( $1, \frac{3+4}{2}$ )  $\equiv$  DCSD. At the weakly correlated equilibrium geometry, the CCSD and ACCSD( $1, \frac{3+4}{2}$ ) data are already quite close to the pertinent FCI energy value, the corresponding errors being 3.744 mE<sub>h</sub> and  $-0.731$  mE<sub>h</sub>, respectively. It is, thus, not surprising that the CAD-FCIQMC[1–5] and CAD-FCIQMC[1,(3+4)/2] energetics can hardly be distinguished from each other at later propagation times (see, for example, Figure 4.4). For the stretched geometry, the deviation between the CCSD and ACCSD( $1, \frac{3+4}{2}$ ) energetics is more pronounced. Although the double bond dissociation of H<sub>2</sub>O involves the entanglement of only four electrons, the presence of quasi-degeneracies has a significant impact on the CCSD energy value, which is characterized by a more than 20 mE<sub>h</sub> error relative to FCI. At the same time, the ACCSD( $1, \frac{3+4}{2}$ ) variant of the ACP schemes, which is well-suited for the study of electronic quasi-degeneracies, offers a dramatically improved description, as is evident by the about 3 mE<sub>h</sub> error relative to the FCI data. Nevertheless, the CAD-FCIQMC[1–5] methodology quickly catches up with CAD-FCIQMC[1,(3+4)/2] and after about 20,000 MC iterations they provide the essentially identical picture (*cf.* Figure 4.4). Thus, in the absence of strong many-electron correlation effects, both of the examined flavors of CAD-FCIQMC provide more or less results of similar quality, even in the presence

of quasi-degeneracies, such as those present in the double bond dissociation of  $\text{H}_2\text{O}$ .

We now compare the performance of the CAD-FCIQMC variants of interest with that of the underlying *i*-FCIQMC simulations. A simple inspection of Figure 4.4 reveals that both the original CAD-FCIQMC[1–5] scheme and its CAD-FCIQMC[1,(3+4)/2] extension to the strong correlation regime are characterized by a rapid convergence to the exact, FCI, energetics, much faster than in the case of *i*-FCIQMC, even when both O–H bonds are stretched to twice their equilibrium value. As shown in Table 4.8, focusing on the more challenging  $R_{\text{O-H}} = 2.0R_e$  nuclear configuration, both CAD-FCIQMC[1–5] and CAD-FCIQMC[1,(3+4)/2] are capable of reproducing the deterministic FCI energy to within a millihartree already at about 40,000 MC iterations, with submillihartree errors achieved at around 100,000 MC iterations. At the same time, the error relative to FCI characterizing the underlying *i*-FCIQMC methodology at 160,000 MC iterations, the last iteration before we stopped the *i*-FCIQMC propagation, is 1.328 mE<sub>h</sub>, which suggests that one needs to keep sampling the many-electron Hilbert space for the *i*-FCIQMC methodology to provide results comparable to CAD-FCIQMC. At this point, it is also interesting to note that the noise inherent to the purely stochastic *i*-FCIQMC simulations propagates to the CAD-FCIQMC calculations through the extracted  $T_2^{(\text{MC})}(\tau)$ ,  $T_3^{(\text{MC})}(\tau)$ , and  $T_4^{(\text{MC})}(\tau)$  amplitudes. Although CAD-FCIQMC[1–5] and CAD-FCIQMC[1,(3+4)/2] cannot eliminate the stochastic noise, they do reduce it, giving rise to considerably smoother energetics (*cf.* Figure 4.4).

The remarkable performance of the CAD-FCIQMC family of methods can be largely attributed to the ability of the *i*-FCIQMC stochastic wavefunction sampling to quickly identify the important triply and quadruply excited Slater determinants that enter the CC system of equations corrected for connected triples and quadruples, Equations (3.29) and (3.40). This is most easily quantified by examining the percentages of triples and quadruples captured by *i*-FCIQMC as functions of the propagation time  $\tau$ . As can be seen in Table 4.8, both variants of CAD-FCIQMC are capable of producing FCI-quality energetics, stable to within a millihartree, once *i*-FCIQMC captures about 17% of triples and about 3% of quadruples



(40,000 MC iterations). This observation implies that not only does *i*-FCIQMC quickly capture the dominant triples and quadruples, but also that their walker populations reflect on the structure of the FCI wavefunction already from the early stages of the propagation. At the same time, the underlying *i*-FCIQMC methodology has only explored a tiny fraction of the many-electron Hilbert space, having captured just 0.02% of the 451,681,246  $S_z = 0$  totally symmetric Slater determinants, using  $C_{2v}$  point group symmetry, spanning the many-electron Hilbert space. These results indicate that the CAD-FCIQMC methodology is capable of producing accurate estimates of the FCI energies out of the early stages of *i*-FCIQMC propagations using computationally affordable CCSD-like computations, even in the presence of quasi-degeneracies such as those characterizing the double bond dissociation of  $H_2O$ .

We are now in a position to proceed to the discussion of the performance of CAD-FCIQMC[1,(3+4)/2] in the presence of strong many-electron correlation effects. To that end, we examine the  $D_{6h}$ - and  $D_{10h}$ -symmetric dissociations of the six- and ten-membered hydrogen rings, respectively. In the case of  $H_6$  we used the cc-pVDZ basis set, while for the larger  $H_{10}$  hydrogen cluster we employed the DZ basis. As already emphasized in this dissertation, the dissociation of equally spaced hydrogen clusters to individual H atoms is characterized by a Mott metal–insulator transition as the system traverses from a weakly correlated metallic phase to a strongly correlated insulating phase, which has a devastating effect on the performance of the hierarchy of traditional CC approaches, including, for example, CCSD and CCSDT. For the sake of completeness, the PECs of the  $H_6$ /cc-pVDZ and  $H_{10}$ /DZ rings resulting from CCSD, CCSDT, and FCI calculations are presented in Figure 4.5. Although the performance of CCSD and CCSDT in describing the  $H_6$  and  $H_{10}$  PECs was discussed extensively in the previous section, here we make a couple of remarks that are useful in the context of the CAD-FCIQMC methodology. In Figure 4.5, we see that CCSD closely reproduces the FCI energetics around the equilibrium geometries of both  $H_6$  and  $H_{10}$ . This suggests that the original CAD-FCIQMC[1–5] scheme, which becomes equivalent

to CCSD for  $\tau = 0$ , will rapidly converge toward the exact description of both hydrogen rings when considering, for example, the structures where the distance between neighboring H atoms is  $R_{\text{H-H}} = 1.0 \text{ \AA}$ , corresponding to the region of minimum on the FCI PEC (cf. Figure 4.5). As one departs from the equilibrium region and approaches the atomization threshold, the performance of CCSD gradually deteriorates, resulting in an unphysical description of both  $\text{H}_6$  and  $\text{H}_{10}$  systems as a consequence of overcorrelating. As discussed earlier in this dissertation, the failure of CCSD is much more dramatic in the case of the  $\text{H}_{10}$  cluster, since no convergence was obtained for distances between neighboring hydrogen atoms larger than  $1.75 \text{ \AA}$ . These observations foreshadow the catastrophe that will befall CAD-FCIQMC[1–5] in the strong correlation regime. In what follows, we demonstrate that the novel CAD-FCIQMC[1,(3+4)/2] methodology introduced in this dissertation, where, out of the five  $\frac{1}{2}T_2^2$  Goldstone–Brandow diagrams shown in Figure 3.5, diagrams D1 and an average of diagrams D3 and D4, which are responsible for capturing strong correlations, are treated deterministically with the rest of  $\frac{1}{2}T_2^2$  calculated using  $T_2^{(\text{MC})}(\tau)$  extracted from FCIQMC, is practically immune to the presence of strong many-electron correlation effects and is characterized by the fastest convergence toward FCI among the examined approaches.

As already mentioned, in the computations regarding the symmetric dissociation of the  $\text{H}_6$  and  $\text{H}_{10}$  rings we employed the cc-pVDZ and DZ basis sets, respectively. The grid of geometries considered in our calculations consisted of the following distances between neighboring hydrogen atoms: 0.6, 0.8, 1.0, 1.25, 1.5, 1.75, and  $2.0 \text{ \AA}$ . The underlying *i*-FCIQMC simulations were performed with HANDE. For both hydrogen clusters and for each geometry of the aforementioned grid, the *i*-FCIQMC propagation was initiated by placing 1,500 walkers on the RHF Slater determinant and setting the  $n_a$  parameter of the initiator algorithm at 3. The time step used in the simulations was  $\Delta\tau = 0.0001 \text{ a.u.}$  and we performed CAD-FCIQMC[1–5] and CAD-FCIQMC[1,(3+4)/2] calculations every 1,000 time steps. The cluster analysis of the *i*-FCIQMC wavefunction and the subsequent CCSD-like computations were performed with codes of the Piecuch group. As was the case with the  $\text{H}_2\text{O}$  system,

the same set of one- and two-body molecular integrals, extracted from GAMESS, was employed for both the *i*-FCIQMC simulations and subsequent CCSD-like computations. The deterministic FCI data, which we needed to judge the performance of its purely stochastic, *i*-FCIQMC, and semi-stochastic, CAD-FCIQMC[1–5] and CAD-FCIQMC[1,(3+4)/2], approximations, were acquired using the determinantal FCI code available in the GAMESS package.

The results of the CAD-FCIQMC[1–5] calculations, the CAD-FCIQMC[1,(3+4)/2] computations, and the underlying *i*-FCIQMC simulations for the H<sub>6</sub>/cc-pVDZ and H<sub>10</sub>/DZ systems are summarized in Figures 4.6 and 4.7 and Tables 4.9 and 4.10. We begin our discussion with the smaller H<sub>6</sub> ring, the dissociation of which involves the entanglement of six electrons. Panels (a) and (b) of Figure 4.6 portray the energies obtained at the *i*-FCIQMC, CAD-FCIQMC[1–5], and CAD-FCIQMC[1,(3+4)/2] levels of theory as functions of the imaginary time  $\tau$  at the structure characterized by  $R_{\text{H-H}} = 1.0 \text{ \AA}$  and the geometry in which each H–H bond is stretched to twice this value, the largest distance considered in our calculations, respectively. Focusing on the weakly correlated  $R_{\text{H-H}} = 1.0 \text{ \AA}$  geometry, we see that both the original CAD-FCIQMC[1–5] and the novel CAD-FCIQMC[1,(3+4)/2] approaches display a remarkably fast convergence toward the exact, FCI, energy value. In fact, Table 4.9 reveals that the energetics of both flavors of CAD-FCIQMC are characterized by stable submillihartree errors relative to FCI already at 20,000 MC iterations or when about 26% of triples and 4% of quadruples are captured by the underlying stochastic wavefunction sampling. Despite the fact that the *i*-FCIQMC propagation has a 110 times larger error relative to FCI at  $\tau = 0$  than CAD-FCIQMC[1,(3+4)/2], it reproduces the FCI value to within about 1.5 millihartree rather quickly (40,000 MC iterations), although the stochastic noise is quite significant.

The picture changes dramatically when one examines the performance of *i*-FCIQMC, CAD-FCIQMC[1–5], and CAD-FCIQMC[1,(3+4)/2] at the stretched geometry in which  $R_{\text{H-H}} = 2.0 \text{ \AA}$ . A simple inspection of panel (b) of Figure 4.6 reveals that the original CAD-

FCIQMC[1–5] scheme is characterized by a slow convergence, comparable to that of the underlying *i*-FCIQMC propagation, toward the FCI energy value. Such behavior was more or less anticipated due to the fact that at  $\tau = 0$  CAD-FCIQMC[1–5]  $\equiv$  CCSD overcorrelates by more than 35 mE<sub>h</sub>. It is, however, interesting to note that, at least for the duration of the particular simulation shown in Figure 4.6(b), *i*-FCIQMC approaches FCI from above while CAD-FCIQMC[1–5] from below. At the same time, the novel CAD-FCIQMC[1,(3+4)/2] methodology introduced in this dissertation is practically immune to the presence of strong many-electron correlation effects. As demonstrated in Table 4.9, CAD-FCIQMC[1,(3+4)/2] faithfully reproduces the FCI energy to within less than 1 mE<sub>h</sub> already at 60,000 MC iterations or when *i*-FCIQMC captures about 41% of triples and 10% of quadruples. Although these percentages are larger than those required for submillihartree accuracy in the case of the corresponding equilibrium geometry, they are still far from the total numbers of triples and quadruples. In fact, at 60,000 MC iterations the *i*-FCIQMC propagation has explored only 2% of the entire many-electron Hilbert space, which is spanned by 2,123,544  $S_z = 0$  totally symmetric Slater determinants using  $D_{2h}$  point group symmetry. This constitutes a tremendous acceleration toward FCI even in the presence of strong non-dynamical correlation effects. The remarkable performance of the CAD-FCIQMC[1,(3+4)/2] approach can be largely attributed to the fact that the  $\frac{1}{2}T_2^2$  Goldstone–Brandow diagram D1 and the average of diagrams D3 and D4 (cf. Figure 3.5), which are responsible for capturing strong correlations, are treated deterministically while the rest of  $\frac{1}{2}T_2^2$  is determined using  $T_2^{(\text{MC})}(\tau)$  extracted from *i*-FCIQMC. Consequently, even at  $\tau = 0$ , CAD-FCIQMC[1,(3+4)/2] is already much closer to FCI than CAD-FCIQMC[1–5], having an error of less than 9 mE<sub>h</sub>, and the gap is rapidly bridged as the simulation progresses.

Further insights into the performance of *i*-FCIQMC, CAD-FCIQMC[1–5], and CAD-FCIQMC[1,(3+4)/2] can be gained by examining the convergence of the entire PEC to its FCI counterpart as a function of MC iterations. This can be found in graphical form in the case of the H<sub>6</sub>/cc-pVDZ system in panels (a), (b), and (c) of Figure 4.7 for 50,000, 100,000,

and 150,000 MC iterations. For the sake of comparison, we also include the information about the deterministic CCSD, CCSDT, and ACCSD( $1, \frac{3+4}{2}$ ) calculations. To begin with, the *i*-FCIQMC approach provides a more or less exact description of the weakly and moderately correlated portions of the PEC at 100,000 MC iterations. However, the energies of the two points closest to the dissociation limit, corresponding to distances between neighboring hydrogen atoms of  $R_{\text{H-H}} = 1.75$  and  $2.0 \text{ \AA}$ , respectively, are far from their FCI counterparts. In fact, even at 100,000 MC iterations *i*-FCIQMC is worse than the deterministic ACCSD( $1, \frac{3+4}{2}$ ) methodology and one needs to go to at least 150,000 MC iterations for *i*-FCIQMC to outperform ACCSD( $1, \frac{3+4}{2}$ ) in the entire range of geometries examined in this dissertation.

Moving on to the original CAD-FCIQMC[1–5] scheme, a simple inspection of Figure 4.7(a) reveals that it provides a practically exact description for the weakly correlated structures corresponding to  $R_{\text{H-H}}$  distances of 0.6, 0.8, 1.0, 1.25, and  $1.5 \text{ \AA}$  already at 50,000 MC iterations, as might have been anticipated. However, after the onset of strong correlations, CAD-FCIQMC significantly overcorrelates even at 50,000 MC iterations, as is evident by the large negative errors with respect to FCI for the  $R_{\text{H-H}} = 1.75$  and  $2.0 \text{ \AA}$  grid points (cf. inset to Figure 4.7). As was the case with the underlying *i*-FCIQMC simulations, one needs to go to 150,000 MC iterations for CAD-FCIQMC[1–5] to provide a PEC of higher quality than ACCSD( $1, \frac{3+4}{2}$ ). It is, however, worth mentioning that CAD-FCIQMC[1–5] converges much faster to the FCI-level energetics at  $R_{\text{H-H}} = 1.75 \text{ \AA}$  than *i*-FCIQMC.

As was expected in light of the above discussion, the CAD-FCIQMC[1,(3+4)/2] methodology is characterized by the fastest convergence toward the exact, FCI, energetics for the entire range of electron correlation effects, ranging from the weakly to the strongly correlated regimes. Even at 50,000 MC iterations, the CAD-FCIQMC[1,(3+4)/2] PEC characterizing the  $D_{6h}$ -symmetric dissociation of the  $\text{H}_6/\text{cc-pVDZ}$  ring is far superior to the one of ACCSD( $1, \frac{3+4}{2}$ ), closely reproducing the FCI data. Indeed, at 100,000 MC iterations one can hardly distinguish the CAD-FCIQMC[1,(3+4)/2] and FCI PECs.

Now, we turn our attention to the larger  $H_{10}$  ring. As was mentioned earlier in this dissertation, the  $D_{10h}$ -symmetric dissociation of  $H_{10}$  involves the entanglement of 10 electrons, *i.e.*, the number of strongly correlated electrons is increased by more than 66% when compared to the smaller  $H_6$  cluster. Panels (c) and (d) of Figure 4.6 show the energies obtained using *i*-FCIQMC, CAD-FCIQMC[1–5], and CAD-FCIQMC[1,(3+4)/2] as functions of the MC iterations at the structure characterized by  $R_{H-H} = 1.0 \text{ \AA}$  and the geometry in which each H–H bond is stretched to twice this value, the largest distance considered in our calculations, respectively. When considering the weakly correlated  $R_{H-H} = 1.0 \text{ \AA}$  geometry, it comes as no surprise that both CAD-FCIQMC variants examined in this dissertation display an equally rapid convergence, faster than that of the underlying *i*-FCIQMC propagation, to the exact, FCI, energy value. It is interesting to note, however, that sub-millihartree accuracies are attained when the *i*-FCIQMC stochastic wavefunction sampling has captured about 42% of triples and 9% of quadruples (40,000 MC iterations). This needs to be contrasted with the 26% of triples and 4% of quadruples that were needed to obtain the same level of accuracy in the case of the  $R_{H-H} = 1.0 \text{ \AA}$  grid point for  $H_6/\text{cc-pVDZ}$ . This indicates the severity of electron correlation effects in  $H_{10}$ , even in the weakly correlated regime. Nevertheless, it is worth emphasizing that at 40,000 MC iterations the underlying *i*-FCIQMC simulation has only captured 0.12% of the entire many-electron Hilbert space, which is spanned by 60,095,104  $S_z = 0$  totally symmetric Slater determinants using  $D_{2h}$  point group symmetry. This is a very interesting observation, because it implies that even if the entire manifolds of triply and quadruply excited Slater determinants need to be captured by FCIQMC so that CAD-FCIQMC produces FCI-quality energetics, they still constitute a tiny fraction of all Slater determinants spanning the many-electron Hilbert space.

The onset of strong non-dynamical correlations has a devastating effect on the original CAD-FCIQMC[1–5] scheme. This is showcased by the fact that no convergence was obtained for  $R_{H-H} = 2.0 \text{ \AA}$  (cf. Table 4.10). In fact, the singularity plaguing the CCSD-like Equations (3.29) and (3.40) with  $\xi_i = 1$ ,  $i = 1-5$ , was so severe that it persisted for the entire *i*-FCIQMC

simulation, independent of the percentages of captured triples and quadruples, and even when we used the converged CAD-FCIQMC[1,(3+4)/2]  $T_1$  and  $T_2$  amplitudes as initial guesses. Despite the success of the original CAD-FCIQMC[1–5] approach, being able to provide fast convergence toward FCI in the presence of quasi-degeneracies such as those characterizing the double bond dissociation of  $\text{H}_2\text{O}$ , it completely breaks down in the presence of strong correlations.

In contrast, the novel CAD-FCIQMC[1,(3+4)/2] methodology is not only well-behaved in the strong correlation regime, but also capable of providing FCI-quality energetics out of the early stages of the *i*-FCIQMC simulation [see, for example, Figure 4.6(d)]. As mentioned earlier in this dissertation, the success behind the CAD-FCIQMC[1,(3+4)/2] approach lies in the fact that, by repartitioning the CC equations projected on doubles, the  $\frac{1}{2}T_2^2$  part responsible for capturing strong correlations is treated deterministically while its complement is extracted from FCIQMC. At  $\tau = 0$ , the error with respect to FCI characterizing CAD-FCIQMC[1,(3+4)/2]  $\equiv \text{ACCS}(1, \frac{3+4}{2})$  amounts to 29.172 mE<sub>h</sub>. At a first glance, such a deviation seems rather large, but we need to keep in mind that the FCI correlation energy at this geometry is −454.768 mE<sub>h</sub>. This implies that the CAD-FCIQMC[1,(3+4)/2] scheme introduced in this dissertation captures about 94% of the FCI correlation energy already at  $\tau = 0$ . Furthermore, after capturing about 70% of triples and 36% of quadruples, CAD-FCIQMC[1,(3+4)/2] steadily recovers 99–101% of the FCI correlation energy. Although the percentages of triples and quadruples are quite large, one has to keep in mind that they constitute a tiny fraction of the entire many-electron Hilbert space. In fact, at this point of the simulation, less than 2% of the Slater determinants spanning the many-electron Hilbert space have been captured. It is, thus, astounding that with such a small subspace of the many-electron Hilbert space recovered, CAD-FCIQMC[1,(3+4)/2] closely reproduces the FCI energy value. At the same time, the underlying purely stochastic *i*-FCIQMC approach is far from attaining such a level of accuracy even at 160,000 MC iterations, the last iteration before we stopped the simulation, where almost all triples and quadruples have

been captured.

A comparison of the convergence of the PECs characterizing the  $D_{10h}$ -symmetric dissociation of  $H_{10}$  obtained using *i*-FCIQMC, CAD-FCIQMC[1–5], and CAD-FCIQMC[1,(3+4)/2] at 50,000, 100,000, and 150,000 MC iterations can be found in panels (d)–(f) of Figure 4.7, respectively. As was the case with the smaller  $H_6$  ring, one needs to go to 150,000 MC iterations for the errors relative to the FCI data characterizing the *i*-FCIQMC energetics to be consistently smaller than those of the deterministic ACCSD( $1, \frac{3+4}{2}$ ) approach. The same applies to the original CAD-FCIQMC scheme, with the exception of the  $R_{H-H} = 2.0$  Å grid point for which no convergence was obtained. The novel CAD-FCIQMC[1,(3+4)/2] methodology is characterized by a rapid convergence to FCI across all grid points sampling the symmetric dissociation of  $H_{10}$ , including both the weakly and strongly correlated regimes. Indeed, CAD-FCIQMC[1,(3+4)/2] faithfully reproduces the FCI PEC already at 100,000 MC iterations, being characterized by smaller than 1% relative errors.

So far, we have seen that both flavors of CAD-FCIQMC considered in this dissertation produce FCI-quality energetics based on information extracted out of the early stages of FCIQMC propagations not only in weakly correlated situations, but also in the presence of quasi-degeneracies such as those characterizing the  $C_{2v}$ -symmetric double bond dissociation of  $H_2O$ . Furthermore, we demonstrated that in the strong correlation regime, the original CAD-FCIQMC[1–5] scheme is characterized by a slow convergence toward the exact energy values or breaks down completely, depending on the number of entangled electrons. On the other hand, the novel CAD-FCIQMC[1,(3+4)/2] methodology is practically immune to the presence of strong correlations and offers a rapid convergence toward FCI-quality energetics for the entire spectrum of electron correlation effects. As a final illustration of the power of CAD-FCIQMC approaches in general, we set out to determine the frozen-core FCI total electronic energy of  $C_6H_6$ , the simplest aromatic compound, as described by the cc-pVDZ basis set at its equilibrium structure. In this case, the size of the many-electron Hilbert space, which is spanned by about  $10^{36}$   $S_z = 0$  Slater determinants without taking advantage



of point group symmetry, renders a brute-force FCI computation impossible. In fact, the dimensionality of the pertinent Hamiltonian matrix exceeds the present-day capabilities of state-of-the-art super computers and matrix diagonalization algorithms by more than 25 orders of magnitude.

At a first glance, it may appear that the near-exact description of the electronic structure of the  $\text{C}_6\text{H}_6/\text{cc-pVDZ}$  system at its equilibrium geometry is child’s play, due to the seemingly absent strong correlations. Although, in general, strong many-electron correlation effects are almost invariably associated with non-dynamical correlations, the minimum-energy structure of  $\text{C}_6\text{H}_6$  is characterized by strong dynamical correlation effects. This can be illustrated by examining the convergence of the hierarchy of traditional CC approaches, including CCSD, CCSDT, and CCSDTQ. For example, the incorporation of three-body clusters, which predominantly recover dynamical correlations, on top of the basic CCSD approach results in a lowering of the CCSD correlation energy by  $-36.45 \text{ mE}_h$  [266] or  $-1.215 \text{ mE}_h$  per electron. For the sake of comparison, the  $(\Delta E_0^{(\text{CCSDT})} - \Delta E_0^{(\text{CCSD})})/N$  correlation energy difference per electron for the  $\text{H}_6/\text{cc-pVDZ}$  system, which is the simplest *ab initio* model of the  $\pi$ -electron network of  $\text{C}_6\text{H}_6/\text{cc-pVDZ}$ , is only  $-0.5368 \text{ mE}_h$ . The effect of connected quadruples in the case of  $\text{C}_6\text{H}_6/\text{cc-pVDZ}$  is far from being negligible, as is evident by the fact that the CCSDTQ correlation energy of  $\Delta E_0^{(\text{CCSDTQ})} = -862.37 \text{ mE}_h$  is lower than the CCSDT one by  $-2.47 \text{ mE}_h$  [266, 317].

As already alluded to above, the situation is further complicated by the size of the problem of distributing the 30 valence electrons of  $\text{C}_6\text{H}_6$  to the 108 correlated orbitals arising from the cc-pVDZ basis. To put it into perspective, the dimension of the many-electron Hilbert space for  $\text{C}_6\text{H}_6/\text{cc-pVDZ}$  is only a few orders of magnitude smaller than the state space of chess, *i.e.*, the number of all possible legal positions of chessmen, as estimated by Shannon [318]. Consequently, the numbers of correlated electrons and correlated orbitals render higher-level SRCC approaches, such as the CC approach with singles, doubles, triples, quadruples, and pentuples (CCSDTQP;  $T^{(\text{CCSDTQP})} = T_1 + T_2 + T_3 + T_4 + T_5$ ) [319], prohibitively expensive

and the same is true for many other conventional quantum chemistry approaches.

The above discussion showcases the fact that the near-exact description of electron correlations in the  $\text{C}_6\text{H}_6/\text{cc-pVDZ}$  system constitutes a great avenue for testing the power of CAD-FCIQMC. So far, in performing CAD-FCIQMC computations, we relied on information extracted from *i*-FCIQMC propagations. However, in the case of the medium-sized  $\text{C}_6\text{H}_6$  molecule that is dominated by strong dynamical correlation effects, *i*-FCIQMC is anticipated to face significant difficulties due to the biasing introduced by the initiator approximation. This becomes apparent once we realize that the proper and accurate description of dynamical correlations requires the stochastic wavefunction sampling to capture a vast number of excited Slater determinants all of which are inhabited by small walker populations. The undersampling of the many-electron Hilbert space induced by the initiator algorithm usually manifests itself in a very slow convergence of *i*-FCIQMC with respect to the total walker population, sometimes so slow that it is essentially impossible to approach the exact, FCI, limit [310]. As a matter of fact, in the case of  $\text{C}_6\text{H}_6$ , the converged *i*-FCIQMC/cc-pVDZ projected energy lies between the CCSD and CCSDT results, being more than  $20 \text{ mE}_\text{h}$  higher than the CCSDTQ correlation energy [310]. Taking into account that in the absence of strong non-dynamical correlations, as in the case of  $\text{C}_6\text{H}_6$  in its equilibrium geometry, CCSDTQ provides energetics that are close to their corresponding FCI values, the conventional *i*-FCIQMC methodology fails to converge to the exact, FCI, limit for this seemingly docile system. This clearly indicates that the wavefunction information provided by *i*-FCIQMC is unsuitable for initializing CAD-FCIQMC computations for  $\text{C}_6\text{H}_6$ .

One possibility to account for the systematic error associated with the initiator approach is to employ a *a posteriori* energy correction based on second-order perturbation theory. In the case of  $\text{C}_6\text{H}_6/\text{cc-pVDZ}$ , *i*-FCIQMC augmented with the aforementioned perturbative correction significantly bridges the gap between *i*-FCIQMC and CCSDTQ, as evident by the converged correlation energy of  $-860.7 \pm 0.7 \text{ mE}_\text{h}$  [310]. However, this result is still higher than the CCSDTQ one by at least  $1 \text{ mE}_\text{h}$ . Taking into consideration the numer-

ical observations that, in the absence of strong non-dynamical correlations, the high-level CC approaches, although not variational, converge to FCI from above, the performance of the perturbation–theory-corrected *i*-FCIQMC methodology is still not satisfactory. In addition, and more importantly for the context of this work, the corresponding wavefunction information is that obtained in the underlying *i*-FCIQMC simulations, which, as already emphasized above, constitutes a poor starting point for performing CAD-FCIQMC calculations. To circumvent all of these difficulties, in our CAD-FCIQMC computations for the C<sub>6</sub>H<sub>6</sub>/cc-pVDZ system, we relied on wavefunctions resulting from the recently proposed AS-FCIQMC methodology of Alavi and co-workers [263]. As mentioned earlier in this dissertation, the AS-FCIQMC methodology ameliorates the bias introduced by the initiator approximation in a *a priori* manner, namely, by making suitable modifications to the initiator algorithm. As a result, even with a relatively modest walker population of 10<sup>8</sup>, the AS-FCIQMC methodology produced the correlation energy for C<sub>6</sub>H<sub>6</sub> that was lower than that of CCSDTQ by about 1 mE<sub>h</sub> (cf. supporting information to Reference [266]), which is already very encouraging.

As already mentioned, in the computations for the C<sub>6</sub>H<sub>6</sub> molecule we employed the cc-pVDZ basis set. The equilibrium geometry of benzene, optimized at the MP2/6-31G\* level of theory, was taken from Reference [320]. The underlying AS-FCIQMC propagations were performed by Alavi and Ghanem [263] using the NECI code [321, 322]. The various details of the AS-FCIQMC simulations can be found in the supporting information to Reference [266]. Here, it suffices to say that the CAD-FCIQMC calculations relied on information extracted from two instantaneous AS-FCIQMC wavefunctions: the wavefunction obtained at the last MC iteration of an AS-FCIQMC simulation with 1 billion (1B) walkers, designated as  $\left| \Phi_{1B}^{(\text{AS-FCIQMC})} \right\rangle$ , and the wavefunction obtained at the end of a AS-FCIQMC propagation with 2 billion (2B) walkers, abbreviated as  $\left| \Phi_{2B}^{(\text{AS-FCIQMC})} \right\rangle$ . To test the numerical stability of our highest-level CAD-FCIQMC results using 2B walkers, we performed an additional CAD-FCIQMC computation in which we replaced the instantaneous  $\left| \Phi_{2B}^{(\text{AS-FCIQMC})} \right\rangle$  wave-

function by the state obtained by averaging the last 100 time steps of the aforementioned AS-FCIQMC simulation with 2 billion walkers, denoted as  $\left| \Phi_{2B}^{(\text{AS-FCIQMC})} (100\text{-avg}) \right\rangle$ . The cluster analysis of the AS-FCIQMC wavefunction and the subsequent CCSD-like computations were performed with codes of the Piecuch group. The same set of one- and two-body molecular integrals, extracted from the MOLPRO program [323, 324], was employed for both the AS-FCIQMC simulations and subsequent CCSD-like computations.

The results of our CAD-FCIQMC[1–5] and CAD-FCIQMC[1,(3+4)/2] computations for the  $\text{C}_6\text{H}_6/\text{cc-pVDZ}$  system are summarized in Table 4.11. The various acronyms shown in Table 4.11 are augmented by either a (1B) or a (2B) suffix, to indicate the total walker population used in the pertinent AS-FCIQMC propagation. For the sake of comparison, we also include the correlation energies obtained from the underlying AS-FCIQMC simulations along with their corresponding error bars. These were obtained by discarding the data points corresponding to the walker growth and equilibration periods and performing blocking analysis [325] on the rest (see the supporting information to Reference [266] for the details). In addition, in Table 4.11, we also report the projective energy corresponding to each instantaneous AS-FCIQMC wavefunction, designated as CAD-FCIQMC-ext, which is computed using Equation (3.5) with the information about the one- and two-body clusters extracted from AS-FCIQMC,  $T_1^{(\text{MC})}(\tau)$  and  $T_2^{(\text{MC})}(\tau)$ , respectively. The difference between the CAD-FCIQMC-ext and CAD-FCIQMC correlation energies provides a valuable diagnostic of the quality of the underlying instantaneous AS-FCIQMC wavefunction, especially of its  $C_n^{(\text{MC})}(\tau)$  with  $n = 1\text{--}4$  components. Indeed, if the initial CAD-FCIQMC-ext correlation energy differs significantly from the final CAD-FCIQMC result, *i.e.*, if the  $T_1^{(\text{MC})}(\tau)$  and  $T_2^{(\text{MC})}(\tau)$  amplitudes extracted from AS-FCIQMC substantially relax during the process of solving the CCSD-like Equations (3.29) and (3.40) in the presence of their  $T_3^{(\text{MC})}(\tau)$  and  $T_4^{(\text{MC})}(\tau)$  counterparts, we can conclude that the AS-FCIQMC wavefunction is not converged yet. The correlation energies reported in the last two rows of Table 4.11, designated as CAD-FCIQMC-ext(2B,100-avg) and CAD-FCIQMC[1–5](2B,100-avg), correspond to the

$\left| \Phi_{2B}^{(\text{AS-FCIQMC})} (100\text{-avg}) \right\rangle$  wavefunction that was obtained by averaging the last 100 time steps of the AS-FCIQMC simulation with 2 billion walkers.

We begin our discussion by focusing on the results arising from the AS-FCIQMC calculation with a total walker population of 1 billion, starting with AS-FCIQMC(1B) itself. The AS-FCIQMC(1B) correlation energy of  $-864.8 \pm 0.5 \text{ mE}_h$  is lower than the CCSDTQ one by at least  $2 \text{ mE}_h$ . At the same time, the CAD-FCIQMC-ext correlation energy is  $-867.010 \text{ mE}_h$ , *i.e.*, about  $2 \text{ mE}_h$  lower than the aforementioned AS-FCIQMC(1B) value. This observation suggests that the instantaneous AS-FCIQMC(1B) wavefunction is not well converged. Indeed, letting the  $T_1$  and  $T_2$  clusters relax in the presence of their  $T_3^{(\text{MC})}(\tau)$  and  $T_4^{(\text{MC})}(\tau)$  counterparts extracted from AS-FCIQMC(1B) increases the correlation energy by about  $3 \text{ mE}_h$ , as evident by the CAD-FCIQMC[1–5](1B) and CAD-FCIQMC[1,(3+4)/2](1B) results. Furthermore, both flavors of CAD-FCIQMC provide correlation energies that are above the upper limit of  $-864.3 \text{ mE}_h$  resulting from the underlying AS-FCIQMC(1B) computations by a fraction of a millihartree. This potentially suggests that AS-FCIQMC(1B) slightly overestimates the correlation energy of the  $\text{C}_6\text{H}_6/\text{cc-pVDZ}$  system. On a side note, the CAD-FCIQMC[1–5](1B) and CAD-FCIQMC[1,(3+4)/2](1B) correlation energies are in excellent agreement with each other, as might have been anticipated due to the absence of strong non-dynamical correlation effects.

We now proceed to the results arising from the largest AS-FCIQMC simulation considered, namely, the one using a total walker population of 2 billion. A simple inspection of Table 4.11 reveals that the AS-FCIQMC(2B) correlation energy of  $-863.7 \pm 0.3 \text{ mE}_h$  is higher than its 1 billion counterpart by about  $1 \text{ mE}_h$ . In fact, there is an excellent agreement between the AS-FCIQMC(2B) value and the CAD-FCIQMC[1–5](1B) and CAD-FCIQMC[1,(3+4)/2](1B) data. This should be contrasted with the fact that the AS-FCIQMC(1B) value is outside the  $\pm 0.3 \text{ mE}_h$  error bars of the more accurate AS-FCIQMC(2B) result. These observations further showcase the spectacular performance of CAD-FCIQMC in accelerating convergence toward the exact, FCI, energetics. Moving on

to our highest-level CAD-FCIQMC results using 2 billion walkers, we notice that the CAD-FCIQMC-ext(2B) correlation energy is in excellent agreement with its AS-FCIQMC(2B) counterpart, suggesting that the instantaneous  $\left| \Phi_{2B}^{(\text{AS-FCIQMC})} \right\rangle$  wavefunction, at least its  $C_1^{(\text{MC})}$  and  $C_2^{(\text{MC})}$  components, are well converged. This is further corroborated by the fact that the CAD-FCIQMC-ext(2B) result can hardly be distinguished from both the CAD-FCIQMC[1–5](2B) and CAD-FCIQMC[1,(3+4)/2](2B) energetics. Indeed, the CAD-FCIQMC-ext(2B), CAD-FCIQMC[1–5](2B), and CAD-FCIQMC[1,(3+4)/2](2B) correlation energies agree with one another to within about 0.02 mE<sub>h</sub>. This clearly demonstrates that the  $T_1^{(\text{MC})}(\tau)$  and  $T_2^{(\text{MC})}(\tau)$  clusters extracted from the instantaneous  $\left| \Phi_{2B}^{(\text{AS-FCIQMC})} \right\rangle$  wavefunction hardly relax during the process of solving the CCSD-like system of equations, Equations (3.29) and (3.40), in the presence of their  $T_3^{(\text{MC})}(\tau)$  and  $T_4^{(\text{MC})}(\tau)$  counterparts. In the spirit of externally corrected CC approaches, the slight relaxation of the one- and two-body clusters in the presence of their three- and four-body counterparts extracted from the AS-FCIQMC(2B) wavefunction implies that  $T_3^{(\text{MC})}(\tau)$  and  $T_4^{(\text{MC})}(\tau)$  are of FCI quality.

As a final test of the numerical stability of our highest-level CAD-FCIQMC results using 2 billion walkers, we examine the CAD-FCIQMC correlation energies arising from processing the  $\left| \Phi_{2B}^{(\text{AS-FCIQMC})}(\text{100-avg}) \right\rangle$  wavefunction. We see that the replacement of the instantaneous  $\left| \Phi_{2B}^{(\text{AS-FCIQMC})} \right\rangle$  wavefunction by its  $\left| \Phi_{2B}^{(\text{AS-FCIQMC})}(\text{100-avg}) \right\rangle$  counterpart, obtained by averaging the last 100 time steps of the AS-FCIQMC simulation with 2 billion walkers, has a minor effect on the CAD-FCIQMC-ext and CAD-FCIQMC[1–5] correlation energies. Indeed, the CAD-FCIQMC-ext(2B,100-avg) and CAD-FCIQMC[1–5](2B,100-avg) data differ from their counterparts using the instantaneous  $\left| \Phi_{2B}^{(\text{AS-FCIQMC})} \right\rangle$  wavefunction by about 0.01 mE<sub>h</sub>. The remarkable consistency between the CAD-FCIQMC energetics using 2 billion walkers gives us further confidence in our results. It is also worth mentioning that the CAD-FCIQMC[1–5](1B) and CAD-FCIQMC[1,(3+4)/2](1B) energetics differ from their counterparts using 2 billion walkers by only about 0.5 mE<sub>h</sub>. The fact that all of our CAD-FCIQMC results reported in this dissertation are within the  $\pm 0.3$  mE<sub>h</sub> error bars

characterizing the largest AS-FCIQMC simulation using 2 billion walkers is also very reassuring. Based on our highest-level CAD-FCIQMC[1–5](2B), CAD-FCIQMC[1,(3+4)/2](2B), and CAD-FCIQMC[1–5](2B,100-avg) results, we estimate the exact, FCI, correlation energy of the  $\text{C}_6\text{H}_6/\text{cc-pVDZ}$  system at its minimum-energy structure to be  $-863.4 \text{ mE}_h$ .

At this point, it is worth mentioning that the calculations for the  $\text{C}_6\text{H}_6/\text{cc-pVDZ}$  system reported in this dissertation formed part of a blind challenge, reported in Reference [266], aimed at determining its frozen-core FCI energy. In addition to the aforementioned AS-FCIQMC and CAD-FCIQMC approaches, the various methodologies that were evaluated in the blind challenge included adaptive sampling CI (ASCI) [326–329], semi-stochastic heat-bath CI (SHCI) [330–336], iterative CI with selection (iCI) [337–340], DMRG [198–201, 341–348], many-body expanded FCI (MBE-FCI) [317, 349–351], and full CC reduction (FCCR) [352]. One of the major findings of that investigation was that, with the exception of the ASCI, iCI, and SHCI results, all correlation energies agreed with one another to within  $0.9 \text{ mE}_h$ , ranging from  $-863.7 \text{ mE}_h$  to  $-862.8 \text{ mE}_h$ . It is also interesting to note that our CAD-FCIQMC result lies more or less in the middle of the aforementioned interval. Based on the findings of the blind challenge, the frozen-core FCI correlation energy of the  $\text{C}_6\text{H}_6$  species at its equilibrium geometry as described by the cc-pVDZ basis set is estimated to be in the neighborhood of  $-863 \text{ mE}_h$ .

Table 4.8: Convergence of the energies resulting from the all-electron *i*-FCIQMC, CAD-FCIQMC[1–5], and CAD-FCIQMC[1,(3+4)/2] calculations with  $\Delta\tau = 0.0001$  a.u. toward FCI for the H<sub>2</sub>O molecule, as described by the cc-pVDZ basis set, at the equilibrium geometry  $R_e$  and the geometry obtained by a simultaneous stretching of both O–H bonds by a factor of 2.0.<sup>a</sup> The *i*-FCIQMC calculations were initiated by placing 1,000 walkers on the RHF determinant and the  $n_a$  parameter of the initiator algorithm was set at 3.

Iterations (I)	%T <sup>b</sup>	%Q <sup>c</sup>	%FCI <sup>d</sup>	$f_I^e$	CAD-FCIQMC		$i$ -FCIQMC
					[1–5]	[1,(3+4)/2]	
$R_{O-H} = R_e$							
0	0	0	0.00	0.09	3.744 <sup>f</sup>	−0.731 <sup>g</sup>	217.821 <sup>h</sup>
20,000	11.8	1.38	0.01	3.95	−0.073	−0.019	1.596
40,000	16.4	2.28	0.01	6.52	−0.211	−0.126	−2.217
60,000	21.3	3.48	0.02	10.3	−0.046	−0.202	1.911
80,000	26.5	5.12	0.02	16.1	0.189	0.210	−0.686
100,000	32.1	7.47	0.04	25.7	−0.036	−0.032	0.139
120,000	38.0	10.3	0.05	40.0	−0.035	−0.061	0.597
140,000	44.2	14.0	0.08	63.5	0.098	0.087	0.080
160,000	50.4	18.3	0.12	100	0.078	0.114	−0.400
∞	100	100	100	—		−76.241860 <sup>i</sup>	
$R_{O-H} = 2.0R_e$							
0	0	0	0.00	0.01	22.032 <sup>f</sup>	3.041 <sup>g</sup>	363.954 <sup>h</sup>
20,000	10.6	1.34	0.01	0.55	8.485	5.656	72.650
40,000	16.6	2.72	0.02	1.29	0.138	−0.232	44.627
60,000	24.5	5.03	0.03	2.85	−0.225	1.026	19.660
80,000	33.2	8.46	0.06	6.01	−0.425	0.812	12.611
100,000	42.5	13.2	0.12	12.4	−0.816	1.125	5.680
120,000	51.7	19.2	0.20	25.1	−0.555	0.534	4.041
140,000	60.9	26.6	0.35	50.3	−0.666	0.498	1.981
160,000	69.5	34.9	0.57	100	−0.434	0.398	1.328
∞	100	100	100	—		−75.951665 <sup>i</sup>	

<sup>a</sup> The equilibrium geometry,  $R_{O-H} = R_e$ , and the geometry obtained by a simultaneous stretching of both O–H bonds by a factor of 2.0 without changing the  $\angle(\text{H-O-H})$  angle,  $R_{O-H} = 2.0R_e$ , were taken from [277] and all electrons were correlated. Unless otherwise stated, all energies are errors relative to FCI in millihartree.

<sup>b</sup> Percentages of triply excited determinants captured during the *i*-FCIQMC propagations.

<sup>c</sup> Percentages of quadruply excited determinants captured during the *i*-FCIQMC propagations.

<sup>d</sup> Percentages of all determinants spanning the entire many-electron Hilbert space captured during the *i*-FCIQMC propagations.

<sup>e</sup> Walker populations characterizing the *i*-FCIQMC propagations reported as percentages of the total walker numbers at  $I = I_{\text{max}} = 160,000$ , which in the specific *i*-FCIQMC runs reported in this table and Figure 4.4 were 1,169,396 at  $R_{O-H} = R_e$  and 10,146,724 at  $R_{O-H} = 2.0R_e$ .

<sup>f</sup> Equivalent to CCSD.

<sup>g</sup> Equivalent to ACCSD(1,  $\frac{3+4}{2}$ ).

<sup>h</sup> Equivalent to RHF.

<sup>i</sup> Total FCI energy in hartree taken from [277].



Table 4.9: Convergence of the energies resulting from the *i*-FCIQMC, CAD-FCIQMC[1–5], and CAD-FCIQMC[1,(3+4)/2] calculations with  $\Delta\tau = 0.0001$  a.u. toward FCI for the symmetric dissociation of the H<sub>6</sub> ring, as described by the cc-pVDZ basis set, at two representative values of the distance between neighboring H atoms, including  $R_{\text{H-H}} = 1.0$  Å (the region of the minimum on the FCI PEC shown in Figure 4.5(a) characterized by weaker correlations) and  $R_{\text{H-H}} = 2.0$  Å (the region characterized by strong correlations involving the entanglement of all six electrons).<sup>a</sup> The *i*-FCIQMC calculations were initiated by placing 1,500 walkers on the RHF determinant and the  $n_a$  parameter of the initiator algorithm was set at 3.

Iterations (I)	%T <sup>b</sup>	%Q <sup>c</sup>	%FCI <sup>d</sup>	$f_I^e$	CAD-FCIQMC		$i$ -FCIQMC
					[1–5]	[1,(3+4)/2]	
$R_{\text{H-H}} = 1.0 \text{ \AA}$							
0	0	0	0.00	0.58	3.328 <sup>f</sup>	1.256 <sup>g</sup>	138.122 <sup>h</sup>
20,000	26.4	4.27	0.84	13.3	0.235	0.047	6.029
40,000	31.7	5.77	1.11	18.5	0.276	0.243	0.598
60,000	37.4	7.67	1.44	25.0	−0.124	−0.096	−0.225
80,000	42.8	9.90	1.86	33.5	−0.005	0.047	−1.680
100,000	47.7	12.4	2.29	43.6	−0.129	−0.146	0.511
120,000	53.6	15.8	2.93	58.4	−0.022	−0.050	−1.338
140,000	59.3	19.0	3.61	75.8	−0.107	−0.178	1.500
160,000	64.0	23.3	4.50	100	0.085	0.129	−0.347
∞	100	100	100	—		−3.387731 <sup>i</sup>	
$R_{\text{H-H}} = 2.0 \text{ \AA}$							
0	0	0	0.00	0.12	−35.048 <sup>f</sup>	8.818 <sup>g</sup>	252.159 <sup>h</sup>
20,000	23.9	3.81	0.83	2.82	−34.263	7.149	119.438
40,000	32.6	6.90	1.51	5.63	−32.884	2.906	70.886
60,000	40.7	10.4	2.33	9.60	−27.807	0.596	43.687
80,000	49.2	14.8	3.41	15.9	−17.090	0.762	26.814
100,000	57.4	20.0	4.77	25.1	−11.815	0.019	16.263
120,000	65.2	26.4	6.61	40.1	−9.077	−0.400	10.560
140,000	72.3	33.4	8.83	63.3	−5.457	−0.114	6.543
160,000	78.5	41.4	11.6	100	−2.401	0.419	4.015
∞	100	100	100	—		−3.062318 <sup>i</sup>	

<sup>a</sup> Unless otherwise stated, all energies are errors relative to FCI in millihartree.

<sup>b</sup> Percentages of triply excited determinants captured during the *i*-FCIQMC propagations.

<sup>c</sup> Percentages of quadruply excited determinants captured during the *i*-FCIQMC propagations.

<sup>d</sup> Percentages of all determinants spanning the entire many-electron Hilbert space captured during the *i*-FCIQMC propagations.

<sup>e</sup> Walker populations characterizing the *i*-FCIQMC propagations reported as percentages of the total walker numbers at  $I = I_{\text{max}} = 160,000$ , which in the specific *i*-FCIQMC runs reported in this table and Figures 4.6(a) and 4.6(b) were 257,301 at  $R_{\text{H-H}} = 1.0$  Å and 1,271,883 at  $R_{\text{H-H}} = 2.0$  Å.

<sup>f</sup> Equivalent to CCSD.

<sup>g</sup> Equivalent to ACCSD(1,  $\frac{3+4}{2}$ ).

<sup>h</sup> Equivalent to RHF.

<sup>i</sup> Total FCI energy in hartree.

Table 4.10: Same as Table 4.9 for the symmetric dissociation of the  $\text{H}_{10}$  ring, as described by the DZ basis set. In analogy to the  $\text{H}_6$  ring,  $R_{\text{H-H}} = 1.0 \text{ \AA}$  corresponds to the region of the minimum on the FCI PEC shown in Figure 4.5(b) characterized by weaker correlations, whereas  $R_{\text{H-H}} = 2.0 \text{ \AA}$  is the region characterized by strong correlations involving the entanglement of all ten electrons.

Iterations (I)	%T	%Q	%FCI	$f_I^a$	CAD-FCIQMC		$i$ -FCIQMC
					[1-5]	[1,(3+4)/2]	
$R_{\text{H-H}} = 1.0 \text{ \AA}$							
0	0	0	0.00	0.14	4.878	2.265	162.374
20,000	34.3	6.14	0.08	7.07	2.083	1.525	14.503
40,000	42.0	9.12	0.12	11.3	0.774	0.785	3.721
60,000	49.2	12.6	0.18	16.6	0.367	0.457	-0.260
80,000	55.9	16.6	0.25	23.6	0.087	0.015	1.991
100,000	61.8	21.4	0.34	33.3	0.343	0.382	1.096
120,000	68.8	27.8	0.48	49.1	-0.092	0.022	-0.083
140,000	74.7	34.7	0.66	70.4	0.231	0.285	-0.388
160,000	79.3	42.2	0.91	100	0.054	0.051	1.394
$\infty$	100	100	100	—		-5.538852	
$R_{\text{H-H}} = 2.0 \text{ \AA}$							
0	0	0	0.00	0.00	NC <sup>b</sup>	29.172	454.768
20,000	37.9	8.92	0.15	0.12	NC <sup>b</sup>	23.004	253.265
40,000	55.1	21.7	0.68	0.56	NC <sup>b</sup>	9.377	163.979
60,000	69.8	36.4	1.90	1.77	NC <sup>b</sup>	3.779	98.996
80,000	80.7	51.7	4.11	4.46	NC <sup>b</sup>	-3.612	63.082
100,000	88.6	65.7	7.54	9.95	NC <sup>b</sup>	-3.565	37.756
120,000	93.5	77.4	12.5	21.4	NC <sup>b</sup>	-3.592	21.909
140,000	96.5	86.0	19.1	45.8	NC <sup>b</sup>	-1.704	11.943
160,000	98.1	91.8	27.3	100	NC <sup>b</sup>	-1.829	7.187
$\infty$	100	100	100	—		-5.079254	

<sup>a</sup> Walker populations characterizing the  $i$ -FCIQMC propagations reported as percentages of the total walker numbers at  $I = I_{\text{max}} = 160,000$ , which in the specific  $i$ -FCIQMC runs reported in this table and Figures 4.6(c) and 4.6(d) were 1,093,428 at  $R_{\text{H-H}} = 1.0 \text{ \AA}$  and 133,246,948 at  $R_{\text{H-H}} = 2.0 \text{ \AA}$ .

<sup>b</sup> NC indicates that no convergence was obtained when the solution of the CC equations defining the deterministic part of the CAD-FCIQMC[1-5] procedure [Equations (3.29) and (3.40), in which  $\xi_i$ ,  $i = 1-5$ , are all set at 1] was carefully continued from the weakly correlated region.

Table 4.11: Results of the CAD-FCIQMC calculations based on the AS-FCIQMC wavefunctions obtained after equilibration runs using 1 billion (1B) and 2 billion (2B) walkers.

Calculation	$\Delta E/mE_h$
<u>1 Billion Walkers</u>	
AS-FCIQMC(1B)	$-864.8 \pm 0.5$
CAD-FCIQMC-ext(1B)	$-867.010$
CAD-FCIQMC[1-5](1B)	$-864.089$
CAD-FCIQMC[1,(3+4)/2](1B)	$-863.861$
<u>2 Billion Walkers</u>	
AS-FCIQMC(2B)	$-863.7 \pm 0.3$
CAD-FCIQMC-ext(2B)	$-863.464$
CAD-FCIQMC[1-5](2B)	$-863.453$
CAD-FCIQMC[1,(3+4)/2](2B)	$-863.438$
CAD-FCIQMC-ext(2B,100-avg)	$-863.460$
CAD-FCIQMC[1-5](2B,100-avg)	$-863.439$

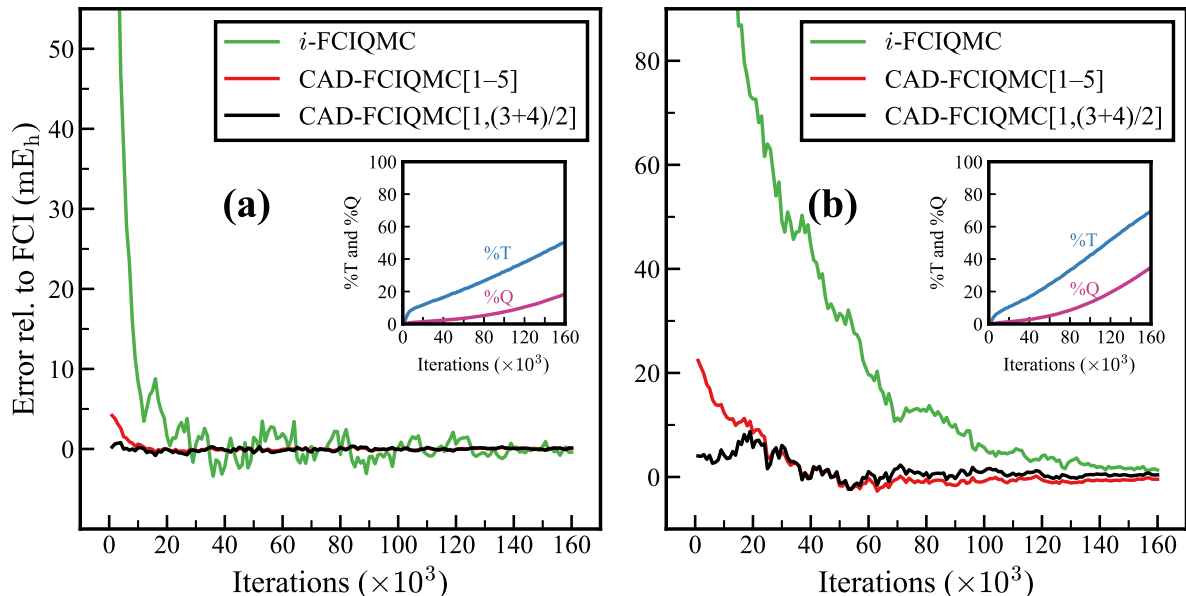


Figure 4.4: Convergence of the energies resulting from the all-electron *i*-FCIQMC, CAD-FCIQMC[1-5], and CAD-FCIQMC[1,(3+4)/2] calculations with  $\Delta\tau = 0.0001$  a.u. toward FCI for the H<sub>2</sub>O molecule, as described by the cc-pVDZ basis set, at (a) the equilibrium geometry and (b) the geometry obtained by a simultaneous stretching of both O-H bonds by a factor of 2 without changing the  $\angle(\text{H-O-H})$  angle (both geometries were taken from [277]). The *i*-FCIQMC calculations were initiated by placing 1,000 walkers on the RHF determinant and the  $n_a$  parameter of the initiator algorithm was set at 3. All energies are errors relative to FCI in millihartree, and the insets show the percentages of triply (%T) and quadruply (%Q) excited determinants captured during the *i*-FCIQMC propagations.

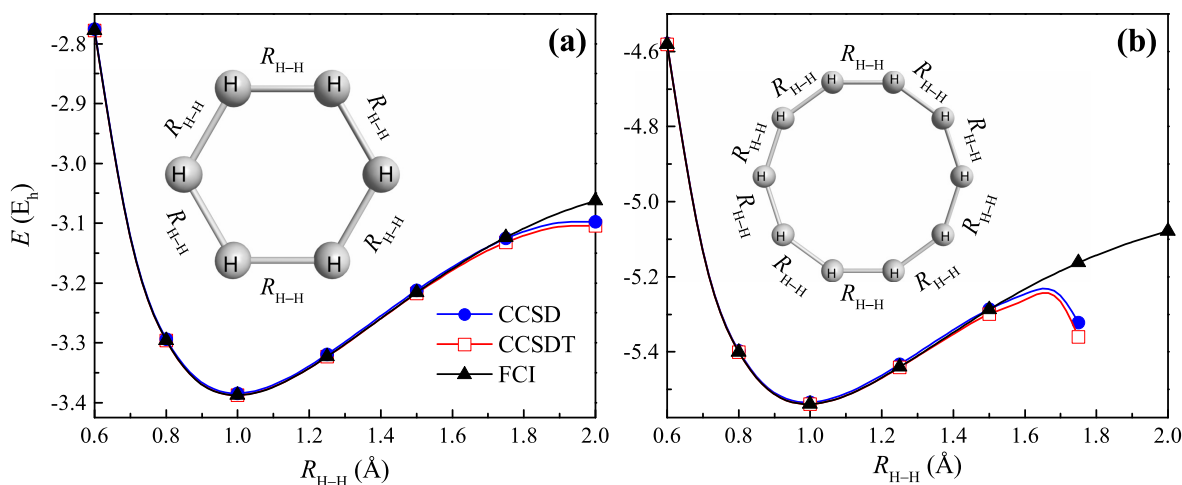


Figure 4.5: Ground-state PECs for the symmetric dissociation of the (a) H<sub>6</sub>/cc-pVDZ and (b) H<sub>10</sub>/DZ systems resulting from the CCSD, CCSDT, and FCI calculations.

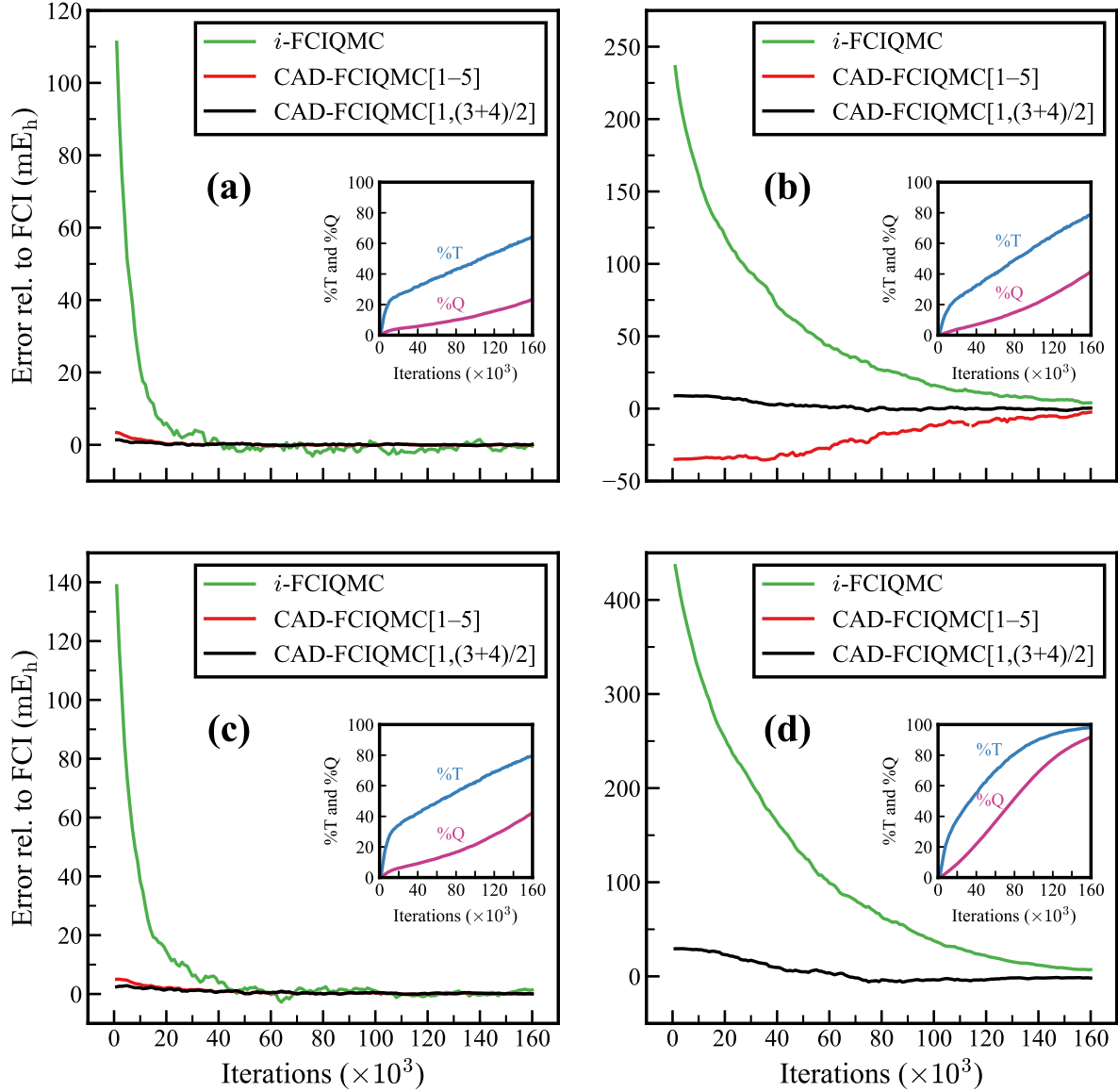


Figure 4.6: Convergence of the energies resulting from the *i*-FCIQMC, CAD-FCIQMC[1–5], and CAD-FCIQMC[1,(3+4)/2] calculations with  $\Delta\tau = 0.0001$  a.u. toward FCI for the symmetric dissociation of the H<sub>6</sub>/cc-pVDZ [panels (a) and (b)] and H<sub>10</sub>/DZ [panels (c) and (d)] systems at two representative values of the distance between neighboring H atoms, including  $R_{\text{H-H}} = 1.0$  Å [panels (a) and (c)] and  $R_{\text{H-H}} = 2.0$  Å [panels (b) and (d)]. The *i*-FCIQMC calculations were initiated by placing 1,500 walkers on the RHF determinant and the  $n_a$  parameter of the initiator algorithm was set at 3. All energies are errors relative to FCI in millihartree, and the insets show the percentages of triply (%T) and quadruply (%Q) excited determinants captured during the *i*-FCIQMC propagations. The CAD-FCIQMC[1–5] curve is absent in panel (d), since the solution of the CC equations defining the deterministic part of the CAD-FCIQMC[1–5] procedure for the H<sub>10</sub>/DZ system could not be continued beyond  $R_{\text{H-H}} = 1.75$  Å.

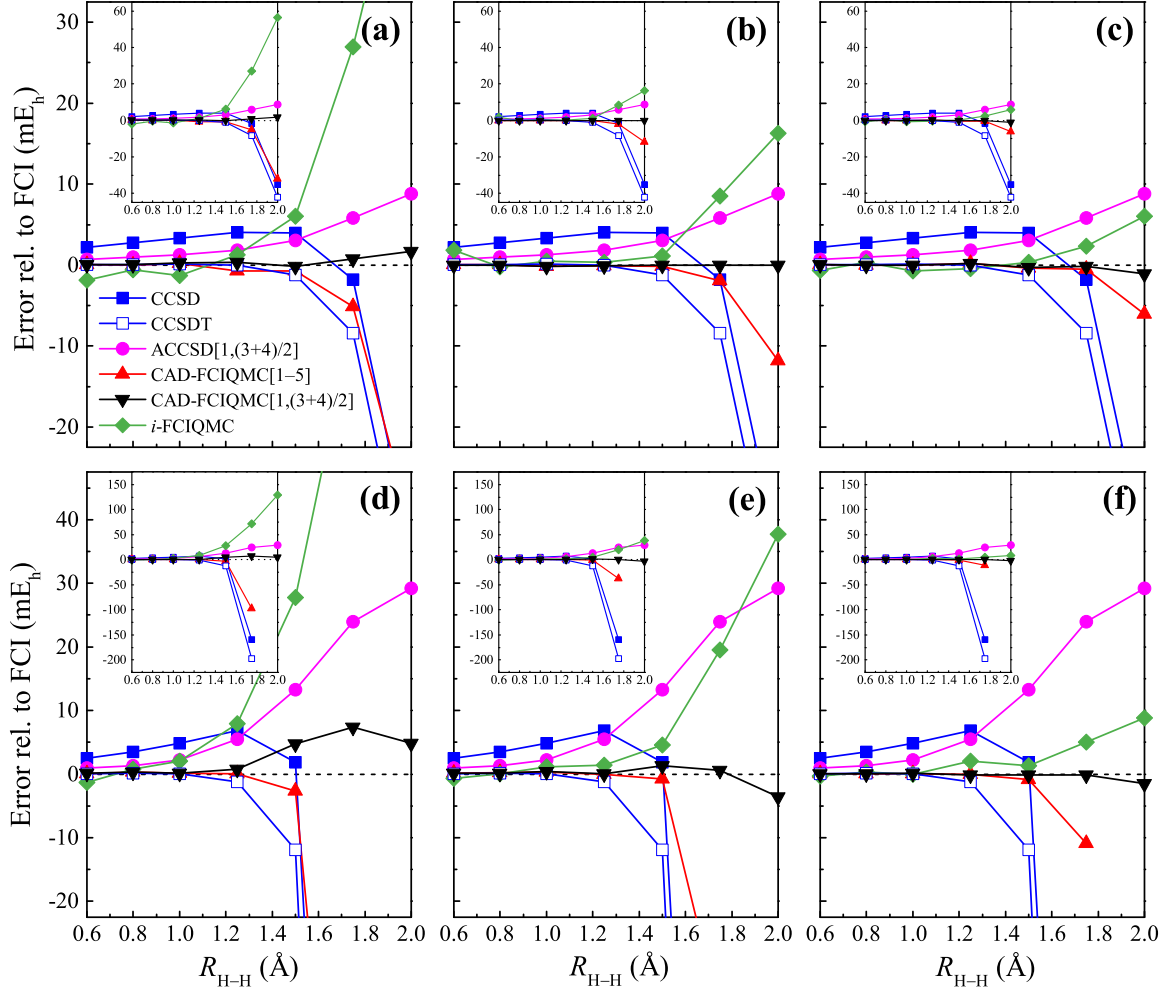


Figure 4.7: A comparison of the energies resulting from the  $i$ -FCIQMC, CAD-FCIQMC[1–5], and CAD-FCIQMC[1,(3+4)/2] calculations at 50,000 [panels (a) and (d)], 100,000 [panels (b) and (e)], and 150,000 [panels (c) and (f)] FCIQMC iterations using time step  $\Delta\tau = 0.0001$  a.u., along with the corresponding fully deterministic CCSD, CCSDT, and ACCSD( $1, 3 \times \frac{n_o}{n_o+n_u} + 4 \times \frac{n_u}{n_o+n_u}$ ) data, for the symmetric dissociation of the  $H_6/cc\text{-pVDZ}$  [panels (a)–(c)] and  $H_{10}/DZ$  [panels (d)–(f)] systems at selected distances between neighboring H atoms,  $R_{H-H}$ , ranging from the weakly correlated (smaller  $R_{H-H}$ ) to the strongly correlated (larger  $R_{H-H}$ ) regions. The  $i$ -FCIQMC calculations were initiated by placing 1,500 walkers on the RHF determinant and the  $n_a$  parameter of the initiator algorithm was set at 3. All energies are errors relative to FCI in millihartree. The insets show the entire range of errors relative to FCI.

## CHAPTER 5

### CONCLUDING REMARKS AND FUTURE OUTLOOK

In this dissertation, we presented recent advances in the development of SRCC approaches for strongly correlated systems, which lie at the heart of contemporary quantum chemistry. After introducing the concept of strong correlation, we argued that the sheer dimensionalities of the underlying model spaces render MR schemes inapplicable to the strong correlation regime, emphasizing the need for robust, yet computationally affordable, single-reference quantum chemistry methodologies. In this dissertation, we focused on SRCC approaches, which, over the years, have been established as the *de facto* standard for high-accuracy electronic structure calculations, even in the presence of quasi-degeneracies such as those characterizing single and double bond dissociations. We presented various numerical examples from the literature that demonstrate that the hierarchy of traditional SRCC approaches, including CCSD, CCSDT, CCSDTQ, *etc.*, completely breaks down in the strong correlation regime of model Hamiltonians. Inspired by the work of Scuseria and co-workers [209], we proved analytically that in the fully correlated limit of the 12-site half-filled attractive pairing Hamiltonian the importance of the many-body components of the cluster operator is reversed, *i.e.*,  $T_2 = T_4 < T_6 < T_8 < T_{10} < T_{12}$  (recall that  $T_{2n+1} = 0, \forall n \in \mathbb{Z}^+ \cup \{0\}$  in the case of the attractive pairing Hamiltonian). Thus, we demonstrated that the fabric of conventional SRCC methodologies is completely torn apart by the onset of strong correlations. Subsequently, we proceeded to the discussion of novel unconventional classes of CC approaches capable of providing an accurate description of the entire spectrum of many-electron correlation effects, ranging from the weakly to the strongly correlated regimes.

In the first part of this dissertation, we examined CC schemes belonging to the family of ACP methodologies, in which one retains all doubly excited cluster amplitudes while using subsets of non-linear diagrams of the CCD/CCSD equations. Although the original ACP schemes were immune to the catastrophic failures exhibited by traditional CC approaches,

such as CCSD and even CCSDT and CCSDTQ, in strongly correlated model systems, their application to realistic problems was hindered by two issues. First, typical ACP approaches neglected the  $T_3$  physics, without which one cannot obtain quantitative accuracy for most problems of chemical interest, while all previous attempts to incorporate the three-body clusters using conventional MBPT-like arguments were only partly successful. Second, the various diagram cancellations defining the ACP methodologies were derived using minimum-basis-set model systems, meaning that they were not necessarily optimum when larger basis sets were employed. Both of these issues were successfully addressed in this dissertation. As far as the neglect of  $T_3$  physics is concerned, we employed active-space ideas to incorporate the leading three-body clusters within the ACP framework in a robust, yet computationally affordable, manner. To extend the ACP schemes to larger basis sets, we introduced a new ACP variant, abbreviated as ACCSD( $1, 3 \times \frac{n_o}{n_o+n_u} + 4 \times \frac{n_u}{n_o+n_u}$ ), that utilized basis-set-dependent scaling factors multiplying the pertinent coupled-pair diagrams. We demonstrated that all of the examined ACP schemes, without and with the connected triples, provided qualitatively correct PECs for the symmetric dissociation of hydrogen clusters as large as the  $H_{50}$  linear chain. In addition, we also showed that all active-space ACP approaches faithfully reproduced their full triples parents, but at a fraction of the computational cost. Furthermore, among the tested ACP methodologies, the novel ACCSD( $1, 3 \times \frac{n_o}{n_o+n_u} + 4 \times \frac{n_u}{n_o+n_u}$ ) scheme corrected for the triples performed the best, consistently recovering about 99–101% of the exact, FCI, or nearly exact, DMRG correlation energies, but at a fraction of the computational cost.

In the second part of this dissertation, we introduced a new class of semi-stochastic approaches capable of extrapolating the exact energetics out of the early stages of FCIQMC simulations, even in the presence of strong many-electron correlation effects. This was accomplished by merging the ACP ideas with the recently proposed CAD-FCIQMC methodology, where, in the spirit of externally corrected CC schemes, one solves CCSD-like equations for the one- and two-body clusters in the presence of their three- and four-body counterparts



extracted from FCIQMC. In its original formulation, this approach was able to accurately extrapolate the exact, FCI, energetics based on the early stages of FCIQMC propagations, even in the presence of quasi-degeneracies such as those characterizing the  $C_{2v}$ -symmetric double bond dissociation of  $H_2O$ . In this dissertation, however, we showed that this scheme was not able to handle strongly correlated systems, due to the singular behavior of CCSD in such situations. Furthermore, we demonstrated that this issue can be remedied by repartitioning the CC equations, so that selected coupled-pair contributions are extracted from FCIQMC as well. In doing so, we treated the part of the  $\langle \Phi_{ij}^{ab} | (V_N \frac{1}{2} T_2^2)_C | \Phi \rangle$  term that is responsible for the good behavior in strongly correlated systems deterministically and extracted the information about its complement from the purely stochastic FCIQMC wavefunction sampling, thus, successfully extending the CAD-FCIQMC methodology to the strong correlation regime. This allowed us to obtain a FCI-quality description of the symmetric dissociation of hydrogen rings into individual H atoms, using the wavefunction information extracted from the early stages of *i*-FCIQMC propagations. As a final illustration of the power of CAD-FCIQMC, we provided an estimate of the frozen-core FCI correlation energy of the  $C_6H_6$  molecule as described by the cc-pVDZ basis at its minimum-energy structure. Our CAD-FCIQMC value was in excellent agreement with the energetics resulting from AS-FCIQMC, MBE-FCI, and DMRG calculations that were performed independently of our CAD-FCIQMC computations.

The ideas and methodologies developed and tested in this dissertation can be expanded in the future in various ways. Focusing on the deterministic ACP methodologies, it would be interesting to replace the active-space treatment of three-body clusters by a CR-CC(2,3)-type non-iterative energy correction. We recall that the CR-CC(2,3) approach [137–140] belongs to the family of left-eigenstate completely renormalized CC/EOMCC methodologies, resulting from the formalism of the method of moments of CC equations [128–144], in which one adds a non-iterative correction to the energies resulting from methods employing a conventional truncation in the cluster operator  $T$ , such as CCSD, for the correlation

effects due to the higher-order connected excitations that are neglected in the initial CC calculation. Taking into account the ability of the various ACCSD approaches to tame strong non-dynamical correlation effects and the fact that CR-CC approaches capture a substantial portion of dynamical correlations, the proposed CR-CC-corrected ACCSD schemes are anticipated to be suitable for the study of the entire spectrum of electron correlation effects. Depending on the outcomes of such an investigation, one can envision correcting the ACCSDt energies for the correlation effects due to the missing triples in the spirit of the CC( $P;Q$ ) framework [37, 38, 144, 161–163], which extends the aforementioned moment expansions to unconventional truncations of the cluster operator such as those defining active-space CC approaches.

Another possibility worth exploring would be to replace the user- and system-dependent active orbitals of ACCSDt schemes by automatically determined active spaces via stochastic wavefunction sampling, as is done, for example, in the recently proposed semi-stochastic CC( $P$ ) methodology and its CC( $P;Q$ ) extension [164–166]. It has been demonstrated, for example, that the semi-stochastic CC( $P$ ) approach is capable of producing CCSDT-level energetics by utilizing active spaces extracted out of the early stages of *i*-FCIQMC or even truncated CI and CC Monte Carlo [353–356], such as CISDT-MC, CISDTQ-MC, and *i*-CCSDT-MC [355], simulations while the semi-stochastic CC( $P;Q$ ) method significantly accelerates the convergence [164, 166]. Naturally, the proposed semi-stochastic extension of the ACCSDt family of methods will be of no use in the study of strongly correlated systems treated by minimum basis sets, such as the  $H_m$ /STO- $n$ G clusters, since the pertinent active spaces are fully determined by the symmetry of the problem. Nevertheless, such an approach will certainly prove useful in the study of realistic strongly correlated systems, including, for example, complexes involving transition metals. Eventually, in the spirit of the semi-stochastic CC( $P;Q$ ) hierarchy, one would like to correct the semi-stochastic ACCSDt results for the correlation effects due to the triples not captured yet by the QMC stochastic wavefunction sampling.

An additional aspect of the ACCSD methodologies and their active-space connected triples extensions that might be interesting to explore in the future is their usefulness as references for obtaining accurate excitation energies, ionization potentials, and electron affinities of strongly correlated systems through the EOM formalism. A straightforward approach in this regard would be to diagonalize a similarity-transformed Hamiltonian constructed using the  $T_1$  and  $T_2$  or  $T_1$ ,  $T_2$ , and  $t_3$  amplitudes resulting from ACCSD or ACCSDt computations, respectively. To the best of our knowledge, there exists only one such investigation based on  $2\text{CC} \equiv \text{ACCSD}(4,5)$  and its connected triples extensions, abbreviated as  $3\text{CC}$  and  $3\text{CC}_m$ , gauging their performance in reproducing the data resulting from their respective EOMCCSD and EOMCCSDT counterparts, FCI, and experiment, when available, [233]. However, the authors did not make any comments regarding the possible merits of using such methods for the treatment excited, ionized, and electron-attached states of systems with strongly correlated electronic ground states. Furthermore, they did not consider ACCSD variants other than ACCSD(4,5). It would be interesting to examine whether the analogous conclusions regarding the performance of the various ground-state ACCSD and ACCSDt methodologies apply to their excited-state, ionized, and electron-attached counterparts. An alternative, and perhaps more suitable, approach for extending the ACCSD and ACCSDt approaches to excited, ionized, and electron-attached states of strongly correlated systems would be to replace the similarity-transformed Hamiltonian of CC theory with an effective Hamiltonian that reflects on the various diagram cancellations/modifications of a given ACCSD/ACCSDt variant. To the best of our knowledge, there exists only one such investigation where the authors studied excited electronic states of organic molecules by diagonalizing effective Hamiltonians corresponding to  $2\text{CC}$ ,  $\text{DCSD}$ , and  $\text{pCCSD}$  reference states [241]. However, they did not consider systems whose ground electronic states are characterized by strong many-electron correlation effects. It would be interesting to examine the performance of the EOM extensions of the ACCSD approaches, without and with triples, examined in this dissertation in the study of challenging strongly correlated systems, where the underlying CCSD

approach produces an unphysical description or even becomes singular.

Turning our attention to the semi-stochastic CAD-FCIQMC family of methods, it would be interesting to attempt to accelerate the convergence toward the exact, FCI, energetics even further by correcting the CAD-FCIQMC energies for the correlation effects associated with the triples and quadruples not yet captured by FCIQMC, in the spirit of the aforementioned  $CC(P;Q)$  hierarchy of methods. Considering that dynamical electron correlation effects are usually more difficult to capture compared to their non-dynamical counterparts during the FCIQMC stochastic wavefunction sampling, such  $CC(P;Q)$ -corrected CAD-FCIQMC approaches are anticipated to accelerate convergence by recovering a substantial portion of dynamical correlations. For example, in the case of CAD-FCIQMC[1–5], the proposed scheme would become equivalent to CR-CC(2,4) at  $\tau = 0$ , which already constitutes a significant improvement over the CCSD starting point of CAD-FCIQMC[1–5]. The suggested *a posteriori* energy corrections are expected to be even more powerful when combined with the CAD-FCIQMC[1,(3+4)/2] scheme, which, as demonstrated in this dissertation, provides an accurate description of strong non-dynamical many-electron correlation effects already from the outset of FCIQMC simulations. Eventually, taking into account that the three- and four-body clusters extracted from FCIQMC wavefunctions become exact only in the  $\tau \rightarrow \infty$  limit, one can even contemplate correcting  $T_3^{(MC)}(\tau)$  and  $T_4^{(MC)}(\tau)$  themselves, in addition to the  $CC(P;Q)$ -type corrections for the triples and quadruples not captured by FCIQMC.

An alternative approach would be to take advantage of the one- and two-body clusters resulting from our CAD-FCIQMC computations and attempt to accelerate the convergence toward FCI of the underlying FCIQMC propagations themselves. This could be accomplished, for example, using the following algorithm. At a given time step, convert the  $T_1$  and  $T_2$  clusters obtained in a CAD-FCIQMC calculation to their  $C_1$  and  $C_2$  counterparts. Subsequently, translate the  $C_1$  and  $C_2$  excitation amplitudes back to walker populations of singly and doubly excited Slater determinants by multiplying them with the population

of walkers residing in the RHF reference determinant (rounding to the nearest integer, if necessary, to enforce integer populations of walkers). Finally, use the list of determinants and updated walker populations to restart the FCIQMC propagation. A much more sophisticated approach that would retain some information regarding the cluster structure of the many-body wavefunction would be as follows. At a given time step, extract a list of all, *i.e.*, up to  $N$ -tuply excited, Slater determinants that are captured by the FCIQMC stochastic wavefunction sampling. Subsequently, cluster analyze the entire FCIQMC wavefunction, extract  $T_1^{(\text{MC})}(\tau) - T_{n-1}^{(\text{MC})}(\tau)$ , and subtract from  $C_3^{(\text{MC})}(\tau) - C_n^{(\text{MC})}(\tau)$  all disconnected components containing  $T_1^{(\text{MC})}(\tau)$  and  $T_2^{(\text{MC})}(\tau)$ . After performing a CAD-FCIQMC computation, restore all disconnected components that were subtracted in the previous step by using  $T_3^{(\text{MC})}(\tau) - T_{n-1}^{(\text{MC})}(\tau)$  and the  $T_1$  and  $T_2$  amplitudes obtained from CAD-FCIQMC. Convert the  $T_1$  and  $T_2$  clusters obtained in a CAD-FCIQMC calculation to their  $C_1$  and  $C_2$  counterparts. Translate all CI excitation amplitudes back to walker populations and restart the FCIQMC simulation. However, the computational complexity associated with such a scheme renders the first algorithm a much more attractive approach for potentially accelerating the convergence of FCIQMC simulations using CAD-FCIQMC.

Another interesting possibility would be to replace the stochastic FCIQMC methodology as the non-CC source of  $T_1$  and  $T_2$  clusters by other wavefunction-based schemes that are also guaranteed to become exact as a given limit is approached. For example, one could use methods that belong to the general category of selected CI (SCI) approaches [357–362]. A typical SCI computation is initiated by diagonalizing the Hamiltonian within an initial variational space that is spanned by one or more selected Slater determinants. Subsequently, the initial variational space is enriched by adding external Slater determinants that satisfy a predefined importance criterion and the Hamiltonian is diagonalized once more. This procedure is repeated until self consistency is reached. This algorithm reveals that as the variational space keeps increasing one arrives at increasingly better approximations to the exact, FCI, energy, and, eventually, SCI becomes equivalent to a FCI diagonalization of

the Hamiltonian matrix. A cluster-analysis-driven SCI (CAD-SCI) is anticipated to have a couple of advantages over the original CAD-FCIQMC family of methods. Unlike the state-of-the-art *i*-FCIQMC and AS-FCIQMC schemes, SCI approaches are variational, suggesting that in every iteration one can extract  $T_3$  and  $T_4$  clusters of increasing quality from the wavefunction of the SCI method of interest. Furthermore, in typical SCI methodologies, the diagonalization of the Hamiltonian matrix is accomplished deterministically, meaning that CAD-SCI will be free of the stochastic noise characterizing CAD-FCIQMC schemes. Time will tell whether such CAD-SCI schemes can provide FCI-quality correlation energies at a smaller computational cost compared to their FCIQMC analogs.

Finally, based on the remarkable performance of CAD-FCIQMC in the case of ground electronic states, it would be worth to extend such approaches to excited electronic states. Taking into account that any excited-state wavefunction that has a non-zero overlap with the HF Slater determinant can be expressed using an exponential ansatz [363], the existing CAD-FCIQMC algorithm, in fact any externally corrected CC approach, can be used for the study of such excited electronic states. This is not surprising, especially when one realizes that the CC equations, which are non-linear, have multiple solutions, some of which correspond to excited electronic states and others that are unphysical [128, 364–376]. However, the study of excited electronic states whose wavefunctions are orthogonal to the HF Slater determinant would only be possible by using, for example, the EOM formalism. In that case, one would need to examine the corresponding EOM equations and identify the  $R_{\mu,n}$  many-body components of the CI-like linear excitation operator  $R_\mu$  that are necessary to determine the pertinent vertical excitation energies,  $\omega_\mu$ . Subsequently, one would need to compare the structure of a generic excited-state wavefunction within the FCI and EOM-FCC formalisms and arrive at a correspondence between the many-body components of the  $C = \sum_{n=0}^N C_n$  operator of FCI and the  $T$  and  $R_\mu$  operators of EOMCC theory. To simplify the process of such a cluster analysis, one could approximate  $T \approx T^{(\text{CCSD})}$ , albeit possibly sacrificing the size-intensivity of the final excitation energies. Of course, such a simplification

will be impossible in situations where CCSD is plagued by singularities.

## APPENDICES



## APPENDIX A

### COMPUTER IMPLEMENTATION OF THE APPROXIMATE COUPLED-PAIR METHODS WITH AN ACTIVE-SPACE TREATMENT OF THREE-BODY CLUSTERS

The active-space triples ACP approaches were implemented by making suitable modifications to the spin-integrated active-space CCSDt code of the Piecuch group, generated by Dr. Jun Shen. The first step in this effort was to identify the five Goldstone–Brandow diagrams associated with the  $\frac{1}{2}T_2^2$  contributions to the CC equations projected on the singlet pp-hh coupled orthogonally spin-adapted doubly excited configuration state functions, shown in Figure 3.5, with their spin-integrated counterparts within the existing CCSDt code. As shown in Table A.1, in spin-orbital form, the  $\langle \Phi_{ij}^{ab} | (V_N \frac{1}{2} T_2^2)_C | \Phi \rangle$  term gives rise to four Hugenholtz diagrams. Thus, we see that the first Hugenholtz diagram of Table A.1 corresponds to the Goldstone–Brandow diagrams D1 and D2 shown in Figure 3.5, while the second, third, and fourth Hugenholtz diagrams correspond to the Goldstone–Brandow diagrams D3, D4, and D5, respectively, of the same figure.

Table A.1: The spin-orbital Hugenholtz and Brandow diagrams and corresponding algebraic expressions arising from the  $\langle \Phi_{ij}^{ab} | (V_N \frac{1}{2} T_2^2)_C | \Phi \rangle$  term. In the last column, we provide the correspondence between the spin-orbital diagrams presented in this table and the spin-adapted ones shown in Figure 3.5.

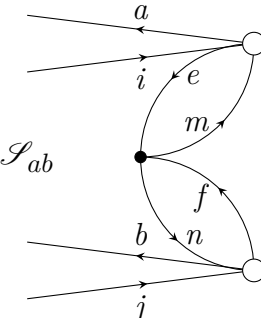
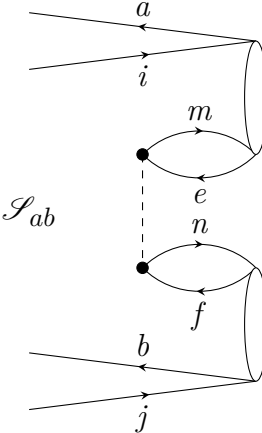
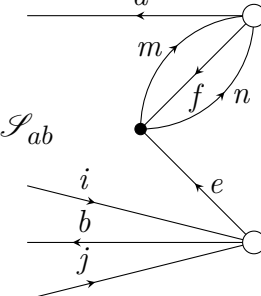
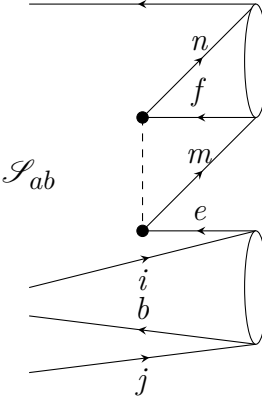
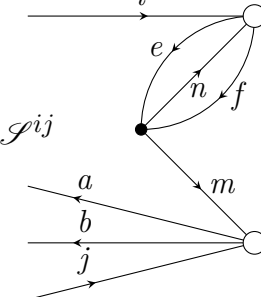
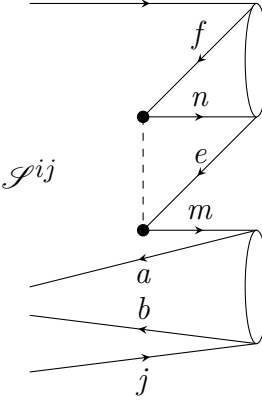
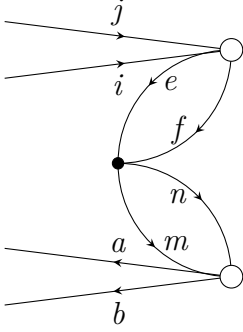
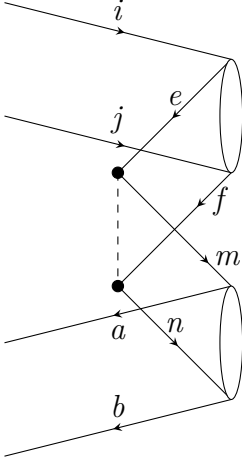
Hugenholtz	Brandow	Expression	Assignment
 <p><math>\mathcal{S}_{ab}</math></p>	 <p><math>\mathcal{S}_{ab}</math></p>	$\mathcal{A}_{ab} v_{mn}^{ef} t_{ae}^{im} t_{bf}^{jn}$	D1 + D2
 <p><math>\mathcal{S}_{ab}</math></p>	 <p><math>\mathcal{S}_{ab}</math></p>	$\frac{1}{2} \mathcal{A}_{ab} v_{mn}^{ef} t_{af}^{nm} t_{be}^{ji}$	D3
 <p><math>\mathcal{S}_{ij}</math></p>	 <p><math>\mathcal{S}_{ij}</math></p>	$\frac{1}{2} \mathcal{A}^{ij} v_{mn}^{ef} t_{ef}^{ni} t_{ab}^{mj}$	D4

Table A.1:(cont'd)

Hugenholtz	Brandow	Expression	Assignment
		$\frac{1}{4}v_{mn}^{ef}t_{ab}^{mn}t_{ef}^{ij}$	D5

Within the spin-integrated formalism, the  $T_2$  operator has three independent components, denoted in this dissertation as  $T_{2A}$ ,  $T_{2B}$ , and  $T_{2C}$ , that are defined as  $T_{2A}|\Phi\rangle = t_{AB}^{IJ}|\Phi_{IJ}^{AB}\rangle$ ,  $T_{2B}|\Phi\rangle = t_{AB}^{I\tilde{J}}|\Phi_{I\tilde{J}}^{A\tilde{B}}\rangle$ , and  $T_{2C}|\Phi\rangle = t_{AB}^{\tilde{I}\tilde{J}}|\Phi_{\tilde{I}\tilde{J}}^{\tilde{A}\tilde{B}}\rangle$ . Here and for the remainder of the Appendices, we explicitly specify the spin of a given spin-orbital as follows. The absence (presence) of the “ $\sim$ ” symbol above a given spatial orbital index indicates an  $\alpha$  ( $\beta$ ) spin-orbital. In analogy with  $T_2$ , the two-body term of the electronic Hamiltonian has three distinct components as well, namely,  $V_N = V_{NA} + V_{NB} + V_{NC}$ . Furthermore, when projecting the connected cluster form of the Schrödinger equation, Equation (3.3), onto doubly excited Slater determinants, one needs to distinguish the following three cases: (a)  $\langle\Phi_{IJ}^{AB}|(H_N e^T)_C|\Phi\rangle = 0$ , (b)  $\langle\Phi_{I\tilde{J}}^{A\tilde{B}}|(H_N e^T)_C|\Phi\rangle = 0$ , and (c)  $\langle\Phi_{\tilde{I}\tilde{J}}^{\tilde{A}\tilde{B}}|(H_N e^T)_C|\Phi\rangle = 0$ . The  $(V_N \frac{1}{2} T_2^2)_C$  connected operator product appearing in these projections gives rise to the terms

$$\begin{aligned}
(V_N \frac{1}{2} T_2^2)_C &= [(V_{NA} + V_{NB} + V_{NC}) \frac{1}{2} (T_{2A} + T_{2B} + T_{2C})^2]_C \\
&= [(V_{NA} + V_{NB} + V_{NC}) \frac{1}{2} (T_{2A}^2 + 2T_{2A}T_{2B} + 2T_{2A}T_{2C} + T_{2B}^2 + 2T_{2B}T_{2C} + T_{2C}^2)]_C \\
&= (V_{NA} \frac{1}{2} T_{2A}^2)_C + (V_{NA} T_{2A} T_{2B})_C + (V_{NB} T_{2A} T_{2B})_C + (V_{NB} T_{2A} T_{2C})_C \\
&\quad + (V_{NA} \frac{1}{2} T_{2B}^2)_C + (V_{NB} \frac{1}{2} T_{2B}^2)_C + (V_{NC} \frac{1}{2} T_{2B}^2)_C + (V_{NB} T_{2B} T_{2C})_C \\
&\quad + (V_{NC} T_{2B} T_{2C})_C + (V_{NC} \frac{1}{2} T_{2C}^2)_C,
\end{aligned}$$

where we used the fact that the various components of  $T_2$  commute with one another and terms whose spin combinations integrate to zero were excluded. Depending on the spin of a particular projection, only a subset of the above terms will be non-zero. Tables A.2, A.3, and A.4 list all  $(V_N \frac{1}{2} T_2^2)_C$  contributions to the spin-integrated CC equations projected onto the doubly excited Slater determinants  $|\Phi_{IJ}^{AB}\rangle$ ,  $|\Phi_{IJ}^{A\tilde{B}}\rangle$ , and  $|\Phi_{IJ}^{\tilde{A}\tilde{B}}\rangle$ , respectively.

Table A.2: The spin-integrated Hugenholtz and Brandow diagrams and corresponding algebraic expressions arising from the  $\langle \Phi_{IJ}^{AB} | (V_N \frac{1}{2} T_2^2)_C | \Phi \rangle$  term. In the last column, we provide the correspondence between the spin-integrated diagrams presented in this table and the spin-adapted ones shown in Figure 3.5.

Hugenholtz	Brandow	Expression	Assignment
$\langle \Phi_{IJ}^{AB}   (V_N \frac{1}{2} T_2^2)_C   \Phi \rangle$			
		$\mathcal{A}_{AB} v_{MN}^{EF} t_{AE}^{IM} t_{BF}^{JN}$	D1 + D2
		$\frac{1}{2} \mathcal{A}_{AB} v_{MN}^{EF} t_{AF}^{NM} t_{BE}^{JI}$	D3

Table A.2:(cont'd)

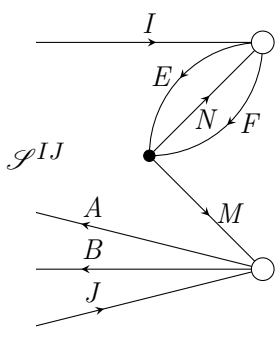
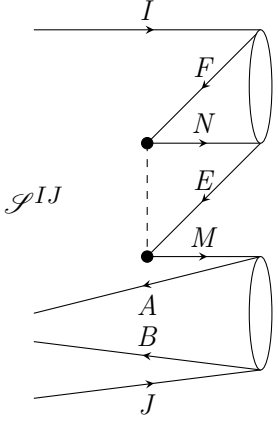
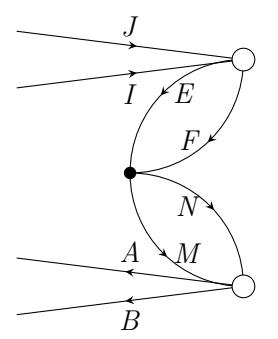
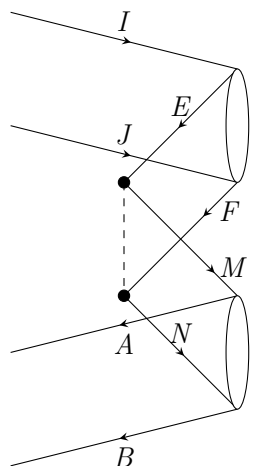
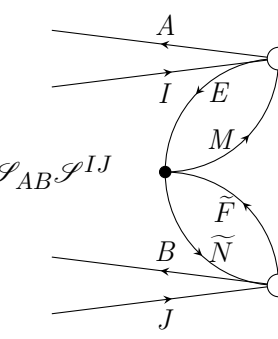
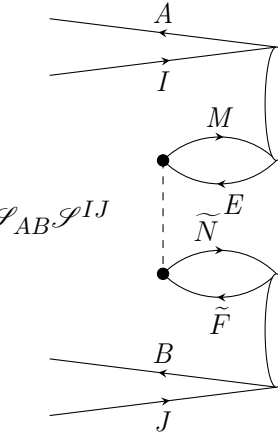
Hugenholtz	Brandow	Expression	Assignment
 $\mathcal{S}^{IJ}$	 $\mathcal{S}^{IJ}$	$\frac{1}{2} \mathcal{A}^{IJ} v_{MN}^{EF} t_{EF}^{NI} t_{AB}^{MJ}$	D4
		$\frac{1}{4} v_{MN}^{EF} t_{EF}^{IJ} t_{AB}^{MN}$	D5
	$\frac{\langle \Phi_{IJ}^{AB}   (V_{NB} T_{2A} T_{2B})_C   \Phi \rangle}{}$		
 $\mathcal{S}_{AB} \mathcal{S}^{IJ}$	 $\mathcal{S}_{AB} \mathcal{S}^{IJ}$	$\mathcal{A}_{AB} \mathcal{A}^{IJ} v_{MN}^{E\tilde{F}} t_{AE}^{IM} t_{BF}^{J\tilde{N}}$	D1

Table A.2:(cont'd)

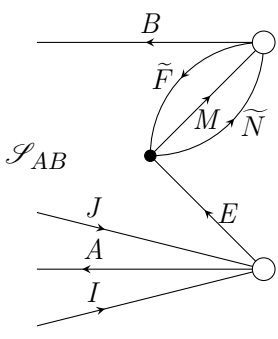
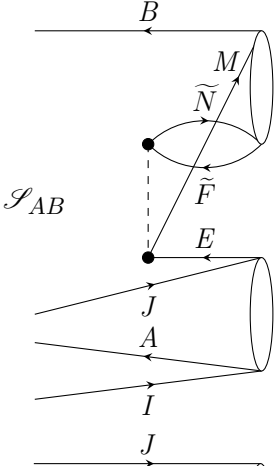
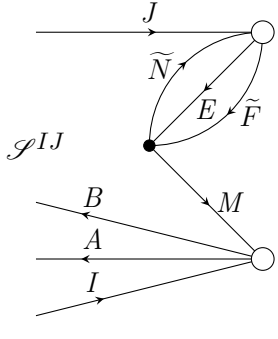
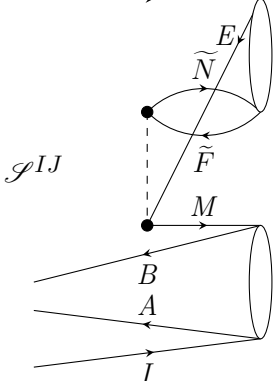
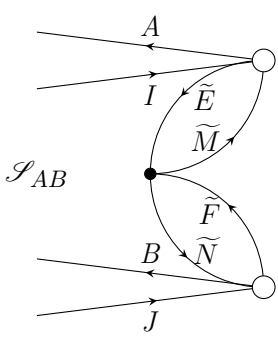
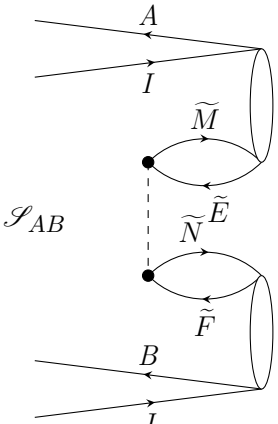
Hugenholtz	Brandow	Expression	Assignment
		$-\mathcal{A}_{AB} v_{M\tilde{N}}^{E\tilde{F}} t_{AE}^{IJ} t_{B\tilde{F}}^{M\tilde{N}}$	D3
		$-\mathcal{A}^{IJ} v_{M\tilde{N}}^{E\tilde{F}} t_{AB}^{IM} t_{EF}^{J\tilde{N}}$	D4
$\langle \Phi_{IJ}^{AB}   (V_{NB} \frac{1}{2} T_{2B}^2)_C   \Phi \rangle$			
		$\mathcal{A}_{AB} v_{M\tilde{N}}^{\tilde{E}\tilde{F}} t_{A\tilde{E}}^{\tilde{I}\tilde{M}} t_{B\tilde{F}}^{J\tilde{N}}$	D1 + D2

Table A.3: The spin-integrated Hugenholtz and Brandow diagrams and corresponding algebraic expressions arising from the  $\langle \Phi_{I\tilde{J}}^{A\tilde{B}} | (V_{\text{N}A} \frac{1}{2} T_2^2)_C | \Phi \rangle$  term. In the last column, we provide the correspondence between the spin-integrated diagrams presented in this table and the spin-adapted ones shown in Figure 3.5.

Hugenholtz	Brandow	Expression	Assignment
$\langle \Phi_{I\tilde{J}}^{A\tilde{B}}   (V_{\text{N}A} T_{2A} T_{2B})_C   \Phi \rangle$			
		$v_{MN}^{EF} t_{AE}^{IM} t_{F\tilde{B}}^{N\tilde{J}}$	D1 + D2
		$\frac{1}{2} v_{MN}^{EF} t_{AF}^{NM} t_{E\tilde{B}}^{I\tilde{J}}$	D3

Table A.3:(cont'd)

Hugenholtz	Brandow	Expression	Assignment
		$\frac{1}{2}v_{MN}^{EF}t_{EF}^{NI}t_{AB}^{MJ}$	D4
		$v_{MN}^{E\tilde{F}}t_{AE}^{IM}t_{B\tilde{F}}^{\tilde{J}\tilde{N}}$	D1
		$v_{MN}^{E\tilde{F}}t_{AF}^{I\tilde{N}}t_{EB}^{MJ}$	D1



Table A.3:(cont'd)

Hugenholtz	Brandow	Expression	Assignment
		$v_{M\tilde{N}}^{E\tilde{F}} t_{A\tilde{F}}^{M\tilde{J}} t_{E\tilde{B}}^{I\tilde{N}}$	D2
		$-v_{M\tilde{N}}^{E\tilde{F}} t_{A\tilde{F}}^{M\tilde{N}} t_{E\tilde{B}}^{I\tilde{J}}$	D3
		$-v_{M\tilde{N}}^{E\tilde{F}} t_{E\tilde{B}}^{M\tilde{N}} t_{A\tilde{F}}^{I\tilde{J}}$	D3

Table A.3:(cont'd)

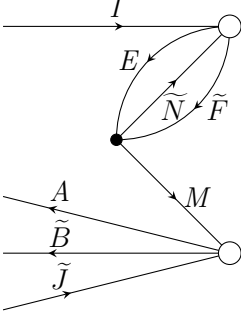
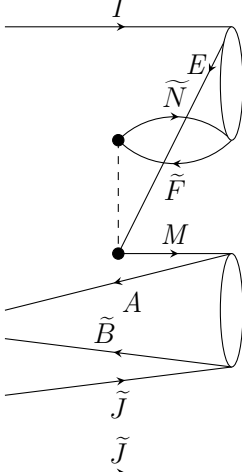
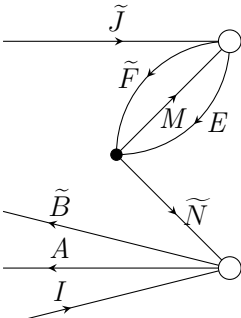
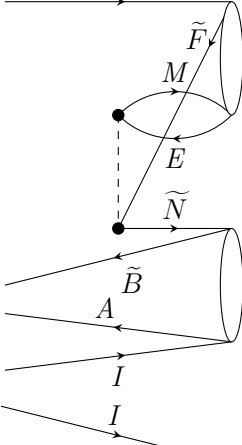
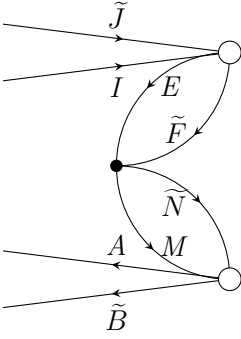
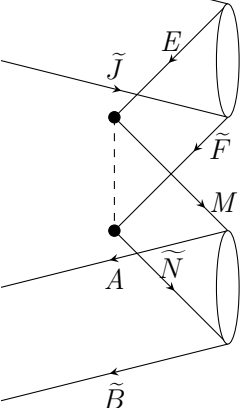
Hugenholtz	Brandow	Expression	Assignment
		$-v_{M\tilde{N}}^{E\tilde{F}} t_{E\tilde{F}}^{I\tilde{N}} t_{A\tilde{B}}^{M\tilde{J}}$	D4
		$-v_{M\tilde{N}}^{E\tilde{F}} t_{E\tilde{F}}^{M\tilde{J}} t_{A\tilde{B}}^{I\tilde{N}}$	D4
		$v_{M\tilde{N}}^{E\tilde{F}} t_{E\tilde{F}}^{I\tilde{J}} t_{A\tilde{B}}^{M\tilde{N}}$	D5

Table A.3:(cont'd)

Hugenholtz	Brandow	Expression	Assignment
$\left\langle \Phi_{IJ}^{AB} \left  (V_{\text{NC}} T_{2\text{B}} T_{2\text{C}})_C \right  \Phi \right\rangle$			
		$v_{\tilde{M}\tilde{N}}^{\tilde{E}\tilde{F}} t_{\tilde{A}\tilde{E}}^{I\tilde{M}} t_{\tilde{B}\tilde{F}}^{\tilde{J}\tilde{N}}$	D1 + D2
		$\frac{1}{2} v_{\tilde{M}\tilde{N}}^{\tilde{E}\tilde{F}} t_{\tilde{A}\tilde{E}}^{I\tilde{J}} t_{\tilde{B}\tilde{F}}^{\tilde{N}\tilde{M}}$	D3
		$\frac{1}{2} v_{\tilde{M}\tilde{N}}^{\tilde{E}\tilde{F}} t_{\tilde{A}\tilde{B}}^{I\tilde{M}} t_{\tilde{E}\tilde{F}}^{\tilde{N}\tilde{J}}$	D4

Table A.4: The spin-integrated Hugenholtz and Brandow diagrams and corresponding algebraic expressions arising from the  $\langle \Phi_{\tilde{I}\tilde{J}}^{\tilde{A}\tilde{B}} | (V_{\text{NA}} \frac{1}{2} T_{2\text{B}}^2)_C | \Phi \rangle$  term. In the last column, we provide the correspondence between the spin-integrated diagrams presented in this table and the spin-adapted ones shown in Figure 3.5.

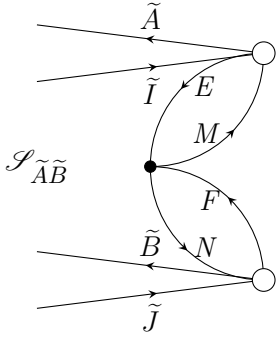
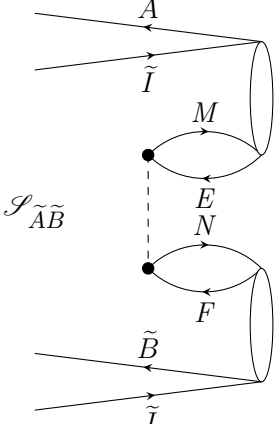
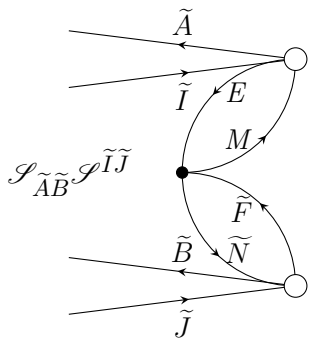
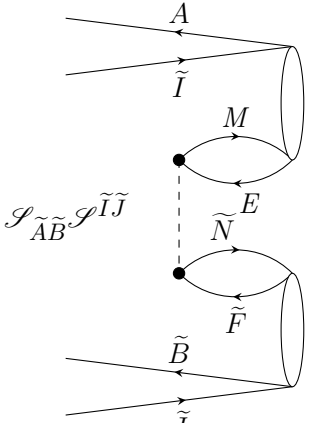
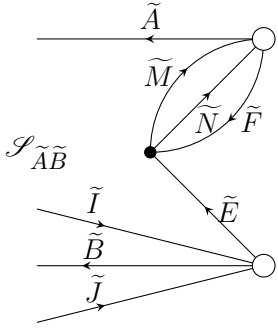
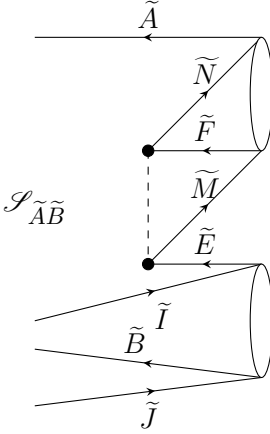
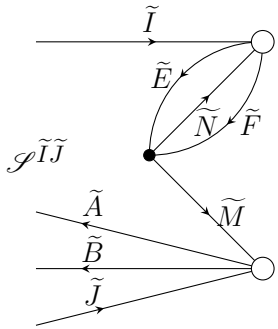
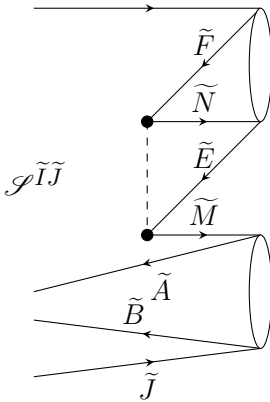
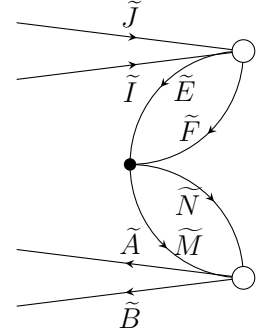
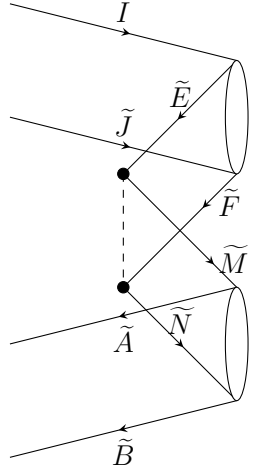
Hugenholtz	Brandow	Expression	Assignment
$\langle \Phi_{\tilde{I}\tilde{J}}^{\tilde{A}\tilde{B}}   (V_{\text{NA}} \frac{1}{2} T_{2\text{B}}^2)_C   \Phi \rangle$			
		$\mathcal{A}_{\tilde{A}\tilde{B}}^{\tilde{v}} t_{MN}^{EF} t_{E\tilde{A}}^{M\tilde{I}} t_{F\tilde{B}}^{\tilde{N}\tilde{J}}$	D1 + D2
$\langle \Phi_{\tilde{I}\tilde{J}}^{\tilde{A}\tilde{B}}   (V_{\text{NB}} T_{2\text{B}} T_{2\text{C}})_C   \Phi \rangle$			
		$\mathcal{A}_{\tilde{A}\tilde{B}}^{\tilde{I}\tilde{J}} v_{M\tilde{N}}^{E\tilde{F}} t_{E\tilde{A}}^{M\tilde{I}} t_{F\tilde{B}}^{\tilde{N}\tilde{J}}$	D1

Table A.4:(cont'd)

Hugenholtz	Brandow	Expression	Assignment
		$-\mathcal{A}_{\tilde{A}\tilde{B}} v_{NM}^{F\tilde{E}} t_{F\tilde{A}}^{N\tilde{M}} t_{\tilde{B}\tilde{E}}^{\tilde{J}\tilde{I}}$	D3
		$-\mathcal{A}^{\tilde{I}\tilde{J}} v_{NM}^{F\tilde{E}} t_{F\tilde{E}}^{N\tilde{I}} t_{\tilde{A}\tilde{B}}^{\tilde{M}\tilde{J}}$	D4
	$\left\langle \Phi_{\tilde{I}\tilde{J}}^{\tilde{A}\tilde{B}} \left  (V_{\text{NC}}^1 T_{2C}^2)_C \right  \Phi \right\rangle$		
		$\mathcal{A}_{\tilde{A}\tilde{B}} v_{\tilde{M}\tilde{N}}^{\tilde{E}\tilde{F}} t_{\tilde{A}\tilde{E}}^{\tilde{I}\tilde{M}} t_{\tilde{B}\tilde{F}}^{\tilde{J}\tilde{N}}$	D1 + D2

Table A.4:(cont'd)

Hugenholtz	Brandow	Expression	Assignment
		$\frac{1}{2} \mathcal{A}_{\tilde{A}\tilde{B}} v_{\tilde{M}\tilde{N}}^{\tilde{E}\tilde{F}} t_{\tilde{A}\tilde{F}}^{\tilde{N}\tilde{M}} t_{\tilde{B}\tilde{E}}^{\tilde{J}\tilde{I}}$	D3
		$\frac{1}{2} \mathcal{A}_{\tilde{I}\tilde{J}} v_{\tilde{M}\tilde{N}}^{\tilde{E}\tilde{F}} t_{\tilde{E}\tilde{F}}^{\tilde{N}\tilde{I}} t_{\tilde{A}\tilde{B}}^{\tilde{M}\tilde{J}}$	D4
		$\frac{1}{4} v_{\tilde{M}\tilde{N}}^{\tilde{E}\tilde{F}} t_{\tilde{E}\tilde{F}}^{\tilde{I}\tilde{J}} t_{\tilde{A}\tilde{B}}^{\tilde{M}\tilde{N}}$	D5

As shown in Tables A.2, A.3, and A.4, there are a total of 30 diagrams, 8 in each of the  $\langle \Phi_{IJ}^{AB} | (V_N \frac{1}{2} T_2^2)_C | \Phi \rangle$  and  $\langle \Phi_{\tilde{I}\tilde{J}}^{\tilde{A}\tilde{B}} | (V_N \frac{1}{2} T_2^2)_C | \Phi \rangle$  updates and 14 diagrams in the case

of  $\langle \Phi_{IJ}^{A\tilde{B}} | (V_N \frac{1}{2} T_2^2)_C | \Phi \rangle$ , that need to be modified in the doubles projections of the spin-integrated CCSDt code. To that end, five single-precision real variables, namely, diag1, diag2, diag3, diag4, and diag5, were introduced into the CCSDt code to scale the various D1, D2, D3, D4, and D5 diagrams. In Figure A.1, we show an excerpt from the Fortran code that illustrates the implementation of the various scaling factors, using the D3 diagram arising from the  $\langle \Phi_{IJ}^{A\tilde{B}} | (V_{NA} T_{2A} T_{2B})_C | \Phi \rangle$  term as an example. In particular, on line 1 of the code presented in Figure A.1, there is an “if” statement that skips the computation of this particular diagram when diag3 = 0. In addition, on line 16, the 0.5 diagrammatic factor is multiplied by the diag3 scaling factor. Taking into consideration the factorized form of the spin-integrated CCSDt code, in scaling the various  $\frac{1}{2} T_2^2$  terms appearing in the CC equations projected on doubly excited Slater determinants, care was taken not to scale intermediates that contribute to additional terms outside  $\frac{1}{2} T_2^2$ . In line 16 of the code presented in Figure A.1, for example, we see that the Q14 variable, which represents the  $\frac{1}{2} v_{MN}^{EF} t_{AF}^{NM}$  intermediate, is added to X5, which, in turn, is multiplied by  $t_{E\tilde{B}}^{I\tilde{J}}$  to give the D3 diagram (not shown). The Q14 variable is then deallocated in line 17, ensuring that only the desired diagram is scaled by this procedure. Out of the 30 intermediates contributing to the 30 spin-integrated diagrams presented in Tables A.2, A.3, and A.4, only four of them were also used in generating additional terms. In each of these four cases, a scaled copy of the intermediate was created and used to multiply the pertinent pair-cluster amplitude, while the original, unscaled, version was employed in constructing the intermediates to the additional terms.

As was anticipated, the spin-integrated diagram D1 and its D2 exchange counterpart are associated with the same Hugenholtz diagram for terms containing antisymmetrized matrix elements of  $V_N$ , namely,  $v_{MN}^{EF}$  and  $v_{M\tilde{N}}^{\tilde{E}\tilde{F}}$  (*cf.* Tables A.2, A.3, and A.4). In such cases, the scaling of the individual D1 and D2 diagrams was accomplished using an addition by subtraction procedure, which we outline using the  $\langle \Phi_{IJ}^{AB} | (V_{NC} \frac{1}{2} T_{2B}^2)_C | \Phi \rangle$  term as an example with the corresponding excerpt of the code provided in Figure A.2. In the first

```

1
2     if (diag3.ne.0) then !skip this part if diag3=0
3         allocate (D1(N0+1:N1,N0+1:N1,N1+1:N3,N1+1:N3))
4         call reorder3421 (N1,N3,N1,N3,N0,N1,N0,N1,
5 &         N0,N1,N0,N1,N1,N3,N1,N3,VAHHPP,D1)
6         allocate (D2(N0+1:N1,N0+1:N1,N1+1:N3,N1+1:N3))
7         call reorder3412 (N1,N3,N1,N3,N0,N1,N0,N1,
8 &         N0,N1,N0,N1,N1,N3,N1,N3,t2A,D2)
9         allocate (Q14(N1+1:N3,N1+1:N3))
10        I1=K3
11        I2=K3
12        I3=K3*K1*K1
13        call EGEMM( I1 , I2 , I3 , D1,D2,Q14)
14        deallocate (D1)
15        deallocate (D2)
16    !
17        call sum21 (N1,N3,N1,N3,X5,Q14,0.500*diag3) !scale D3 by diag3
18        deallocate (Q14)
19    endif

```

Figure A.1: Excerpt of the code that computes the scaled  $\frac{1}{2}v_{MN}^{EF}t_{AF}^{NM}$  intermediate, which eventually multiplies  $t_{E\tilde{B}}^{I\tilde{J}}$  and results in the D3 contribution of the  $\left\langle \Phi_{I\tilde{J}}^{A\tilde{B}} \left| (V_{\text{NA}}T_{2A}T_{2B})_C \right| \Phi \right\rangle$  term (*cf.* Table A.3).

step, we replace the antisymmetrized  $v_{MN}^{\tilde{E}\tilde{F}}$  matrix element by its non-antisymmetrized  $v_{MN}^{E\tilde{F}}$  counterpart, essentially eliminating the D2 contribution (line 3 of the code shown in Figure A.2). In the second step, the D1 diagram is multiplied by a factor of  $\text{diag1} - \text{diag2}$  (lines 26 and 27 of the code shown in Figure A.2). In the third and final step, an extra D1 + D2 term is added, this time scaled by  $\text{diag2}$  (lines 57 and 58 of the code shown in Figure A.2). The net result of this process is:  $(\text{diag1} - \text{diag2}) \times \text{D1} + \text{diag2} \times (\text{D1} + \text{D2}) = \text{diag1} \times \text{D1} + \text{diag2} \times \text{D2}$ .



```

1      if (diag1.ne.diag2) then
2          allocate (D1(N0+1:N2,N2+1:N3,N0+1:N2,N2+1:N3))
3          call reorder4231 (N2,N3,N2,N3,N0,N2,N0,N2,N0,N2,N2,N3,N0,N2,N2,N3,VBHHPP,D1)
4          allocate (D2(N0+1:N2,N2+1:N3,N1+1:N3,N0+1:N1))
5          call reorder3124 (N2,N3,N1,N3,N0,N2,N0,N1,N0,N2,N2,N3,N1,N3,N0,N1,t2B,D2)
6          allocate (S40(N1+1:N3,N0+1:N1,N0+1:N2,N2+1:N3))
7          I1=K4*K2
8          I2=K1*K3
9          I3=K4*K2
10         call EGEVM(I1,I2,I3,D1,D2,S40)
11         deallocate (D1)
12         deallocate (D2)
13     !
14         allocate (D1(N0+1:N2,N2+1:N3,N1+1:N3,N0+1:N1))
15         call reorder3412 (N1,N3,N0,N1,N0,N2,N2,N3,N0,N2,N3,N1,N3,N0,N1,S40,D1)
16         allocate (D2(N0+1:N2,N2+1:N3,N1+1:N3,N0+1:N1))
17         call reorder3124 (N2,N3,N1,N3,N0,N2,N0,N1,N0,N2,N2,N3,N1,N3,N0,N1,t2B,D2)
18         allocate (U41(N1+1:N3,N0+1:N1,N1+1:N3,N0+1:N1))
19         I1=K1*K3
20         I2=K1*K3
21         I3=K4*K2
22         call EGEVM(I1,I2,I3,D1,D2,U41)
23         deallocate (D1)
24         deallocate (D2)
25     !
26         call sum1423 (N1,N3,N1,N3,N0,N1,N0,N1,V2A,U41,-diag1+diag2)
27         call sum1324 (N1,N3,N1,N3,N0,N1,N0,N1,V2A,U41,diag1-diag2)
28         deallocate (U41)
29         deallocate (S40)
30     endif
31 !
32     if (diag2.ne.0) then
33         allocate (D1(N0+1:N2,N2+1:N3,N0+1:N2,N2+1:N3))
34         call reorder4231 (N2,N3,N2,N3,N0,N2,N0,N2,N0,N2,N2,N3,N0,N2,N2,N3,VCHHPP,D1)
35         allocate (D2(N0+1:N2,N2+1:N3,N1+1:N3,N0+1:N1))
36         call reorder3124 (N2,N3,N1,N3,N0,N2,N0,N1,N0,N2,N2,N3,N1,N3,N0,N1,t2B,D2)
37         allocate (S40(N1+1:N3,N0+1:N1,N0+1:N2,N2+1:N3))
38         I1=K4*K2
39         I2=K1*K3
40         I3=K4*K2
41         call EGEVM(I1,I2,I3,D1,D2,S40)
42         deallocate (D1)
43         deallocate (D2)
44     !
45         allocate (D1(N0+1:N2,N2+1:N3,N1+1:N3,N0+1:N1))
46         call reorder3412 (N1,N3,N0,N1,N0,N2,N2,N3,N0,N2,N2,N3,N1,N3,N0,N1,S40,D1)
47         allocate (D2(N0+1:N2,N2+1:N3,N1+1:N3,N0+1:N1))
48         call reorder3124 (N2,N3,N1,N3,N0,N2,N0,N1,N0,N2,N2,N3,N1,N3,N0,N1,t2B,D2)
49         allocate (U41(N1+1:N3,N0+1:N1,N1+1:N3,N0+1:N1))
50         I1=K1*K3
51         I2=K1*K3
52         I3=K4*K2
53         call EGEVM(I1,I2,I3,D1,D2,U41)
54         deallocate (D1)
55         deallocate (D2)
56     !
57         call sum1423 (N1,N3,N1,N3,N0,N1,N0,N1,V2A,U41,-diag2)
58         call sum1324 (N1,N3,N1,N3,N0,N1,N0,N1,V2A,U41,diag2)
59         deallocate (U41)
60         deallocate (S40)
61     endif

```

Figure A.2: Excerpt of the code that computes the scaled D1 and D2 diagrams arising from the  $\langle \Phi_{IJ}^{AB} | (V_{NC} \frac{1}{2} T_{2B}^2)_C | \Phi \rangle$  term (*cf.* Table A.2).

## APPENDIX B

### COMPUTER IMPLEMENTATION OF THE CLUSTER-ANALYSIS-DRIVEN FULL CONFIGURATION INTERACTION QUANTUM MONTE CARLO APPROACH FOR STRONGLY CORRELATED SYSTEMS

The first step in developing CAD-FCIQMC was the extraction of the information about the FCIQMC wavefunction up to quadruples at a given propagation time  $\tau$ . To that end, we utilized the existing infrastructure that Dr. J. Emiliano Deustua, a former graduate student in the Piecuch research group, generated in the context of the semi-stochastic CC( $P;Q$ ) methodology. To be precise, Dr. J. Emiliano Deustua created a modified version of the HANDE code that was printing lists of Slater determinants along with their signed walker populations at given intervals of the FCIQMC simulation time  $\tau$ . A small portion of such a list is given in Figure B.1 in the case of  $H_{10}/DZ$ . For example, the first determinant on the list shown in Figure B.1 is populated by 17,613 walkers, while the second one is inhabited by  $-1,785$  walkers.

1	17613	1	2	3	4	5	6	7	8	9	10
2	-1785	1	2	3	4	5	6	7	8	11	12
3	-20	1	3	4	5	6	8	9	10	11	12
4	60	1	2	3	4	7	8	11	12	13	14
5	-62	2	3	4	6	7	8	9	10	11	15
6	-256	1	2	3	4	5	8	9	10	12	15
7	-4	1	2	5	6	7	8	10	11	12	15
8	-255	1	2	4	5	6	8	9	10	13	15
9	-95	2	4	5	6	7	8	9	10	13	15
10	-9	2	3	4	6	7	10	11	12	13	15
...											

Figure B.1: Portion of a list containing Slater determinants and numbers of signed walkers inhabiting them corresponding to the last time step, namely, 160,000 MC iterations, of a  $i$ -FCIQMC simulation for  $H_{10}/DZ$  with  $R_{H-H} = 1.0$  Å. The first column contains serial numbers for each determinant. The second column contains the information about the signed walker populations while the remaining columns list the spin-orbital indices occupied in a given determinant. Odd (even) spin-orbital indices correspond to  $\alpha$  ( $\beta$ ) spin functions.

The first step in the CAD-FCIQMC algorithm is to scan the list of Slater determinants and compute their excitation rank with respect to the reference determinant, usually the HF Slater determinant  $|\Phi\rangle$  (see, for example, the first Slater determinant on the list shown in Figure B.1). Taking advantage of routines available in the HANDE code, this is most easily accomplished by encoding each Slater determinant into a binary string, *i.e.*, employing occupation number representation, and performing a bit-wise exclusive OR operation between a given binary string and the one representing the reference determinant. The excitation rank is equal to the count of the number of bits set to 1 divided by two. The signed walker populations and spin-orbital indices of up to quadruples are stored for processing while the rest of the information is discarded.

Subsequently, for each excited Slater determinant, we identify the spatial orbitals involved in the excitation and distinguish between the various spin cases. This step is required, since the CC routines of the Piecuch group are spin-integrated. Thus, one can distinguish between two types of singly excited Slater determinants, namely,  $|\Phi_I^A\rangle$  and  $|\Phi_{\tilde{I}}^{\tilde{A}}\rangle$ , which are associated with  $\alpha \rightarrow \alpha$  and  $\beta \rightarrow \beta$  spin-orbital excitations, respectively. Similarly, there exist three kinds of doubly excited Slater determinants within the spin-integrated formalism, denoted as  $|\Phi_{IJ}^{AB}\rangle$ ,  $|\Phi_{IJ}^{A\tilde{B}}\rangle$ , and  $|\Phi_{\tilde{I}\tilde{J}}^{\tilde{A}\tilde{B}}\rangle$ , while triply excited Slater determinants have four, namely,  $|\Phi_{IJK}^{ABC}\rangle$ ,  $|\Phi_{IJK}^{AB\tilde{C}}\rangle$ ,  $|\Phi_{IJK}^{A\tilde{B}\tilde{C}}\rangle$ , and  $|\Phi_{\tilde{I}\tilde{J}\tilde{K}}^{\tilde{A}\tilde{B}\tilde{C}}\rangle$ , and quadruply excited Slater determinants have five, denoted as  $|\Phi_{IJKL}^{ABCD}\rangle$ ,  $|\Phi_{IJKL}^{ABC\tilde{D}}\rangle$ ,  $|\Phi_{IJKL}^{AB\tilde{C}\tilde{D}}\rangle$ ,  $|\Phi_{IJKL}^{A\tilde{B}\tilde{C}\tilde{D}}\rangle$ , and  $|\Phi_{\tilde{I}\tilde{J}\tilde{K}\tilde{L}}^{\tilde{A}\tilde{B}\tilde{C}\tilde{D}}\rangle$ . For example, within this scheme, the second determinant on the list shown in Figure B.1 is denoted as  $|\Phi_{55}^{66}\rangle$ .

Based on the above analysis, it comes as no surprise that the CI excitation operators  $C_1$ ,  $C_2$ ,  $C_3$ , and  $C_4$  have 2, 3, 4, and 5 distinct components within the spin-integrated formalism, *i.e.*,  $C_1 = C_{1A} + C_{1B}$ ,  $C_2 = C_{2A} + C_{2B} + C_{2C}$ ,  $C_3 = C_{3A} + C_{3B} + C_{3C} + C_{3D}$ , and  $C_4 = C_{4A} + C_{4B} + C_{4C} + C_{4D} + C_{4E}$ . The various components of  $C_1$ – $C_4$  are defined as follows:

$$C_{1A}|\Phi\rangle = c_A^I|\Phi_I^A\rangle, \quad (\text{B.1a})$$

$$C_{1B} |\Phi\rangle = c_{\tilde{A}}^{\tilde{I}} \left| \Phi_{\tilde{I}}^{\tilde{A}} \right\rangle, \quad (\text{B.1b})$$

$$C_{2A} |\Phi\rangle = c_{AB}^{IJ} \left| \Phi_{IJ}^{AB} \right\rangle, \quad (\text{B.1c})$$

$$C_{2B} |\Phi\rangle = c_{\tilde{A}\tilde{B}}^{I\tilde{J}} \left| \Phi_{\tilde{I}\tilde{J}}^{A\tilde{B}} \right\rangle, \quad (\text{B.1d})$$

$$C_{2C} |\Phi\rangle = c_{\tilde{A}\tilde{B}}^{\tilde{I}\tilde{J}} \left| \Phi_{\tilde{I}\tilde{J}}^{\tilde{A}\tilde{B}} \right\rangle, \quad (\text{B.1e})$$

$$C_{3A} |\Phi\rangle = c_{ABC}^{IJK} \left| \Phi_{IJK}^{ABC} \right\rangle, \quad (\text{B.1f})$$

$$C_{3B} |\Phi\rangle = c_{\tilde{A}\tilde{B}\tilde{C}}^{I\tilde{J}\tilde{K}} \left| \Phi_{\tilde{I}\tilde{J}\tilde{K}}^{A\tilde{B}\tilde{C}} \right\rangle, \quad (\text{B.1g})$$

$$C_{3C} |\Phi\rangle = c_{\tilde{A}\tilde{B}\tilde{C}}^{\tilde{I}\tilde{J}\tilde{K}} \left| \Phi_{\tilde{I}\tilde{J}\tilde{K}}^{\tilde{A}\tilde{B}\tilde{C}} \right\rangle, \quad (\text{B.1h})$$

$$C_{3D} |\Phi\rangle = c_{\tilde{A}\tilde{B}\tilde{C}}^{\tilde{I}\tilde{J}\tilde{K}} \left| \Phi_{\tilde{I}\tilde{J}\tilde{K}}^{\tilde{A}\tilde{B}\tilde{C}} \right\rangle, \quad (\text{B.1i})$$

$$C_{4A} |\Phi\rangle = c_{ABCD}^{IJKL} \left| \Phi_{IJKL}^{ABCD} \right\rangle, \quad (\text{B.1j})$$

$$C_{4B} |\Phi\rangle = c_{\tilde{A}\tilde{B}\tilde{C}\tilde{D}}^{I\tilde{J}\tilde{K}\tilde{L}} \left| \Phi_{\tilde{I}\tilde{J}\tilde{K}\tilde{L}}^{A\tilde{B}\tilde{C}\tilde{D}} \right\rangle, \quad (\text{B.1k})$$

$$C_{4C} |\Phi\rangle = c_{\tilde{A}\tilde{B}\tilde{C}\tilde{D}}^{\tilde{I}\tilde{J}\tilde{K}\tilde{L}} \left| \Phi_{\tilde{I}\tilde{J}\tilde{K}\tilde{L}}^{\tilde{A}\tilde{B}\tilde{C}\tilde{D}} \right\rangle, \quad (\text{B.1l})$$

$$C_{4D} |\Phi\rangle = c_{\tilde{A}\tilde{B}\tilde{C}\tilde{D}}^{\tilde{I}\tilde{J}\tilde{K}\tilde{L}} \left| \Phi_{\tilde{I}\tilde{J}\tilde{K}\tilde{L}}^{\tilde{A}\tilde{B}\tilde{C}\tilde{D}} \right\rangle, \quad (\text{B.1m})$$

and

$$C_{4E} |\Phi\rangle = c_{\tilde{A}\tilde{B}\tilde{C}\tilde{D}}^{\tilde{I}\tilde{J}\tilde{K}\tilde{L}} \left| \Phi_{\tilde{I}\tilde{J}\tilde{K}\tilde{L}}^{\tilde{A}\tilde{B}\tilde{C}\tilde{D}} \right\rangle. \quad (\text{B.1n})$$

However, before we are able to extract the corresponding CI excitation amplitudes, we need to take into consideration the phase factor associated with a given Slater determinant. These sign factors arise from the action of the elementary annihilation and creation operators on the antisymmetric Slater determinants, *i.e.*,

$$a_p \left| n_1 \dots n_{p-1} n_p n_{p+1} \dots \right\rangle = (-1)^{\sum_{k=1}^{p-1} n_k} n_p \left| n_1 \dots n_{p-1} (1 - n_p) n_{p+1} \dots \right\rangle \quad (\text{B.2})$$

and

$$a^p \left| n_1 \dots n_{p-1} n_p n_{p+1} \dots \right\rangle = (-1)^{\sum_{k=1}^{p-1} n_k} (1 - n_p) \left| n_1 \dots n_{p-1} (1 - n_p) n_{p+1} \dots \right\rangle, \quad (\text{B.3})$$

respectively, with  $n_i = 0$  or  $1$  denoting the occupation number of spin-orbital  $i$ . The sign factor of a given excited Slater determinant is computed using the following procedure. First,

we form two strings of pairs of creation and annihilation operators, one for the  $\alpha$  and another for the  $\beta$  excitations. Within each of the two groups, the pairs of creation and annihilation operators are listed in descending order of spin-orbital indices. Finally, we let the string of pairs of creation and annihilation operators associated with  $\alpha$  spin-orbitals act first on the reference Slater determinant followed by the  $\beta$  string. This procedure is illustrated using the second,  $|\Phi_{55}^{66}\rangle$ , and third,  $|\Phi_{41}^{66}\rangle$ , Slater determinants on the list shown in Figure B.1 as examples. In the occupation number representation, we obtain

$$\begin{aligned}
a^{12}a_{10}a^{11}a_9|1111111111\rangle &= a^{12}a_{10}a^{11}|1111111101\rangle \\
&= -a^{12}a_{10}|11111111011\rangle \\
&= -a^{12}|11111111001\rangle \\
&= |11111111001\rangle
\end{aligned} \tag{B.4}$$

and

$$\begin{aligned}
a^{12}a_2a^{11}a_7|1111111111\rangle &= a^{12}a_2a^{11}|1111110111\rangle \\
&= -a^{12}a_2|11111101111\rangle \\
&= a^{12}|10111101111\rangle \\
&= -|10111101111\rangle.
\end{aligned} \tag{B.5}$$

After assigning the proper phase factor to the population of walkers inhabiting each Slater determinant, the CAD-FCIQMC algorithm extracts the  $C_1^{(\text{MC})}(\tau)$ – $C_4^{(\text{MC})}(\tau)$  excitation amplitudes by dividing each walker population by that of the reference determinant. For example, the CI excitation amplitudes of the aforementioned  $|\Phi_{55}^{66}\rangle$  and  $|\Phi_{41}^{66}\rangle$  Slater determinants are  $c_{66}^{55} = \frac{-1785}{17613} = -0.101$  and  $c_{66}^{41} = -\frac{20}{17613} = 0.00114$ , respectively. Subsequently, the  $C_{2A}$ ,  $C_{2C}$ ,  $C_{3A}$ ,  $C_{3B}$ ,  $C_{3C}$ ,  $C_{3D}$ ,  $C_{4A}$ ,  $C_{4B}$ ,  $C_{4C}$ ,  $C_{4D}$ , and  $C_{4E}$  operators are properly antisymmetrized.

The next step in the CAD-FCIQMC algorithm is the cluster analysis of the FCIQMC wavefunction up to quadruples. In complete analogy to the CI excitation operators, the many-body components of the cluster operator will be denoted as  $T_1 = T_{1A} + T_{1B}$ ,  $T_2 =$

$T_{2A} + T_{2B} + T_{2C}$ ,  $T_3 = T_{3A} + T_{3B} + T_{3C} + T_{3D}$ , and  $T_4 = T_{4A} + T_{4B} + T_{4C} + T_{4D} + T_{4E}$ .

Using Equation (3.16) with  $m = 1-4$  yields, within a spin-integrated formalism,

$$T_{1A} = C_{1A}, \quad (\text{B.6a})$$

$$T_{1B} = C_{1B}, \quad (\text{B.6b})$$

$$T_{2A} = C_{2A} - \frac{1}{2}C_{1A}^2, \quad (\text{B.6c})$$

$$T_{2B} = C_{2B} - C_{1A}C_{1B}, \quad (\text{B.6d})$$

$$T_{2C} = C_{2C} - \frac{1}{2}C_{1C}^2, \quad (\text{B.6e})$$

$$T_{3A} = C_{3A} - C_{2A}C_{1A} + \frac{1}{3}C_{1A}^3, \quad (\text{B.6f})$$

$$T_{3B} = C_{3B} - C_{2A}C_{1B} - C_{2B}C_{1A} + C_{1A}^2C_{1B}, \quad (\text{B.6g})$$

$$T_{3C} = C_{3C} - C_{2B}C_{1B} - C_{2C}C_{1A} + C_{1A}C_{1B}^2, \quad (\text{B.6h})$$

$$T_{3D} = C_{3D} - C_{2C}C_{1B} + \frac{1}{3}C_{1B}^3, \quad (\text{B.6i})$$

$$T_{4A} = C_{4A} - C_{3A}C_{1A} - \frac{1}{2}C_{2A}^2 + C_{2A}C_{1A}^2 - \frac{1}{4}C_{1A}^4, \quad (\text{B.6j})$$

$$T_{4B} = C_{4B} - C_{3A}C_{1B} - C_{3B}C_{1A} - C_{2A}C_{2B} + 2C_{2A}C_{1A}C_{1B} + C_{2B}C_{1A}^2 - C_{1A}^3C_{1B}, \quad (\text{B.6k})$$

$$T_{4C} = C_{4C} - C_{3B}C_{1B} - C_{3C}C_{1A} - \frac{1}{2}C_{2B}^2 - C_{2A}C_{2C} + C_{2A}C_{1B}^2 + 2C_{2B}C_{1B}C_{1A} \\ + C_{2C}C_{1A}^2 - \frac{3}{2}C_{1A}^2C_{1B}^2, \quad (\text{B.6l})$$

$$T_{4D} = C_{4D} - C_{3C}C_{1B} - C_{3D}C_{1A} - C_{2B}C_{2C} + 2C_{2C}C_{1B}C_{1A} + C_{2B}C_{1B}^2 - C_{1A}C_{1B}^3, \quad (\text{B.6m})$$

and

$$T_{4E} = C_{4E} - C_{3D}C_{1B} - \frac{1}{2}C_{2C}^2 + C_{2C}C_{1B}^2 - \frac{1}{4}C_{1B}^4. \quad (\text{B.6n})$$

The explicit algebraic expressions connecting the cluster and CI excitation amplitudes can be derived diagrammatically by using Equation (B.6) and computing matrix elements of the form  $\langle \Phi_{I_1 \dots I_{n-1} I_n}^{A_1 \dots A_{n-1} A_n} | T_{nA} | \Phi \rangle$ ,  $\langle \Phi_{I_1 \dots I_{n-1} \tilde{I}_n}^{A_1 \dots A_{n-1} \tilde{A}_n} | T_{nB} | \Phi \rangle$ , *etc.* This procedure gives rise to the following correspondence between the spin-integrated cluster and CI excitation amplitudes

up to quadruples,

$$t_A^I = c_A^I, \quad (B.7a)$$

$$t_{\tilde{A}}^{\tilde{I}} = c_{\tilde{A}}^{\tilde{I}}, \quad (B.7b)$$

$$t_{AB}^{IJ} = c_{AB}^{IJ} - \mathcal{A}^{IJ} c_A^I c_B^J, \quad (B.7c)$$

$$t_{A\tilde{B}}^{I\tilde{J}} = c_{A\tilde{B}}^{I\tilde{J}} - c_A^I c_{\tilde{B}}^{\tilde{J}}, \quad (B.7d)$$

$$t_{\tilde{A}\tilde{B}}^{\tilde{I}\tilde{J}} = c_{\tilde{A}\tilde{B}}^{\tilde{I}\tilde{J}} - \mathcal{A}^{\tilde{I}\tilde{J}} c_{\tilde{A}}^{\tilde{I}} c_{\tilde{B}}^{\tilde{J}}, \quad (B.7e)$$

$$t_{ABC}^{IJK} = c_{ABC}^{IJK} - \mathcal{A}_{AB/C} \mathcal{A}^{IJ/K} c_{AB}^{IJ} c_C^K + 2\mathcal{A}^{IJK} c_A^I c_B^J c_C^K, \quad (B.7f)$$

$$t_{ABC}^{IJ\tilde{K}} = c_{ABC}^{IJ\tilde{K}} - c_{AB}^{IJ} c_{\tilde{C}}^{\tilde{K}} - \mathcal{A}_{AB} \mathcal{A}^{IJ} c_{AC}^{I\tilde{K}} c_B^J + 2\mathcal{A}^{IJ} c_A^I c_B^J c_{\tilde{C}}^{\tilde{K}}, \quad (B.7g)$$

$$t_{\tilde{A}\tilde{B}\tilde{C}}^{I\tilde{J}\tilde{K}} = c_{\tilde{A}\tilde{B}\tilde{C}}^{I\tilde{J}\tilde{K}} - \mathcal{A}_{\tilde{B}\tilde{C}} \mathcal{A}^{\tilde{J}\tilde{K}} c_{\tilde{A}}^{I\tilde{J}} c_{\tilde{C}}^{\tilde{K}} - c_{\tilde{B}\tilde{C}}^{\tilde{J}\tilde{K}} c_A^I + 2\mathcal{A}^{\tilde{J}\tilde{K}} c_A^I c_{\tilde{B}}^{\tilde{J}} c_{\tilde{C}}^{\tilde{K}}, \quad (B.7h)$$

$$t_{\tilde{A}\tilde{B}\tilde{C}}^{\tilde{I}\tilde{J}\tilde{K}} = c_{\tilde{A}\tilde{B}\tilde{C}}^{\tilde{I}\tilde{J}\tilde{K}} - \mathcal{A}_{\tilde{A}\tilde{B}/\tilde{C}} \mathcal{A}^{\tilde{I}\tilde{J}/\tilde{K}} c_{\tilde{A}\tilde{B}}^{\tilde{I}\tilde{J}} c_{\tilde{C}}^{\tilde{K}} + 2\mathcal{A}^{\tilde{I}\tilde{J}\tilde{K}} c_{\tilde{A}}^{\tilde{I}} c_{\tilde{B}}^{\tilde{J}} c_{\tilde{C}}^{\tilde{K}}, \quad (B.7i)$$

$$\begin{aligned} t_{ABCD}^{IJKL} &= c_{ABCD}^{IJKL} - \mathcal{A}_{ABC/D} \mathcal{A}^{IJK/L} c_{ABC}^{IJK} c_D^L - \mathcal{A}^{IJ/KL} \mathcal{A}_{A/CD} c_{AB}^{IJ} c_{CD}^{KL} \\ &\quad + 2\mathcal{A}_{AB/CD} \mathcal{A}^{IJ/K/L} c_{AB}^{IJ} c_C^K c_D^L - 6\mathcal{A}^{IJKL} c_A^I c_B^J c_C^K c_D^L, \end{aligned} \quad (B.7j)$$

$$\begin{aligned} t_{ABC\tilde{D}}^{IJK\tilde{L}} &= c_{ABC\tilde{D}}^{IJK\tilde{L}} - c_{ABC}^{IJK} c_{\tilde{D}}^{\tilde{L}} - \mathcal{A}_{AB/C} \mathcal{A}^{IJ/K} c_{AB\tilde{D}}^{IJ\tilde{L}} c_C^K - \mathcal{A}_{AB/C} \mathcal{A}^{IJ/K} c_{AB}^{IJ} c_{\tilde{D}}^{K\tilde{L}} \\ &\quad + 2\mathcal{A}_{AB/C} \mathcal{A}^{IJ/K} c_{AB}^{IJ} c_C^K c_{\tilde{D}}^{\tilde{L}} + 2\mathcal{A}_{A/BC} \mathcal{A}^{IJK} c_{A\tilde{D}}^{I\tilde{L}} c_B^J c_C^K - 6\mathcal{A}^{IJK} c_A^I c_B^J c_C^K c_{\tilde{D}}^{\tilde{L}}, \end{aligned} \quad (B.7k)$$

$$\begin{aligned} t_{AB\tilde{C}\tilde{D}}^{I\tilde{J}\tilde{K}\tilde{L}} &= c_{AB\tilde{C}\tilde{D}}^{I\tilde{J}\tilde{K}\tilde{L}} - \mathcal{A}_{\tilde{C}\tilde{D}} \mathcal{A}^{\tilde{K}\tilde{L}} c_{AB\tilde{C}}^{I\tilde{J}\tilde{K}} c_{\tilde{D}}^{\tilde{L}} - \mathcal{A}_{AB} \mathcal{A}^{IJ} c_{A\tilde{C}\tilde{D}}^{I\tilde{K}\tilde{L}} c_B^J - \mathcal{A}_{AB} \mathcal{A}^{IJ} \mathcal{A}^{\tilde{K}\tilde{L}} c_{A\tilde{C}}^{I\tilde{K}} c_{\tilde{B}\tilde{D}}^{J\tilde{L}} \\ &\quad - c_{AB}^{IJ} c_{\tilde{C}\tilde{D}}^{\tilde{K}\tilde{L}} + 2\mathcal{A}^{\tilde{K}\tilde{L}} c_{AB}^{IJ} c_{\tilde{C}}^{\tilde{K}} c_{\tilde{D}}^{\tilde{L}} + 2\mathcal{A}_{AB} \mathcal{A}_{\tilde{C}\tilde{D}}^{IJ} \mathcal{A}^{\tilde{K}\tilde{L}} c_A^I c_{\tilde{C}}^{\tilde{K}} c_{\tilde{B}\tilde{D}}^{\tilde{L}} \\ &\quad + 2\mathcal{A}^{IJ} c_A^I c_B^J c_{\tilde{C}\tilde{D}}^{\tilde{K}\tilde{L}} - 6\mathcal{A}^{IJ} \mathcal{A}^{\tilde{K}\tilde{L}} c_A^I c_B^J c_{\tilde{C}}^{\tilde{K}} c_{\tilde{D}}^{\tilde{L}}, \end{aligned} \quad (B.7l)$$

$$\begin{aligned} t_{\tilde{A}\tilde{B}\tilde{C}\tilde{D}}^{I\tilde{J}\tilde{K}\tilde{L}} &= c_{\tilde{A}\tilde{B}\tilde{C}\tilde{D}}^{I\tilde{J}\tilde{K}\tilde{L}} - \mathcal{A}_{\tilde{B}\tilde{C}/\tilde{D}} \mathcal{A}^{\tilde{J}\tilde{K}/\tilde{L}} c_{\tilde{A}\tilde{B}\tilde{C}}^{I\tilde{J}\tilde{K}} c_{\tilde{D}}^{\tilde{L}} - c_{\tilde{B}\tilde{C}\tilde{D}}^{\tilde{J}\tilde{K}\tilde{L}} c_{\tilde{A}}^I - \mathcal{A}_{\tilde{B}/\tilde{C}\tilde{D}} \mathcal{A}^{\tilde{J}/\tilde{K}\tilde{L}} c_{\tilde{A}\tilde{B}}^{I\tilde{J}} c_{\tilde{C}\tilde{D}}^{\tilde{K}\tilde{L}} \\ &\quad + 2\mathcal{A}_{\tilde{B}/\tilde{C}\tilde{D}} \mathcal{A}^{\tilde{J}/\tilde{K}\tilde{L}} c_{\tilde{C}\tilde{D}}^{\tilde{K}\tilde{L}} c_{\tilde{B}}^{\tilde{J}} c_{\tilde{A}}^I + 2\mathcal{A}_{\tilde{B}/\tilde{C}\tilde{D}} \mathcal{A}^{\tilde{J}\tilde{K}\tilde{L}} c_{\tilde{A}\tilde{B}}^{I\tilde{J}} c_{\tilde{C}}^{\tilde{K}} c_{\tilde{D}}^{\tilde{L}} - 6\mathcal{A}^{\tilde{J}\tilde{K}\tilde{L}} c_A^I c_{\tilde{B}}^{\tilde{J}} c_{\tilde{C}}^{\tilde{K}} c_{\tilde{D}}^{\tilde{L}}, \end{aligned} \quad (B.7m)$$

and

$$\begin{aligned}
t_{\tilde{A}\tilde{B}\tilde{C}\tilde{D}}^{\tilde{I}\tilde{J}\tilde{K}\tilde{L}} &= c_{\tilde{A}\tilde{B}\tilde{C}\tilde{D}}^{\tilde{I}\tilde{J}\tilde{K}\tilde{L}} - \mathcal{A}_{\tilde{A}\tilde{B}\tilde{C}/\tilde{D}} \mathcal{A}^{\tilde{I}\tilde{J}\tilde{K}/\tilde{L}} c_{\tilde{A}\tilde{B}\tilde{C}}^{\tilde{I}\tilde{J}\tilde{K}} c_{\tilde{D}}^{\tilde{L}} - \mathcal{A}^{\tilde{I}\tilde{J}/\tilde{K}\tilde{L}} \mathcal{A}_{\tilde{A}/\tilde{C}\tilde{D}} c_{\tilde{A}\tilde{B}}^{\tilde{I}\tilde{J}} c_{\tilde{C}\tilde{D}}^{\tilde{K}\tilde{L}} \\
&\quad + 2\mathcal{A}_{\tilde{A}\tilde{B}/\tilde{C}\tilde{D}} \mathcal{A}^{\tilde{I}\tilde{J}/\tilde{K}/\tilde{L}} c_{\tilde{A}\tilde{B}}^{\tilde{I}\tilde{J}} c_{\tilde{C}}^{\tilde{K}} c_{\tilde{D}}^{\tilde{L}} - 6\mathcal{A}^{\tilde{I}\tilde{J}\tilde{K}\tilde{L}} c_{\tilde{A}}^{\tilde{I}} c_{\tilde{B}}^{\tilde{J}} c_{\tilde{C}}^{\tilde{K}} c_{\tilde{D}}^{\tilde{L}}.
\end{aligned} \tag{B.7n}$$

Subsequently, the  $T_{2A}$ ,  $T_{2C}$ ,  $T_{3A}$ ,  $T_{3B}$ ,  $T_{3C}$ ,  $T_{3D}$ ,  $T_{4A}$ ,  $T_{4B}$ ,  $T_{4C}$ ,  $T_{4D}$ , and  $T_{4E}$  operators are properly antisymmetrized.

As already mentioned earlier in this dissertation, in the final step of the CAD-FCIQMC approach, one solves a CCSD-like system of equations, Equations (3.29) and (3.30), for  $T_1$  and  $T_2$  in the presence of  $T_3^{(\text{MC})}(\tau)$  and  $T_4^{(\text{MC})}(\tau)$  resulting from the cluster analysis of the FCIQMC wavefunction at time  $\tau$ . To that end, the cluster analysis algorithm was interfaced with the spin-integrated CCSD code of the Piecuch group corrected for  $T_3$  and  $T_4$  terms. To further assist convergence, one also has the option of using  $T_1^{(\text{MC})}(\tau)$  and  $T_2^{(\text{MC})}(\tau)$  extracted from the FCIQMC wavefunction as an initial guess.

At this point, it is worth mentioning that the CAD-FCIQMC code is flexible enough that it can be used for performing externally corrected CC calculations using arbitrary sources of three- and four-body clusters. The only requirement is a list of up to quadruply excited Slater determinants and their coefficients, in the format outlined in Figure B.1, originating from the non-CC approach of interest. One needs to pay attention, however, to the way the Slater determinants are encoded in different programs, as this might potentially introduce additional phase factors. For example, the determinantal truncated CI and FCI routines in GAMESS, like many other CI codes, place the string of  $\alpha$  spin-orbitals in front of the  $\beta$  ones. In interfacing GAMESS with CAD-FCIQMC, one needs to extract lists of coefficients and determinants, where the latter are represented by alternating  $\alpha/\beta$  pairs, taking into account any additional sign factors that might arise.

The implementation of the CAD-FCIQMC methodology as outlined above, albeit correct, suffers from unfavorable memory and disk requirements associated with the handling of the amplitudes of the  $C_4 = C_{4A} + C_{4B} + C_{4C} + C_{4D} + C_{4E}$  and  $T_4 = T_{4A} + T_{4B} + T_{4C} + T_{4D} + T_{4E}$  operators. The computational resources consumed by the CAD-FCIQMC code are dramat-



ically reduced by processing quadruples, *i.e.*,  $C_4^{(\text{MC})}(\tau)$  and  $T_4^{(\text{MC})}(\tau)$ , on-the-fly. To that end, the  $\langle \Phi_{ij}^{ab} | \left[ V_N T_4^{(\text{MC})}(\tau) \right]_C | \Phi \rangle$  contributions to Equation (3.30), whose number equals that of doubly excited Slater determinants  $|\Phi_{ij}^{ab}\rangle$ , are computed once and stored on the disk. By doing that, we avoid storing or keeping in memory  $C_4^{(\text{MC})}(\tau)$  and  $T_4^{(\text{MC})}(\tau)$ . The details of this implementation can be found in Dr. J. Emiliano Deustua's Ph.D. dissertation. In principle, a similar approach could be adopted for  $C_3^{(\text{MC})}(\tau)$  and  $T_3^{(\text{MC})}(\tau)$ , especially in the case of the linear terms  $\langle \Phi_i^a | \left[ V_N T_3^{(\text{MC})}(\tau) \right]_C | \Phi \rangle$  and  $\langle \Phi_{ij}^{ab} | \left[ F_N T_3^{(\text{MC})}(\tau) \right]_C | \Phi \rangle$  terms. The only problem is how to handle the last  $T_3^{(\text{MC})}(\tau)$ -containing term in Equations (3.29) and (3.30), namely,  $\langle \Phi_{ij}^{ab} | \left[ V_N T_3^{(\text{MC})}(\tau) T_1 \right]_C | \Phi \rangle$ , in which  $T_3^{(\text{MC})}(\tau)$  is fixed and  $T_1$  is updated. One possibility would be to approximate this term by replacing  $T_1$  by the fixed  $T_1^{(\text{MC})}(\tau)$ . Alternatively, one could precompute and store on the disk the  $\left[ V_N T_3^{(\text{MC})}(\tau) \right]_C$  intermediate at the cost of de-vectorizing the CC code. Due to the aforementioned considerations, the latest implementation of the CAD-FCIQMC methodology precomputes and stores the  $T_4^{(\text{MC})}(\tau)$ -containing terms while the  $T_3^{(\text{MC})}(\tau)$  amplitudes are stored on disk.

The CAD-FCIQMC methodology was extended to the strong correlation regime by taking advantage of the ACP ideas. Consequently, suitable modifications were made to the spin-integrated CCSD code corrected for  $T_3$  and  $T_4$  terms that guaranteed not only the good behavior in the presence of strong many-electron correlation effects, but also exactness in the infinite imaginary-time limit. The first step in this direction was to introduce in the CCSD-like equations projected on doubles the identical modifications to the  $\frac{1}{2}T_2^2$  terms discussed in Appendix A. Although this renders the CAD-FCIQMC methodology well-suited for the description of strong correlation, CAD-FCIQMC is not exact anymore in the  $\tau \rightarrow \infty$  limit, since one is not solving CCSD equations corrected for connected triples and quadruples. As discussed earlier in this dissertation, to restore exactness in the infinite time limit, each coupled-pair contribution was augmented by its complement extracted from FCIQMC [*cf.* Equation (3.40)].

In Figures B.2 and B.3 we show excerpts of the modified CAD-FCIQMC code, focusing

on the D3 contribution of the  $\langle \Phi_{IJ}^{AB} | (V_{\text{NA}} \frac{1}{2} T_{2A}^2)_C | \Phi \rangle$  term, that showcase the changes that needed to be made to allow for the treatment of strong correlation. In line 30 of the code presented in Figure B.2, we multiply the 0.5 diagrammatic factor by the real variable `diag3`. This is one of the terms responsible for the good behavior in the presence of strong correlations and is, thus, treated deterministically. In Figure B.3, we show the complement to the aforementioned term that is treated stochastically. To begin with, the “if” statement on line 1 of the code shown in Figure B.3 reveals that this term only contributes if this is an externally corrected calculation (`ext_cor=.TRUE.`) and the `diag3` variable is not equal to 1. On lines 8 and 22, we see that the `t2a` variable appearing in Figure B.2 is replaced by its stochastically determined counterpart `t2a_mc`. Finally, the 0.5 diagrammatic weight is multiplied by the  $(1 - \text{diag3})$  scaling factor. The final result of these particular alterations to the code is the replacement of the  $\Lambda_3^{(2)}$  term by  $\text{diag3} \times \Lambda_3^{(2)} + (1 - \text{diag3}) \times \Lambda_3^{(2),(\text{MC})}$ . Similar modifications were made to all diagrams arising from the  $\frac{1}{2} T_2^2$  contributions to the CC equations projected on doubly excited Slater determinants.

```

1      if(diag3.eq.0) goto 5001      !skip this term if diag3=0
2      allocate(d1(n0+1:n1,n0+1:n1,n1+1:n3,n1+1:n3))
3      call reorder2134(n0,n3,n0,n3,n0,n3,n0,n3,
4      &    n0,n1,n0,n1,n1,n3,n1,n3,intr,d1)
5      allocate(d2(n0+1:n1,n0+1:n1,n1+1:n3,n1+1:n3))
6      call reorder3412(n1,n3,n1,n3,n0,n1,n0,n1,
7      &    n0,n1,n0,n1,n1,n3,n1,n3,t2a,d2)
8      allocate(q11(n1+1:n3,n1+1:n3))
9      i1=k3
10     i2=k3
11     i3=k3*k1*k1
12     call egemm(i1,i2,i3,d1,d2,q11)
13     deallocate(d1)
14     deallocate(d2)
15 !
16     allocate(b1(n1+1:n3,n1+1:n3))
17     call reorder21(n1,n3,n1,n3,
18     &    n1,n3,n1,n3,q11,b1)
19     allocate(d2(n1+1:n3,n1+1:n3,n0+1:n1,n0+1:n1))
20     call reorder1234(n1,n3,n1,n3,n0,n1,n0,n1,
21     &    n1,n3,n1,n3,n0,n1,n0,n1,t2a,d2)
22     allocate(z54(n1+1:n3,n0+1:n1,n0+1:n1,n1+1:n3))
23     i1=k3
24     i2=k1*k1*k3
25     i3=k3
26     call egemm(i1,i2,i3,b1,d2,z54)
27     deallocate(b1)
28     deallocate(d2)
29 !
30     factor=-0.500*diag3      !scale D3 by diag3
31     call
32     &    sum1342(n1,n3,n1,n3,n0,n1,n0,n1,v2a,z54,factor)
33     factor=-factor
34     call
35     &    sum2341(n1,n3,n1,n3,n0,n1,n0,n1,v2a,z54,factor)
36     deallocate(z54)
37     deallocate(q11)
38     factor=0

```

Figure B.2: Excerpt of the code that computes the deterministic  $\text{diag3} \times \Lambda_3^{(2)}$  contribution of the  $\langle \Phi_{IJ}^{AB} | (V_{\text{NA}} \frac{1}{2} T_{2A}^2)_C | \Phi \rangle$  term (*cf.* Table A.2).

```

1  !complementary acc-d3_mc term
2  5001  if (ext_cor.and.diag3.ne.1) then
3      allocate (d1_mc(n0+1:n1,n0+1:n1,n1+1:n3,n1+1:n3))
4      call reorder2134(n0,n3,n0,n3,n0,n3,n0,n3,
5      & n0,n1,n0,n1,n1,n3,n1,n3,intr,d1_mc)
6      allocate (d2_mc(n0+1:n1,n0+1:n1,n1+1:n3,n1+1:n3))
7      call reorder3412(n1,n3,n1,n3,n0,n1,n0,n1,
8      & n0,n1,n0,n1,n1,n3,n1,n3,t2a_mc,d2_mc)
9      allocate (q11_mc(n1+1:n3,n1+1:n3))
10     i1=k3
11     i2=k3
12     i3=k3*k1*k1
13     call egemm(i1,i2,i3,d1_mc,d2_mc,q11_mc)
14     deallocate (d1_mc)
15     deallocate (d2_mc)
16  !
17     allocate (b1_mc(n1+1:n3,n1+1:n3))
18     call reorder21(n1,n3,n1,n3,
19     & n1,n3,n1,n3,q11_mc,b1_mc)
20     allocate (d2_mc(n1+1:n3,n1+1:n3,n0+1:n1,n0+1:n1))
21     call reorder1234(n1,n3,n1,n3,n0,n1,n0,n1,
22     & n1,n3,n1,n3,n0,n1,n0,n1,t2a_mc,d2_mc)
23     allocate (z54_mc(n1+1:n3,n0+1:n1,n0+1:n1,n1+1:n3))
24     i1=k3
25     i2=k1*k1*k3
26     i3=k3
27     call egemm(i1,i2,i3,b1_mc,d2_mc,z54_mc)
28     deallocate (q11_mc)
29     deallocate (b1_mc)
30     deallocate (d2_mc)
31  !
32     factor=-0.500*(1.0-diag3) !scale D3^(MC) by 1-diag3
33     call
34     & sum1342(n1,n3,n1,n3,n0,n1,n0,n1,v2a,z54_mc,factor)
35     factor=-factor
36     call
37     & sum2341(n1,n3,n1,n3,n0,n1,n0,n1,v2a,z54_mc,factor)
38     deallocate (z54_mc)
39     factor=0
40  endif

```

Figure B.3: Excerpt of the code that computes the stochastic  $(1 - \text{diag3}) \Lambda_3^{(2),(\text{MC})}$  contribution of the  $\langle \Phi_{IJ}^{AB} | (V_{\text{NA}} \frac{1}{2} T_{2A}^2)_C | \Phi \rangle$  term (*cf.* Table A.2).

## BIBLIOGRAPHY

## BIBLIOGRAPHY

- [1] E. Schrödinger, *Ann. Phys.* **384**, 361 (1926).
- [2] E. Schrödinger, *Ann. Phys.* **384**, 489 (1926).
- [3] E. Schrödinger, *Ann. Phys.* **384**, 734 (1926).
- [4] E. Schrödinger, *Ann. Phys.* **385**, 437 (1926).
- [5] E. Schrödinger, *Ann. Phys.* **386**, 109 (1926).
- [6] E. Schrödinger, *Phys. Rev.* **28**, 1049 (1926).
- [7] Ø. Burrau, *Naturwiss.* **15**, 16 (1927).
- [8] W. Heitler and F. London, *Z. Phys.* **44**, 455 (1927).
- [9] K. Gavroglu and A. Simões, *Neither Physics nor Chemistry: A History of Quantum Chemistry* (The MIT Press, 2012).
- [10] P. A. M. Dirac, *Proc. R. Soc. London A* **123**, 714 (1929).
- [11] M. Born and R. Oppenheimer, *Ann. Phys.* **389**, 457 (1927).
- [12] P. A. M. Dirac, *Proc. R. Soc. London A* **117**, 610 (1928).
- [13] P. A. M. Dirac, *Proc. R. Soc. London A* **118**, 351 (1928).
- [14] T. Saue, *ChemPhysChem* **12**, 3077 (2011).
- [15] D. R. Hartree, *Math. Proc. Cambridge Philos. Soc.* **24**, 89 (1928).
- [16] D. R. Hartree, *Math. Proc. Cambridge Philos. Soc.* **24**, 111 (1928).
- [17] W. Pauli, *Z. Phys.* **31**, 765 (1925).
- [18] W. Pauli, *Phys. Rev.* **58**, 716 (1940).
- [19] J. C. Slater, *Phys. Rev.* **34**, 1293 (1929).
- [20] V. Fock, *Z. Phys.* **61**, 126 (1930).

- [21] V. Fock, *Z. Phys.* **62**, 795 (1930).
- [22] J. C. Slater, *Phys. Rev.* **35**, 210 (1930).
- [23] P. Hohenberg and W. Kohn, *Phys. Rev.* **136**, B864 (1964).
- [24] W. Kohn and L. J. Sham, *Phys. Rev.* **140**, A1133 (1965).
- [25] G. G. Hall, *Proc. R. Soc. London A* **205**, 541 (1951).
- [26] C. C. J. Roothaan, *Rev. Mod. Phys.* **23**, 69 (1951).
- [27] H. Fukutome, *Prog. Theor. Phys.* **52**, 115 (1974).
- [28] H. Fukutome, *Int. J. Quantum Chem.* **20**, 955 (1981).
- [29] M. S. Gordon and D. G. Truhlar, *Theor. Chim. Acta* **71**, 1 (1987).
- [30] E. Wigner, *Phys. Rev.* **46**, 1002 (1934).
- [31] P.-O. Löwdin, *Adv. Chem. Phys.* **2**, 207 (1959).
- [32] O. Sinanoğlu and D. F.-T. Tuan, *J. Chem. Phys.* **38**, 1740 (1963).
- [33] P.-O. Löwdin, *Int. J. Quantum Chem.* **55**, 77 (1995).
- [34] H. Weyl, *The Classical Groups: Their Invariants and Representations* (Princeton University Press, 1946).
- [35] J. Paldus, *J. Chem. Phys.* **61**, 5321 (1974).
- [36] G. Rasskazov, M. Nairat, I. Magoulas, V. V. Lozovoy, P. Piecuch, and M. Dantus, *Chem. Phys. Lett.* **683**, 121 (2017).
- [37] I. Magoulas, N. P. Bauman, J. Shen, and P. Piecuch, *J. Phys. Chem. A* **122**, 1350 (2018).
- [38] S. H. Yuwono, I. Magoulas, J. Shen, and P. Piecuch, *Mol. Phys.* **117**, 1486 (2019).
- [39] S. H. Yuwono, I. Magoulas, and P. Piecuch, *Sci. Adv.* **6**, eaay4058 (2020).
- [40] J. Lahiri, M. Moemeni, J. Kline, B. Borhan, I. Magoulas, S. H. Yuwono, P. Piecuch, J. E. Jackson, M. Dantus, and G. J. Blanchard, *J. Phys. Chem. B* **123**, 8448 (2019).
- [41] J. Lahiri, M. Moemeni, I. Magoulas, S. H. Yuwono, J. Kline, B. Borhan, P. Piecuch,

- J. E. Jackson, G. J. Blanchard, and M. Dantus, *Phys. Chem. Chem. Phys.* **22**, 19613 (2020).
- [42] J. Lahiri, M. Moemeni, J. Kline, I. Magoulas, S. H. Yuwono, M. Laboe, J. Shen, B. Borhan, P. Piecuch, J. E. Jackson, G. J. Blanchard, and M. Dantus, *J. Chem. Phys.* **153**, 224301 (2020).
- [43] F. Coester, *Nucl. Phys.* **7**, 421 (1958).
- [44] F. Coester and H. Kümmel, *Nucl. Phys.* **17**, 477 (1960).
- [45] J. Čížek, *J. Chem. Phys.* **45**, 4256 (1966).
- [46] J. Čížek, *Adv. Chem. Phys.* **14**, 35 (1969).
- [47] J. Čížek and J. Paldus, *Int. J. Quantum Chem.* **5**, 359 (1971).
- [48] J. Paldus, J. Čížek, and I. Shavitt, *Phys. Rev. A* **5**, 50 (1972).
- [49] K. A. Brueckner, *Phys. Rev.* **100**, 36 (1955).
- [50] J. Goldstone, *Proc. R. Soc. London A Math. Phys. Eng. Sci.* **239**, 267 (1957).
- [51] J. Hubbard, *Proc. R. Soc. London A Math. Phys. Eng. Sci.* **240**, 539 (1957).
- [52] N. M. Hugenholtz, *Physica* **23**, 481 (1957).
- [53] J. Paldus and X. Li, *Adv. Chem. Phys.* **110**, 1 (1999).
- [54] P. Piecuch and K. Kowalski, *Int. J. Mol. Sci.* **3**, 676 (2002).
- [55] R. J. Bartlett and M. Musiał, *Rev. Mod. Phys.* **79**, 291 (2007).
- [56] D. I. Lyakh, M. Musiał, V. F. Lotrich, and R. J. Bartlett, *Chem. Rev.* **112**, 182 (2012).
- [57] K. Emrich, *Nucl. Phys. A* **351**, 379 (1981).
- [58] K. Emrich, *Nucl. Phys. A* **351**, 397 (1981).
- [59] J. Geertsen, M. Rittby, and R. J. Bartlett, *Chem. Phys. Lett.* **164**, 57 (1989).
- [60] D. C. Comeau and R. J. Bartlett, *Chem. Phys. Lett.* **207**, 414 (1993).
- [61] J. F. Stanton and R. J. Bartlett, *J. Chem. Phys.* **98**, 7029 (1993).



- [62] G. D. Purvis, III and R. J. Bartlett, *J. Chem. Phys.* **76**, 1910 (1982).
- [63] J. M. Cullen and M. C. Zerner, *J. Chem. Phys.* **77**, 4088 (1982).
- [64] J. Noga and R. J. Bartlett, *J. Chem. Phys.* **86**, 7041 (1987), *ibid.* **89**, 3401 (1988) [Erratum].
- [65] G. E. Scuseria and H. F. Schaefer, III, *Chem. Phys. Lett.* **152**, 382 (1988).
- [66] N. Oliphant and L. Adamowicz, *J. Chem. Phys.* **95**, 6645 (1991).
- [67] S. A. Kucharski and R. J. Bartlett, *Theor. Chim. Acta* **80**, 387 (1991).
- [68] S. A. Kucharski and R. J. Bartlett, *J. Chem. Phys.* **97**, 4282 (1992).
- [69] K. Kowalski and P. Piecuch, *J. Chem. Phys.* **115**, 643 (2001).
- [70] K. Kowalski and P. Piecuch, *Chem. Phys. Lett.* **347**, 237 (2001).
- [71] M. Kállay and P. R. Surján, *J. Chem. Phys.* **113**, 1359 (2000).
- [72] S. Hirata, M. Nooijen, and R. J. Bartlett, *Chem. Phys. Lett.* **326**, 255 (2000).
- [73] S. A. Kucharski, M. Włoch, M. Musiał, and R. J. Bartlett, *J. Chem. Phys.* **115**, 8263 (2001).
- [74] S. Hirata, *J. Chem. Phys.* **121**, 51 (2004).
- [75] M. Kállay and J. Gauss, *J. Chem. Phys.* **121**, 9257 (2004).
- [76] M. Nooijen and R. J. Bartlett, *J. Chem. Phys.* **102**, 3629 (1995).
- [77] M. Nooijen and R. J. Bartlett, *J. Chem. Phys.* **102**, 6735 (1995).
- [78] S. Hirata, M. Nooijen, and R. J. Bartlett, *Chem. Phys. Lett.* **328**, 459 (2000).
- [79] M. Musiał and R. J. Bartlett, *J. Chem. Phys.* **119**, 1901 (2003).
- [80] J. R. Gour, P. Piecuch, and M. Włoch, *J. Chem. Phys.* **123**, 134113 (2005).
- [81] J. R. Gour, P. Piecuch, and M. Włoch, *Int. J. Quantum Chem.* **106**, 2854 (2006).
- [82] J. R. Gour and P. Piecuch, *J. Chem. Phys.* **125**, 234107 (2006).
- [83] M. Nooijen and J. G. Snijders, *Int. J. Quantum Chem. Symp.* **26**, 55 (1992).

- [84] M. Nooijen and J. G. Snijders, *Int. J. Quantum Chem.* **48**, 15 (1993).
- [85] J. F. Stanton and J. Gauss, *J. Chem. Phys.* **101**, 8938 (1994).
- [86] R. J. Bartlett and J. F. Stanton, in *Reviews in Computational Chemistry*, Vol. 5, edited by K. B. Lipkowitz and D. B. Boyd (VCH Publishers, New York, 1994) pp. 65–169.
- [87] M. Musiał, S. A. Kucharski, and R. J. Bartlett, *J. Chem. Phys.* **118**, 1128 (2003).
- [88] M. Musiał and R. J. Bartlett, *Chem. Phys. Lett.* **384**, 210 (2004).
- [89] Y. J. Bomble, J. C. Saeh, J. F. Stanton, P. G. Szalay, and M. Kállay, *J. Chem. Phys.* **122**, 154107 (2005).
- [90] M. Kamiya and S. Hirata, *J. Chem. Phys.* **125**, 074111 (2006).
- [91] M. Nooijen and R. J. Bartlett, *J. Chem. Phys.* **106**, 6441 (1997).
- [92] M. Nooijen, *Int. J. Mol. Sci.* **3**, 656 (2002).
- [93] K. W. Sattelmeyer, H. F. Schaefer, III, and J. F. Stanton, *Chem. Phys. Lett.* **378**, 42 (2003).
- [94] M. Musiał, A. Perera, and R. J. Bartlett, *J. Chem. Phys.* **134**, 114108 (2011).
- [95] M. Musiał, S. A. Kucharski, and R. J. Bartlett, *J. Chem. Theory Comput.* **7**, 3088 (2011).
- [96] T. Kuś and A. I. Krylov, *J. Chem. Phys.* **135**, 084109 (2011).
- [97] T. Kuś and A. I. Krylov, *J. Chem. Phys.* **136**, 244109 (2012).
- [98] J. Shen and P. Piecuch, *J. Chem. Phys.* **138**, 194102 (2013).
- [99] J. Shen and P. Piecuch, *Mol. Phys.* **112**, 868 (2014).
- [100] A. O. Ajala, J. Shen, and P. Piecuch, *J. Phys. Chem. A* **121**, 3469 (2017).
- [101] J. R. Reimers, J. Shen, M. Kianinia, C. Bradac, I. Aharonovich, M. J. Ford, and P. Piecuch, *Phys. Rev. B* **102**, 144105 (2020).
- [102] O. Sinanoğlu, *Proc. Natl. Acad. Sci. U. S. A.* **47**, 1217 (1961).
- [103] O. Sinanoğlu, *J. Chem. Phys.* **36**, 3198 (1962).

- [104] O. Sinanoğlu, *Adv. Chem. Phys.* **6**, 315 (1964).
- [105] M. Schütz and H.-J. Werner, *J. Chem. Phys.* **114**, 661 (2001).
- [106] H.-J. Werner and M. Schütz, *J. Chem. Phys.* **135**, 144116 (2011).
- [107] J. Yang, G. K.-L. Chan, F. R. Manby, M. Schütz, and H.-J. Werner, *J. Chem. Phys.* **136**, 144105 (2012).
- [108] M. Schwilk, Q. Ma, C. Köppl, and H.-J. Werner, *J. Chem. Theory Comput.* **13**, 3650 (2017).
- [109] Q. Ma, M. Schwilk, C. Köppl, and H.-J. Werner, *J. Chem. Theory Comput.* **13**, 4871 (2017).
- [110] Q. Ma and H.-J. Werner, *J. Chem. Theory Comput.* **14**, 198 (2018).
- [111] S. Li, J. Shen, W. Li, and Y. Jiang, *J. Chem. Phys.* **125**, 074109 (2006).
- [112] W. Li, P. Piecuch, J. R. Gour, and S. Li, *J. Chem. Phys.* **131**, 114109 (2009).
- [113] W. Li and P. Piecuch, *J. Phys. Chem. A* **114**, 6721 (2010).
- [114] W. Li and P. Piecuch, *J. Phys. Chem. A* **114**, 8644 (2010).
- [115] C. Riplinger and F. Neese, *J. Chem. Phys.* **138**, 034106 (2013).
- [116] C. Riplinger, B. Sandhoefer, A. Hansen, and F. Neese, *J. Chem. Phys.* **139**, 134101 (2013).
- [117] M. Saitow, U. Becker, C. Riplinger, E. F. Valeev, and F. Neese, *J. Chem. Phys.* **146**, 164105 (2017).
- [118] F. Pavošević, C. Peng, P. Pinski, C. Riplinger, F. Neese, and E. F. Valeev, *J. Chem. Phys.* **146**, 174108 (2017).
- [119] Y. S. Lee and R. J. Bartlett, *J. Chem. Phys.* **80**, 4371 (1984).
- [120] Y. S. Lee, S. A. Kucharski, and R. J. Bartlett, *J. Chem. Phys.* **81**, 5906 (1984), *ibid.* **82**, 5761 (1985) [Erratum].
- [121] J. Noga, R. J. Bartlett, and M. Urban, *Chem. Phys. Lett.* **134**, 126 (1987).
- [122] G. W. Trucks, J. Noga, and R. J. Bartlett, *Chem. Phys. Lett.* **145**, 548 (1988).

- [123] S. A. Kucharski and R. J. Bartlett, *Chem. Phys. Lett.* **158**, 550 (1989).
- [124] K. Raghavachari, *J. Chem. Phys.* **82**, 4607 (1985).
- [125] M. Urban, J. Noga, S. J. Cole, and R. J. Bartlett, *J. Chem. Phys.* **83**, 4041 (1985), *ibid.* **85**, 5383 (1986) [Erratum].
- [126] K. Raghavachari, G. W. Trucks, J. A. Pople, and M. Head-Gordon, *Chem. Phys. Lett.* **157**, 479 (1989).
- [127] S. A. Kucharski and R. J. Bartlett, *J. Chem. Phys.* **108**, 9221 (1998).
- [128] P. Piecuch and K. Kowalski, in *Computational Chemistry: Reviews of Current Trends*, Vol. 5, edited by J. Leszczyński (World Scientific, Singapore, 2000) pp. 1–104.
- [129] K. Kowalski and P. Piecuch, *J. Chem. Phys.* **113**, 18 (2000).
- [130] K. Kowalski and P. Piecuch, *J. Chem. Phys.* **113**, 5644 (2000).
- [131] P. Piecuch, S. A. Kucharski, and K. Kowalski, *Chem. Phys. Lett.* **344**, 176 (2001).
- [132] K. Kowalski and P. Piecuch, *J. Chem. Phys.* **115**, 2966 (2001).
- [133] K. Kowalski and P. Piecuch, *J. Chem. Phys.* **116**, 7411 (2002).
- [134] K. Kowalski and P. Piecuch, *J. Chem. Phys.* **120**, 1715 (2004).
- [135] P.-D. Fan, K. Kowalski, and P. Piecuch, *Mol. Phys.* **103**, 2191 (2005).
- [136] M. D. Lodriguito, K. Kowalski, M. Włoch, and P. Piecuch, *J. Mol. Struct.: THEOCHEM* **771**, 89 (2006).
- [137] P. Piecuch and M. Włoch, *J. Chem. Phys.* **123**, 224105 (2005).
- [138] P. Piecuch, M. Włoch, J. R. Gour, and A. Kinal, *Chem. Phys. Lett.* **418**, 467 (2006).
- [139] M. Włoch, M. D. Lodriguito, P. Piecuch, and J. R. Gour, *Mol. Phys.* **104**, 2149 (2006), *ibid.* **124**, 2291 (2006) [Erratum].
- [140] M. Włoch, J. R. Gour, and P. Piecuch, *J. Phys. Chem. A* **111**, 11359 (2007).
- [141] P. Piecuch, J. R. Gour, and M. Włoch, *Int. J. Quantum Chem.* **109**, 3268 (2009).
- [142] P. Piecuch, K. Kowalski, I. S. O. Pimienta, and M. J. McGuire, *Int. Rev. Phys. Chem.* **21**, 527 (2002).

- [143] P. Piecuch, K. Kowalski, I. S. O. Pimienta, P.-D. Fan, M. Lodriguito, M. J. McGuire, S. A. Kucharski, T. Kuś, and M. Musiał, *Theor. Chem. Acc.* **112**, 349 (2004).
- [144] J. Shen and P. Piecuch, *Chem. Phys.* **401**, 180 (2012).
- [145] N. Oliphant and L. Adamowicz, *J. Chem. Phys.* **94**, 1229 (1991).
- [146] N. Oliphant and L. Adamowicz, *J. Chem. Phys.* **96**, 3739 (1992).
- [147] P. Piecuch, N. Oliphant, and L. Adamowicz, *J. Chem. Phys.* **99**, 1875 (1993).
- [148] P. Piecuch and L. Adamowicz, *Chem. Phys. Lett.* **221**, 121 (1994).
- [149] P. Piecuch and L. Adamowicz, *J. Chem. Phys.* **100**, 5792 (1994).
- [150] P. Piecuch and L. Adamowicz, *J. Chem. Phys.* **102**, 898 (1995).
- [151] V. Alexandrov, P. Piecuch, and L. Adamowicz, *J. Chem. Phys.* **102**, 3301 (1995).
- [152] K. B. Ghose, P. Piecuch, and L. Adamowicz, *J. Chem. Phys.* **103**, 9331 (1995).
- [153] K. B. Ghose, P. Piecuch, S. Pal, and L. Adamowicz, *J. Chem. Phys.* **104**, 6582 (1996).
- [154] P. Piecuch, S. A. Kucharski, and R. J. Bartlett, *J. Chem. Phys.* **110**, 6103 (1999).
- [155] P. Piecuch, S. A. Kucharski, and V. Špirko, *J. Chem. Phys.* **111**, 6679 (1999).
- [156] K. Kowalski and P. Piecuch, *Chem. Phys. Lett.* **344**, 165 (2001).
- [157] K. Kowalski and P. Piecuch, *J. Chem. Phys.* **113**, 8490 (2000).
- [158] K. Kowalski, S. Hirata, M. Włoch, P. Piecuch, and T. L. Windus, *J. Chem. Phys.* **123**, 074319 (2005).
- [159] P. Piecuch, S. Hirata, K. Kowalski, P.-D. Fan, and T. L. Windus, *Int. J. Quantum Chem.* **106**, 79 (2006).
- [160] P. Piecuch, *Mol. Phys.* **108**, 2987 (2010).
- [161] J. Shen and P. Piecuch, *J. Chem. Phys.* **136**, 144104 (2012).
- [162] J. Shen and P. Piecuch, *J. Chem. Theory Comput.* **8**, 4968 (2012).
- [163] N. P. Bauman, J. Shen, and P. Piecuch, *Mol. Phys.* **115**, 2860 (2017).

- [164] J. E. Deustua, J. Shen, and P. Piecuch, *Phys. Rev. Lett.* **119**, 223003 (2017).
- [165] S. H. Yuwono, A. Chakraborty, J. E. Deustua, J. Shen, and P. Piecuch, *Mol. Phys.* **118**, e1817592 (2020).
- [166] J. E. Deustua, J. Shen, and P. Piecuch, *J. Chem. Phys.*, In press (2021), arXiv:2102.10158.
- [167] N. F. Mott, *Proc. Phys. Soc. A* **62**, 416 (1949).
- [168] N. F. Mott, *Rev. Mod. Phys.* **40**, 677 (1968).
- [169] N. F. Mott, *Metal-Insulator Transitions* (Taylor and Francis, London, 1974; 2nd edition 1990, 1990).
- [170] J. Hubbard, *Proc. R. Soc. London A Math. Phys. Eng. Sci.* **276**, 238 (1963).
- [171] J. Hubbard, *Proc. R. Soc. London A Math. Phys. Eng. Sci.* **277**, 237 (1964).
- [172] J. Hubbard, *Proc. R. Soc. London A Math. Phys. Eng. Sci.* **281**, 401 (1964).
- [173] D. Vollhardt, *Rev. Mod. Phys.* **56**, 99 (1984).
- [174] M. Imada, A. Fujimori, and Y. Tokura, *Rev. Mod. Phys.* **70**, 1039 (1998).
- [175] J. Hachmann, W. Cardoen, and G. K.-L. Chan, *J. Chem. Phys.* **125**, 144101 (2006).
- [176] G. L. Bendazzoli, S. Evangelisti, and A. Monari, *Int. J. Quantum Chem.* **111**, 3416 (2011).
- [177] M. Motta, D. M. Ceperley, G. K.-L. Chan, J. A. Gomez, E. Gull, S. Guo, C. A. Jiménez-Hoyos, T. N. Lan, J. Li, F. Ma, A. J. Millis, N. V. Prokof'ev, U. Ray, G. E. Scuseria, S. Sorella, E. M. Stoudenmire, Q. Sun, I. S. Tupitsyn, S. R. White, D. Zgid, and S. Zhang, *Phys. Rev. X* **7**, 031059 (2017).
- [178] T. Tsuchimochi and G. E. Scuseria, *J. Chem. Phys.* **131**, 121102 (2009).
- [179] A. V. Sinitskiy, L. Greenman, and D. A. Mazziotti, *J. Chem. Phys.* **133**, 014104 (2010).
- [180] D. Kats and F. R. Manby, *J. Chem. Phys.* **139**, 021102 (2013).
- [181] E. Pastorczak, J. Shen, M. Hapka, P. Piecuch, and K. Pernal, *J. Chem. Theory Comput.* **13**, 5404 (2017).
- [182] R. Pauncz, J. de Heer, and P.-O. Löwdin, *J. Chem. Phys.* **36**, 2247 (1962).

- [183] R. Pauncz, J. de Heer, and P.-O. Löwdin, *J. Chem. Phys.* **36**, 2257 (1962).
- [184] R. Pariser and R. G. Parr, *J. Chem. Phys.* **21**, 466 (1953).
- [185] R. Pariser and R. G. Parr, *J. Chem. Phys.* **21**, 767 (1953).
- [186] J. A. Pople, *Trans. Faraday Soc.* **49**, 1375 (1953).
- [187] J. Paldus, M. Takahashi, and R. W. H. Cho, *Phys. Rev. B* **30**, 4267 (1984).
- [188] J. Paldus, M. Takahashi, and R. W. H. Cho, *Int. J. Quantum Chem. Symp.* **18**, 237 (1984).
- [189] M. Takahashi and J. Paldus, *Phys. Rev. B* **31**, 5121 (1985).
- [190] P. Piecuch, S. Zarrabian, J. Paldus, and J. Čížek, *Phys. Rev. B* **42**, 3351 (1990).
- [191] P. Piecuch and J. Paldus, *Int. J. Quantum Chem. Symp.* **25**, 9 (1991).
- [192] J. Paldus and P. Piecuch, *Int. J. Quantum Chem.* **42**, 135 (1992).
- [193] P. Piecuch, J. Čížek, and J. Paldus, *Int. J. Quantum Chem.* **42**, 165 (1992).
- [194] R. Podeszwa, S. A. Kucharski, and L. Z. Stolarczyk, *J. Chem. Phys.* **116**, 480 (2002).
- [195] J. Li, Y. Yao, A. A. Holmes, M. Otten, Q. Sun, S. Sharma, and C. J. Umrigar, *Phys. Rev. Research* **2**, 012015(R) (2020).
- [196] K. Ruedenberg, M. W. Schmidt, M. M. Gilbert, and S. T. Elbert, *Chem. Phys.* **71**, 41 (1982).
- [197] B. O. Roos, *Adv. Chem. Phys.* **69**, 399 (1987).
- [198] S. R. White, *Phys. Rev. Lett.* **69**, 2863 (1992).
- [199] S. R. White and R. L. Martin, *J. Chem. Phys.* **110**, 4127 (1999).
- [200] A. O. Mitrushenkov, G. Fano, F. Ortolani, R. Linguerri, and P. Palmieri, *J. Chem. Phys.* **115**, 6815 (2001).
- [201] G. K.-L. Chan and M. Head-Gordon, *J. Chem. Phys.* **116**, 4462 (2002).
- [202] S. Keller, M. Dolfi, M. Troyer, and M. Reiher, *J. Chem. Phys.* **143**, 244118 (2015).

- [203] G. K.-L. Chan, A. Keselman, N. Nakatani, Z. Li, and S. R. White, *J. Chem. Phys.* **145**, 014102 (2016).
- [204] Y. Kurashige and T. Yanai, *J. Chem. Phys.* **135**, 094104 (2011).
- [205] S. Guo, M. A. Watson, W. Hu, Q. Sun, and G. K.-L. Chan, *J. Chem. Theory Comput.* **12**, 1583 (2016).
- [206] N. Nakatani and S. Guo, *J. Chem. Phys.* **146**, 094102 (2017).
- [207] S. Sharma and G. K.-L. Chan, *J. Chem. Phys.* **141**, 111101 (2014).
- [208] L. Freitag, S. Knecht, C. Angeli, and M. Reiher, *J. Chem. Theory Comput.* **13**, 451 (2017).
- [209] M. Degroote, T. M. Henderson, J. Zhao, J. Dukelsky, and G. E. Scuseria, *Phys. Rev. B* **93**, 125124 (2016).
- [210] I. W. Bulik, T. M. Henderson, and G. E. Scuseria, *J. Chem. Theory Comput.* **11**, 3171 (2015).
- [211] J. A. Gomez, M. Degroote, J. Zhao, Y. Qiu, and G. E. Scuseria, *Phys. Chem. Chem. Phys.* **19**, 22385 (2017).
- [212] J. A. Gomez, T. M. Henderson, and G. E. Scuseria, *Mol. Phys.* **115**, 2673 (2017).
- [213] D. J. Thouless, *Nucl. Phys.* **21**, 225 (1960).
- [214] D. J. Thouless, *The Quantum Mechanics of Many-Body Systems* (Academic Press, 1961).
- [215] P.-O. Löwdin, *Phys. Rev.* **97**, 1509 (1955).
- [216] P.-O. Löwdin, *J. Appl. Phys. Suppl.* **33**, 251 (1962).
- [217] P.-O. Löwdin, *Rev. Mod. Phys.* **34**, 520 (1962).
- [218] P.-O. Löwdin, *Adv. Chem. Phys.* **14**, 283 (1969).
- [219] P. Piecuch, R. Toboła, and J. Paldus, *Phys. Rev. A* **54**, 1210 (1996).
- [220] J. Paldus, J. Čížek, and M. Takahashi, *Phys. Rev. A* **30**, 2193 (1984).
- [221] Y. Qiu, T. M. Henderson, and G. E. Scuseria, *J. Chem. Phys.* **145**, 111102 (2016).



- [222] Y. Qiu, T. M. Henderson, and G. E. Scuseria, *J. Chem. Phys.* **146**, 184105 (2017).
- [223] T. M. Henderson and G. E. Scuseria, *Phys. Rev. A* **96**, 022506 (2017).
- [224] B. G. Adams, K. Jankowski, and J. Paldus, *Chem. Phys. Lett.* **67**, 144 (1979).
- [225] K. Jankowski and J. Paldus, *Int. J. Quantum Chem.* **18**, 1243 (1980).
- [226] B. G. Adams, K. Jankowski, and J. Paldus, *Phys. Rev. A* **24**, 2316 (1981).
- [227] B. G. Adams, K. Jankowski, and J. Paldus, *Phys. Rev. A* **24**, 2330 (1981).
- [228] R. A. Chiles and C. E. Dykstra, *Chem. Phys. Lett.* **80**, 69 (1981).
- [229] S. M. Bachrach, R. A. Chiles, and C. E. Dykstra, *J. Chem. Phys.* **75**, 2270 (1981).
- [230] P. Piecuch and J. Paldus, *Theor. Chim. Acta* **78**, 65 (1990).
- [231] P. Piecuch, R. Toboła, and J. Paldus, *Int. J. Quantum Chem.* **55**, 133 (1995).
- [232] R. J. Bartlett and M. Musiał, *J. Chem. Phys.* **125**, 204105 (2006).
- [233] M. Musiał and R. J. Bartlett, *J. Chem. Phys.* **127**, 024106 (2007).
- [234] L. M. J. Huntington and M. Nooijen, *J. Chem. Phys.* **133**, 184109 (2010).
- [235] V. Rishi and E. F. Valeev, *J. Chem. Phys.* **151**, 064102 (2019).
- [236] D. Kats, *J. Chem. Phys.* **141**, 061101 (2014).
- [237] D. Kats, D. Kreplin, H.-J. Werner, and F. R. Manby, *J. Chem. Phys.* **142**, 064111 (2015).
- [238] D. Kats, *J. Chem. Phys.* **144**, 044102 (2016).
- [239] D. Kats, *Mol. Phys.* **116**, 1435 (2018).
- [240] V. Rishi, A. Perera, and R. J. Bartlett, *J. Chem. Phys.* **144**, 124117 (2016).
- [241] V. Rishi, A. Perera, M. Nooijen, and R. J. Bartlett, *J. Chem. Phys.* **146**, 144104 (2017).
- [242] D. Kats and A. Köhn, *J. Chem. Phys.* **150**, 151101 (2019).
- [243] J. Paldus, *J. Math. Chem.* **55**, 477 (2017).

- [244] P. Piecuch, A. E. Kondo, V. Špirko, and J. Paldus, *J. Chem. Phys.* **104**, 4699 (1996).
- [245] A. Hall, *Messeng. Math.* **2**, 113 (1873).
- [246] G.-L. L. de Buffon, *Essai d'arithmétique morale* (1777).
- [247] J. D. Hey, T. M. Neugebauer, and C. M. Pasca, “Georges-Louis Leclerc de Buffon’s ‘Essays on Moral Arithmetic’,” in *The Selten School of Behavioral Economics: A Collection of Essays in Honor of Reinhard Selten*, edited by A. Sadrieh and A. Ockenfels (Springer Berlin Heidelberg, Berlin, Heidelberg, 2010) pp. 245–282.
- [248] J. H. Halton, *SIAM Rev.* **12**, 1 (1970).
- [249] N. Metropolis, *Los Alamos Sci.* **15**, 125 (1987).
- [250] N. Metropolis and S. Ulam, *J. Am. Stat. Assoc.* **44**, 335 (1949).
- [251] N. Metropolis, A. W. Rosenbluth, M. N. Rosenbluth, A. H. Teller, and E. Teller, *J. Chem. Phys.* **21**, 1087 (1953).
- [252] R. Eckhardt, *Los Alamos Sci.* **15**, 131 (1987).
- [253] B. M. Austin, D. Y. Zubarev, and W. A. Lester, Jr., *Chem. Rev.* **112**, 263 (2012).
- [254] W. L. McMillan, *Phys. Rev.* **138**, A442 (1965).
- [255] D. Ceperley, G. V. Chester, and M. H. Kalos, *Phys. Rev. B* **16**, 3081 (1977).
- [256] J. B. Anderson, *J. Chem. Phys.* **63**, 1499 (1975).
- [257] J. B. Anderson, *J. Chem. Phys.* **65**, 4121 (1976).
- [258] P. J. Reynolds, D. M. Ceperley, B. J. Alder, and W. A. Lester, Jr., *J. Chem. Phys.* **77**, 5593 (1982).
- [259] J. B. Anderson, *Int. Rev. Phys. Chem.* **14**, 85 (1995).
- [260] G. H. Booth, A. J. W. Thom, and A. Alavi, *J. Chem. Phys.* **131**, 054106 (2009).
- [261] D. Cleland, G. H. Booth, and A. Alavi, *J. Chem. Phys.* **132**, 041103 (2010).
- [262] D. M. Cleland, G. H. Booth, and A. Alavi, *J. Chem. Phys.* **134**, 024112 (2011).
- [263] K. Ghanem, A. Y. Lozovoi, and A. Alavi, *J. Chem. Phys.* **151**, 224108 (2019).

- [264] K. Ghanem, K. Guthrie, and A. Alavi, *J. Chem. Phys.* **153**, 224115 (2020).
- [265] J. E. Deustua, I. Magoulas, J. Shen, and P. Piecuch, *J. Chem. Phys.* **149**, 151101 (2018).
- [266] J. J. Eriksen, T. A. Anderson, J. E. Deustua, K. Ghanem, D. Hait, M. R. Hoffmann, S. Lee, D. S. Levine, I. Magoulas, J. Shen, N. M. Tubman, K. B. Whaley, E. Xu, Y. Yao, N. Zhang, A. Alavi, G. K.-L. Chan, M. Head-Gordon, W. Liu, P. Piecuch, S. Sharma, S. L. Ten-no, C. J. Umrigar, and J. Gauss, *J. Phys. Chem. Lett.* **11**, 8922 (2020).
- [267] J. Paldus and J. Planelles, *Theor. Chim. Acta* **89**, 13 (1994).
- [268] L. Z. Stolarczyk, *Chem. Phys. Lett.* **217**, 1 (1994).
- [269] G. Peris, J. Planelles, and J. Paldus, *Int. J. Quantum Chem.* **62**, 137 (1997).
- [270] G. Peris, J. Planelles, J.-P. Malrieu, and J. Paldus, *J. Chem. Phys.* **110**, 11708 (1999).
- [271] X. Li and J. Paldus, *J. Chem. Phys.* **107**, 6257 (1997).
- [272] X. Li and J. Paldus, *J. Chem. Phys.* **124**, 174101 (2006).
- [273] G. J. R. Aroeira, M. M. Davis, J. M. Turney, and H. F. Schaefer, III, *J. Chem. Theory Comput.* **17**, 182 (2021).
- [274] I. Magoulas, K. Gururangan, P. Piecuch, J. E. Deustua, and J. Shen, *J. Chem. Theory Comput.* Submitted (2021), arXiv:2102.10143.
- [275] S. Hirata, *Theor. Chem. Acc.* **129**, 727 (2011).
- [276] T. H. Dunning, Jr., *J. Chem. Phys.* **90**, 1007 (1989).
- [277] J. Olsen, P. Jørgensen, H. Koch, A. Balkova, and R. J. Bartlett, *J. Chem. Phys.* **104**, 8007 (1996).
- [278] J. Paldus and M. J. Boyle, *Int. J. Quantum Chem.* **22**, 1281 (1982).
- [279] P. Kramer and M. Moshinsky, in *Group Theory and its Applications*, edited by E. M. Loebl (Academic Press, 1968) pp. 339–468.
- [280] C. A. Coulson and G. S. Rushbrooke, *Math. Proc. Cambridge Philos. Soc.* **36**, 193 (1940).
- [281] S. N. Dixit and S. Mazumdar, *Phys. Rev. B* **29**, 1824 (1984).

- [282] R. W. Richardson and N. Sherman, *Nucl. Phys.* **52**, 221 (1964).
- [283] R. W. Richardson, *Phys. Rev.* **141**, 949 (1966).
- [284] R. W. Richardson, *J. Math. Phys.* **9**, 1327 (1968).
- [285] L. N. Cooper, *Phys. Rev.* **104**, 1189 (1956).
- [286] J. Bardeen, L. N. Cooper, and J. R. Schrieffer, *Phys. Rev.* **106**, 162 (1957).
- [287] J. Bardeen, L. N. Cooper, and J. R. Schrieffer, *Phys. Rev.* **108**, 1175 (1957).
- [288] J. Paldus, *J. Chem. Phys.* **67**, 303 (1977).
- [289] B. G. Adams and J. Paldus, *Phys. Rev. A* **20**, 1 (1979).
- [290] P. Piecuch and J. Paldus, *Int. J. Quantum Chem.* **36**, 429 (1989).
- [291] J. A. Pople, R. Krishnan, H. B. Schlegel, and J. S. Binkley, *Int. J. Quantum Chem.* **14**, 545 (1978).
- [292] R. J. Bartlett and G. D. Purvis, III, *Int. J. Quantum Chem.* **14**, 561 (1978).
- [293] J. Paldus, B. G. Adams, and J. Čížek, *Int. J. Quantum Chem.* **11**, 813 (1977).
- [294] J. H. Van Vleck, *Rev. Mod. Phys.* **7**, 167 (1935).
- [295] S. A. Kucharski and R. J. Bartlett, *Adv. Quantum Chem.* **18**, 281 (1986).
- [296] W. Meyer, *Int. J. Quantum Chem.* **5**, 341 (1971).
- [297] W. Meyer, *J. Chem. Phys.* **58**, 1017 (1973).
- [298] R. Ahlrichs, H. Lischka, V. Staemmler, and W. Kutzelnigg, *J. Chem. Phys.* **62**, 1225 (1975).
- [299] P. R. Taylor, G. B. Bacskay, N. S. Hush, and A. C. Hurley, *Chem. Phys. Lett.* **41**, 444 (1976).
- [300] P. R. Taylor, G. B. Bacskay, N. S. Hush, and A. C. Hurley, *J. Chem. Phys.* **69**, 1971 (1978).
- [301] P. R. Taylor, G. B. Bacskay, N. S. Hush, and A. C. Hurley, *J. Chem. Phys.* **69**, 4669 (1978).

- [302] R. Ahlrichs, *Comput. Phys. Commun.* **17**, 31 (1979).
- [303] A. C. Hurley, *Electron Correlation in Small Molecules* (Academic Press, New York, 1976).
- [304] W. Kutzelnigg, in *Methods of Electronic Structure Theory*, edited by H. F. Schaefer, III (Springer, Boston, 1977) pp. 129–188.
- [305] W. Meyer, in *Methods of Electronic Structure Theory*, edited by H. F. Schaefer, III (Springer, Boston, 1977) pp. 413–446.
- [306] W. J. Hehre, R. F. Stewart, and J. A. Pople, *J. Chem. Phys.* **51**, 2657 (1969).
- [307] M. W. Schmidt, K. K. Baldridge, J. A. Boatz, S. T. Elbert, M. S. Gordon, J. H. Jensen, S. Koseki, N. Matsunaga, K. A. Nguyen, S. Su, T. L. Windus, M. Dupuis, and J. A. Montgomery, Jr., *J. Comput. Chem.* **14**, 1347 (1993).
- [308] M. S. Gordon and M. W. Schmidt, in *Theory and Applications of Computational Chemistry: The First Forty Years*, edited by C. E. Dykstra, G. Frenking, K. S. Kim, and G. E. Scuseria (Elsevier, Amsterdam, 2005) pp. 1167–1189.
- [309] G. M. J. Barca, C. Bertoni, L. Carrington, D. Datta, N. De Silva, J. E. Deustua, D. G. Fedorov, J. R. Gour, A. O. Gunina, E. Guidez, T. Harville, S. Irle, J. Ivanic, K. Kowalski, S. S. Leang, H. Li, W. Li, J. J. Lutz, I. Magoulas, J. Mato, V. Mironov, H. Nakata, B. Q. Pham, P. Piecuch, D. Poole, S. R. Pruitt, A. P. Rendell, L. B. Roskop, K. Ruedenberg, T. Sattasathuchana, M. W. Schmidt, J. Shen, L. Slipchenko, M. Sosonkina, V. Sundriyal, A. Tiwari, J. L. Galvez Vallejo, B. Westheimer, M. Włoch, P. Xu, F. Zahariev, and M. S. Gordon, *J. Chem. Phys.* **152**, 154102 (2020).
- [310] N. S. Blunt, A. J. W. Thom, and C. J. C. Scott, *J. Chem. Theory Comput.* **15**, 3537 (2019).
- [311] T. H. Dunning, Jr., *J. Chem. Phys.* **53**, 2823 (1970).
- [312] T. H. Dunning, Jr. and P. J. Hay, in *Methods of Electronic Structure Theory*, edited by H. F. Schaefer, III (Springer, Boston, 1977) pp. 1–27.
- [313] J. Ivanic and K. Ruedenberg, *Theor. Chem. Acc.* **106**, 339 (2001).
- [314] J. Ivanic, *J. Chem. Phys.* **119**, 9364 (2003).
- [315] J. Ivanic, *J. Chem. Phys.* **119**, 9377 (2003).
- [316] J. S. Spencer, N. S. Blunt, W. A. Vigor, F. D. Malone, W. M. C. Foulkes, J. J. Shepherd, and A. J. W. Thom, *J. Open Res. Software* **3**, e9 (2015).

- [317] J. J. Eriksen and J. Gauss, *J. Phys. Chem. Lett.* **10**, 7910 (2019).
- [318] C. E. Shannon, *London, Edinburgh, Dublin Philos. Mag. J. Sci.* **41**, 256 (1950).
- [319] M. Musiał, S. A. Kucharski, and R. J. Bartlett, *J. Chem. Phys.* **116**, 4382 (2002).
- [320] M. Schreiber, M. R. Silva-Junior, S. P. A. Sauer, and W. Thiel, *J. Chem. Phys.* **128**, 134110 (2008).
- [321] G. H. Booth and A. Alavi *et al.*, Standalone NECI Codebase Designed for FCIQMC and Other Stochastic Quantum Chemistry Methods, [https://github.com/ghb24/NECI\\_STABLE](https://github.com/ghb24/NECI_STABLE), 2013.
- [322] K. Guthrie, R. J. Anderson, N. S. Blunt, N. A. Bogdanov, D. Cleland, N. Dattani, W. Dobrutz, K. Ghanem, P. Jeszenszki, N. Liebermann, G. L. Manni, A. Y. Lozovoi, H. Luo, D. Ma, F. Merz, C. Overy, M. Rampp, P. K. Samanta, L. R. Schwarz, J. J. Shepherd, S. D. Smart, E. Vitale, O. Weser, G. H. Booth, and A. Alavi, *J. Chem. Phys.* **153**, 034107 (2020).
- [323] H.-J. Werner, P. J. Knowles, G. Knizia, F. R. Manby, and M. Schütz, *WIREs Comput. Mol. Sci.* **2**, 242 (2012).
- [324] H.-J. Werner, P. J. Knowles, F. R. Manby, J. A. Black, K. Doll, A. Heßelmann, D. Kats, A. Köhn, T. Korona, D. A. Kreplin, Q. Ma, T. F. Miller, III, A. Mitrushchenkov, K. A. Peterson, I. Polyak, G. Rauhut, and M. Sibaev, *J. Chem. Phys.* **152**, 144107 (2020).
- [325] H. Flyvbjerg and H. G. Petersen, *J. Chem. Phys.* **91**, 461 (1989).
- [326] N. M. Tubman, J. Lee, T. Y. Takeshita, M. Head-Gordon, and K. B. Whaley, *J. Chem. Phys.* **145**, 044112 (2016).
- [327] D. Hait, N. M. Tubman, D. S. Levine, K. B. Whaley, and M. Head-Gordon, *J. Chem. Theory Comput.* **15**, 5370 (2019).
- [328] N. M. Tubman, C. D. Freeman, D. S. Levine, D. Hait, M. Head-Gordon, and K. B. Whaley, *J. Chem. Theory Comput.* **16**, 2139 (2020).
- [329] D. S. Levine, D. Hait, N. M. Tubman, S. Lehtola, K. B. Whaley, and M. Head-Gordon, *J. Chem. Theory Comput.* **16**, 2340 (2020).
- [330] F. R. Petruzielo, A. A. Holmes, H. J. Changlani, M. P. Nightingale, and C. J. Umrigar, *Phys. Rev. Lett.* **109**, 230201 (2012).
- [331] A. A. Holmes, H. J. Changlani, and C. J. Umrigar, *J. Chem. Theory Comput.* **12**, 1561 (2016).

- [332] A. A. Holmes, N. M. Tubman, and C. J. Umrigar, *J. Chem. Theory Comput.* **12**, 3674 (2016).
- [333] S. Sharma, A. A. Holmes, G. Jeanmairet, A. Alavi, and C. J. Umrigar, *J. Chem. Theory Comput.* **13**, 1595 (2017).
- [334] B. Smith, J. E. T. Mussard, A. A. Holmes, and S. Sharma, *J. Chem. Theory comput.* **13**, 5468 (2017).
- [335] A. A. Holmes, C. J. Umrigar, and S. S., *J. Chem. Phys.* **147**, 164111 (2017).
- [336] J. Li, M. Otten, A. A. Holmes, S. Sharma, and C. J. Umrigar, *J. Chem. Phys.* **149**, 214110 (2018).
- [337] W. Liu and M. R. Hoffmann, *Theor. Chem. Acc.* **133**, 1481 (2014).
- [338] W. Liu and M. R. Hoffmann, *J. Chem. Theory Comput.* **12**, 1169 (2016).
- [339] Y. Lei, W. Liu, and M. R. Hoffmann, *Mol. Phys.* **115**, 2696 (2017).
- [340] N. Zhang, W. Liu, and M. R. Hoffmann, *J. Chem. Theory Comput.* **16**, 2296 (2020).
- [341] S. R. White, *Phys. Rev. B* **48**, 10345 (1993).
- [342] O. Legeza, J. Röder, and B. A. Hess, *Phys. Rev. B* **67**, 125114 (2003).
- [343] G. K.-L. Chan and S. Sharma, *Annu. Rev. Phys. Chem.* **62**, 465 (2011).
- [344] S. Sharma and G. K.-L. Chan, *J. Chem. Phys.* **136**, 124121 (2012).
- [345] S. Wouters and D. Van Neck, *Eur. Phys. J. D* **68**, 272 (2014).
- [346] R. Olivares-Amaya, W. Hu, N. Nakatani, S. Sharma, J. Yang, and G. K.-L. Chan, *J. Chem. Phys.* **142**, 034102 (2015).
- [347] T. Yanai, Y. Kurashige, W. Mizukami, J. Chalupský, T. N. Lan, and M. Saitow, *Int. J. Quantum Chem.* **115**, 283 (2015).
- [348] S. Knecht, E. D. Hedegård, S. Keller, A. Kovyrshin, Y. Ma, A. Muolo, C. J. Stein, and M. Reiher, *Chimia* **70**, 244 (2016).
- [349] J. J. Eriksen, F. Lipparini, and J. Gauss, *J. Phys. Chem. Lett.* **8**, 4633 (2017).
- [350] J. J. Eriksen and J. Gauss, *J. Chem. Theory Comput.* **14**, 5180 (2018).

- [351] J. J. Eriksen and J. Gauss, *J. Chem. Theory Comput.* **15**, 4873 (2019).
- [352] E. Xu, M. Uejima, and S. L. Ten-no, *Phys. Rev. Lett.* **121**, 113001 (2018).
- [353] A. J. W. Thom, *Phys. Rev. Lett.* **105**, 263004 (2010).
- [354] R. S. T. Franklin, J. S. Spencer, A. Zoccante, and A. J. W. Thom, *J. Chem. Phys.* **144**, 044111 (2016).
- [355] J. S. Spencer and A. J. W. Thom, *J. Chem. Phys.* **144**, 084108 (2016).
- [356] C. J. C. Scott and A. J. W. Thom, *J. Chem. Phys.* **147**, 124105 (2017).
- [357] C. F. Bender and E. R. Davidson, *Phys. Rev.* **183**, 23 (1969).
- [358] J. L. Whitten and M. Hackmeyer, *J. Chem. Phys.* **51**, 5584 (1969).
- [359] B. Huron, M. J.-P., and P. Rancurel, *J. Chem. Phys.* **58**, 5745 (1973).
- [360] R. J. Buenker and S. D. Peyerimhoff, *Theor. Chim. Acta* **35**, 33 (1974).
- [361] R. J. Harrison, *J. Chem. Phys.* **94**, 5021 (1991).
- [362] F. Illas, J. Rubio, J. M. Ricart, and P. S. Bagus, *J. Chem. Phys.* **95**, 1877 (1991).
- [363] F. E. Harris, *Int. J. Quantum Chem. Symp.* **11**, 403 (1977).
- [364] T. P. Živković and H. J. Monkhorst, *J. Math. Phys.* **19**, 1007 (1978).
- [365] L. Meissner, A. Balková, and R. J. Bartlett, *Chem. Phys. Lett.* **212**, 177 (1993).
- [366] K. Jankowski, K. Kowalski, and P. Jankowski, *Chem. Phys. Lett.* **222**, 608 (1994).
- [367] K. Jankowski, K. Kowalski, and P. Jankowski, *Int. J. Quantum Chem.* **50**, 353 (1994).
- [368] K. Jankowski, K. Kowalski, and P. Jankowski, *Int. J. Quantum Chem.* **53**, 501 (1995).
- [369] K. Kowalski and K. Jankowski, *Phys. Rev. Lett.* **81**, 1195 (1998).
- [370] K. Jankowski and K. Kowalski, *J. Chem. Phys.* **110**, 3714 (1999).
- [371] K. Jankowski and K. Kowalski, *J. Chem. Phys.* **110**, 9345 (1999).
- [372] K. Jankowski and K. Kowalski, *J. Chem. Phys.* **111**, 2940 (1999).



- [373] R. Podeszwa and L. Z. Stolarczyk, *Chem. Phys. Lett.* **366**, 426 (2002).
- [374] R. Podeszwa, L. Z. Stolarczyk, K. Jankowski, and K. Rubiniec, *Theor. Chem. Acc.* **109**, 309 (2003).
- [375] N. J. Mayhall and K. Raghavachari, *J. Chem. Theory Comput.* **6**, 2714 (2010).
- [376] J. Lee, D. W. Small, and M. Head-Gordon, *J. Chem. Phys.* **151**, 214103 (2019).